



THE UNIVERSITY *of* EDINBURGH

This thesis has been submitted in fulfilment of the requirements for a postgraduate degree (e.g. PhD, MPhil, DClinPsychol) at the University of Edinburgh. Please note the following terms and conditions of use:

- This work is protected by copyright and other intellectual property rights, which are retained by the thesis author, unless otherwise stated.
- A copy can be downloaded for personal non-commercial research or study, without prior permission or charge.
- This thesis cannot be reproduced or quoted extensively from without first obtaining permission in writing from the author.
- The content must not be changed in any way or sold commercially in any format or medium without the formal permission of the author.
- When referring to this work, full bibliographic details including the author, title, awarding institution and date of the thesis must be given.



**A Study of the Molecular Details of p53 Redox-Regulation using
Fourier Transform Ion Cyclotron Resonance
Mass Spectrometry**

A thesis submitted for the degree of
Doctor of Philosophy

by

Jenna Scotcher

School of Chemistry
College of Science and Engineering
The University of Edinburgh

October 2010

Declaration

I declare that this thesis was composed by myself and is based on work carried out at the University of Edinburgh during the period 2007-10. Unless stated otherwise, this work is wholly original and has not been submitted in partial or complete form for any other degree or professional qualification.

October 2010

Acknowledgements

Firstly, I would like to acknowledge Dr. Claudia Blindauer (University of Warwick) for thoughtfully suggesting that I consider a PhD at the University of Edinburgh under the supervision of Prof. Peter Sadler. I am immensely grateful to Peter for subsequently introducing me to the Doctoral Training Centre in Proteomic Technologies, and I would like to thank him for his continued support and guidance over the past three years, despite having left Edinburgh prior to the start date of my PhD!

I would like to thank Dr. Penka Nikolova (King's College London) for donation of the p53 expression vector, welcoming me into her lab at KCL, and her continued support and interest in my progress. I am also grateful to Prof. Ted Hupp (Edinburgh Cancer Research Centre) for his support, Seema Patel (King's College London) for teaching me the p53 expression and purification procedure, Dr. Jennifer Fraser (Edinburgh Cancer Research Centre) for help with the DNA-binding assay and the Campopiano group (University of Edinburgh) for access to their protein purification equipment.

I am grateful to the funding bodies, the EPSRC and the BBSRC, for their financial support, without which the work presented in this thesis would not have been possible. I would also like to thank the IRColl RASOR and the BMSS for providing financial assistance with travel and subsistence expenses.

I would like to express my sincere gratitude to each member of SIRCAMS (the Scottish Instrumentation and Resource Centre for *Measurement Science*), past and present, for contributing to a fun and friendly working environment. I owe a debt of gratitude to Dr. David Clarke and to Dr. Stefan Weidt for their consistently invaluable advice and assistance in the face of relentless scientific-interrogation and sometimes shouting. I would like to thank Dr. Logan Mackay for his continued support and generosity, and Dr. David Kilgour for his patience and enthusiasm for reading the same sentence repeatedly.

Finally, I would like to gratefully acknowledge my unique and distinguished PhD supervisor, and the founding member of SIRCAMS, Dr. Pat Langridge-Smith.

Abstract

Reactive oxygen species (ROS) such as hydrogen peroxide (H_2O_2) and superoxide ($\text{O}_2^{\cdot -}$) have been shown to serve as messengers in biological signal transduction, and many prokaryotic and eukaryotic proteins are now known to have their function controlled via ROS-mediated oxidation reactions occurring on critical cysteine residues.

The tumour-suppressor protein p53 is involved in the regulation of a diverse range of cellular processes including apoptosis, differentiation, senescence, DNA-repair, cell-cycle arrest, autophagy, glycolysis and oxidative stress. However, little is understood about the specific molecular mechanisms that allow p53 to discriminate between these various different functions. p53 is a multiple cysteine-containing protein and there is mounting evidence to suggest that redox-modification of p53 Cys residues participate in control of its biological activity. Furthermore, p53 activity has been linked to intracellular ROS levels.

Fourier transform ion cyclotron resonance mass spectrometry (FT-ICR MS) offers superior mass resolving power and mass measurement accuracy, which is beneficial for the study of intact proteins and the characterisation of their post-translational modifications (PTMs). The primary goal of the work described in this thesis was to employ FT-ICR mass spectrometry to investigate the molecular details of p53 redox-regulation.

The relative reactivity of each of the ten cysteine residues in the DNA-binding core domain of recombinant human p53 was characterised by treatment with the Cys-alkylating reagent *N*-ethylmaleimide (NEM) under various conditions. A combination of top-down and middle-down FT-ICR MS was used to unambiguously identify Cys182 and Cys277 as sites of preferential alkylation. These results were confirmed by site-directed mutagenesis. Interestingly, Cys182 and Cys277 have previously been implicated in p53 redox-regulation. Alkylation beyond these two residues was found to trigger rapid alkylation of the remaining Cys residues, presumably accompanied by protein unfolding. These observations have implications

for the re-activation of mutant p53 with Cys-targeting compounds which result in the death of cancer-cells.

Furthermore, the molecular interaction between p53 and the ROS hydrogen peroxide was investigated. p53 was found to form two disulfide bonds upon treatment with H₂O₂. An enrichment strategy was developed to purify oxidised p53 and top-down FT-ICR mass spectrometry revealed unambiguously that Cys176, 182, 238 and 242 were the oxidised residues. Interestingly, Cys176, 238 and 242 are Zn²⁺-binding residues suggesting that p53 contains a zinc-redox switch. The mechanism of H₂O₂ oxidation was investigated, and revealed that oxidation via an alternative pathway results in indiscriminate over-oxidation of p53. Moreover, Cys176, 238 or 242 was shown to act as a nucleophile, and the intracellular antioxidant glutathione (GSH) did not prevent oxidation of the Zn²⁺-binding Cys residues, providing further evidence for a role in p53 redox-regulation.

This study has revealed hitherto unknown details regarding the chemistry of cysteine residues within the important tumour-suppressor protein p53. Furthermore, the analytical power of FT-ICR MS for the study of multiple Cys-containing proteins has been very clearly demonstrated.

Table of Contents

Declaration	i
Acknowledgements	ii
Abstract	iii
Table of Contents	v
List of Figures	x
List of Tables	xiii
Glossary	xiv
Chapter 1 Introduction	1
1.1 Biological Redox Signalling	2
1.1.1 Reactive Oxygen Species as Signalling Molecules	2
1.1.2 The Chemistry of Cysteine	3
1.1.3 Redox-Regulated Proteins	5
1.2 Tumour-Suppressor Protein p53	8
1.2.1 Introduction	8
1.2.2 Domain Structure of p53	9
1.2.3 p53 Core Domain	10
1.2.4 Evidence for p53 Redox-Regulation	15
1.3 Analysis of Multiple Cys-Containing Proteins	18
1.4 Protein Mass Spectrometry	20
1.4.1 Bottom-up Mass Spectrometry	20
1.4.2 Top-down Mass Spectrometry	21
1.4.3 Middle-down Mass Spectrometry	26
1.5 Electrospray Ionisation Mass Spectrometry	26
1.6 FT-ICR Mass Spectrometry	30
1.7 Fragmentation of Ions	36
1.7.1 Nomenclature	37
1.7.2 Collision-Induced Dissociation	38
1.7.3 Electron Capture Dissociation	39

Chapter 2	Materials and Methods	42
2.1	Materials	43
2.2	Molecular Biology	43
2.2.1	Bacterial Growth Media	43
2.2.2	Amplification and Purification of Plasmid DNA	43
2.2.3	Restriction Digest and Agarose Gel Electrophoresis	43
2.2.4	Site-Directed Mutagenesis	44
2.2.5	DNA Sequencing	44
2.2.6	Expression of Wild-Type and Mutant p53 Core Domain	44
2.2.7	Protein Purification	45
2.2.7.1	Ion Exchange Chromatography	45
2.2.7.2	Gel Filtration Chromatography	45
2.2.8	Protein Gel Electrophoresis	46
2.2.9	DNA-Binding Assay	46
2.3	Protein Chemistry	47
2.3.1	Reaction Buffer	47
2.3.2	Protein Concentration	47
2.3.3	Cysteine Alkylation	47
2.3.3.1	Confirmation of Free Cysteine Residues	47
2.3.3.2	Concentration-Dependent Alkylation	47
2.3.3.3	Time-Dependent Alkylation	48
2.3.4	p53 Oxidation	48
2.3.4.1	H ₂ O ₂ Titration	48
2.3.4.2	H ₂ O ₂ Oxidation over Time	48
2.3.4.3	Oxidation in Excess Dimedone, Zn ²⁺ or GSH	48
2.3.5	TCA Precipitation	48
2.3.6	Affinity Purification of Oxidised p53	49
2.3.6.1	Biotinylation	49
2.3.6.2	Capture and Elution	49
2.3.7	Proteolytic Digestion	49
2.3.7.1	Trypsin or Lys-C Digestion of 2NEM-p53	49

2.3.7.2	Trypsin Digestion of Oxidised p53	50
2.3.7.3	Desalting	50
2.4	Liquid Chromatography	50
2.5	Mass Spectrometry	50
2.5.1	Sample Preparation	50
2.5.1.1	Denaturing Conditions	51
2.5.1.2	Native Conditions	51
2.5.2	Ionisation Source	51
2.5.2.1	ESI	51
2.5.2.2	Nano-ESI	51
2.5.3	FT-ICR Mass Spectrometry	51
2.5.4	Tandem FT-ICR Mass Spectrometry	52
2.5.4.1	CID	52
2.5.4.2	ECD	52
2.5.5	Calibration	53
2.5.6	Data Analysis	53
2.5.6.1	Isotope Modelling and Mass Measurement Error	53
2.5.6.2	Neutral Spectra	53
2.5.6.3	Fragmentation Data	53
2.5.6.4	Trypsin Digest Spectra	54
2.6	X-ray Crystal Structures	54
Chapter 3	Recombinant p53 Core Domain	55
3.1	Introduction	56
3.2	Expression and Purification	57
3.3	Characterisation by FT-ICR Mass Spectrometry	59
3.3.1	Denaturing Conditions	59
3.3.2	Native Conditions	62
3.3.3	Confirmation of Free Cysteine Residues	63
3.4	DNA-Binding Assay	64
3.5	p53 Cysteine Mutants	64
3.6	p53 Cancer Mutant R175H	68

Chapter 4 Identification of Reactive Cysteine Residues	70
4.1 Introduction	71
4.2 Alkylation of p53 Cysteine Residues	72
4.2.1 Concentration Dependence	72
4.2.2 Time Dependence	75
4.2.3 Alkylation at Physiological Temperature	75
4.3 Identification of Reactive Cysteine Residues	77
4.3.1 Top-Down Mass Spectrometry	77
4.3.2 Middle-Down Mass Spectrometry	82
4.3.3 Bottom-Up Mass Spectrometry	91
4.4 Alkylation of p53 Cysteine Mutants	91
4.5 Preferential Alkylation of Cys182 and Cys277	95
4.6 Identification of the Third Site of Alkylation	99
4.7 Disruption of Secondary Structure and Protein Unfolding	103
4.8 Conclusion	105
4.9 Future Work	106
Chapter 5 Oxidation of p53 by Reactive Oxygen Species	108
5.1 Introduction	109
5.2 Air Oxidation	109
5.3 Mixtures of Oxidised and Reduced p53	112
5.4 H ₂ O ₂ Oxidation	112
5.4.1 Disulfide Bond Formation	112
5.4.2 Effect on Protein Structure	115
5.4.3 Labelling of Free Thiol Groups	116
5.5 Affinity Purification of Oxidised p53	119
5.5.1 Methodology	119
5.5.2 Biotinylation	124
5.5.3 Capture	124
5.5.4 Elution	125
5.6 Identification of Oxidised Cysteine Residues	125

5.7	Cysteine Connectivity	130
5.8	Oxidation of Zinc-Binding Cysteines	131
5.9	Trapping of Sulfenic Acid	134
5.10	Oxidation of p53 Cysteine Mutant C182S	135
5.11	Effect of Zn ²⁺ on Oxidation of p53	138
5.12	Effect of GSH on Oxidation of p53	140
5.13	Conclusion	143
5.14	Future Work	144
	References	145
	Appendix A Overview of FT-ICR MS Instrumentation	181
	Appendix B Mass Assignments for Fragment Ions	183
	Appendix C Publications, Course and Conference Attendance	198
	Appendix D Publication Reprints	202

List of Figures

1.1	Univalent reduction of oxygen to water	2
1.2	Deprotonation of cysteine	3
1.3	Domain structure of p53	9
1.4	Primary sequence of human p53	11
1.5	X-ray crystal structure of a p53-DNA complex	12
1.6	Secondary structural elements of p53 core domain	13
1.7	X-ray crystal structure of a p53 core domain highlighting Cys	14
1.8	Mutant p53-reactivating molecules	17
1.9	Principles of bottom-up Mass Spectrometry	22
1.10	Principles of top-down Mass Spectrometry	23
1.11	Principles of middle-down Mass Spectrometry	24
1.12	Schematic of electrospray ionisation	27
1.13	Charge state distributions in a protein ESI spectrum	29
1.14	Cyclotron motion of a positive and negative ion	30
1.15	Schematic of a cylindrical ICR cell	32
1.16	An FT-ICR MS experiment	34
1.17	Simplified overview of FT-ICR MS instrumentation	35
1.18	Fragment ions resulting from dissociation of polypeptide backbone	37
3.1	Ion exchange and gel filtration chromatograms of p53 core domain	58
3.2	Protein gel electrophoresis of p53 core domain	59
3.3	Denatured MS of recombinant p53 core domain	60
3.4	Native MS of recombinant p53 core domain	61
3.5	MS of p53 core domain alkylated with an excess of NEM	63
3.6	DNA-binding assay of p53 by EMSA	65
3.7	Isotope distributions of p53 core domain cysteine mutants	66
3.8	Native MS of p53 core domain cysteine mutants	67
4.1	Alkylation of cysteine by NEM	71
4.2	Reaction of p53 core domain with NEM; titration and time course	73

4.3	Isotope distributions of alkylated forms of p53	74
4.4	Reaction of p53 with NEM at 37°C; titration and time course	76
4.5	CID MS of 2NEM-p53	78
4.6	ECD MS of 2NEM-p53	79
4.7	Fragment map for top-down MS of 2NEM-p53	81
4.8	MS of Lys-C digest of 2NEM-p53	83
4.9	CID MS of dialkylated p53 Lys-C peptide Gln165-Lys291	84
4.10	ECD MS of dialkylated p53 Lys-C peptide Gln165-Lys291	85
4.11	Diagnostic <i>y</i> ion from middle-down MS of 2NEM-p53 _{Lys-C}	87
4.12	Fragment map for middle-down MS of 2NEM-p53	88
4.13	MS of trypsin digest of 2NEM-p53 and sequence coverage	89
4.14	Isotopic distribution and CID MS of alkylated p53 peptide VCACPGR	90
4.15	Reaction of p53C182S with NEM; titration and time course	92
4.16	Reaction of p53C277S with NEM; titration and time course	93
4.17	Reaction of p53C182/277S with NEM; titration and time course	94
4.18	X-ray crystal structure of p53 core domain; surface and buried cysteines	97
4.19	CID MS of 3NEM-p53	100
4.20	Fragment map for top-down MS of 3NEM-p53	102
4.21	Diagnostic <i>b</i> and <i>y</i> ion from top-down MS of 3NEM-p53	103
5.1	Overlapping isotope distributions of air oxidised p53	111
5.2	Isotope distributions of p53 treated with H ₂ O ₂	113
5.3	Charge state distributions of p53 treated with H ₂ O ₂	114
5.4	Oxidation of p53 over time; H ₂ O ₂ treatment and NEM alkylation	117
5.5	Isotope distributions of p53 treated with H ₂ O ₂ and alkylated with NEM	118
5.6	Biotinylation of cysteine with Biotin-HPDP	120
5.7	Method for affinity purification of oxidised p53	121
5.8	MS of oxidised p53 and MS of biotinylated p53	122
5.9	Tolerance of avidin-biotin complex to guanidine	123
5.10	MS of oxidised p53 after affinity enrichment	125
5.11	CID MS of 6NEM-p53	126
5.12	Fragment map for top-down MS of 6NEM-p53	128

5.13	Diagnostic γ ion from top-down MS of 6NEM-p53	129
5.14	X-ray crystal structure of p53 core domain; zinc-binding cysteines	133
5.15	Reaction of cysteine with dimedone	134
5.16	Oxidation of p53C182S over time.	136
5.17	Oxygen incorporation into p53C182S compared to wt p53	137
5.18	H ₂ O ₂ oxidation of p53 in the presence of excess Zn ²⁺	139
5.19	<i>S</i> -glutathionylation of cysteine	140
5.20	H ₂ O ₂ oxidation of p53 in the presence of excess GSH	141
5.21	Isotope distributions of <i>S</i> -glutathionylated p53	142

List of Tables

1.1	Common redox- modifications of cysteine	4
1.2	Examples of redox-regulated proteins and complexes	6
2.1	Primers used in site-directed mutagenesis	44
3.1	Average molecular masses of p53 core domain variants	57
4.1	Permutations of 2NEM-p53 and number of assigned fragment ions	80
4.2	Permutations of 2NEM-p53 _{Lys} -C and number of assigned fragment ions	86
4.3	Solvent accessibility of p53 thiol groups	96
4.4	Permutations of 3NEM-p53 and number of assigned fragment ions	101
5.1	Permutations of 6NEM-p53 and number of assigned fragment ions	127
5.2	Monoisotopic masses of cross-linked p53 tryptic peptides	130

Glossary

15d-PGJ ₂	15-deoxy- $\Delta^{12,14}$ -prostaglandin J ₂
2-YT	2 x yeast tryptone
a.a.	Amino acid(s)
A _{280nm}	Absorbance measured at 280 nm
AI	Activated-ion
AMT	Accurate mass and time tag
<i>apo</i> -p53	Zn ²⁺ -free p53
BCA	Bicinchoninic acid
Biotin-HPDP	N-[6-(Biotinamido)hexyl]-3'-(2'-pyridyldithio) propionamide
BIRD	Blackbody infrared dissociation
BNPS-skatole	3-bromo-3-methyl-2-(<i>o</i> -nitrophenylsulfenyl)indolenine
CID	Collision-induced dissociation
CT	p53 C-terminal regulatory domain
Dimedone	5,5-dimethyl-1,3-cyclohexanedione
DNA	Deoxyribonucleic acid
DsbA	Disulfide bond isomerase A
DTT	1,4-dithiothreitol
<i>E. coli</i>	<i>Escherichia coli</i>
ECD	Electron capture dissociation
EDTA	Ethylenediaminetetraacetic acid
ELISA	Enzyme-linked immunosorbent assay
EMSA	Electrophoretic mobility shift assay
ESI	Electrospray ionisation
EtBr	Ethidium bromide
ETD	Electron transfer dissociation
FPLC	Fast protein liquid chromatography
FT-ICR	Fourier transform ion cyclotron resonance
FWHM	Full width at half maximum
GPX1	Glutathione peroxidase-1

GRX	Glutaredoxin
GSH	Glutathione
GSSG	Glutathione disulfide
HEPES	4-(2-hydroxyethyl)-1-piperazineethanesulfonic acid
<i>holo</i> -p53	Zn ²⁺ -bound p53
HPLC	High performance liquid chromatography
HSA	Human serum albumin
Hsp33	Heat shock protein 33
IPTG	Isopropyl β-D-thiogalactoside
IRMPD	Infrared multiphoton dissociation
LB	Luria Bertani
LC	Liquid chromatography
MALDI	Matrix-assisted laser desorption/ionisation
MeOH	Methanol
MES	2-(<i>N</i> -morpholino)ethanesulfonic acid
MGMT	O(6)-methylguanine-DNA methyltransferase
MME	Mass measurement error
MQ	Methylene quinuclidinone
MRM	Multiple reaction monitoring
mRNA	Messenger ribonucleic acid
MS	Mass spectrometry
MS/MS	Tandem mass spectrometry
Msr	Methionine sulfoxide reductase
MWCO	Molecular weight cut off
NADPH	Reduced form of nicotinamide adenine dinucleotide phosphate
NEM	<i>N</i> -ethylmaleimide
nESI	Nano-electrospray ionisation
NF-κB	Nuclear factor κB
NMR	Nuclear magnetic resonance
<i>n</i> NEM-p53	p53 modified with <i>n</i> NEM groups
NQO1	Quinone oxidoreductase

OD _{600nm}	Optical density measured at 600 nm
p53 _{Lys-C}	p53 peptide Gln165 – Lys291
PAGE	Polyacrylamide gel electrophoresis
PAR	4-(2-pyridylazo) resorcinol
PDB	Protein data bank
PKC	Protein kinase C
Poly[dI-dC]	poly(deoxyinosinic-deoxycytidylic) acid
POX	Proline oxidase
PRR	Proline-rich region
psi	Pounds per square inch
PTEN	Phosphatase and tensin homolog
PTM	Post-translational modification
PTP	Protein tyrosine phosphatase
Ref-1	Redox factor 1
RNS	Reactive nitrogen species
ROS	Reactive oxygen species
rpm	Revolutions per minute
SDS	Sodium dodecyl sulfate
SeMet	Selenomethionine
SESN1	Mammalian sestrin homologue
SOC	Super optimal broth with catabolite repression
SOD	Superoxide dismutase
TAD	p53 N-terminal transactivation domain
TAE	Tris-acetate-EDTA
TCA	Trichloroacetic acid
TET	p53 tetramerization domain
TNB	thionitrobenzoate
TOF	Time-of-flight
Trx	Thioredoxin
UV	Ultraviolet
wt	Wild type

Chapter 1: Introduction

1.1 Biological Redox Signalling

1.1.1 Reactive Oxygen Species as Signalling Molecules

Reactive oxygen species (ROS) is a collective term used to describe derivatives of molecular oxygen (O_2), excluding water, that are encountered by biological systems. They include the free radicals superoxide ($O_2^{\bullet-}$), hydroxyl (HO^{\bullet}) and singlet oxygen ($^1O_2^*$), in addition to non-radicals such as hydrogen peroxide (H_2O_2), hypochlorite (OCl^-) and ozone (O_3) [1-6]. Aerobic organisms are continuously exposed to ROS as they are generated as products or by-products from a vast array of cellular processes. For example, it is estimated that 1-3% of O_2 reduced in the mitochondrial electron transport chain forms $O_2^{\bullet-}$, which is further reduced to H_2O_2 by the antioxidant enzyme superoxide dismutase (SOD) [2]. Hydrogen peroxide can be decomposed to water and O_2 by peroxidase enzymes or undergo Fenton chemistry (iron-catalysed oxygen free radical reactions) to form the hydroxyl radical [2, 7]. Figure 1.1 shows the ROS that arise along the univalent reduction pathway of O_2 to water.

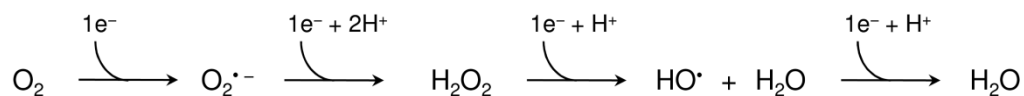


Figure 1.1 The univalent reduction pathway of oxygen to water.

ROS are traditionally associated with disease, dysfunction and ageing, owing to their increased reactivity relative to O_2 and their propensity to indiscriminately oxidise biomolecules including lipids, proteins, and nucleic acids. Indeed, hyper-physiological levels of ROS cause cellular damage and are implicated in numerous pathological conditions such as Alzheimer's disease, cancer, coronary artery disease and diabetes [8-11]. However, it is now clear that the cellular role of ROS is not exclusively detrimental, and there is a large body of evidence supporting a role for ROS in biological signal transduction [2, 12-15]. ROS are now known to partake in well-defined, highly-specific protein oxidation reactions that mediate specific physiological responses by regulating protein function. The action of ROS as messengers in biological systems is known as redox-signalling, and relies on the

distinct preferences of ROS for different cellular targets as a result of their intrinsic chemical properties.[†] For example, $O_2^{\bullet -}$ is known to preferentially react with iron-sulfur ([Fe-S]) clusters due to a high electrostatic attraction, whereas H_2O_2 , which is uncharged, displays a preference for the sulfur-containing amino acids methionine and cysteine [4, 5, 16, 17].

1.1.2 The Chemistry of Cysteine

The thiol group ($-SH$) of cysteine can be deprotonated to form the thiolate anion ($-S^-$; see Figure 1.2), which is the most powerful nucleophile among proteinogenic amino acid side chains [18]. This property qualifies cysteine as an oxidizable target in ROS-mediated redox-signalling. The pK_a of the thiol proton in free cysteine is 8.3.

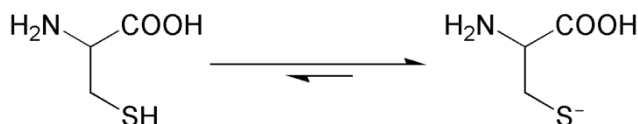


Figure 1.2 Depending on the surrounding protein environment, the amino acid cysteine is deprotonated to form the thiolate anion (S^-) at physiological pH.

However, this can vary dramatically depending on the surrounding environment within a protein [19]. For example, the pK_a of the catalytic cysteine in disulfide bond isomerase A (DsbA) is lowered to 3.5 due to stabilisation of the resulting thiolate by a nearby cationic histidine residue [20]. Variation in cysteine thiol pK_a 's is reflected in the wide range of rate constants measured for their reaction with H_2O_2 (10 - $10^6 M^{-1} s^{-1}$) [5] and provides the basis for selectivity in cysteine-based redox-signalling mechanisms [4, 12, 16, 17].

Unlike oxygen, sulfur is able to exist in multiple oxidation states, from -2 to $+6$, owing to its position in the second row of the periodic table and the availability of

[†]Reactive nitrogen species (RNS) such as nitric oxide (NO^\bullet) and peroxynitrite ($ONOO^-$) are also involved in redox-signalling. However, they will not be discussed further here.

Table 1.1 Common redox-modifications of cysteine. The oxidation state of the cysteine sulfur atom is stated.

Name	Structure	Oxidation State
Thiol	Cys-S-H	-2
Disulfide	Cys-S-S-R	-1
Thioether	Cys-S-R	-2
Sulfenic acid	Cys-S-OH	0
Sulfinic acid	Cys-S(O)-OH	+2
Sulfonic acid	Cys-S(O) ₂ -OH	+4
Sulfenamide	Cys-S-N-R ₂	0
S-nitrosothiol	Cys-S-N=O	-2
Thiosulfinate	Cys-S(O)-S-R	+1
Thiyl radical	Cys-S [•]	-1

d orbitals [14, 21]. Hence, a multitude of cysteine redox-modifications have been confirmed or postulated to exist *in vivo*, some of which are shown in Table 1.1.

Nucleophilic attack of the O–O bond in hydrogen peroxide by the Cys thiolate leads to release of H₂O and the formation of a sulfenic acid (–SOH). Sulfenic acids are typically unstable and represent a cross-road in the H₂O₂-mediated oxidation mechanism of cysteine; they can condense with a nearby Cys residue to form an intra or intermolecular disulfide bond, condense with a low molecular weight thiol such as glutathione (GSH) to form a mixed disulfide, be further oxidised by H₂O₂ to form sulfinic or sulfonic acids (–SO₂H and –SO₃H respectively) or react with a proximal nitrogen to form a sulfenamide (–S–N–) (this list is by no means exhaustive and other reaction pathways, e.g. with RNS, also occur) [5, 12, 14, 17].

In order to be effective in redox-signalling, cysteine redox-modifications must be reversible under physiological conditions – allowing specific cysteines residues to act as molecular switches. Sulfenic acids are reduced to disulfide bonds by cysteine thiolates (as described above) and disulfide bonds are reduced back to thiol groups either by thioredoxin (Trx) or glutaredoxin (GRX), which themselves are reduced by NADPH-dependent Trx- and glutathione reductases [2, 5]. Sulfinic acids were thought to be an irreversible product of cysteine over-oxidation. However, a class of

enzymes, sulfiredoxins, was recently discovered which reduce sulfinic acids *in vivo*, indicating that they may take part in redox-signalling mechanisms [22].

Methionine also participates in biological redox-chemistry, illustrated by the existence of enzymes dedicated to the reduction of oxidised forms of the amino acid such as methionine sulfoxide reductases (Msr). The oxidation of methionine in proteins to methionine sulfoxide ($R_2S=O$) has known physiological roles [14, 18, 23]. However, the redox-chemistry of the thioether group (R-S-R) of methionine is far less extensive than for the thiol group of cysteine, and methionine will be not be elaborated on further here.

The oxidation state of cysteine (or methionine) can regulate protein function in the same way as any other post-translational modification (PTM) i.e. by promoting or inhibiting a protein-substrate interaction; for example, by blocking the catalytic site of an enzyme. Examples of redox-regulated proteins are discussed below.

1.1.3 Redox-Regulated Proteins

A growing number of prokaryotic and eukaryotic proteins are now known to have their function controlled via specific redox-reactions occurring on critical cysteine residues. Table 1.2 lists some examples of redox-regulated proteins from different protein classes and the effect that specific Cys-oxidation states have on their activity. The importance of ROS-mediated redox-signalling has only become evident over the past decade. Hence, the field is still in its infancy and the significance of oxidation *in vivo* for many of the proteins listed remains to be determined.

In the case of the redox-regulated mammalian protein complex NRF2/KEAP1, the physiological response to oxidation is well characterised yet the exact oxidative-modifications that modulate the activity of this complex are not well defined. NRF2 is an important transcription factor that regulates the expression of detoxification enzymes in response to oxidant and xenobiotic stresses. Under non-stress conditions, NRF2 is prevented from nuclear localisation by the multiple Cys-containing protein KEAP1. NRF2 binds to the KEAP1 homodimer via two binding sites with amino acid (a.a.) sequences DLG and ETGE. This mode of binding facilitates ubiquitination

Table 1.2 Examples of redox-regulated proteins and complexes. Adapted from Ref. [12].

	Protein/Complex	Cys Redox-State [†]	Effect	Ref.
Phosphatases	Cdc25	S–S; SOH	Inactivates	[24]
	LMW-PTPs	S–S; SOH	Inactivates	[25]
	PTEN	S–S; SOH	Inactivates	[26]
	PTP1B	S–S; SOH; S–N	Inactivates	[27]
	PTP2 α	S–S; SOH; S–N	Inactivates	[28]
	SHP-1/SHP-2	S–S; SOH	Inactivates	[29]
Kinases	ASK1	S–S	Initiates oligomerization/activates	[30]
	PKA RI	S–S	Activates	[31]
	PKG-1 α	S–S	Enhances affinity for substrates	[32]
	Src tyrosine kinase	S–S	Activates/inactivates	[33]
	Sty1/Tpx1	S–S	Activates	[34]
Transcription Factors	AP-1 (Fos/Jun)	S–S	Inhibits DNA-binding	[35]
	FoxO4/p300/CBP	S–S	Acetylates/inactivates	[36]
	Hsf1	S–S	Activates	[37]
	Nrf-2/Keap-1	S–S	Enhances Nrf-2 stability	[38]
	OhrR	S–S; SOH	Inhibits DNA-binding	[39]
	OxyR	S–S; SOH	Activates	[40]
	SarZ	S–S; SOH	Inhibits DNA-binding	[41]
	Yap1/Gpx3	S–S; SOH	Activates	[42]
Other	DJ-1	SO ₂ H	Locates to mitochondria	[43]
	GDE2	S–S	Inactivates	[44]
	HDAC4/DnaJb5	S–S	Inhibits complex formation	[45]
	Hsp33	S–S	Activates	[46]
	MMP-7	SO ₂ H	Activates	[47]

[†]S–S intra or intermolecular disulfide bond; SOH sulfenic acid; S–N sulfenamide; SO₂H sulfinic acid.

of NRF2, which targets the protein for proteosomal degradation. In the presence of H₂O₂, cysteine residues in KEAP1 are oxidised, inducing a conformational change which results in decreased affinity for NRF2 at the DLG site, thus allowing a third protein, p21, to bind to this motif. Binding of p21 prevents the ubiquitination and subsequent degradation of NRF2, therefore allowing accumulation in the nucleus and transactivation of target genes [5, 12, 38]. KEAP1 is a zinc-binding protein and it has been suggested that KEAP1 sensing of NRF2 inducers involves zinc-binding cysteine residues [48]. However, this remains to be tested.

Contrary to the commonly held view that Zn^{2+} protects thiol groups from oxidation, many protein zinc-binding centres have been recognised to serve in a redox-activating capacity, by increasing the reactivity of the cysteine thiol towards ROS. Zn^{2+} is a Lewis acid, therefore it lowers the pK_a of the coordinating thiol, potentially modifying its reactivity. Furthermore, as Zn^{2+} is redox-inert, redox chemistry occurring at the zinc-binding domain will be ligand-centred (i.e. on the thiol) rather than metal-centred (as observed with [Fe-S] clusters) [5, 49, 50]. Oxidation of zinc-binding Cys residues leads to release of the metal ion, possibly accompanied by a conformational change. Conversely, reduction of oxidised Cys residues can facilitate binding of Zn^{2+} , thus forming a basis for the link between intracellular redox-state and zinc homeostasis [51, 52].

Heat shock protein 33 (Hsp33), protein kinase C (PKC or PKA RI) and the anti-sigma factor RsrA are among an increasing number of proteins confirmed to contain a ‘zinc-redox switch’ [49, 50, 53, 54]. Hsp33 is a bacterial molecular chaperone that contains 6 Cys residues. In its monomeric inactive form, 4 of these cysteines are involved in the tetrahedral coordination of a Zn^{2+} ion. Upon a combination of heat and oxidative stress (i.e. elevated levels of ROS), the zinc-binding Cys residues are oxidised to form two intramolecular disulfide bonds and Zn^{2+} is released, resulting in unfolding of the C-terminal domain and the subsequent formation of active Hsp33 dimers [46]. Disulfide bonds are commonly believed to be stabilising features which promote protein folding [55]. However, Hsp33 presents a novel facet of disulfide bond formation whereby they can cause destabilisation of protein structure and induce protein unfolding.

The recent substantiation that the tumour-suppressor PTEN (phosphatase and tensin homolog) can be used as a biomarker for predicting the sensitivity of cancer patients to trastuzumab (trade name Herceptin) treatment has generated increased interest in this protein [56]. PTEN is a protein tyrosine phosphatase (PTP) that serves as a tumour-suppressor by inhibiting phosphoinositide 3-kinase (PI3K)-dependent activation of the anti-apoptotic protein AKT. PTEN contains 10 cysteine residues and, analogous to other PTPs, its catalytic activity is inhibited via oxidation of the active site cysteine residue (Cys124) [26, 57]. The increased levels of ROS

associated with many pathological conditions, such as chronic inflammation, may undesirably inactivate PTEN, thereby allowing cells to avoid apoptosis and possibly result in the onset of tumourigenesis [57]. Glutathione has recently been shown to be involved in the reduction of Cys124 *in vivo* [58]. The role of the remaining PTEN Cys residues is as of yet unknown.

Oxidative-modification of Cys residues is also known to play an important role in regulating the activity of the tumour-suppressor protein p53.

1.2 Tumour-Suppressor Protein p53

1.2.1 Introduction

p53 is a transcription factor best known for its key role in mediating cell cycle arrest, apoptosis or senescence in response to numerous different forms of cellular stress [59, 60]. Since its discovery in 1979, p53 has been the subject of intense research due to its clear role as a potent tumour-suppressor in humans and mammals [61, 62]. Ref. [63] provides an excellent account of the first 30 years of p53 research.

p53 serves as a tumour-suppressor by protecting the integrity of the genome thereby preventing the proliferation of potentially cancerous cells. For example, DNA-damage upon UV radiation results in activation of p53 and cell cycle arrest in the G₁ phase followed by induction of DNA-repair mechanisms. If the damage is repaired, the cell is allowed to re-enter the cell cycle. However, if the damage cannot be repaired, p53 mediated-apoptosis ensues, thereby eliminating a potentially cancerous cell and preventing the development of a tumour [64, 65]. The importance of p53 is illustrated by the fact that loss or mutation of the p53 gene (*TP53*) is strongly associated with an increased susceptibility to cancer. Around half of all human cancers contain a mutated form of this protein [63, 66-68].

In addition to the well established roles mentioned above, p53 has also been implicated in the regulation of many other cellular processes including glycolysis, autophagy, angiogenesis, oxidative stress and differentiation [69, 70]. Furthermore, p53 has recently been shown to exert a pro-apoptotic effect independent of its transcriptional activity [71]. Despite over three decades of extensive research,

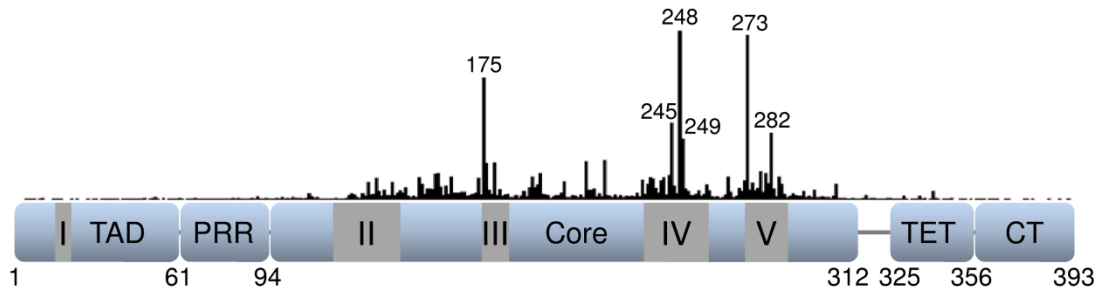


Figure 1.3 Domain structure of human p53 consisting of an N-terminal transactivation domain (TAD), a proline-rich region (PRR), a DNA-binding core domain (Core) and a C-terminal tetramerization (TET) and regulatory (CT) domain. The five regions of the p53 gene that highly conserved across species are shown (I-V). The histogram indicates the position and relative frequency of tumour-derived mutations. The six 'hot-spot' mutations are annotated. Figure adapted from Refs. [72] and [73].

relatively little is known about the specific molecular mechanisms that allow p53 to discriminate between its different functions, and there is particular current interest in determining how p53 differentially activates expression of its target genes [74]. The major drive for understanding the molecular details of the regulatory-mechanisms that control p53 activity is the rational design or identification of effective chemotherapeutics that are able to induce the pro-apoptotic activity of both wild type (wt) and mutant forms of p53 [70, 75-77].

1.2.2 Domain Structure of p53

p53 is active as a homo-tetramer. Each monomer of human p53 consists of 393 amino acids (UniProt accession no. P04637) that can be divided into five structural domains, each with their own individual function. p53 also contains five regions, termed 'BOXES', that are highly conserved across species. Figure 1.3 illustrates the different functional domains of monomeric p53 along with the five highly conserved regions (I-V). The position and relative frequency of tumour-derived mutations are also shown, according to the most recent version (R14; November 2009; N=22416) of the International Agency for Research on Cancer (IARC) TP53 mutation database (<http://www-p53.iarc.fr>) [78]. The primary sequence of human p53 is shown in

Figure 1.4. BOXES I-V constitute amino acids 13-19, 117-142, 171-181, 234-258 and 270-286 respectively [79].

The N-terminal region of p53 is natively unfolded[‡] and contains an acidic transactivation domain (TAD; a.a. 1-61) and a proline-rich region (PRR; a.a. 61-94). The TAD is the binding site for numerous interacting proteins such as p53's negative regulator, MDM2, or components of the transcription machinery. The exact role for the proline-rich region is poorly understood, though it may play a role in mediating protein-protein interactions. The p53 core domain (a.a. 94-312) comprises a compact, folded structure and is responsible for the specific DNA-binding activity of p53. The C-terminal region contains a structured tetramerization domain (TET; a.a. 325-356) that regulates the oligomerization of p53, and a natively unfolded regulatory domain (CT; a.a. 356-393) that is known to regulate protein function and protein levels via extensive post-translational modification. The CT also binds to DNA non-specifically [72, 73].

The structure of individual domains of p53 have been well characterised by both NMR spectroscopy and X-ray crystallography [73]. However, a solution or crystal structure of wild type full length p53 remains to be solved due to its size (which is too large for protein NMR spectroscopy) and its regions of unfolded structure (which hinder crystallisation).

1.2.3 p53 Core Domain

The p53 core domain is the site of four of the five highly conserved regions and contains over 95% of the tumour-derived mutations (according to the iarc mutation database), including the six most frequently mutated residues, known as 'hot-spots', observed in human cancers (R175, G245, R248, R249, R273 and R282) [66, 68, 78]. The primary sequence of the p53 core domain is displayed in Figure 1.4. As previously mentioned, this central portion of p53 is folded and is responsible for the specific DNA-binding activity of p53 [81].

[‡]Natively unfolded proteins lack ordered structure under physiological conditions. They typically undergo transition to a folded form upon binding to their target substrates [80].

```

      10      20      30      40
MEEPQSDPSV EPPLSQETF S DLWKLLPENN VLSPLPSQAM
      50      60      70      80
DDLMLSPDDI EQWFTEDPGP DEAPRMPEAA PPVAPAPAAP
      90     100     110     120
TPAAPAPAPS WPLSSSVPSQ KTYQGSYGFR LGFLHSGTAK
     130     140     150     160
SVTCTYSPAL NKMFCQLAKT CPVQLWVDST PPPGTRVRAM
     170     180     190     200
AIYKQSQHMT EVVRRCPHHE RCSDSDGLAP PQHLIRVEGN
     210     220     230     240
LRVEYLDDRN TFRHSVVVPY EPPEVGSDCT TIHYNYMCNS
     250     260     270     280
SCMGGMNRRP ILTIITLED S SGNLLGRNSF EVRVCACPGR
     290     300     310     320
DRRTEENLR KKGEPHHELP PGSTKRALPN NTSSSPQPKK
     330     340     350     360
KPLDGEYFTL QIRGRERFEM FRELNEALEL KDAQAGKEPG
     370     380     390
GSRAHSSHLK SKKGQSTRH KKLMFKTEGP DSD

```

Figure 1.4 The primary sequence of human full-length p53 (UniProt accession no. P04637). The core domain (a.a. 94-312) is highlighted in black, the 10 cysteine residues (Cys124, 135, 141, 176, 182, 229, 238, 242, 275 and 277) are highlighted in bold and the zinc-binding residues (Cys176, 238 and 242 and His179) are highlighted in red.

The promoter region of p53 responsive-genes contains two copies of the double-stranded palindromic sequence 5'-PuPuPuC(A/T)(A/T)GPyPyPy-3' (where Pu is a purine base, A or G, and Py is a pyrimidine base, C or T) which may be separated by up to 13 base pairs [60]. p53 binds to consensus DNA as a tetramer structured in the form of a dimer of dimers (via the oligomerization domain), with each dimer binding to one copy of the consensus sequence [73, 82, 83]. The X-ray crystal structure of monomeric p53 core domain specifically bound to a consensus DNA sequence was first reported in 1994 (PDB ID 1TUP), and revealed that the a.a. residues most frequently mutated in cancer are at, or near to, the protein-DNA interface [72]. Conversely, residues infrequently mutated are generally located far away from the DNA. This observation confirmed the importance of the specific DNA-binding function of p53 for its tumour-suppressor activity. A plethora of crystal structures of

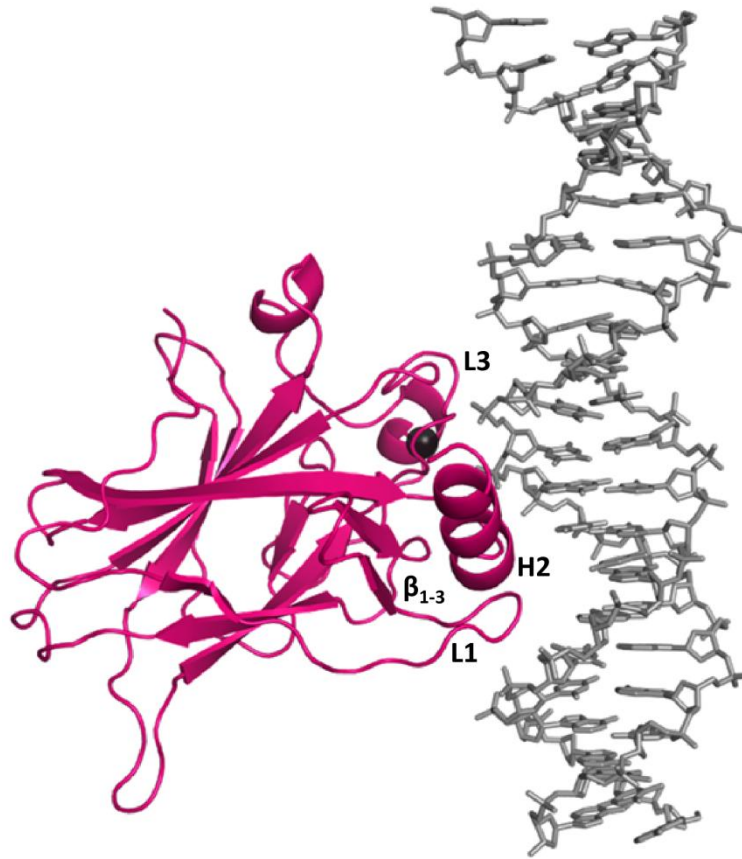


Figure 1.5 X-ray crystal structure (PDB ID 1TUP) of p53 core domain in complex with consensus DNA [72]. The loop-sheet-helix motif (L1- β 1-3-H2) interacts with the major groove of DNA whilst the L3 loop (L3) interacts with the minor groove. The Zn²⁺ ion is shown in black. The L1- β 1-3-H2 motif and L3 contain some of the most frequently mutated residues in human cancer.

p53 core domain have since been solved [73]. These include wild-type and mutant p53 in the absence of DNA [84, 85], p53 from different species [82] and p53 in complex with different target DNA [86] or bound to domains of target proteins [87].

The X-ray crystal structure of wild-type p53 core domain bound to a consensus DNA sequence is shown in Figure 1.5. The main structural feature of the p53 core domain is a β -sandwich which is composed of two anti-parallel β -sheets. The stabilising β -sandwich acts as a scaffold for the less rigid structures that comprise the DNA-binding surface. Namely, a loop- β -sheet- α -helix motif and two large loops

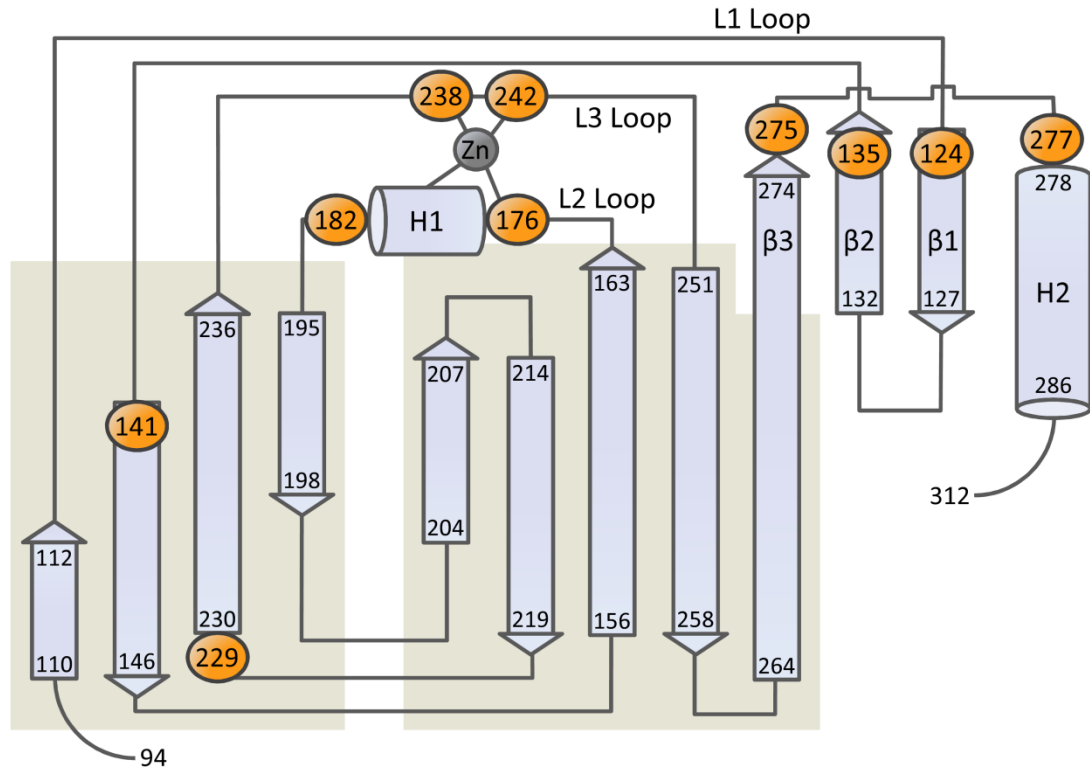


Figure 1.6 Topological diagram of the secondary structural elements of p53 core domain. The boundaries of the two anti-parallel β -sheets that make up the β -sandwich are highlighted in grey and the components of the DNA-binding surface (L1-L3, β 1- β 3 and H2) are labelled. The locations of the 10 Cys residues are shown in orange. Figure adapted from Ref. [72].

(L2 and L3; a.a. 163-195 and 237-250 respectively) which are held together by a tetrahedrally coordinated Zn^{2+} ion. A topological diagram of the structural elements that make up the core domain is shown in Figure 1.6 (along with the positions of p53 cysteine residues, which are addressed below). The loop-sheet-helix motif is comprised of loop L1 (112-124), the H2 helix (278-286) and a short three-stranded β -sheet (β_{1-3} ; 124-127, 132-135 and 270-274). Residues from this motif, including the second most frequently mutated residues in human cancer, Arg273, interact with the major groove of DNA. The most frequently mutated residue, Arg248, is located in the L3 loop and is responsible for the interaction of p53 with the minor groove of DNA [72]. Crystal structures of p53 core domain in the absence of DNA have very similar overall structures to that of DNA-bound protein, suggesting that a significant conformational change does not occur upon DNA-binding [72, 85].

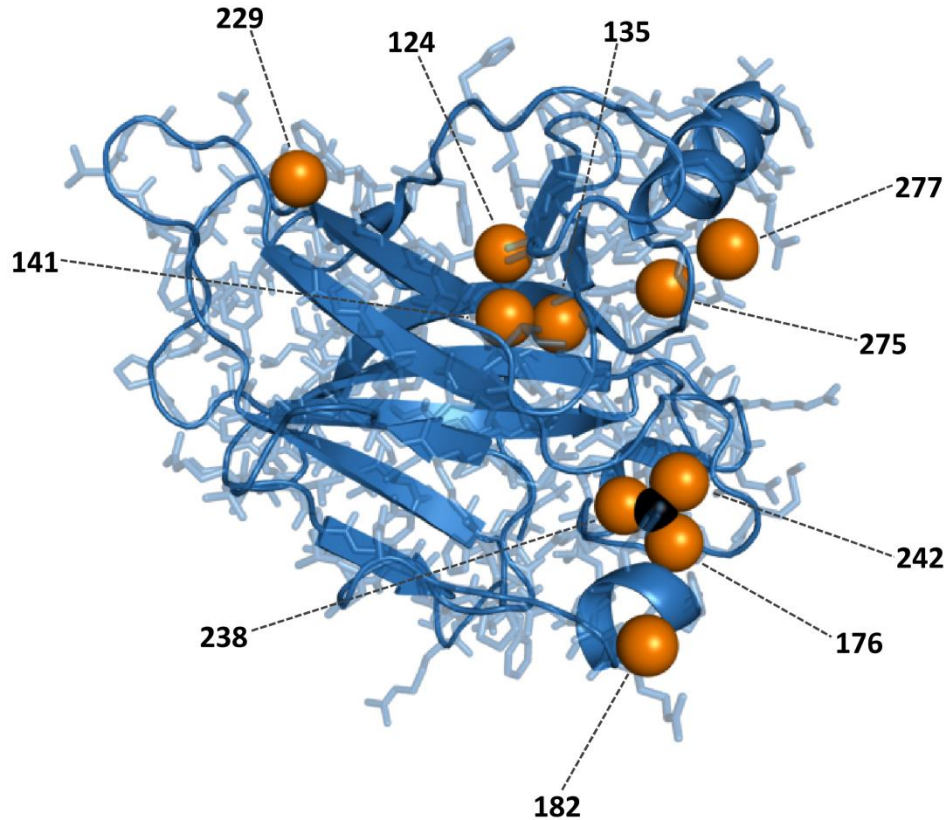


Figure 1.7 X-ray crystal structure (PDB ID 1TUP) of p53 core domain [72]. The sulfur atoms of the ten Cys residues are labelled and shown in orange. The Zn^{2+} ion is shown in black.

Analogous to many other transcription factors, the DNA-binding domain of p53 contains a non-covalently bound Zn^{2+} ion [88]. The co-ordinating ligands are the thiol groups of three cysteine residues (Cys176, 238 and 242) and a nitrogen of one histidine residue (His179) [72]. Several studies have shown that Zn^{2+} plays a critical structural role and is necessary for the specific DNA-binding function of p53 [89-91]. Removal of the metal ion causes p53 to adopt a ‘mutant-like’ conformation (recognised by the monoclonal antibody PAb240, specific for unfolded, mutant p53) which displays decreased ability to bind to consensus DNA [89, 90].

Human p53 contains 10 cysteine residues (Cys124, 135, 141, 176, 182, 229, 238, 242, 275 and 277), all of which are contained within the core domain. Nine of the Cys residues are highly conserved across mammalian species (all but Cys299) [79] and three are involved in coordination of a Zn^{2+} ion. Figure 1.6 shows their position

relative to the secondary structural elements of p53 and Figure 1.7 shows the sulfur atoms of each of the Cys residues in the crystal structure of p53 [85]. Mounting evidence suggests that p53 cysteine residues play a fundamental role in regulating the activity of this important tumour-suppressor protein.

1.2.4 Evidence for p53 Redox-Regulation

Redox-modification of p53 thiol groups was first suggested as a potential mechanism to regulate the transcriptional activity of p53 in 1993, when Hupp *et al.* found that treatment of recombinant p53 with thiol-alkylating and oxidising agents inhibited specific DNA-binding [92]. Over the following years, several investigations demonstrated the effect of cysteine alkylation, oxidation or mutation on the specific DNA-binding activity of p53 [93-99]. It was generally found by electromobility shift assays (EMSA) that modification of p53 Cys residues disrupted the specific interaction between p53 and consensus DNA. The ability of oxidised p53 to bind to DNA in a non-specific manner was, however, retained [96]. In the case of p53 treated with oxidising agents, disulfide bond reducing agents were able to restore the specific DNA-binding activity of p53.

In contrast to previous results, Buzek *et al.* later discovered that p53 oxidation does not universally disrupt specific p53-DNA binding [100]. They found that oxidised p53 differentially binds to DNA depending on the consensus sequence. Site-directed mutagenesis revealed that the redox-state of Cys277 directly altered the affinity of p53 for its target genes; oxidation decreased the affinity for the GADD45 response element (involved in DNA-repair) yet had no apparent effect on binding of p53 to the p21 response element (involved in cell-cycle arrest). These results suggest that redox-regulation of p53 plays an important role in differential gene recognition in DNA-damaged cells.

Additional evidence suggesting a regulatory role for p53 cysteine residues is the occurrence of endogenous oxidised Cys residues *in vivo*, in both stressed and unstressed cells [99, 101-103]. However, only one study to date, by Held *et al.*, has specifically and unambiguously identified an oxidised p53 Cys residue *in vivo* (discussed below) [103].

Interestingly, intracellular levels of hydrogen peroxide are known to be linked to p53 activity (see Chapter 5 for further details) [104-106]. Furthermore, proteins that are responsible for modulating Cys-redox state, such as thioredoxin (Trx) and Redox factor 1 (Ref-1), are known to participate in the regulation of p53 activity [107-111]. Both Trx and Ref-1 have been shown to activate the transcriptional activity of p53 *in vivo* [107, 108]. However, the exact mechanisms by which Trx and Ref-1 control p53 function are not fully understood. Trx and Ref-1 also regulate the DNA-binding activity of numerous other cysteine-containing transcription factors, including nuclear factor- κ B (NF- κ B), and Fos/Jun (AP-1) [112, 113].

Shortly after Buzek *et al.* described a role for Cys277 in discriminating between genes involved in DNA-repair and cell cycle arrest, Seo *et al.* reported that selenomethionine (SeMet; a major dietary source of selenium with anti-cancer properties) activated p53-dependent DNA-repair via a DNA damage-independent pathway [102]. DNA-repair was shown to be activated by a Ref-1-dependent redox-mechanism involving reduction of p53 cysteine residues. Using a C-terminal peptide containing only Cys residues 275 and 277, Seo *et al.* demonstrated that these two residues are possible substrates for SeMet-mediated reduction. This was achieved by labelling the free thiol groups (-SH) with biotin and measuring the degree of biotinylation before and after SeMet treatment by Western blot. However, it is unknown if the remaining cysteines are a target for SeMet-mediated redox-modification. It has since been postulated that the redox-state of Cys277 serves as a switch to activate the DNA-repair machinery [65].

Published studies regarding redox-states of p53 cysteine residues and their role in regulating p53 activity represent an extremely minor proportion of p53 research reported over the past three decades. However, the recent discovery of small electrophilic compounds that covalently bind to thiol groups and reactivate mutant forms of the protein *in vivo*, leading to the death of tumour cells, is most notably responsible for awakening p53 researchers to the importance of cysteine residues in regulating p53 function [114-117]. Figure 1.8 shows a selection of compounds that have been shown to restore the specific DNA-binding function of tumour-derived

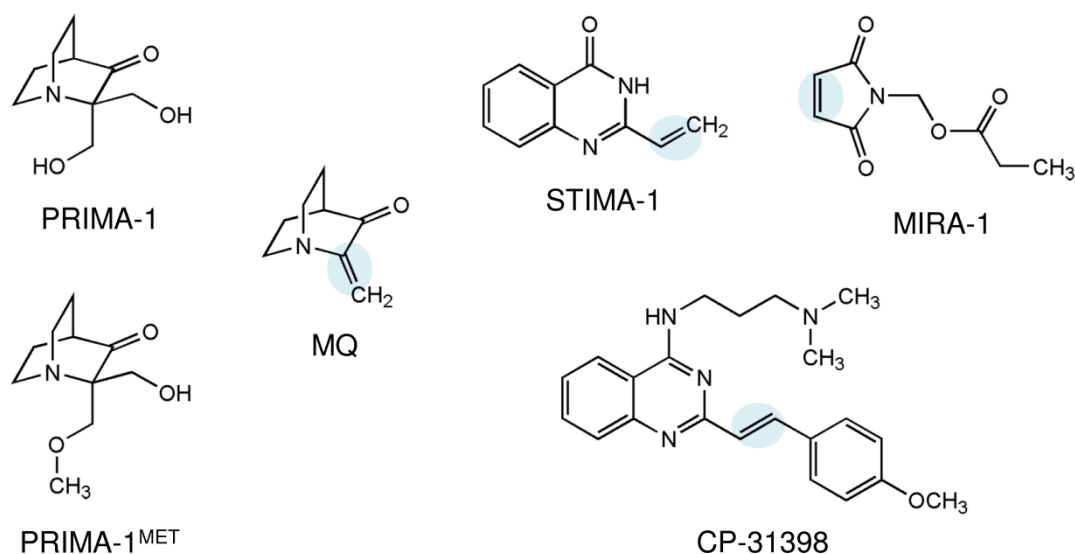


Figure 1.8 Mutant p53-reactivating molecules. Electrophilic C=C double bonds which react with nucleophilic thiol groups are indicated. PRIMA-1 and PRIMA-1^{MET} do not contain a reactive C=C bond. However, a common decomposition product of these molecules, methylene quinuclidinone (MQ), contains this functional group.

p53 mutants (and misfolded wild-type p53) *in vivo*, thereby inducing up-regulation of pro-apoptotic p53 target genes and subsequent cell death [115-117]. PRIMA-1 and PRIMA-1^{MET} themselves do not reactivate mutant p53, but a decomposition product of these compounds, methylene quinuclidinone (MQ), is the active molecule. The mutant-reactivating compounds share a common feature; an electrophilic double bond able to react with nucleophilic thiol groups. MQ was recently confirmed to covalently bind to p53 cysteine residues by mass spectrometry [117]. However, the specific Cys residues that are targeted by MQ (or indeed any of the Cys-targeting anti-tumour molecules) and the exact molecular mechanism of mutant p53 reactivation upon thiol modification is unknown. PRIMA-1^{MET} is currently undergoing clinical trial [77]. Conventional anti-cancer drugs, such as cisplatin, generally have little effect on tumour cells harbouring wild-type p53. Hence, the development of novel mutant p53-reactivating drugs should have a major impact on the treatment of cancer [77, 118].

Three studies explicitly regarding investigation of p53 Cys-modifications have been published within the past year [103, 119, 120]. Kim *et al.* used site-directed

mutagenesis to show that an electrophilic cyclopentenone prostaglandin[§], 15-deoxy- $\Delta^{12,14}$ -prostaglandin J₂, (15d-PGJ₂), binds to Cys277 *in vivo*, leading to an increase in its stability and reduction of its transcriptional activity [119]. Intriguingly, 15d-PGJ₂ has previously been shown to induce p53-mediated apoptosis [122]. Held *et al.* described a highly sensitive mass spectrometry based approach used to quantify oxidised cysteine residues in p53 *in vivo* [103]. From the eight Cys residues that they were able to detect, they found Cys182 to be the most susceptible to diamide oxidation. During the preparation of this thesis, Kaar *et al.* reported the use of various techniques, including mass spectrometry (MS) and X-ray crystallography, to investigate the binding and stabilisation of mutant p53 by cysteine-targeting electrophilic compounds identified from a chemical library [120]. The electron density in the crystal structure was insufficient to model unambiguously the Cys-modifications. Also, the orders of cysteine reactivity, as determined from MS and crystallography, were found to be inconsistent and are discussed further in Chapter 4.5.

1.3 Analysis of Multiple Cys-Containing Proteins

It is clear that redox-modification of cysteine residues participates in functional control of the important tumour-suppressor protein p53. Several investigations have implicated specific Cys residues in p53 redox-regulation, most notably Cys277. However, no single study has provided unambiguous site-specific information on each of the 10 Cys residues in p53. This is partly due to the lack of experimental tools that allow unambiguous identification and localisation of protein post-translational modifications. As a result, unravelling the molecular details of p53 redox-regulation - and indeed the regulatory mechanisms of many other multiple Cys-containing proteins - is generally proving to be a challenging and onerous process.

The nucleophilic nature of thiol groups can be exploited in the study of cysteine-containing proteins and a variety of chemical derivatising reagents exist that can be

[§]Prostaglandins are a group of lipid compounds involved in cellular signalling. They have a diverse range of biological functions including roles in cell growth, proliferation and differentiation [121].

used to exclusively label free thiol groups; they are typically based on maleimide, alkyl halide or disulfide compounds. However, alternative reagents such as electrophilic selenium and mercury derivatives may also be used [123]. Labelling free thiol groups can potentially allow the extent and location of redox-modifications to be determined. If the derivatising agent is functionalised with a radioisotope, a fluorophore or an epitope/affinity tag, the labelled thiol groups can be detected and quantified by autoradiography, fluorescence detection or Western blot/enzyme-linked immunosorbent assay (ELISA) respectively. However, when analysing an intact protein containing multiple cysteine residues, these techniques do not allow for localisation of the modified thiol groups. Furthermore, the identity of unknown thiol oxidation-states cannot be determined. Site-directed mutagenesis and the analysis of cysteine-mutants can provide site-specific information. Analysis of Cys-mutants using the aforementioned techniques still does not, however, provide information regarding the identity of unknown redox-modifications.

X-ray crystallography and mass spectrometry are tools that allow unambiguous characterisation and localisation of cysteine redox-states [124, 125]. However, the challenges associated with protein crystallisation and the timescales involved are notorious. Furthermore, reaction kinetics or real-time changes in protein conformation cannot be monitored with this technique. Mass spectrometry allows covalent cysteine modifications to be both identified and located without the need for numerous and time-consuming crystallisation trials, antibodies, functionalised reagents (i.e. fluorophores or radioisotopes) or the cloning, expression and purification of recombinant Cys-mutants. Furthermore, MS requires relatively small sample amounts (μl of μM concentration and below) and can also be used to probe protein conformation at low resolution and measure rates of reactions.

The overall aim of the work presented in the following chapters of this thesis was to use high resolution mass spectrometry to investigate the molecular details of p53 redox-regulation and, in doing so, demonstrate the power of FT-ICR MS for the study of multiple Cys-containing proteins.

1.4 Protein Mass Spectrometry

The development of two ionisation techniques – electrospray ionisation (ESI) and matrix-assisted laser desorption/ionisation (MALDI) – in the late 1980s transformed the field of biological mass spectrometry by enabling the formation of intact molecular ions of non-volatile polar macromolecules such as proteins [126, 127]. The subsequent drive to improve the performance and versatility of MS instrumentation has made mass spectrometry now one of the most important and mainstream analytical techniques for protein research and the study of biomolecules in general [128].

Mass spectrometry is central to the field of proteomics, which involves identification of proteins in complex mixtures such as cell lysates, tissue extracts or clinical fluids [129]. Tandem mass spectrometry (MS/MS) can assist in protein identification and also allows *de novo* sequencing of species with unknown primary structure [130]. Post-translational modifications (PTMs) can be characterised and the use of stable isotopes enables quantitation of modification states or protein expression levels [128, 131]. A unique feature of ESI and MALDI is the preservation of non-covalent interactions [132]. Hence, non-covalent protein complexes can be studied and the tertiary and quaternary structure of intact proteins can be probed using MS [133].

A feature of MS pertinent to this study is the ability to localise a PTM to a specific amino acid residue. This can be achieved using three different approaches: bottom-up, top-down or middle-down mass spectrometry.

1.4.1 Bottom-Up Mass Spectrometry

Bottom-up protein mass spectrometry is the most traditional and commonly employed method for the identification and localisation of protein PTMs [128, 129, 131, 134]. The defining step in the bottom-up approach is cleavage of the intact protein(s) into small peptides (generally < 3 kDa) prior to MS. Figure 1.9 illustrates the workflow of a typical bottom-up experiment. The intact protein is cleaved into its constituent peptides by a suitable enzyme, usually trypsin (which cleaves the C-terminal side of Lys or Arg residues except when followed by Pro). The peptides

are optionally fractionated followed by MS analysis. In classical proteomic experiments which aim to identify proteins from a mixture, the masses of individual peptides are searched against a database and used as a 'mass fingerprint' to identify the parent protein. Furthermore, tandem mass spectrometry can be employed to fragment the detected peptides, thus providing more detailed sequence information and greater assurance in protein identification. When mapping PTMs, the accurate mass of a modified peptide may be sufficient to locate the modification to a specific residue i.e. if the peptide contains only one possible modification site. If there is ambiguity regarding the locality of a PTM, MS/MS can be performed.

A major limitation in protein mass spectrometry in general is the large size of the intact macromolecules. Proteolysis prior to MS therefore makes the bottom-up MS independent of protein size, and this is one of the major advantages of this strategy. Furthermore, bottom-up methods are well-established, highly sensitive and amenable to automated and high-throughput studies. However, proteolysis and the lack of an intact protein mass results in the bottom-up approach having distinct disadvantages for protein and PTM characterisation. Namely, incomplete sequence coverage and no knowledge of the relationship between peptides and the modification state or isoform of the parent protein. 100% sequence coverage is rarely achieved in bottom-up MS, meaning that important information, e.g. the presence of a PTM, is often lost. Furthermore, when analysing differentially modified proteins, the combination that PTMs occur in or their hierarchy (i.e. which PTM occurs 1st, 2nd, 3rd etc.) cannot be determined because the mass of the peptides cannot be directly related back to mass of the parent protein. These limitations can be overcome using the top-down approach for protein and PTM characterisation.

1.4.2 Top-Down Mass Spectrometry

Figure 1.10 illustrates the workflow of a typical top-down MS experiment. In contrast to bottom-up approach to protein and PTM characterisation, proteolysis is not performed prior to MS analysis [131, 135-138]. Rather, the accurate mass of an intact protein is measured and the whole protein is directly fragmented inside the mass spectrometer. The masses of the resulting fragment ions are searched against

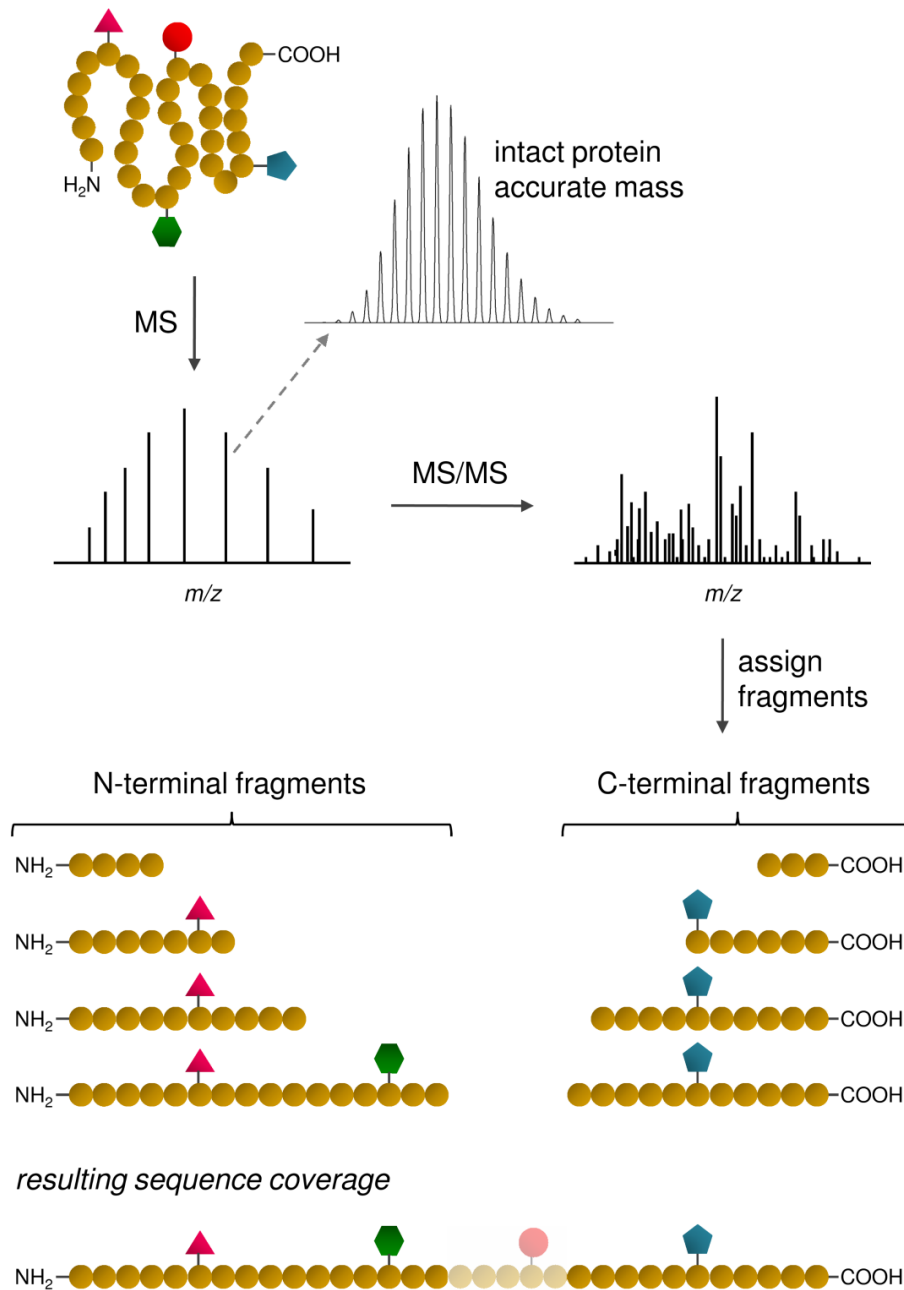


Figure 1.10 The top-down approach to PTM identification and localisation by MS. The accurate mass of the intact protein is measured followed by direct fragmentation which results in a complex MS/MS spectrum. The masses of the fragment ions are searched against a database or the primary sequence of a known protein and N- and C-terminal fragments are assigned. The identity and combination of PTMs present may be known from the mass of the intact protein. However, top-down MS of large proteins ($> \sim 30$ kDa) typically results in poor sequence coverage over the internal region of the protein which may preclude the unambiguous assignment of a PTM location.

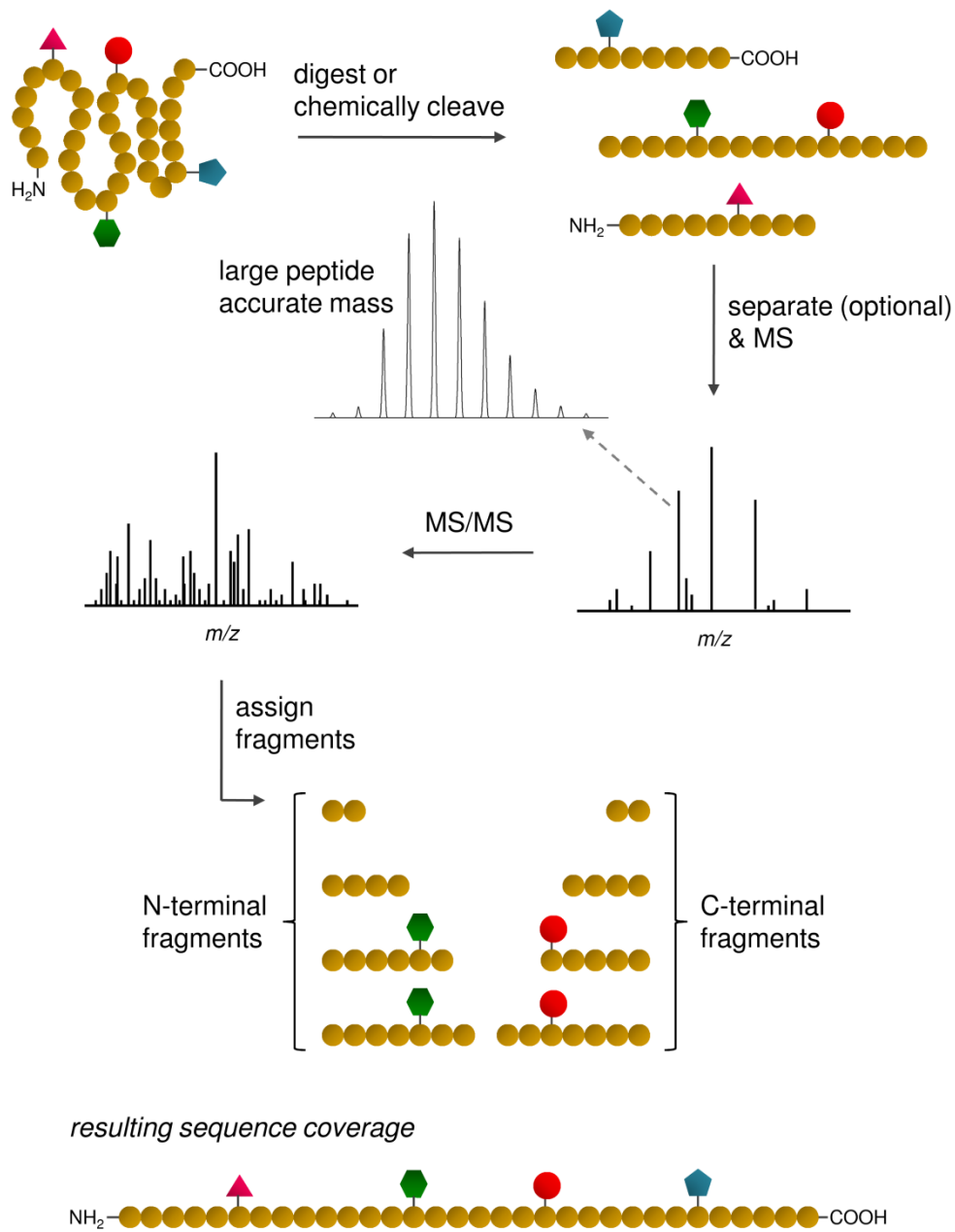


Figure 1.11 The middle-down approach to PTM identification and localisation by MS. The intact protein is cleaved into large peptides using enzymatic digestion or a chemical cleaving reagent. The large peptides may contain multiple PTM sites yet be small enough to allow extensive fragmentation, thus allowing unambiguous assignment of PTMs. Middle-down MS is particularly useful for providing comprehensive sequence coverage over the internal region of a large protein.

the primary sequence of a known protein, or against a database in the case of an unknown protein. To simplify the data analysis, only the N- and C-terminal fragments are assigned (see Section 1.7 for further details regarding fragmentation of protein ions).

The accurate mass of an intact protein or protein complex can provide important information such as the identity of PTMs and their respective stoichiometries. Knowledge of the molecular mass, together with the ability to isolate individual modification states or isoforms inside the mass spectrometer, e.g. with a mass resolving quadrupole, means that the relationship between the parent protein and fragment ions is known. Top-down MS therefore allows the unambiguous assignment of protein PTM states and their hierarchy to be determined.

Furthermore, top-down MS typically results in far greater cleavage of inter-residue bonds compared to bottom-up MS, because the entire protein sequence is available for interrogation rather than only a few peptides. However, the number of cleaved inter-residue bonds typically reduces with increasing protein mass due to the decreased dissociation efficiency and fragmentation over the internal region of larger proteins ($> \sim 30$ kDa) is often not sufficient to unambiguously locate the site of a PTM (knowledge of the intact mass does, however, indicate their existence). Above a molecular mass of ~ 50 kDa, fragmentation of an intact protein becomes substantially problematic due to the increased complexity of the molecular ions' gas-phase tertiary structure [139]. These limitations of protein size can be overcome using the middle-down approach described below.

MS/MS is an inherent part of the top-down approach, whereas it is an optional step in the bottom-up approach, when analysing the constituent proteolytic peptides of a protein. Fragmentation of an intact protein generates a complex MS/MS spectrum with many overlapping, multiply-charged fragment ions. As a result, high-performance mass spectrometers which offer superior resolving power and mass accuracy, such as FT-ICR instruments (see section 1.6), are preferred for top-down analysis of proteins. In addition to protein size, the requirement and cost of such instruments is a limiting factor in top-down MS protein studies.

1.4.3 Middle-Down Mass Spectrometry

The advantages of bottom-up and top-down MS are combined in the middle-down approach to protein and PTM characterisation, namely, proteolysis to form peptides more amenable to MS, yet large enough (typically > 3 kDa) to contain multiple PTM sites and provide substantial sequence information [136, 138]. Figure 1.11 highlights the main steps in a typical middle-down experiment. The intact protein is cleaved into large peptides using an enzyme or chemical cleaving reagent that targets less abundant amino acids than trypsin. For example, polypeptides can be cleaved at the relatively rare amino acid tryptophan using BNPS-skatole, at methionine residues using cyanogen bromide (CNBr), or at Asp or Glu residues using the proteases AspN and GluC respectively [136, 140]. The resulting large peptides can be optionally separated followed by accurate mass measurement of the precursor ion and fragmented to yield a relatively complex MS/MS spectrum similar to top-down MS. The masses of the fragment ions are searched against the known primary sequence or a database and the N- and C-terminal fragments are assigned. Fragmentation of these intermediate sized peptides results in increased dissociation efficiency compared to the intact protein therefore sequence coverage is improved. Middle-down is particularly useful for providing extensive sequence coverage^{**} over the internal regions of larger proteins which top-down MS typically fails to achieve.

1.5 Electrospray Ionisation Mass Spectrometry

Two principal methods are used to ionise peptides/proteins and introduce them into the gas-phase; matrix-assisted laser desorption/ionisation (MALDI) and electrospray ionisation (ESI). Both techniques are ‘soft’ ionisation methods meaning that gas-phase ions are generated without fragmentation. The development and application of MALDI and ESI to large polar macromolecules such as proteins and oligonucleotides revolutionised the field of biological mass spectrometry. This was

^{**}When discussing top-down or middle-down MS, ‘sequence-coverage’ typically refers to the number of inter-residue bonds cleaved. E.g. 100% sequence coverage in top-down protein MS would mean that each inter-residue bond was cleaved, and the corresponding fragment ions detected, across the entire primary sequence.

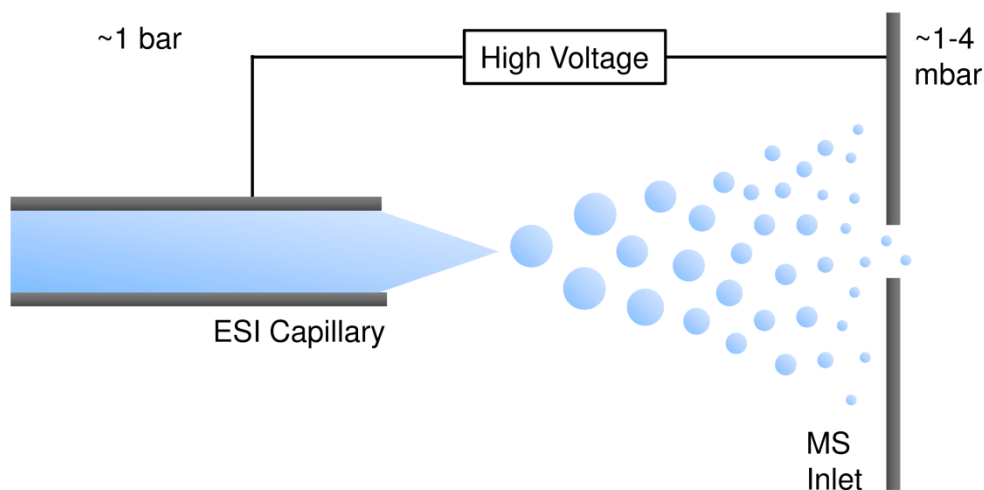


Figure 1.12 Schematic of electrospray ionisation. A capillary is held at high voltage with respect to the inlet of the mass spectrometer resulting in a fine mist of charged droplets ('electrospray') containing the analyte. The droplets reduce in size via solvent evaporation and 'Coulombic explosions' (see text) during their transition down a pressure and potential gradient towards the entrance to the MS. Gas-phase ions are formed during desolvation however the exact mechanism for this is unknown.

recognised by the award of the 2002 Nobel Prize in Chemistry to Koichi Tanaka and John Fenn for the development of MALDI and ESI for mass spectrometric analyses of biological macromolecules respectively^{††} [142, 143].

MALDI involves co-crystallisation of analyte molecules with a large excess of a light-absorbing matrix compound, followed by laser irradiation of the resulting solid layer. The energy uptake upon irradiation results in desorption and ionisation of the analyte which can then be detected by a suitable mass analyser. MALDI typically results in predominately singly charged ions. Therefore, analysis of large intact proteins by MALDI-MS is limited to mass analysers with an extended mass range, such as time-of-flight (TOF) instruments [144].

A schematic of the ESI process is provided in Figure 1.12. During ESI, a solution containing the analyte, e.g. intact protein, is passed through a capillary held at a high potential. The effect of a large electric field at the tip of the capillary causes the

^{††}However, controversy exists regarding the award to Koichi Tanaka, due to a publication by Karas *et al* in 1985, where "matrix-assisted" laser desorption ionisation was first reported [141].

solution to emerge as a fine mist of charged droplets ('electrospray') which are drawn towards the entrance of the mass spectrometer by a potential and pressure gradient. During this transition, the droplets reduce in size by evaporation of solvent (aided by a heated drying gas) until the surface tension can no longer sustain the increasing charge density (Rayleigh limit) and they fragment due to 'Coulomb explosion'. This process continues until all of the solvent is evaporated. Gas-phase ions are formed during the electrospray process. However, the exact mechanism for this is still being debated [144-146]. Further information regarding the development of ESI and the proposed mechanisms of ion formation can be found in Refs. [143, 144, 147].

Conventional ESI is typically operated at flow rates of 1-20 $\mu\text{l}/\text{min}$. Miniaturising the electrospray and reducing flow rates to 20-50 nl/min – known as nanoESI (nESI) – generates smaller charged droplets and increases the efficiency of desolvation. Furthermore, sample consumption is substantially reduced with nESI [144-146, 148].

In contrast to MALDI, ESI characteristically results in the formation of multiply charged ions. This is advantageous for the study of intact proteins because the mass to charge ratios (m/z) can be reduced to within the detectable m/z range of the majority of mass analysers, including quadrupoles and ion traps [144, 145, 149]. Furthermore, higher charge states provide more scope for fragmentation and detection of product ions. For example, dissociation of a singly charged polypeptide will result in one singly charged product ion and one neutral molecule, which cannot be detected by MS.

Separation of complex samples, or desalting, is often required prior to mass spectrometry of biological molecules. ESI involves the direct sampling of analytes from solution at atmospheric pressure. This allows high performance liquid chromatography (HPLC) to be interfaced to an ESI source, and sample separation/desalting steps can, therefore, be directly coupled to MS analysis (known as 'on-line' LC-MS). In addition to increasing sensitivity, directly coupling chromatographic separations to MS is useful in high-throughput proteomics experiments whereby retention time can be used in combination with accurate mass

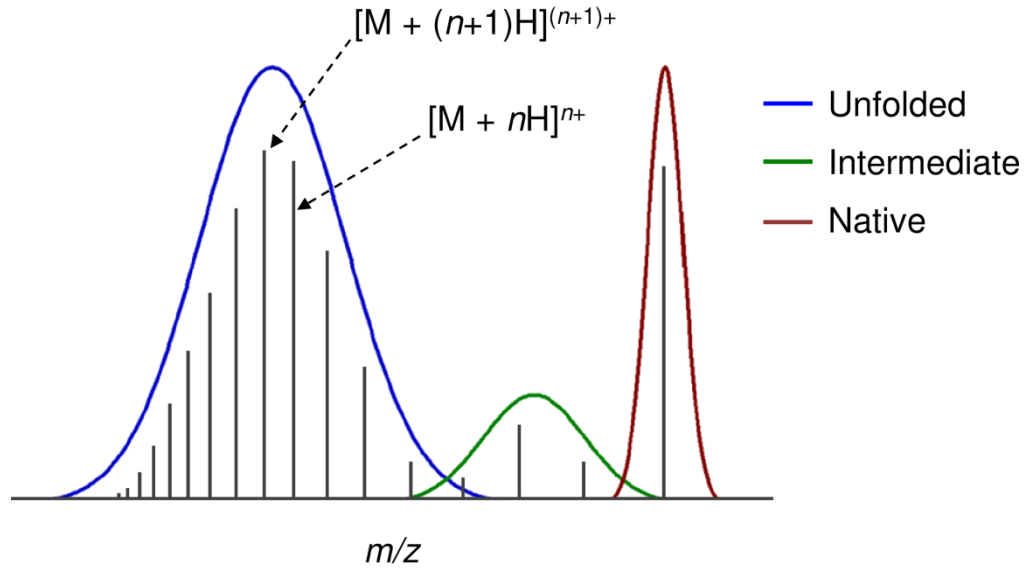


Figure 1.13 Charge state distributions that may be observed in a protein ESI mass spectrum depending on the conformations present in solution.

measurements (AMT; accurate mass and time tag) to identify peptides from complex samples [150].

ESI-MS can also be used to probe the higher-order structure of intact proteins. Figure 1.13 shows the charge state distributions typically observed in a protein ESI mass spectrum, depending on the conformations present in solution [151-153]. Proteins can become multiply protonated due to the presence of many basic amino acid side chains (Arg, Lys and His). Protein conformation dictates the solvent exposure of these residues. For example, a protein in its native conformation will typically be folded with a compact tertiary structure. Many of the basic side chains will be buried, inaccessible to bulk solvent and therefore protected from protonation. This is reflected in the mass spectrum of a native protein by a relatively narrow charge state distribution at high m/z . Conversely, the basic side chains in an unfolded protein will be exposed to the solvent, resulting in higher charge states which span a broader m/z range. Many proteins may adopt intermediate conformations between their folded and unfolded states, which are typically observed as relatively low-abundance ions of intermediate charge in an ESI mass spectrum.

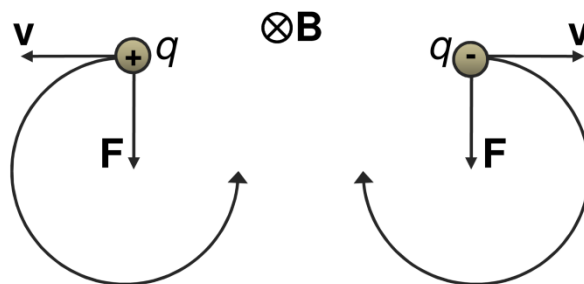


Figure 1.14 Cyclotron motion of a positive and negative ion. Charged particles (with a charge q), with a velocity \mathbf{v} , in a static magnetic field \mathbf{B} (directed perpendicular to the paper), will undergo cyclic motion due to the Lorentz force, \mathbf{F} . The direction of orbit is dependent on the polarity of the ion. Figure adapted from Ref. [154].

The observed charge state distributions may be affected by the solvent conditions. Denaturing conditions (typically 50% organic solvent and 0.1% volatile organic acid) promote protein unfolding by disrupting non-covalent interactions which hold the protein in its native, folded conformation. Denaturing conditions, therefore, generally result in the broad charge state distribution observed for unfolded proteins. Native conditions (neutral pH and typically 10% organic solvent to aid the desolvation process) preserve non-covalent interactions therefore the native tertiary structure is maintained during ESI-MS, resulting in the characteristic narrow charge state distribution observed for folded proteins. Native conditions also facilitate the study of non-covalent interactions of proteins with metal ions or ligands such as peptide aptamers, drug molecules or DNA [133, 155, 156].

1.6 FT-ICR MS

The accurate mass measurement of an intact protein can be used to confidently assign many features, including the oxidation state of metal centres (± 1 Da or more), the presence of a disulfide bond (-2 Da), or the deamidation of asparagine and glutamine residues ($+1$ Da) [131, 157-159]. Isotopic resolution is required in order to achieve high mass measurement accuracy, which is defined as ± 10 parts per million (ppm) in MS-based protein identification studies [160, 161]. When dealing with intact proteins, the resolving power required to separate the isotopic variants

(differing in the number of ^{13}C or other heavy isotopes of constituent atoms) [162] is typically in the order of 10^5 - 10^6 . Fourier transform ion cyclotron resonance mass spectrometry (FT-ICR MS) offers the highest mass measurement accuracy and mass resolving power of any mass spectrometer, and resolving powers $> 1,000,000$ and sub-ppm mass accuracies can be routinely obtained [154, 163].

The superior resolving power and mass accuracy that FT-ICR MS offers is of major benefit when analysing the many multiply charged fragments that arise from fragmentation of an intact protein. Furthermore, FT-ICR mass spectrometers are versatile instruments which are compatible with a wide range of fragmentation techniques (discussed below). As a result, FT-ICR MS is the method of choice for top-down protein mass spectrometry [131, 164, 165].

FT-ICR MS is based on the principle that an ion with velocity \mathbf{v} moving in a homogenous magnetic field will undergo cyclic motion in the plane perpendicular to the direction of the magnetic field [146, 163, 166, 167]. This cyclotron motion is due to the Lorentz force (\mathbf{F}), which is a vector cross product of the magnetic field strength (\mathbf{B}) and the velocity (\mathbf{v}), multiplied by the charge (q) (in S.I. units):

$$\mathbf{F} = q\mathbf{v} \times \mathbf{B} \quad 1.1$$

Figure 1.14 shows the Lorentz force acting on a positively and negatively charged particle. Providing no collisions occur, the magnetic field will bend the ion path into a complete circle. The direction of orbit is dependent on the polarity of the ion. The frequency with which an ion repeats its orbit is known as the cyclotron frequency, ν_c , and is dependent on the magnetic field, the mass of the ion, m , and its charge according to the following equation (in S.I. units):

$$\nu_c = \frac{qB}{2\pi m} \quad 1.2$$

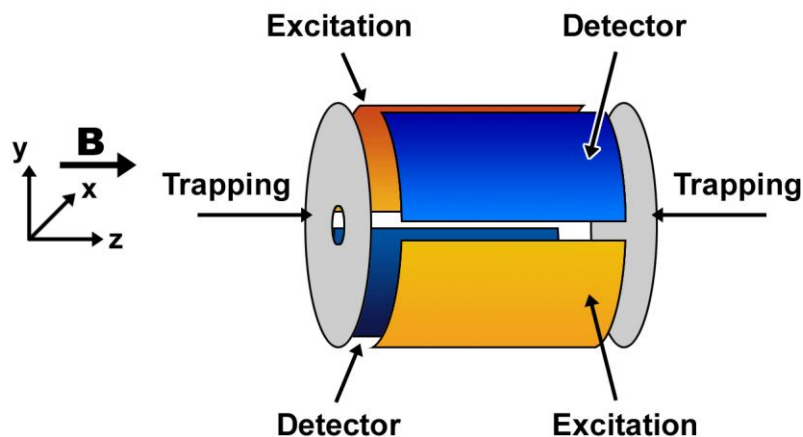


Figure 1.15 A schematic of a cylindrical ICR cell. A static electric field is applied to the end trapping plates to trap ions in the z direction. An oscillating electric field is applied to the excitation plates to increase the cyclotron radius of the ions and the resulting induced current is detected by the detection plates. Figure courtesy of Chris Whyte (PhD Thesis, University of Edinburgh, 2004)

A derivation of Equation 1.2 is provided in Ref. [166]. This equation can be expressed in terms of the more familiar mass to charge ratio, m/z , which is used in mass spectrometry, where m is in Daltons (Da), z is equal to q/e where e is the elementary charge (in S.I. units) and u is the atomic mass unit (in S.I. units):

$$\nu_c = \left(\frac{e}{2\pi u} \right) \frac{B}{m/z} = \frac{1.5 \times 10^7 B}{m/z} \quad 1.3$$

Rearranging Equation 1.3 gives:

$$m/z \propto \frac{B}{\nu_c} \quad 1.4$$

which illustrates the fundamental relationship exploited in FT-ICR mass spectrometry; m/z is directly proportional to magnetic field and inversely proportional to cyclotron frequency. For example, an ion with 1000 m/z will have a

cyclotron frequency of 141 kHz in a uniform 9.4 Tesla (T) magnetic field, increasing to 180 kHz in a uniform 12 T magnetic field.

The high mass measurement accuracy associated with FT-ICR MS stems from inherently accurate frequency measurements. Furthermore, the cyclotron frequency of an ion is independent of its kinetic energy (K.E.). Resolution is therefore not limited by the spread in the K.E. distribution of the ions, as is seen with TOF and sector mass analysers. The insensitivity of cyclotron frequency to K.E. is one of the principle reasons why FT-ICR MS is able to achieve ultra-high resolution. Increasing the magnetic field strength increases resolving power by increasing the cyclotron frequency of an ion, i.e. many more measurements can be taken in a certain time. The difference between two cyclotron frequencies is also increased, corresponding to greater resolving power and peak capacity [154, 163]. A historical account of the development of FT-ICR MS is given in Ref. [168].

During FT-ICR MS, ions are trapped in an ICR cell which is located within a uniform magnetic field. The ICR cell typically consists of a pair of end trapping plates, a pair of excitation plates and a pair of detection plates as shown in Figure 1.15. A static electric field is applied to the end trapping plates to prevent ions from leaving the cell. A coherent radiofrequency pulse is applied to the excitation plates in order to form a coherent ion packet and increase the cyclotron radius of the ions out towards the detection plates. This radiofrequency sweep sequentially excites all ions at resonance within the m/z range of interest. The resulting induced current is detected by the detection plates and amplified to give a transient ion image current. Fourier transform is applied to this image current resulting in the frequency spectrum, which is then converted to the corresponding m/z spectrum. These steps are illustrated in Figure 1.16.

It is important to note that electric fields are present within the ICR cell, arising from either the ions themselves (known as space-charge effects) or trapping potentials, which affect the motion of ions within the cell. Equations 1.2 and 1.3 are based on an ideal case which does not take into account these effects, and therefore deal with the “unperturbed” cyclotron frequency. The observed cyclotron frequency, ν_{obs} , is dependent on numerous other parameters including ion charge density,

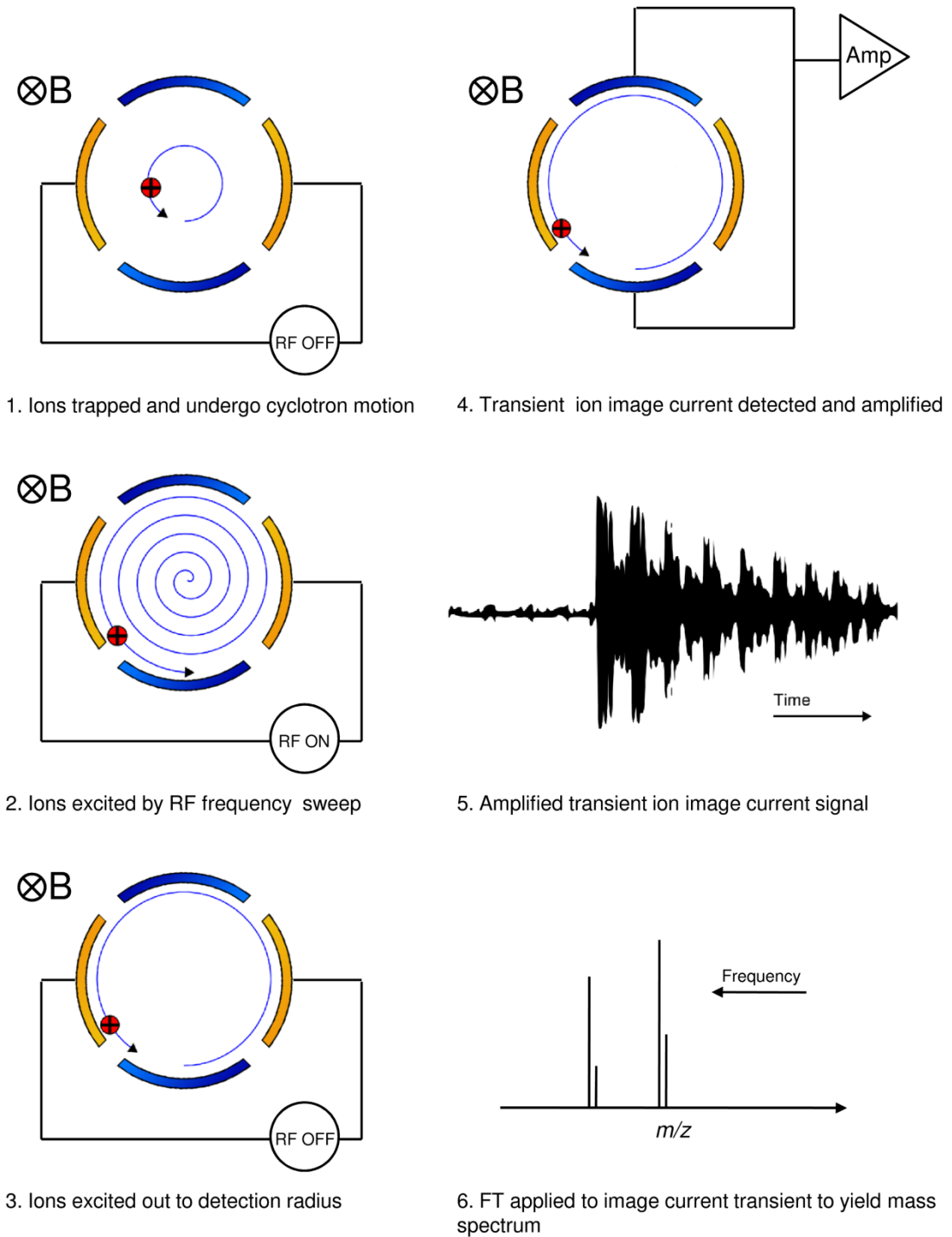


Figure 1.16 An FT-ICR MS experiment. Ions are trapped in an ICR cell (the excitation and detection plates are shown) and undergo cyclotron motion at a frequency dependent on their m/z and the magnetic field. Ions are then excited out to the detection radius by a radiofrequency (RF) sweep and the resulting transient image current is recorded. Fourier transform is applied to the time domain signal which is calibrated to yield a mass spectrum.

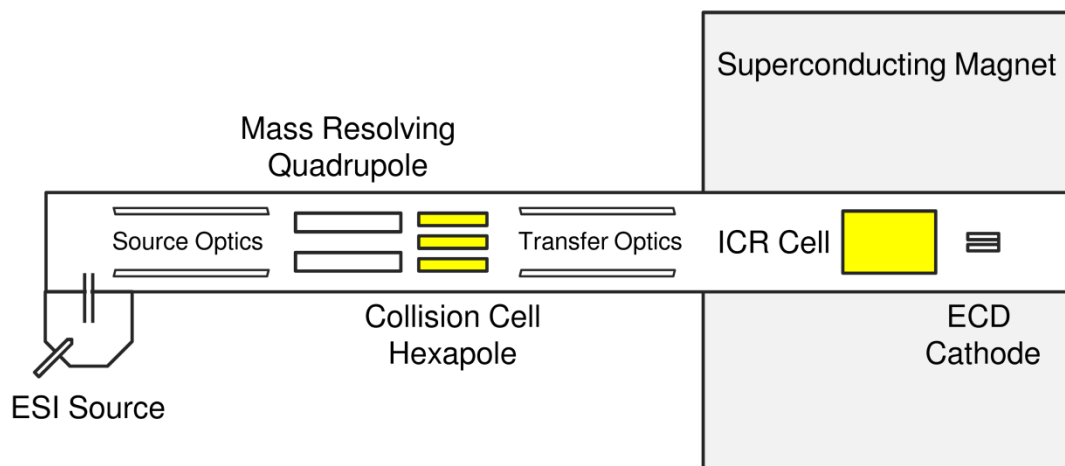


Figure 1.17 Simplified overview of the Bruker Daltonics apex-Qe FT-ICR mass spectrometer. Regions highlighted in yellow indicate where MS/MS may be performed. Ions of a specific m/z can be selected and isolated in the mass resolving quadrupole prior to CID in the adjacent hexapole, or ECD in the ICR cell. A more detailed overview of this instrument including the vacuum stages and ion optics is given in Appendix A.

geometry of the ICR cell and trapping potentials, in addition to the magnetic field and mass-to-charge ratio. Shifts in m/z arising from the presence of electric fields within the ICR cell are corrected by calibration (see Ref. [169] for an in depth discussion of the calibration equations used in FT-ICR MS) and do not normally pose a problem. Further discussion of the theory of FT-ICR MS is out with the scope of this introduction and the reader is directed to the following Refs. for more in-depth reviews: [166, 170].

The spatial confinement of ions within an ICR cell allows for a wide variety of ion manipulation and fragmentation techniques to be employed. Excitation waveforms can be tailored to excite ions at one frequency or eject unwanted ions from the cell [146, 171-173]. Techniques for fragmentation of ions within the ICR cell include sustained off-resonance irradiation collision-induced dissociation (SORI-CID), infrared multiphoton dissociation (IRMPD), blackbody infrared dissociation (BIRD), surface-induced dissociation (SID) and electron capture dissociation (ECD) [154, 163, 167, 171, 174-178]. Hybrid FT-ICR instruments allow ions to be fragmented before they reach the ICR cell, therefore expanding the range

of dissociation techniques which may be utilised and also increasing the scope for MSⁿ experiments.

A hybrid instrument, the Bruker Daltonics apex-Qe FT-ICR mass spectrometer, was used extensively to record the MS and MS/MS spectra presented in this thesis. Figure 1.17 shows a simplified overview of the main components on this instrument. A more detailed overview, showing the various vacuum regions, ion optics and source configuration is given in Appendix A. Ions are generated by ESI and guided along the flight tube to the ICR cell by various sets of ion optics, including ion funnels and steering plates. The ICR cell resides in a 12 T superconducting magnet. A mass resolving quadrupole and collision cell hexapole are located between the source optics and the transfer optics. For MS/MS, ions of a specified m/z can be isolated in the quadrupole followed by CID in the hexapole or ECD in the ICR cell. As mentioned above, the ability to accurately measure the m/z of large multiply charged precursor ions in addition to the fragment ions makes FT-ICR MS a powerful tool for structural characterisation of proteins.

1.7 Fragmentation of Ions

As previously discussed, fragmentation of the polypeptide backbone can provide primary sequence information, and unambiguously locate a post-translational modification to within one residue. Collision-induced dissociation (CID) is traditionally used to fragment peptides or intact proteins. However, many fragmentation techniques exist (a selection of techniques compatible with FT-ICR MS is discussed in Section 1.6), each with associated advantages and disadvantages, and new or improved methods to generate fragment ions are in a continual state of development. A recent example is electron transfer dissociation (ETD) [179]. This technique involves the transfer of an electron from a radical anion with low electron affinity (such as anthracene) to a multiply protonated peptide/protein. The energy released upon recombination of an electron and a multiply protonated polypeptide induces fragmentation of the peptide backbone in a manner analogous to that observed in electron capture dissociation (ECD; see 1.7.3). In addition to the

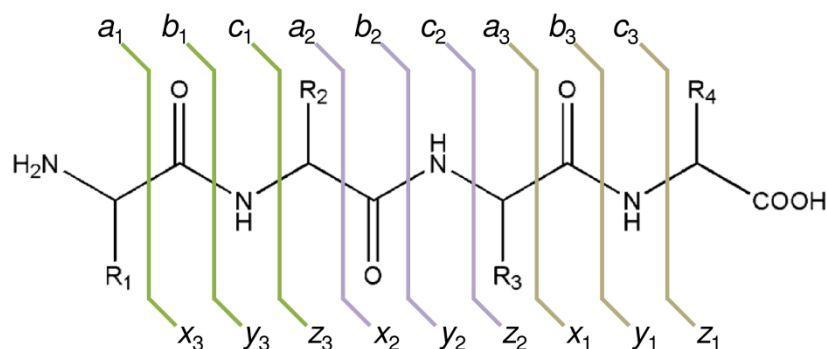


Figure 1.18 Fragment ions that may arise upon fragmentation of a polypeptide backbone. *a*, *b* and *c* ions are N-terminal fragments and *x*, *y* and *z* ions are C-terminal fragments. The subscript denotes the number of residues in the fragment, counting from the N-terminal for *a*, *b* and *c* ions or the C-terminal for *x*, *y* and *z* ions.

advantages described for ECD (below), ETD is compatible with a wider range of MS instrumentation and can be used to dissociate both anionic and cationic precursor ions [180].

The fragmentation techniques utilised for MS/MS experiments presented in this thesis were collision-induced dissociation and electron capture dissociation.

1.7.1 Nomenclature

Figure 1.18 shows the types of fragment ions that may be observed in the MS/MS spectrum of a polypeptide. The polypeptide backbone can be cleaved in one of three positions; the C_{α} —C bond, the C—N bond (amide or peptide bond) or the N— C_{α} bond [130, 181, 182]. These cleavages result in *a* and *x*, *b* and *y*, or *c* and *z* ions respectively. The backbone is preferentially cleaved at a certain position depending on the fragmentation technique used. *a*, *b* and *c* ions are N-terminal fragments and *x*, *y* and *z* ions are C-terminal fragments. A subscript is used to denote the number of amino acids in the fragment, counting from the N-terminus in the case of *a*, *b* and *c* ions, and the C-terminus in the case of *x*, *y* and *z* ions. Internal fragments (i.e. where cleavage occurs at more than one place along the backbone resulting in a fragment that contains neither the original N nor C-terminus) and cleavage of the amino acid side chains may also occur during fragmentation. However, these fragments were not

considered during data-analysis of any MS/MS spectra included in this thesis and their associated nomenclature will not be discussed here. The presence of side-chain and internal fragments increases the complexity of MS/MS spectrum. However, they can be minimised by utilisation of fragmentation methods that are highly-specific for a particular backbone bond-type, such as ECD (see below).

1.7.2 Collision-Induced Dissociation

Collision-induced dissociation (CID), also known as collisional-activated dissociation (CAD), is the most commonly used method for tandem mass spectrometry of peptides and proteins. In CID, the internal energy of the precursor ion is increased by energetic collisions with a neutral target gas (typically argon, helium or nitrogen) leading to fragmentation and the formation of product ions [183-186]. Depending on the type of instrumentation, high-energy CID (typically time of flight and sector instruments) or low-energy CID (typically multipole e.g. quadrupole and ion trap instruments) is performed. The CID experiments conducted here were carried out in a hexapole collision cell (indicated in Figure 1.17) and ions were fragmented using low-energy CID (eV rather than keV precursor ion kinetic energies).

Low-energy CID falls into the category of so called ‘slow-heating’ techniques, along with numerous other MS/MS technologies including infrared multi-photon dissociation (IRMPD), sustained off-resonance irradiation CID (SORI-CID) and blackbody infrared radiative dissociation (BIRD) [175-177, 186, 187]. In these methods, dissociation is mainly a result of internal (e.g. vibrational and rotational) excitation of the precursor ion [129, 184, 185]. In the case of CID, each collision with the inert gas increases the internal energy until enough internal energy is accumulated to overcome the bond energy, thus resulting in dissociation. Fragmentation of polypeptides using slow-heating methods results primarily in dissociation of the backbone amide bond, giving *b* and *y* fragment ions. Slow-heating techniques result in fragmentation via the lowest energy pathway. Hence, cleavage of the peptide backbone is generally not random and specific product ions e.g. those resulting from cleavage of the facile amide bond on the *N*-terminal side of proline,

may predominate the MS/MS spectrum [171]. The loss of side chains and small neutral molecules (such as H₂O and NH₃) are also typically observed.

Collision-induced dissociation is the most robust and readily applied method for fragmentation of peptide and protein ions in tandem mass spectrometry, owing to its relative simplicity (in terms of its application), efficiency and reproducibility [183]. However, a limitation of CID that is particularly relevant to top-down MS (involving the analysis of intact proteins) is the inverse relationship between molecular mass and dissociation efficiency. As the size of a molecule increases, the number of degrees of freedom increases ($3N - 6$ vibrational modes in a nonlinear ion with N atoms) meaning that many more energy channels exist whereby the internal energy of an excited ion may be dissipated [183-185]. The net result is a decrease in the yield of fragment ions thus less extensive sequence coverage is generally achieved as protein size increases. Furthermore, the tendency for CID to result in side-chain losses (particularly with high-energy CID) is not ideal for the study of protein PTMs [188].

Further information regarding dissociation mechanisms and the history of CID and associated methods can be found in Refs. [184-186].

1.7.3 Electron Capture Dissociation

Electron capture dissociation (ECD) is a relatively new fragmentation technique for tandem mass spectrometry of peptides and proteins [174]. Multiply protonated peptides or proteins are irradiated with low-energy electrons (< 1 eV) resulting in dissociation processes entirely distinct from those observed in CID and the conventional slow-heating techniques. The exact mechanism of ECD is a subject of much debate and is beyond the scope of the general introduction provided here. The reader is directed towards Refs. [189-198] for further information regarding ECD mechanism.

During ECD, a multiply charged polypeptide, $[M + nH]^{n+}$, captures an electron resulting in charge neutralisation and the formation of an excited radical species, $[M + nH]^{(n-1)+\bullet}$. The excited radical ions may undergo very rapid dissociation of the N—C_α bond leading to predominately c and z' ions. However, the majority of

electron capture events do not result in fragmentation and lead only to charge-reduction. Hence, ECD is a relatively inefficient MS/MS technology and a high abundance of precursor ion is ideally required for extensive fragmentation of the polypeptide backbone [171, 185, 199, 200].

Capture of an electron by a singly protonated precursor ion results in a neutral species. Thus, the precursor ion must be at least doubly charged in order for the resulting fragment ions to be observable by MS. ECD is therefore only suited to ionisation methods that generate multiply protonated polypeptides, such as ESI. Furthermore, ECD is generally limited to the ICR cell of FT-ICR instruments (see Figure 1.17) due to the long residence times of ions (at least several ms) necessary to ensure capture of electrons by a notable proportion of precursor ions, and the ability to accommodate low-energy electrons (which cannot be trapped in instruments that use a radio frequency electrostatic field to trap ions i.e. quadrupole ion traps) [179, 200]. ECD has been implemented in less expensive quadrupole ion-trap instruments with limited success [201, 202]. However, a recently developed alternative to ECD, electron transfer dissociation (ETD; see Section 1.5), uses ion-ion reactions to transfer an electron to the analyte, rather than direct ion-electron reactions [179, 180]. ETD provides polypeptide backbone cleavage in a manner characteristic to that observed for ECD, with the advantage of being amenable to quadrupole ion trap mass spectrometers.

ECD is a ‘non-ergodic’ process, meaning that bond dissociation occurs before the additional energy can be redistributed away from the capture site [174, 199]. This fast dissociation is advantageous for tandem MS of polypeptides because the lowest energy fragmentation pathways are not favoured (as with CID), resulting in extensive cleavage across the backbone. Furthermore, internal fragments usually occur with much lower abundance than typically observed for conventional MS/MS techniques. In addition to reducing the complexity of MS/MS spectra, ECD is therefore a valuable tool for the study of labile PTMs such as phosphorylation, sulfation and γ -carboxylation, which are found to be retained in ECD fragments [203, 204].

The non-ergodic nature of ECD also allows non-covalent interactions to be preserved during fragmentation and can, therefore, be employed to investigate

protein-ligand binding sites [205]. However, the preservation of non-covalent bonding can be disadvantageous when fragmenting relatively large intact proteins, due to extensive intramolecular non-covalent interactions. The peptide backbone may undergo fragmentation but the resulting fragments are essentially held together as a large non-covalent complex, thus appearing as a charged-reduced species in the MS/MS spectrum [206]. To overcome this problem, precursor ions can be vibrationally excited using slow-heating methods such as CID or IRMPD prior to or during electron capture. This technique is known as activated ion (AI) ECD and serves to disrupt higher-order structure of larger ions therefore increasing sequence coverage [206].

A feature of ECD which contributes to the gas-phase disruption of protein tertiary structure is the preferential reduction of disulfide bonds [207-209]. Cleavage of disulfide bonds during ECD precludes the requirement of a reduction step prior to MS for many proteins and can potentially be utilised in the study of redox-regulated proteins.

Chapter 2: Materials and Methods

2.1 Materials

All materials, solvents and reagents were purchased from Sigma-Aldrich or Fisher Scientific unless stated otherwise.

2.2 Molecular Biology

2.2.1 Bacterial Growth Media

LB broth base and powdered 2-YT medium were purchased from Invitrogen and made up according to the manufacturer's instructions. Recipes for growth media can be found in Ref. [210]. All media was sterilised in an autoclave at 121°C and 15 psi for 15 min prior to use.

2.2.2 Amplification and Purification of Plasmid DNA

A pRSET(A) vector (Invitrogen) containing a segment of the wild-type human p53 gene encoding the core domain (a.a. residues 94-312) was kindly donated by Penka Nikolova (King's College London). Competent *E. coli* DH5 α cells (Invitrogen) were transformed as described below in Section 2.2.6. LB medium (10 ml) supplemented with ampicillin (100 μ g/ml) was inoculated with a single colony of transformed cells and grown overnight at 37°C and 250 rpm. Plasmid DNA was purified from the bacteria using a QIAprep Spin Miniprep Kit (Qiagen) according to the manufacturer's instructions. Plasmids were stored at -20°C.

2.2.3 Restriction Digest and Agarose Gel Electrophoresis

In order to determine the size of the gene insert in the pRSET(A) vector, a restriction digest was performed and the resulting fragments were analysed by agarose gel electrophoresis. Purified plasmid DNA (8 μ l) was incubated with the restriction enzymes NdeI and HindIII (New England BioLabs; 0.5 μ l of each) in NEBuffer 2 (New England BioLabs; 1 μ l) at 37°C for 2 h. DNA loading buffer [210] was added to each sample followed by separation on a 1% Tris-acetate-EDTA (TAE) agarose gel [210] containing ethidium bromide (EtBr) at a final concentration of 0.5 μ g/ml, at 100 V for ~1 h. The gel was visualised under UV light.

Table 2.1 Primers used in site-directed mutagenesis of human p53 core domain.

Mutation	Primers
C182S	Forward 5'-CCACCATGAGCGCTCCTCAGATAGCGATGGTCTGG-3' Reverse 5'-CCAGACCATCGCTATCTGAGGAGCGCTCATGGTGG -3'
C277S	Forward 5'-GTGCGTGTTTGTGCCTCTCCTGGGAGAGACCGGCGCAC-3' Reverse 5'-TGTGCGCCGGTCTCTCCAGGAGAGGCACAAACACGCAC-3'
R175H	Forward 5'-GGAGGTTGTGAGGCACTGCCCCACCATGAGC -3' Reverse 5'-GTCATGGTGGGGGCAGTGCCTCACAACTCC -3'

2.2.4 Site-Directed Mutagenesis

Site-directed mutagenesis was performed using the QuikChange Site-Directed Mutagenesis Kit (Stratagene) according to the manufacturer's instructions. The primers used for each mutation are listed in Table 2.1.

2.2.5 DNA Sequencing

The p53 encoding region of plasmid DNA was sequenced using the T7 promoter and T7 reverse primers (Invitrogen) by the University of Edinburgh School of Biological Sciences Sequencing Service. Sequencing data was analysed using Vector NTI Advance software (Invitrogen).

2.2.6 Expression of Wild-Type and Mutant p53 Core Domain

Competent *E. coli* C41(DE3) cells (Cambridge Bioscience) were transformed as follows: cells (50 µl) were incubated on ice with plasmid DNA (1 µl) for 30 min, heat-shocked at 42°C for 45 s and placed back on ice for 2 min. SOC medium (100 µl) was added and the suspension was shaken at 37°C for 1 h. Cells (50 µl) were spread onto selective agar plates (100 µg/ml ampicillin) supplemented with 1% glucose and incubated at 37°C overnight. Sub-cultures were prepared by inoculating 2-YT medium (12x5 ml; pH 7.2) supplemented with ampicillin (100 µl/mg) with a single colony of transformed cells followed by incubation at 37°C and 250 rpm overnight. These sub-cultures were used to inoculate 3 L of 2-YT medium (12x250 ml; pH 7.2) supplemented with ampicillin (100 µl/mg) and the cells were

grown to an $OD_{600nm} \sim 0.6-0.8$ at 37°C and 225 rpm. The temperature was reduced to 22°C and overnight expression was induced with 1 mM isopropyl β -D-thiogalactoside (IPTG). Cells were harvested by centrifugation at 3000 rpm and 4°C for 20-30 min. The resulting cell pellet (typically ~36 g) was frozen in liquid nitrogen and stored at -80°C.

2.2.7 Protein Purification

Cells overexpressing p53 core domain were defrosted and lysed using BugBuster Protein Extraction Reagent (Novagen; 5 ml per gram of cells) supplemented with 4 mM dithiothreitol (DTT), EDTA-free protease inhibitor tablet (Roche; 1 tablet per 50 ml) and benzonase nuclease (Novagen; 25 units per ml) on ice for 20-40 min. Insoluble protein and cell debris were removed by centrifugation at 16,000 rpm and 4°C for 25 min and the supernatant was filtered (0.45 μ m). p53 core domain was purified from the soluble protein fraction by fast protein liquid chromatography (FPLC) using an ÄKTA FPLC system (GE Healthcare) at 4°C.

2.2.7.1 Ion Exchange Chromatography

The soluble protein fraction was loaded onto a Resource S (Amersham Biosciences) cation exchange column (prepared in-house; 10 ml) or a HiTrap SP XL column (GE Healthcare; 5 ml) equilibrated with 25 mM sodium phosphate (pH 7.2) and 4 mM DTT. Protein was eluted with a linear salt gradient of 0-1 M NaCl, 25 mM sodium phosphate buffer (pH 7.2) and 4 mM DTT over 15 column volumes. Protein gel electrophoresis was performed to confirm p53 expression and check purity. Fractions containing p53 were pooled and concentrated using a spin filtration device (Vivaspin 20; 10,000 MWCO). Protein concentration was determined as described in 2.3.2. Purified protein was frozen in liquid nitrogen and stored at -80°C in the presence of 10% glycerol (v/v).

2.2.7.2 Gel Filtration Chromatography^{##}

Protein purity can be increased by performing gel filtration chromatography

^{##}This 'polishing' purification step can be omitted in order to reduce protein loss.

following the ion exchange step. Fractions containing p53 were pooled, concentrated to ~10 ml and loaded onto a HiLoad 16/60 Superdex 75 pg column (GE Healthcare; 120 ml) equilibrated with 25 mM sodium phosphate buffer (pH 7.2), 4 mM DTT and 200 mM NaCl. Protein was eluted under isocratic conditions and fractions containing p53 were treated as described in Section 2.2.7.1.

2.2.8 Protein Gel Electrophoresis

Proteins were analysed on the basis of their molecular weight by protein gel electrophoresis. Denaturing protein loading buffer [210] was added to each sample prior to heating in a boiling water bath for 5 min. Samples were separated on pre-cast NuPAGE 12% Bis-Tris gels (Invitrogen) in MES buffer (Invitrogen) at 200 V for ~1 h. Gels were visualised with Coomassie Brilliant Blue [210] or GelCode Blue Stain Reagent (Pierce).

2.2.9 DNA-Binding Assay

Specific DNA-binding activity of recombinant human p53 core domain was assessed by electrophoretic mobility shift assay (EMSA). 0, 200, 400 or 600 ng of purified p53 core domain was incubated with 60 ng of ³²P end-labeled double-stranded p21 promoter [211] (5'-TGGCCATCAGGAACATGTCCCAACATGTTGAGCTCTGGCA-3' and 5'-TGCCAGAGCTCAACATGTTGGGACATGTTTCCTGATGGCC A-3'), 1 µg of poly(deoxyinosinic-deoxycytidylic) acid (Poly[dI-dC]·Poly[dI-dC]) and 0.5 µg of salmon sperm DNA (Invitrogen) in 30 mM HEPES (pH 7.5), 50 mM KCl, 5% glycerol (v/v), 4 mM DTT, 0.6 mg/ml bovine serum albumin (BSA) and 0.5% triton-X-100 (v/v) in a total volume of 12 µl on ice for 30 min. Specific p53-DNA binding was verified using a competition assay. A sample containing 400 ng of p53 core domain was prepared as described above, with the addition of 600 ng of unlabeled ("cold") p21 promoter. DNA loading buffer [210] was added to each sample followed by separation on a 5% nondenaturing polyacrylamide Tris borate gel [210] at 35 mA and 4°C for ~3 h. The gel was dried onto filter paper and visualised by phosphorimaging.

2.3 Protein Chemistry

2.3.1 Reaction Buffer

Unless stated otherwise, all protein alkylation and oxidation experiments were performed in 25 mM sodium phosphate (pH 7.2), 100 mM KCl, 0.2 mM EDTA and 20% glycerol (v/v). Buffer exchange from storage to reaction buffer was performed using PD MiniTrap G-25 columns (GE Healthcare).

2.3.2 Protein Concentration

Protein concentration was determined using the BCA Protein Assay Kit (Pierce) or from $A_{280\text{nm}}$ using the extinction coefficient $\epsilon = 17,130 \text{ M}^{-1} \text{ cm}^{-1}$ [212]. $A_{280\text{nm}}$ was measured using a NanoDrop Spectrophotometer ND-1000 (Thermo Scientific).

2.3.3 Cysteine Alkylation

2.3.3.1 Confirmation of Free Cysteine Residues

p53 core domain (30 μM) in 6 M guanidine-HCl and 25 mM sodium phosphate (pH 7.2) was incubated with 20 mM *N*-ethylmaleimide (NEM) for at least 10 min followed by desalting with off-line reverse phase LC (see Section 2.4) and analysis by MS.

2.3.3.2 Concentration-Dependent Alkylation

Wild-type or mutant p53 (35 μM) was incubated with 0 mM, 0.05 mM, 0.1 mM, 0.2 mM, 0.5 mM, 1 mM, 2 mM or 5 mM NEM for 15 min at 22°C or 37°C. At 22°C, cysteine alkylation was quenched by the addition of dithiothreitol (DTT) to a final concentration of 25 mM. At 37°C, alkylation was quenched by TCA precipitation (see 2.3.5) and precipitated protein was re-suspended in 6 M guanidine-HCl, 25 mM sodium phosphate (pH 7.2) and 25 mM DTT. Quenched samples were analysed by on-line LC-MS.

For top-down MS, p53 incubated with 0.1 mM NEM for 15 min was quenched by DTT and desalted by off-line reverse-phase LC. The fraction containing intact NEM-labelled p53 was manually collected and directly infused into the mass spectrometer.

2.3.3.3 Time-Dependent Alkylation

Wild-type or mutant p53 (35 μ M) was incubated with 1 mM (22°C) or 0.5 mM (37°C) NEM and aliquots were removed at various time points. Alkylation was quenched with DTT or TCA precipitation as described above, followed by on-line LC-MS.

2.3.4 p53 Oxidation

2.3.4.1 H₂O₂ Titration

p53 core domain (15 μ M) in 100 mM ammonium acetate was incubated with 0 mM, 1 mM, 2 mM or 10 mM hydrogen peroxide (H₂O₂) for 1 min at room temperature. The reaction was quenched by a 5 fold dilution with denaturing MS solution (50% methanol and 0.1% formic acid), followed by direct infusion into the mass spectrometer.

2.3.4.2 H₂O₂ Oxidation Over Time

Wild type or mutant p53 core domain (concentrations ranged from 100 – 150 μ M and are quoted in the text) was incubated with 4 mM H₂O₂ on ice. Aliquots were removed at various time points and oxidation was quenched by TCA precipitation. The resulting protein pellet was re-suspended in 6 M guanidine hydrochloride and 25 mM sodium phosphate (pH 7.2) supplemented with 10 mM NEM. The reaction was allowed to proceed for at least 10 min prior to on-line LC-MS.

2.3.4.3 Oxidation in the Presence of Excess Dimedone, Zn²⁺ or GSH

p53 was incubated with 4 mM H₂O₂ on ice for 1 h with the addition of either 5 mM dimedone, 2 mM zinc sulfate or 2 mM glutathione (GSH). Oxidation was quenched and free thiol groups were alkylated as described above. Protein was analysed by on-line LC-MS.

2.3.5 TCA Precipitation

p53 was precipitated using trichloroacetic acid (TCA). Ice cold 20% TCA (w/v) was added to protein samples in a 1:1 volume ratio followed by refrigeration on ice for

20-30 min. Precipitated protein was collected by centrifugation at 13,000 rpm for 5 min and protein pellets were washed with 1% TCA (w/v).

2.3.6 Affinity Purification of Oxidised p53

2.3.6.1 Biotinylation

Oxidised, NEM-labelled p53 core domain was buffer exchanged into reaction buffer containing 50 mM DTT followed by TCA precipitation. Precipitated protein was re-suspended in 6 M guanidine-HCl and 25 mM sodium phosphate (pH 7.2) supplemented with 0.4 mM EZ-Link Biotin-HPDP (Pierce). The reaction was allowed to proceed for at least 1 h at room temperature prior to avidin capture.

2.3.6.2 Capture & Elution

Biotinylated p53 was buffer exchanged into 4 M guanidine-HCl, 25 mM sodium phosphate (pH 7.2) and 200 mM KCl. Protein was mixed with monomeric avidin agarose slurry (Pierce) in a 1:2 ratio (v/v). The immobilised avidin was collected by centrifugation at 5,000 rpm and repeatedly washed with 25 mM sodium phosphate and 200 mM KCl buffer. p53 was eluted from the immobilised avidin by re-suspension in 4 M guanidine-HCl, sodium phosphate and KCl supplemented with 50 mM DTT. The p53-containing supernatant was removed and analysed by on-line LC-MS. For top-down MS, off-line LC was performed and the fraction containing intact NEM-labelled p53 was manually collected and directly infused into the mass spectrometer.

2.3.7 Proteolytic Digestion

2.3.7.1 Trypsin or Lys-C Digestion of 2NEM-p53

Quenched samples of p53 treated with 0.1 mM NEM for 15 min at 22°C were incubated with trypsin (Promega) or Lys-C (Roche) for 4 h at 37°C at an enzyme to protein ratio of ~1:20 by weight. Following Lys-C digestion, precipitated protein was collected by centrifugation at 13,000 rpm for 5 min and re-suspended in 6 M guanidine-HCl, 25 mM sodium phosphate (pH 7.2) and 10 mM DTT.

2.3.7.2 Trypsin Digestion of Oxidised p53

Precipitated p53 (~0.05mg) treated with H₂O₂ for 1 h was re-suspended in 10 µl 6 M guanidine and 25 mM sodium phosphate (pH 7.2) supplemented with 5 mM NEM. The reaction was allowed to proceed for at least 5 min prior to reduction of the guanidine concentration to 0.5 M by a 12 fold dilution with reaction buffer. Trypsin was added to give an enzyme to protein ratio of ~1:40 by weight and the solution was incubated at 37°C for 4 h.

2.3.7.3 Desalting

All digested samples were desalted and buffer exchanged into 50% acetonitrile and 0.6% formic acid using C₁₈ ZipTip pipette tips (Millipore) prior to direct infusion into the mass spectrometer.

2.4 Liquid Chromatography

Reverse-phase high performance liquid chromatography (HPLC) was performed using an Ultimate 3000 HPLC system (Dionex) equipped with a monolithic PS-DVB (500 µm X 50 mm) reverse-phase analytical column (Dionex). Buffer A consisted of 2% acetonitrile and 0.1% formic acid, and Buffer B consisted of 80% acetonitrile and 0.1% formic acid. Protein (typically ~5 pmoles) was loaded directly onto the column (maintained at 60°C) followed by a 5 min washing step (diverted to waste) with 4% Buffer B. Protein was eluted from the column during a 10 min linear gradient from 4% - 100% Buffer B (20 µl/min flow rate).

On-line LC-MS was achieved by coupling the reverse-phase column to a Triversa NanoMate (Advion BioSciences) for nano-electrospray ionisation (nanoESI). Acquisition of LC-MS data was controlled by HyStar software (Bruker Daltonics).

2.5 Mass Spectrometry

2.5.1 Sample Preparation

For direct MS analysis of purified recombinant wt and mutant p53 core domain, protein was buffer exchanged into 50 mM ammonium acetate (~ pH 7) using

PD MiniTrap G-25 columns (GE Healthcare) followed by dilution with the appropriate MS solvent.

2.5.1.1 Denaturing Conditions

For denatured protein mass spectra, p53 was typically diluted to a concentration of ~10 μ M with 50% methanol (MeOH) and 0.1% formic acid.

2.5.1.2 Native Conditions

For native protein mass spectra, p53 was typically diluted to a concentration of ~15 μ M with 50 mM ammonium acetate (~pH 7) and 10% MeOH was added to aid desolvation.

2.5.2 Ionisation Source

2.5.2.1 ESI

Electrospray ionisation was achieved using an electrospray nebulizer (Bruker Daltonics). The capillary voltage and end plate offset were typically 4500 V and -500 V respectively.

2.5.2.2 Nano-ESI

Nano-electrospray ionisation (nESI) was achieved using the TriVersa NanoMate (Advion BioSciences). The NanoMate was operated in 'infusion' mode for direct infusion of protein/peptide samples into the mass spectrometer or 'LC chip coupling' mode for on-line LC-MS. Gas pressure was typically ~0.4 psi and spray voltage ~1.5 kV.

2.5.3 FT-ICR Mass Spectrometry

All mass spectra, with the exception of those displayed in Figures 3.8, 4.3, 4.14, 4.15 and 4.16, were recorded on an apex-Qe FT-ICR mass spectrometer equipped with a 12 Tesla superconducting magnet (Bruker Daltonics). The remaining spectra were recorded on a solariX FT-ICR mass spectrometer equipped with a 12 T magnet (Bruker Daltonics). Source pressure was typically $\sim 4 \times 10^{-6}$ mbar. Ion and source

accumulation times were typically 0.7 s on the apex-Qe and 0.1 s on the solariX instrument. Ions were trapped using a 6 cm × 10 cm Infinity cell Penning trap (Bruker Daltonics), and the front and back plate trapping potentials were typically 1.4 V on the apex-Qe, and 0.4 V and 0.6 V respectively on the solariX. Trapped ions were excited by a frequency chirp and detected over an m/z range of 500-3800 for denaturing conditions, and an m/z range of 800-4000 for native conditions. Direct infusion spectra were typically the sum of 100 acquisitions. Each individual LC-MS spectrum was the sum of 2 acquisitions. Transient data size was 512 kword for each acquisition and sine-bell multiplication apodization was applied to each transient during FT-MS post-processing.

2.5.4 Tandem FT-ICR Mass Spectrometry

MS/MS was performed on an apex-Qe FT-ICR mass spectrometer. Specific ion species were isolated using the mass resolving quadrupole and MS/MS was performed using either collision-induced dissociation (CID) or electron capture dissociation (ECD). Ion accumulation time was often increased to at least 1 s in order to maximise ion abundance. Fragmentation spectra were the sum of 100-500 acquisitions over a typical m/z range of 500-3800.

2.5.4.1 CID

Typical collision energy values for fragmentation of intact p53 or the p53 peptide Gln165 - Lys291 were between -10 and -22 eV. The collision energy used to fragment the p53 tryptic peptide VCACPGR was -29 eV.

2.5.4.2 ECD

For ECD fragmentation of intact p53 or the p53 peptide Gln165 - Lys291, 1.8 A was applied to the hollow dispenser cathode (HeatWave Technologies) and pulse lengths were between 8 -18 ms. The ECD lens and bias voltages were typically 20.0 V and 1.2 V respectively.

2.5.5 Calibration

All mass spectra were calibrated externally using ESI tuning mix (1 in 20 dilution with acetonitrile) or ESI-L low concentration tuning mix (Agilent Technologies).

2.5.6 Data Analysis

All mass spectra were analysed using DataAnalysis software (Bruker Daltonics).

2.5.6.1 Isotope Modelling and Mass Error

Isotope distributions of specific charge states were predicted from theoretical empirical formulae (determined using Bruker Daltonics IsotopePattern software). These were overlaid upon recorded experimental distributions as scatter plots, with the theoretical apex of each isotope peak designated by a circle. Mass measurement error (MME) was calculated in parts per million (ppm) from the most abundant isotope peak of a specific charge state using the following equation, where m_{ex} is the experimental m/z (or mass in Da) and m_{cal} is the calculated m/z (or mass in Da) [213]:

$$\text{MME (ppm)} = \frac{m_{\text{ex}} - m_{\text{cal}}}{m_{\text{cal}}} \times 10^6$$

2.5.6.2 Neutral Spectra

Neutral spectra were created using Maximum Entropy deconvolution and relative ratios of alkylated forms of p53 were calculated from peak heights [214].

2.5.6.3 Fragmentation Data

The SNAP algorithm was used for automated monoisotopic peak peaking of fragmentation spectra. The resulting mass lists were searched for b and y or c and z ions corresponding to each permutation of the relevant amino acid sequence modified with the relevant number of NEM groups using BioTools software (Bruker Daltonics). Each permutation was then ranked by the associated number of assigned non-redundant fragments ions and the highest-ranked results were further

interrogated using ProSight PTM software [215]. Mass error tolerances were exclusively 10 ppm.

2.5.6.4 Trypsin Digest Spectra

Monoisotopic peak lists were generated as described above and searched for tryptic peptides corresponding to the relevant form of alkylated p53 using BioTools software (Bruker Daltonics). Three missed cleavages were allowed and the error tolerance was 10 ppm. Mass spectra of digested oxidised p53 were also manually searched for crosslinked peptides.

2.6 X-ray Crystal Structures

X-ray crystal structures were obtained from the RCSB Protein Data Bank (PDB). Figures were generated using PyMol software (DeLano Scientific) and PDB IDs are stated in the figure captions and in the text.

Chapter 3: Recombinant p53 Core Domain

3.1 Introduction

All experiments detailed in this thesis were performed using recombinant human p53 core domain (a.a. residues 94-312). As described in Section 1.2.3, the core domain contains each of the ten cysteine residues in human p53 and comprises an independently folded, compact structural region of the full length protein. This domain is responsible for the specific DNA-binding function of p53 and contains the majority of mutation sites that are identified in human cancers [66, 68, 72, 81]. There are several major advantages associated with studying the p53 core domain rather than the full length protein, which is very sensitive towards thermal denaturation and spontaneously unfolds and aggregates at physiological temperature *in vitro* [216, 217].

Recombinant expression of full length p53 in *E. coli* results in the accumulation of insoluble inclusion bodies and several denaturing and renaturation steps are required for purification of the folded active protein, often resulting in low yields [218, 219]. Soluble, folded full length p53 can successfully be expressed in insect cells using a baculovirus expression system. However, the protein will be post-translationally modified resulting in a heterogeneous protein mixture [220]. The p53 core domain is known to be more stable in solution than full length p53 [217], and recombinant expression in *E. coli* provides soluble, unmodified protein which requires a simple one- or two-step purification procedure, resulting in a moderate protein yield (~5 mg/L of cell culture). Moreover, because dissociation efficiency decreases as protein size increases [131], top-down fragmentation of the p53 core domain is likely to yield higher sequence coverage and to provide more unambiguous information about the location of Cys-modifications when compared to a similar analysis of full length p53. At 46 kDa, full length p53 is near to the ~50 kDa dissociation limit using post-source fragmentation techniques, whereas at 25 kDa, the core domain is well within this limit [165]. Clearly, the disadvantage of only studying the core domain is that the affect of the N-terminal transactivation domain and C-terminal regulatory domain on cysteine reactivity will be unknown.

Table 3.1 Average molecular masses of p53 variants studied for this thesis.

Variant	Average Molecular Mass / Da	
	<i>apo</i>	<i>holo</i>
wt p53	24,550.64	24,616.04
C182S and C277S	24,534.57	24,599.97
C182/277S	24,518.51	24,583.90

In this chapter a brief account of the expression and purification of wild type (wt) and several mutant forms of the p53 core domain is provided (see Section 2.2 for a detailed description of the expression and purification methods), together with a description of the initial characterisation of the recombinant p53 variants by FT-ICR mass spectrometry. The specific DNA-binding activity of wt p53 core domain was also assessed. For reference, the average molecular masses of the *apo* (no zinc) and *holo* (zinc bound) forms of the p53 variants described in this thesis are listed in Table 3.1.

3.2 Expression and Purification

Untagged human p53 core domain was overexpressed from the pRSET(A) vector in *E. coli* C41(DE3). *E. coli* C41(DE3) is a mutant strain of BL21(DE3), which is often used for over-production of toxic or insoluble recombinant proteins [221, 222]. p53 core domain was initially purified on the basis of its charge using ion exchange chromatography [223]. A typical cation exchange chromatogram for wt p53 (purified on a 10 ml Resource S column) is shown in Figure 3.1A. At pH 7.2, p53 core domain elutes at a NaCl concentration of approximately 200 mM.

The level of p53 purity obtained from ion exchange chromatography was sufficient for the experiments described throughout this thesis. However, protein purity can be increased by performing gel filtration chromatography (purification on the basis of molecular weight) [223] following the ion exchange step. A typical gel filtration chromatogram for wt p53 core domain is shown in Figure 3.1B. A single symmetrical peak was obtained, indicating protein homogeneity, and the volume at which the protein eluted corresponded to the monomeric form of p53 core domain

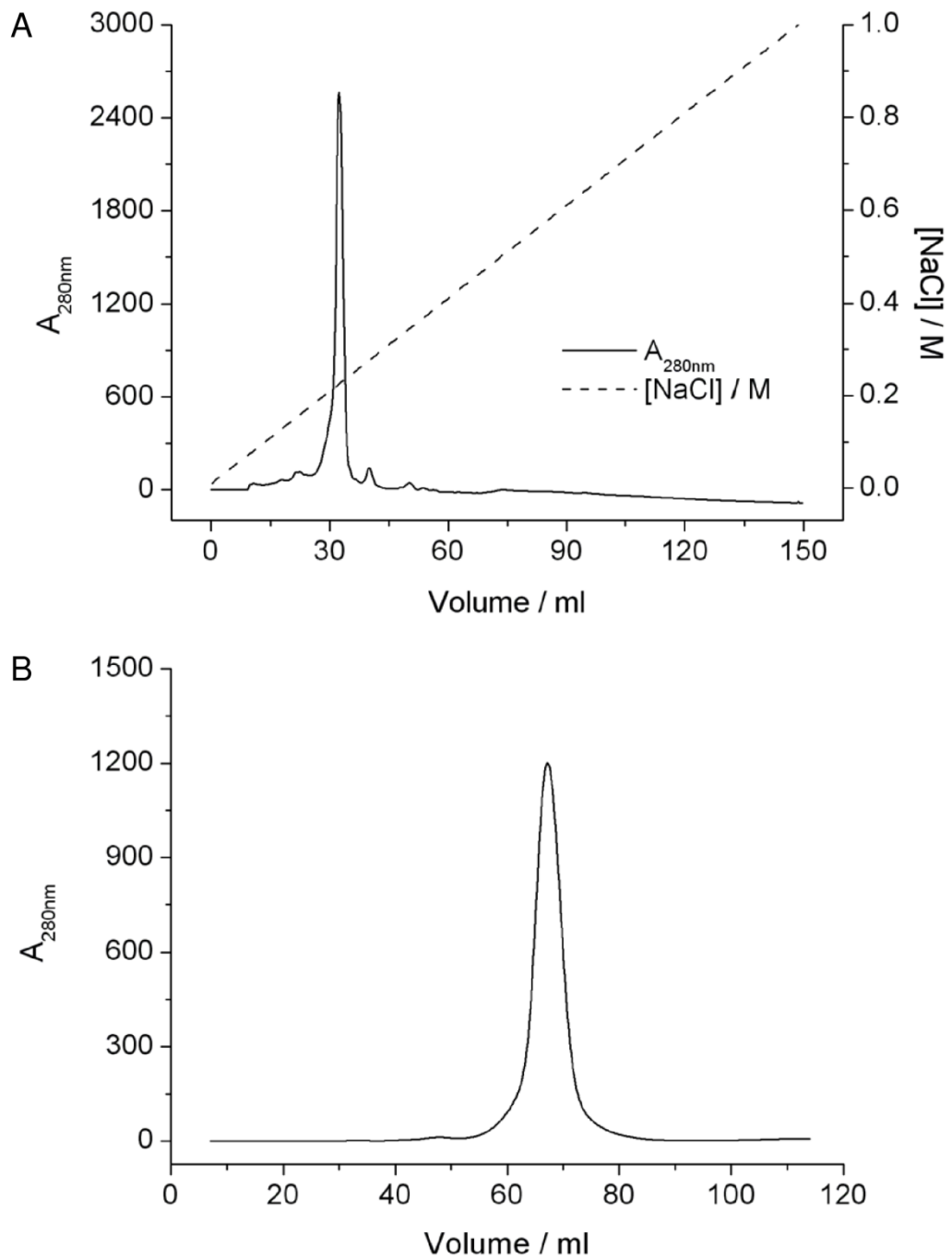


Figure 3.1 Purification of wt p53 core domain. **(A)** Ion exchange chromatogram. Purification on the basis of protein charge using a Resource S cation exchange column over a NaCl gradient from 0-1 M. **(B)** Gel filtration chromatogram. Purification on the basis of molecular weight using a Superdex 75 column under isocratic conditions.

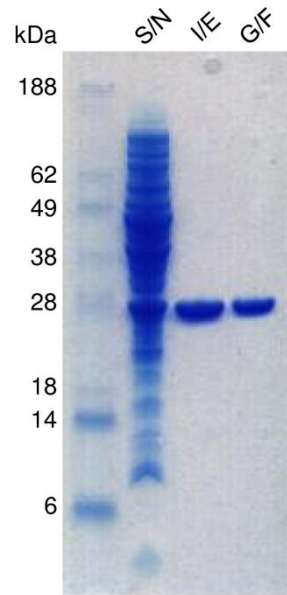


Figure 3.2 Purification of wt p53 core domain. Protein gel electrophoresis of supernatant containing soluble protein from lysed *E. coli* (S/N), combined protein-containing fractions from ion exchange chromatography (I/E) and combined protein-containing fractions from gel filtration chromatography (G/F). The molecular weight (M_w) of the purified protein is consistent with the M_w of p53 core domain (25 kDa).

(based on the calibration curve for the column used). p53 overexpression and purification by ion exchange and gel filtration chromatography was checked by protein gel electrophoresis (see Figure 3.2). Protein bands are consistent with the molecular weight of p53 core domain and the gel indicated < 95% purity.

A typical yield of wt p53 core domain was found to be ~4 mg/L of cell culture. Interestingly, the yield of each of the cysteine to serine mutants was ~6 mg/L of cell culture.

3.3 Characterisation by FT-ICR Mass Spectrometry

3.3.1 Denaturing Conditions

Recombinantly produced wt p53 core domain was analysed by nESI FT-ICR mass spectrometry under protein denaturing conditions (50% methanol, 50% water and 0.1% formic acid). A typical mass spectrum is shown in Figure 3.3. The charge state

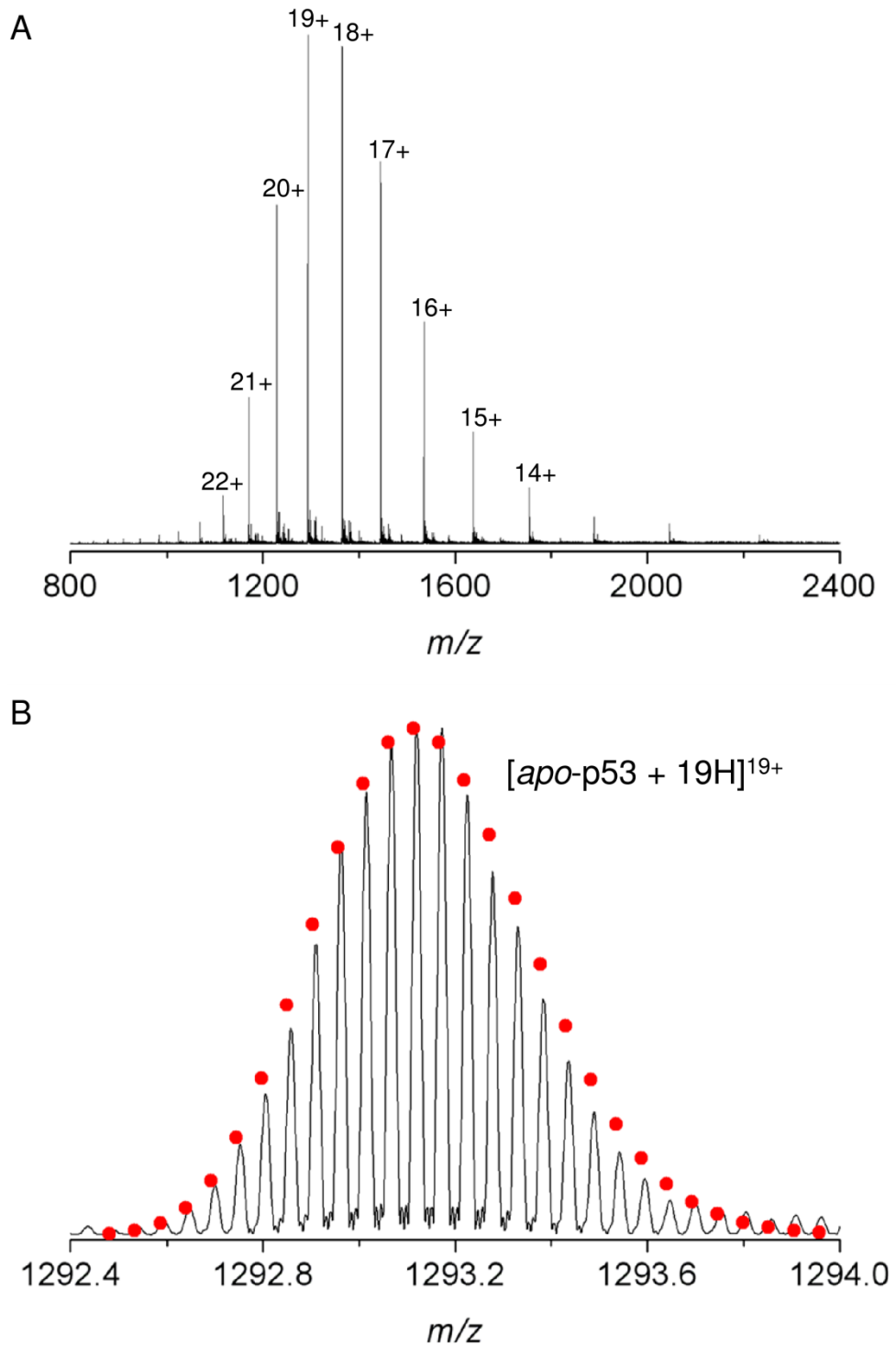


Figure 3.3 nESI FT-ICR MS of recombinant p53 core domain recorded under denaturing conditions. **(A)** Charge state distribution. **(B)** 19+ charge state. The simulated isotope distribution is consistent with the experimental isotope distribution for unmodified p53 core domain (empirical formula $[C_{1055}H_{1692}N_{321}O_{324}S_{16}]^{19+}$; •; 5 ppm MME).

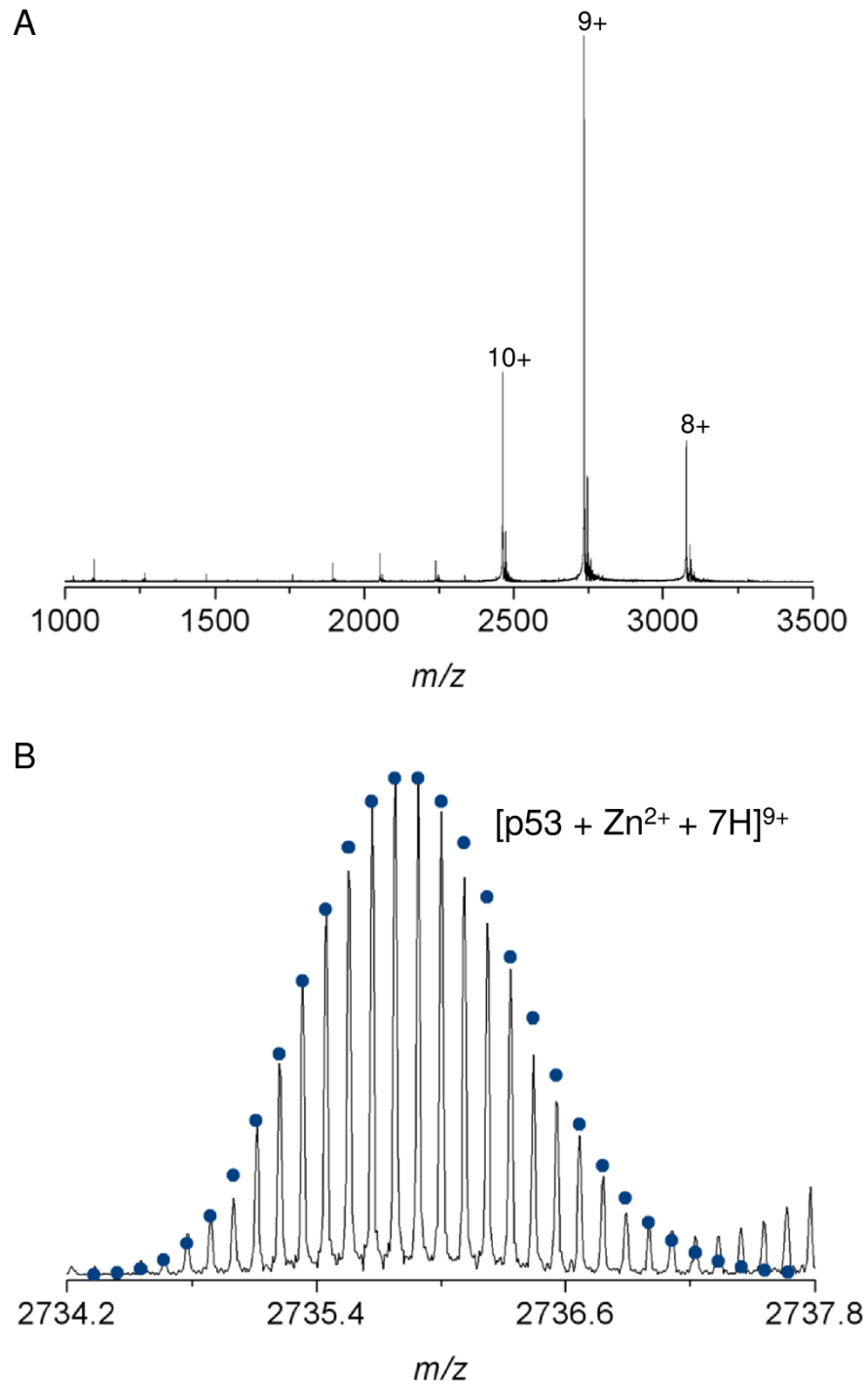


Figure 3.4 nESI FT-ICR MS of recombinant p53 core domain recorded under native conditions. **(A)** Charge state distribution. **(B)** 9+ charge state. The simulated isotope distribution is consistent with the experimental isotope distribution for p53 core domain non-covalently bound to one zinc ion (empirical formula $[C_{1055}H_{1680}N_{321}O_{324}S_{16}Zn]^{9+}$; •; MME < 1 ppm).

distribution is relatively broad, from $[M + 11H]^{11+}$ to $[M + 29H]^{29+}$, consistent with the protein being denatured and losing its native fold. The simulated isotope distribution for the 19+ charge state of *apo* wt p53 core domain is consistent with the experimental isotope distribution, confirming that recombinant p53 core domain is unmodified and that each Cys residue is in the reduced form. As expected, the non-covalent interaction between p53 and zinc was not retained under these denaturing conditions. The deconvoluted mass of *apo*-p53 calculated from the most abundant measured isotope was 24,550.2743 Da. This varied from the theoretical deconvoluted mass by 0.1178 Da, corresponding to an MME of 5 ppm.

3.3.2 Native Conditions

Recombinant wt p53 core domain was analysed by nESI FT-ICR MS under native conditions (50 mM ammonium acetate ~pH 7 and 10% methanol). A resulting mass spectrum is shown in Figure 3.4. The most abundant molecular ion has a charge of 9+, compared to 19+ for p53 in denaturing conditions, and the predominate charge states form a much narrower distribution than the distribution that is observed in the spectrum for denatured p53. The theoretical isotope distribution for the 9+ charge state of *holo*-p53 core domain is consistent with the experimental isotope distribution, illustrating that the non-covalent interaction between p53 and one Zn^{2+} ion was retained. No *apo*-p53 was detected in the spectrum. However, adducts of 98 Da were observed, corresponding with the non-covalent interaction between p53 and either an inorganic phosphate ($[H_2PO_4]^-$) or sulfate ($[HSO_4]^-$) ion. The deconvoluted mass of *holo*-p53 calculated from the most abundant measured isotope was 24,615.0065 Da. This varied from the theoretical deconvoluted mass by 0.0117 Da, corresponding to an MME of less than 1 ppm.

Zinc is known to induce p53 to fold into its active wt conformation [90]. Therefore, the data shown here indicate that recombinant wt p53 core domain is correctly folded into its native, active conformation. The p53 DNA-binding domain has been shown to cycle through various folded, unfolded and partially folded states *in vitro* [91, 224, 225]. A distribution of low abundance charge states, from 11+ to

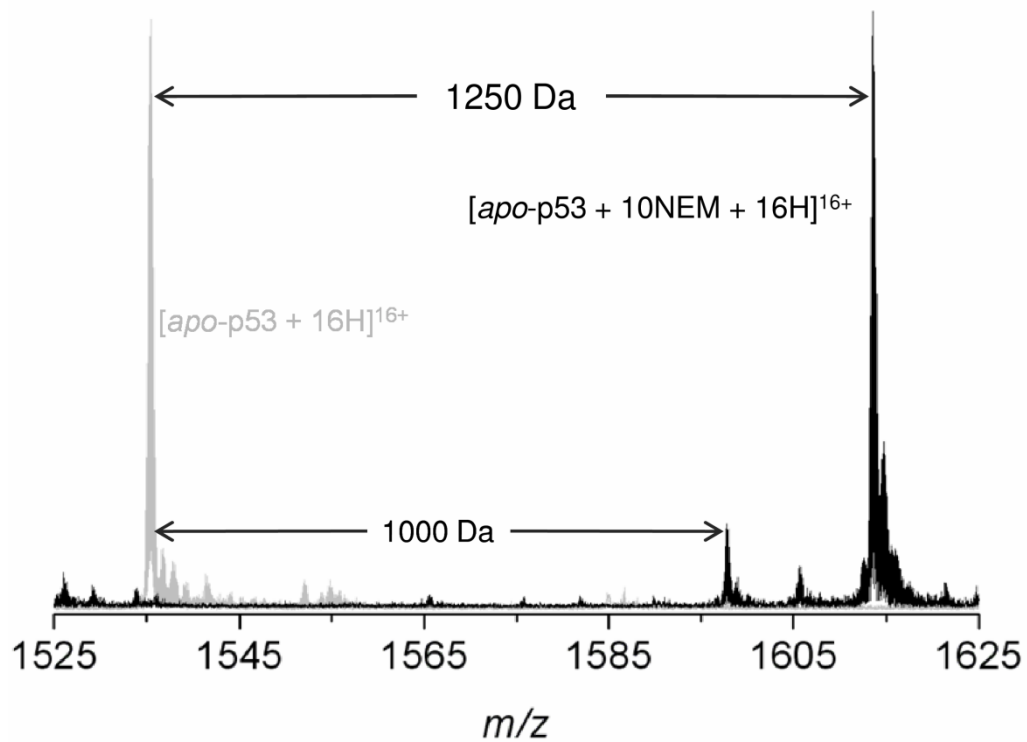


Figure 3.5 Confirmation of free cysteine residues in recombinant p53 core domain. p53 was incubated with the thiol alkylating reagent *N*-ethylmaleimide (NEM; 125 Da) followed by FT-ICR MS analysis. The observed mass shift from untreated p53 was consistent with the addition of 10 NEM groups.

14+, was observed in the native mass spectrum of p53 core domain. These low abundance species of intermediate charge may represent a partially unfolded form of *holo*-p53. Unfolding of the p53 DNA-binding domain could be further interrogated by recording ESI mass spectra over a range of pH values [151, 152].

3.3.3 Confirmation of Free Cysteine Residues

In order to test for the presence of ten free thiol groups in the recombinant p53 core domain, purified wt p53 (~30 μ M) was incubated with an excess of the thiol alkylating reagent *N*-ethylmaleimide (NEM; 125 kDa; 20 mM) followed by off-line reverse phase liquid chromatography (LC) and analysis by nESI-FT-ICR MS. In Figure 3.5, the resulting mass spectrum is overlaid upon a mass spectrum of untreated p53 core domain to illustrate the mass increase upon reaction with NEM.

The 1250 Da mass increase is consistent with the addition of 10 NEM groups, confirming the presence of 10 Cys residues in the reduced form. Interestingly, a small degree of p53 core domain modified with 8 NEM groups was also observed, suggesting that one disulfide bond was present. This observation is discussed further in Chapter 5.2.

3.4 DNA-Binding Assay

In order to verify correct protein folding, purified wt p53 core domain was assessed for its specific DNA-binding activity by electromobility shift assay (EMSA). p53 (0 ng, 200 ng, 400 ng and 600 ng) was incubated with a ^{32}P -labelled consensus DNA sequence followed by separation on a non-denaturing polyacrylamide gel, as shown in Figure 3.6. It can be seen that as p53 concentration increased, the formation of a protein-DNA complex increased, and the amount of free consensus DNA (free probe) decreased. The addition of an excess of unlabeled consensus DNA (cold probe) resulted in a decrease in p53-DNA signal, indicating that the unlabeled DNA was competing with the labelled DNA for the same binding site, and that the p53-DNA interaction was specific. These results suggest that recombinantly produced p53 core domain was in its native folded form.

3.5 p53 Cysteine Mutants

Several experiments described in this thesis involved the analysis of p53 core domain in which the cysteine residues had been mutated to serine residues. Serine is structurally similar to cysteine, the only difference being the substitution of the thiol group ($-\text{SH}$) for a hydroxyl ($-\text{OH}$) group. Oxygen is far more electronegative than sulfur. Therefore, thiols are generally better nucleophiles than analogous oxygen compounds, and unlike cysteine, serine is not susceptible to oxidation. Cys-Ser mutations can, therefore, be used to investigate sites of Cys-modification whilst limiting the effect on protein conformation.

The p53 core domain Cys-Ser mutants studied for this thesis were C182S, C277S and the double mutant C182/277S. Site-directed mutagenesis was performed in order

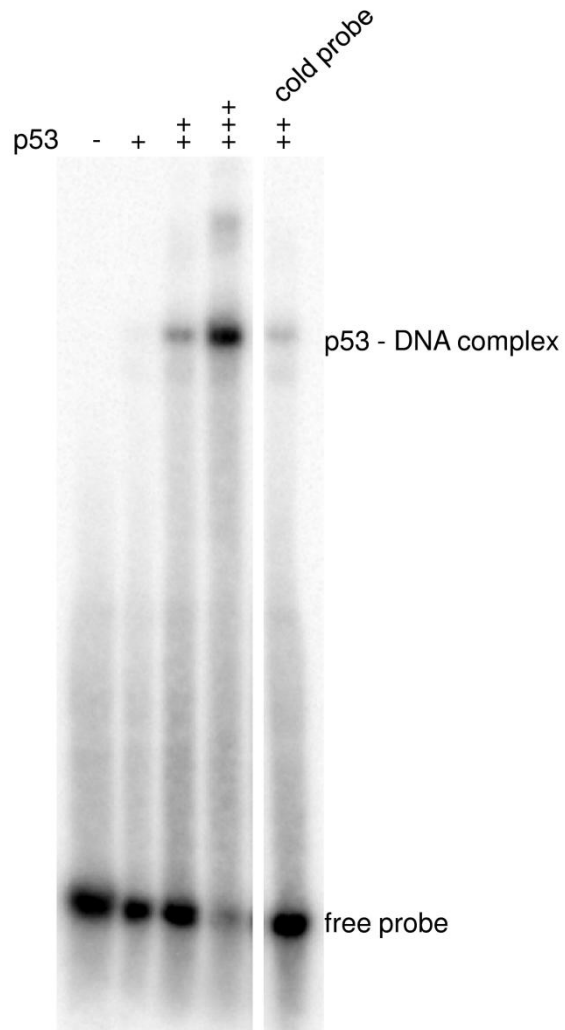


Figure 3.6 Specific DNA-binding of recombinant p53 core domain. Wt p53 (0 ng, 200 ng, 400 ng or 600 ng) was incubated with ^{32}P -labeled p21 promoter and analysed by electromobility shift assay (EMSA). Specific DNA-binding was verified by the addition of an excess of unlabeled p21 promoter (cold probe).

to create the necessary single point mutations in the p53 gene insert of plasmid DNA and each Cys mutant was expressed and purified following the methods described above. Each mutant was analysed by reverse phase LC FT-ICR MS and the resulting isotope distributions are displayed in Figure 3.7. The theoretical isotope distribution is consistent with the experimental isotope distribution for each mutant, corresponding to the correct replacement of a Cys residue with a Ser residue in each case.

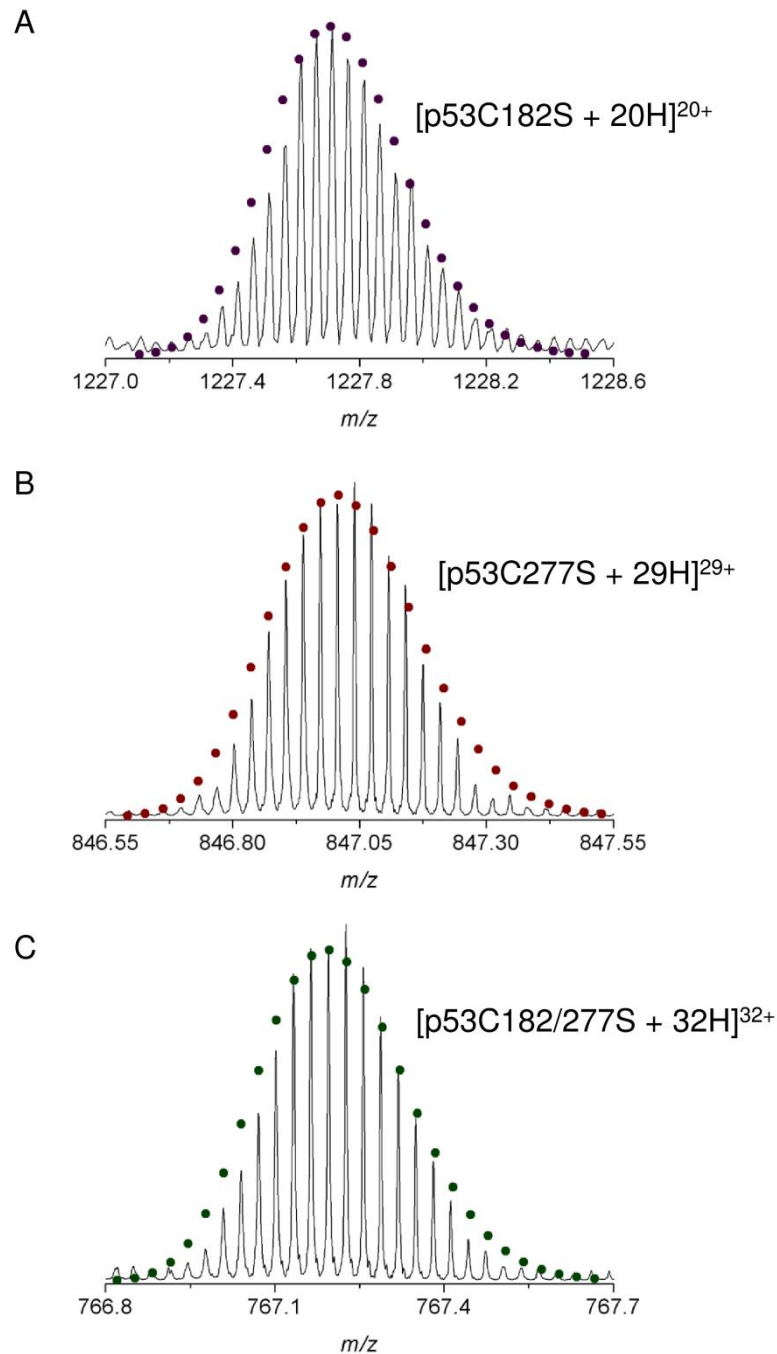


Figure 3.7 Isotope distributions of recombinant p53 core domain cysteine to serine mutants. Theoretical isotope distributions are consistent with the experimental isotope distributions of **(A)** p53C182S (20+ charge state; empirical formula $[C_{1055}H_{1693}N_{321}O_{325}S_{15}]^{20+}$; •) **(B)** p53C277S (29+ charge state; empirical formula $[C_{1055}H_{1702}N_{321}O_{325}S_{15}]^{29+}$; •) and **(C)** p53C182/277S (32+ charge state; empirical formula $[C_{1055}H_{1705}N_{321}O_{326}S_{14}]^{32+}$; •). The MME for each species is 3 ppm.

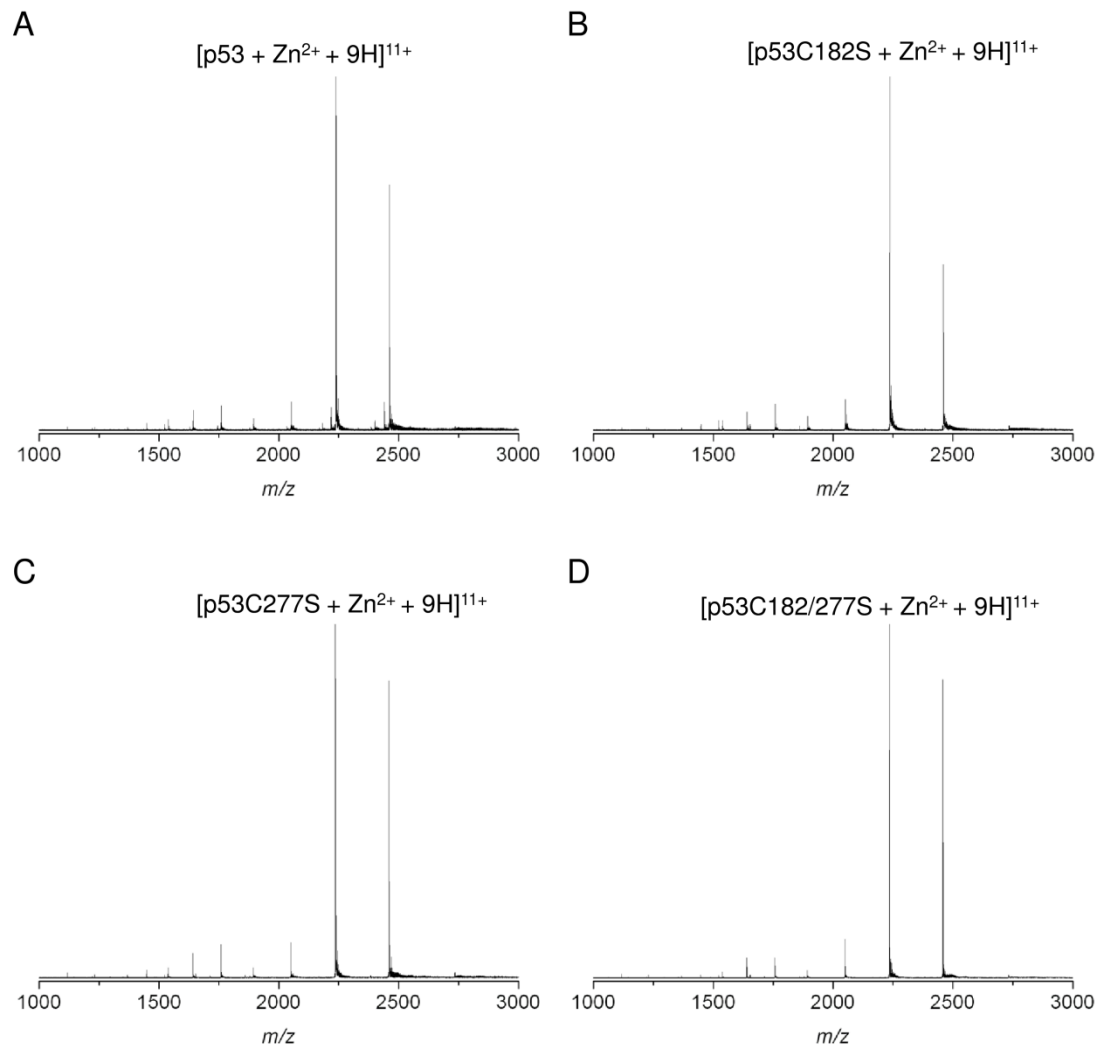


Figure 3.8 ESI FT-ICR mass spectra of recombinant wt and mutant p53 core domain recorded under native MS conditions. **(A)** wt p53 **(B)** p53C182S **(C)** p53C277S and **(D)** p53C182/277S. The native charge state distributions of the Cys mutants are consistent with the charge state distribution of native wt p53, indicating correct folding of the p53 core domain mutants.

Each Cys mutant was also analysed by ESI^{§§}-FT-ICR MS under native conditions in order to evaluate the affect of the mutations on zinc-binding and protein folding. The mass spectra of the mutant proteins display similar charge state distributions to the wt protein (see Figure 3.8) and the deconvoluted masses were consistent with the theoretical relative molecular masses for *holo* C182S, C277S and C182/277S. Taken together, these observations show that recombinant p53 core domain Cys-Ser mutants retain the ability to bind to Zn²⁺ and suggest that each mutant was correctly folded in solution.

3.6 p53 Cancer Mutant R175H

Arginine 175 is one of the six most frequently mutated residues in p53 found in human cancers (along with G245, R248, R249, R273 and R282), with mutation to a histidine residue being the most predominate substitution [226]. Of the most commonly occurring p53 cancer hotspot mutants, R175H has the lowest thermodynamic stability [212, 227] and displays a substantially enhanced rate of Zn²⁺ loss compared to wt p53 [91]. Recombinant expression and purification of p53 core domain mutant R175H was attempted in order to interrogate the zinc-binding and cysteine redox properties of this important, predominately unfolded, cancer mutant using high resolution FT-ICR mass spectrometry. It has been proposed that the R175H mutant is prone to cysteine oxidation, due to perturbation of the tetrahedral geometry of the zinc-binding domain [118]. FT-ICR MS of p53 core domain R175H has the ability to unambiguously determine the oxidation state of each of the 10 Cys residues in this protein, as demonstrated in Chapters 4 and 5.

Site-directed mutagenesis was performed in order to create the single point mutation in the plasmid DNA necessary to code for His instead of Arg at codon 175. The correct sequence over the p53 encoding region of the plasmid was confirmed by DNA-sequencing. However, the protein expression protocol described in Chapter 2.2 repeatedly failed to result in overexpression of the R175H mutant. Low-level expression of R175H did occur, as confirmed by FT-ICR MS, following ion

^{§§}Standard ESI was found to be more effective than nano-ESI for FT-ICR MS of p53 under native conditions.

exchange chromatography and extensive concentration of the FPLC fraction at the expected time of protein elution (data not shown). The protocol for recombinant expression of R175H p53 core domain described in Ref. [212] was also followed, and the Invitrogen Cell-Free Expression System was used. However, neither of these methods resulted in overexpression of R175H p53. Steps that can be taken in the future to try and induce the recombinant overexpression of p53 R175H mutant include lowering the expression temperature to 18°C [91] and supplementing the growth medium with Zn^{2+} in an attempt to prevent aggregation [91]. Additionally, alternative strains of *E. coli* could be tested, such as the BL21 Star (DE3) strains (available from Invitrogen), which have increased mRNA stability [228].

Chapter 4: Identification of Reactive Cysteine Residues

4.1 Introduction

As described in Chapter 1.1.2, the reactivity of cysteine residues varies depending on the pK_a of the thiol proton. For example, the two reduced Cys residues present in the active site of *E. coli* thioredoxin, Cys32 and Cys35, display markedly different reactivity towards the thiol alkylating reagent iodoacetic acid at pH 8.0, due to their respective pK_a values of 6.2 and 9.0 [229].

The relative reactivity of each cysteine residue within p53 is yet to be clearly defined. This is due, in part, to an inability of the methods used previously to determine the modification/oxidation state of each of the 10 Cys residues within p53. Here, the reactivity of p53 Cys residues towards alkylation with the thiol-derivatizing reagent *N*-ethylmaleimide (NEM; Figure 4.1) has been investigated [230]. NEM is a α,β -unsaturated carbonyl compound and nucleophilic thiols undergo conjugate addition to the electrophilic C=C double bond (isolated C=C double bonds are nucleophilic but C=C double bonds conjugated with carbonyl groups are electrophilic) [231]. The addition of one NEM group to a Cys residue corresponds with a monoisotopic mass increase of 125.0477 Da.

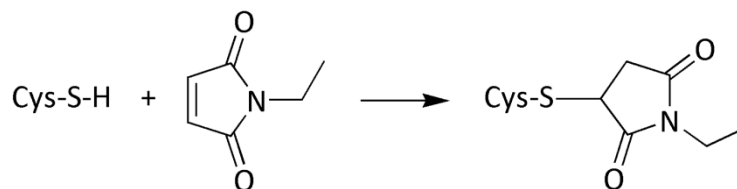


Figure 4.1 Alkylation of cysteine by *N*-ethylmaleimide (NEM).

Interestingly, NEM has been shown to have a concentration-dependent affect on specific DNA-binding of p53. Relatively low concentrations of NEM have previously been shown to increase binding of p53 to a consensus oligonucleotide [232], whereas an excess of NEM has been shown to result in decreased DNA-binding [95]. A similar trend has also been observed for alkylation of wt and mutant p53 by the anti-tumour maleimide compound MIRA-1 and its analogues [115].

FT-ICR mass spectrometry of intact p53 core domain alkylated under various conditions has revealed that alkylation of p53 proceeds in distinct steps. Furthermore, the use of top-down and middle-down MS allowed the oxidation/modification state of each of the 10 Cys residues to be defined, thus revealing the most reactive cysteine residues present in the p53 tumour-suppressor protein and providing evidence for their role in p53 redox-regulation.

4.2 Alkylation of p53 Cysteine Residues

4.2.1 Concentration Dependence

p53 core domain (35 μ M) was incubated with increasing concentrations of NEM for 15 min at 22°C. Cysteine alkylation was quenched by the addition of an excess of the thiol-containing reducing agent dithiothreitol (DTT) and the degree of p53 alkylation was monitored by reverse-phase on-line liquid chromatography FT-ICR MS. Neutral mass spectra were created using maximum entropy deconvolution and the relative ratio of alkylated/non-alkylated forms of p53 were calculated from MS peak heights. This method for measuring the relative amounts of differentially modified proteins is based on the principle that the ionisation efficiency of an intact protein (> ~10 kDa) is not significantly affected by its PTM state [233, 234].

The neutral mass spectra are shown in Figure 4.2A and clearly show that, at low concentrations of alkylating reagent (NEM < 1 mM), p53 was predominantly modified with two NEM groups (2NEM-p53), and at higher concentrations of alkylating reagent (NEM > 1 mM), p53 was predominately modified with 10 NEM groups, i.e. all Cys residues had been alkylated. At 0.1 mM NEM, 80% of p53 was dialkylated and at 2 mM NEM, 67% of the protein was fully alkylated. Approximately 100% of p53 had been converted to 10NEM-p53 with 5 mM NEM. Interestingly, the formation of tri-alkylated p53 correlated with the formation of fully alkylated p53, and only relatively small amounts of species with intermediate stages of alkylation (4NEM-p53 – 9NEM-p53) were detected. At 1 mM NEM, 34% of p53 was dialkylated, 29% of p53 was fully alkylated, 5% of p53 was modified with four NEM groups, 5% of p53 was modified with five NEM groups and 3% of p53 was modified with six NEM groups.

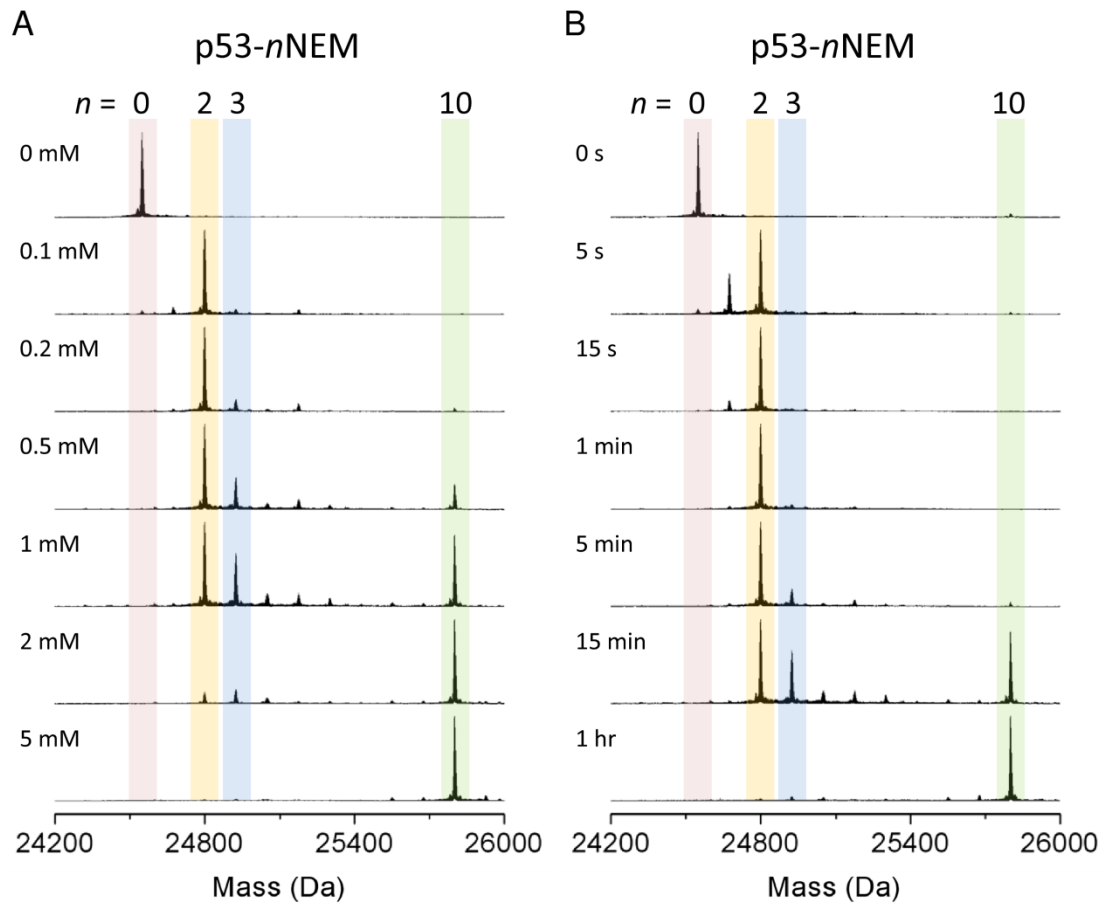


Figure 4.2 Reaction of p53 core domain with *N*-ethylmaleimide. **(A)** NEM titration. p53 was incubated with varying concentrations of NEM for 15 min. Deconvoluted mass spectra are shown. **(B)** Cysteine alkylation over time. p53 was incubated with 1 mM NEM and deconvoluted mass spectra are shown for various time points.

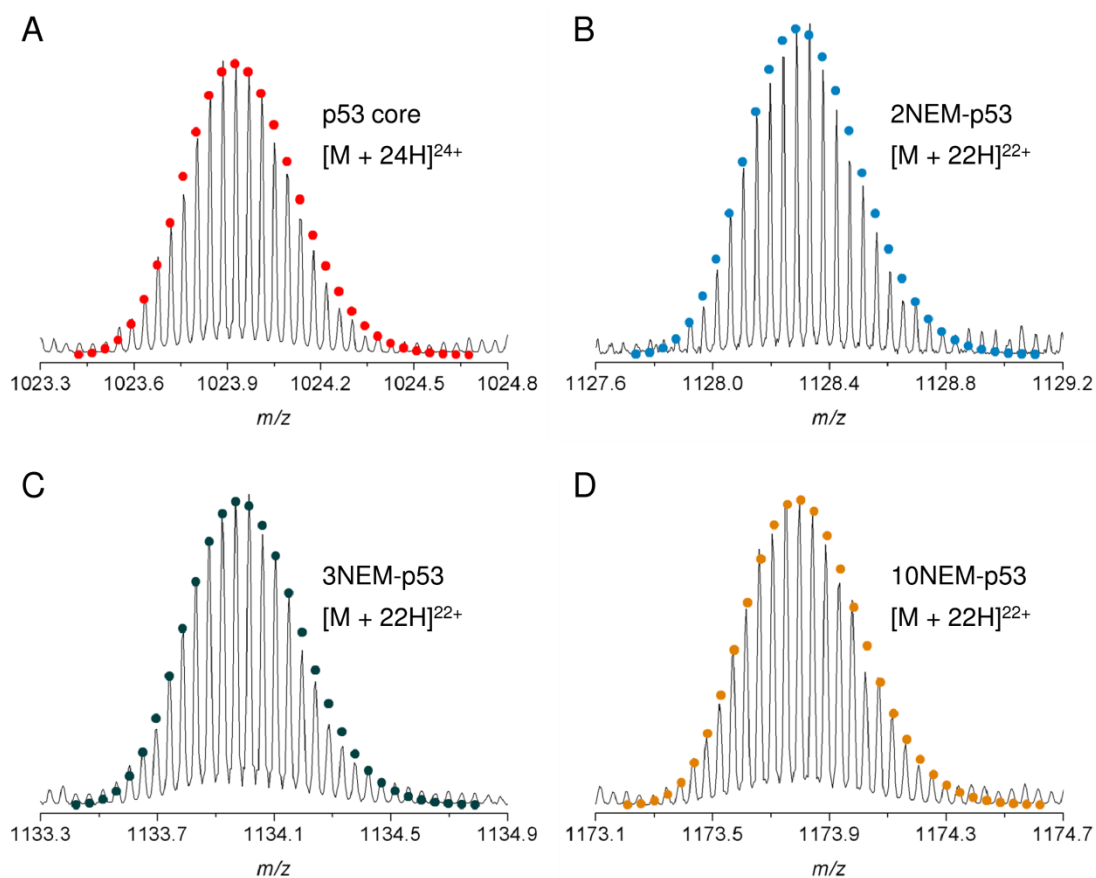


Figure 4.3 Isotope distributions of p53 core domain recorded before and after alkylation with NEM. Theoretical isotope distributions are consistent with the experimental isotope distributions for **(A)** fully reduced unmodified p53 core domain (24+ charge state; empirical formula $[C_{1055}H_{1697}N_{321}O_{324}S_{16}]^{24+}$; •; 2 ppm MME) **(B)** 2NEM-p53 (22+ charge state; empirical formula $[C_{1067}H_{1709}N_{323}O_{328}S_{16}]^{22+}$; •; 3 ppm MME) **(C)** 3NEM-p53 (22+ charge state; empirical formula $[C_{1073}H_{1716}N_{324}O_{330}S_{16}]^{22+}$; •; 3 ppm MME) and **(D)** 10NEM-p53 (22+ charge state; empirical formula $[C_{1115}H_{1765}N_{331}O_{344}S_{16}]^{22+}$; •; 1 ppm MME).

The identity of each p53 species was confirmed by comparison of the theoretical isotope distributions with the experimental isotope distributions observed in the undeconvoluted spectra (see Figure 4.3). The MME for each species was < 4 ppm.

4.2.2 Time Dependence

To monitor the time dependence of alkylation, p53 (35 μ M) was incubated with 1 mM NEM at 22°C, and the reaction was quenched with an excess of DTT at various time points followed by on-line LC FT-ICR MS. The neutral mass spectra (see Figure 4.2B) clearly show that two Cys residues in p53 react rapidly to form a dialkylated species. After 5 s, 32% of p53 was monoalkylated and 63% of p53 dialkylated. By 15 s, the proportion of 2NEM-p53 had increased to 85% and by the 1 min time point 100% of p53 had been dialkylated. Alkylation of a third Cys residue was not apparent until 5 min, at which point the formation of 10NEM-p53 was also observed.

Taken together, the concentration and time-dependence results show that alkylation of p53 cysteine residues proceeds in distinct steps. Initially, two Cys residues are alkylated to form a stable dialkylated species. An increase in NEM concentration or time results in alkylation of a third Cys residue, which appears to trigger rapid alkylation of the remaining seven Cys residues, illustrated by the relative low abundance of intermediate stages of alkylated p53 in the mass spectra.

4.2.3 Alkylation at Physiological Temperature

The p53 core domain is known to have a low thermodynamic stability [235] and to unfold at body temperature [236]. Therefore, concentration and time dependence of p53 alkylation was investigated at 37°C. p53 (35 μ M) was incubated with increasing concentrations of NEM for 15 min, or 0.5 mM NEM was incubated with p53 for increasing amounts of time. Protein precipitation was observed at 37°C. Hence, cysteine alkylation was quenched by TCA precipitation followed by re-suspension of protein in 6 M guanidine and 25 mM DTT. This ensured that all protein was in solution prior to LC FT-ICR MS analysis.

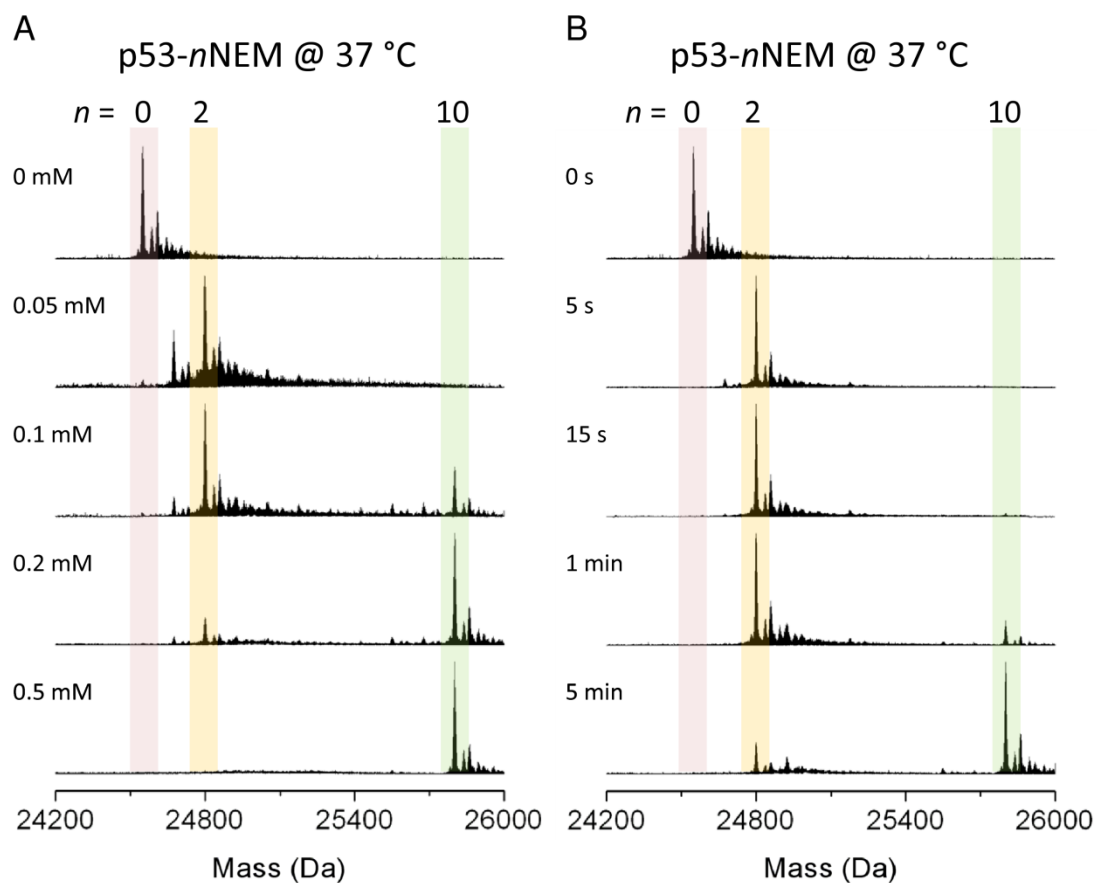


Figure 4.4 Reaction of p53 core domain with *N*-ethylmaleimide at physiological temperature. **(A)** NEM titration. p53 was incubated with varying concentrations of NEM for 15 min at 37°C. Deconvoluted mass spectra are shown. **(B)** Cysteine alkylation over time. p53 was incubated with 0.5 mM NEM at 37 °C. Deconvoluted mass spectra are shown for various time points.

It is evident from the neutral mass spectra shown in Figure 4.4 that a similar pattern of p53 alkylation occurs at 37°C; namely initial reaction of two Cys residues to form a stable dialkylated species, followed by direct conversion of 3NEM-p53 to 10NEM-p53 upon increasing NEM concentration or time. At a NEM concentration of 0.1 mM, 46% of p53 was dialkylated and 20% of p53 was fully alkylated. At the 1 min time point, 68% of p53 was dialkylated and 14% of p53 was fully alkylated. By 5 min these values had decreased and increased to 17% and 69% respectively. As observed at 22°C, minimal intermediate stages of alkylated p53 were detected, providing further evidence that alkylation of a third Cys triggers cooperative alkylation of the remaining seven Cys residues.

As expected, alkylation of p53 occurs at a faster rate at 37°C than at ambient temperature. At 37°C, 0.2 mM NEM resulted in 68% of p53 becoming fully alkylated, compared to 3% at 22°C. 69% of p53 was fully alkylated by the 5 min time point with 0.5 mM NEM at 37°C, whereas only 15% of p53 was converted to 10NEM-p53 by this time with 1 mM NEM at 22°C.

Intriguingly, increased formation of p53 salt adducts was observed at body temperature compared to ambient temperature, most prominent being $[M + K^+]$ and $[M + K^+ + Na^+]$.

4.3 Identification of Reactive Cysteine Residues

4.3.1 Top-Down FT-ICR Mass Spectrometry

Top-down FT-ICR mass spectrometry was employed in order to identify the two cysteine residues in p53 that are initially alkylated by NEM. p53 core domain was incubated with 0.1 mM NEM for 15 min, quenched with DTT followed by off-line reverse phase HPLC, and the p53 containing fraction was manually collected and directly infused into the mass spectrometer. Individual charge states of the 2NEM-p53 species (26+, 29+, 31+ and 32+) were sequentially isolated and fragmented using collision-induced dissociation (CID) or electron capture dissociation (ECD). A typical CID and ECD spectrum of 2NEM-p53 is shown in Figure 4.5 and Figure 4.6, respectively.

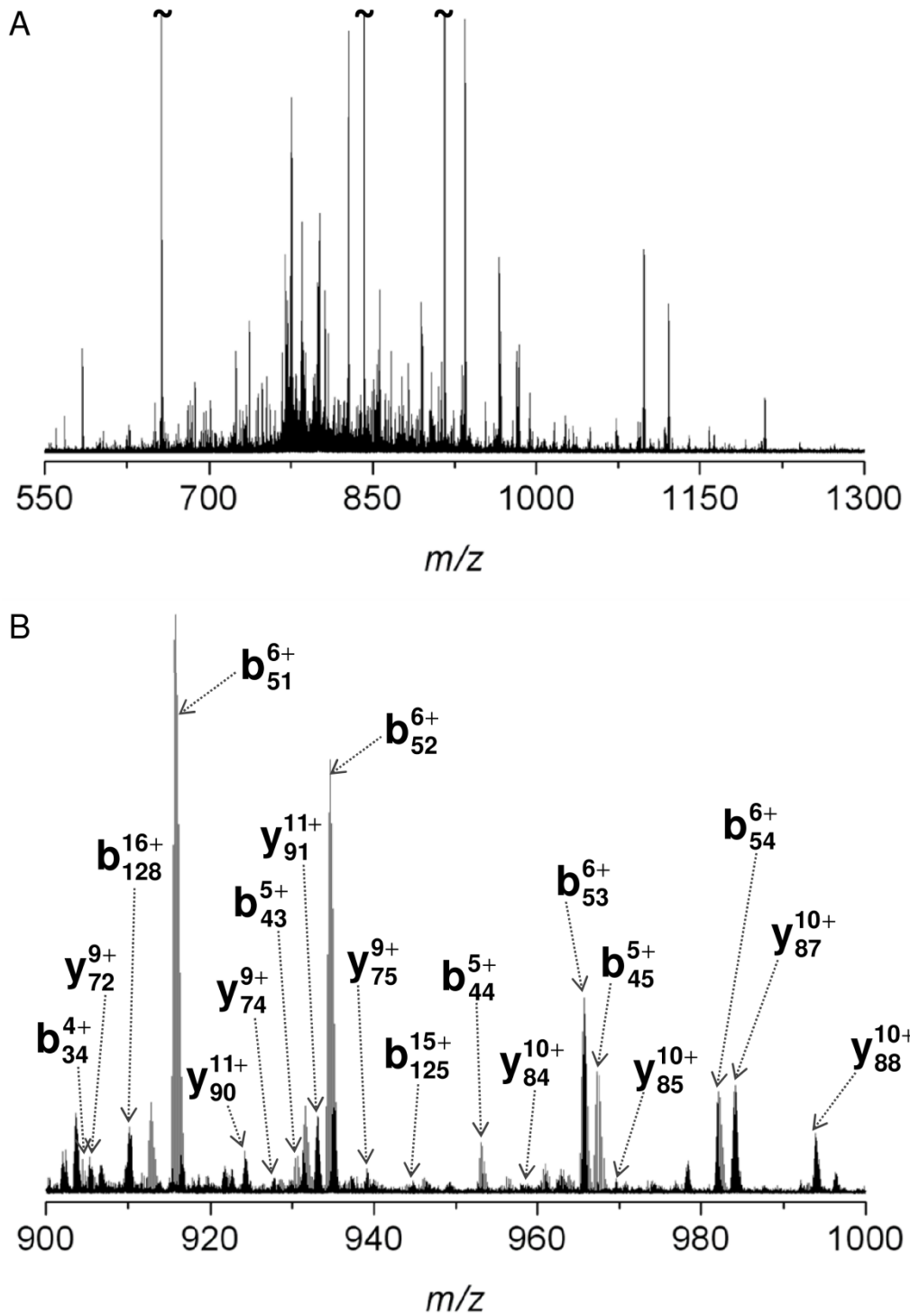


Figure 4.5 Top-down FT-ICR MS of 2NEM-p53. **(A)** CID mass spectrum of the 32+ charge state (776 m/z) of 2NEM-p53. **(B)** Expansion of the region 900-1000 m/z . Assigned b and y ions are annotated.

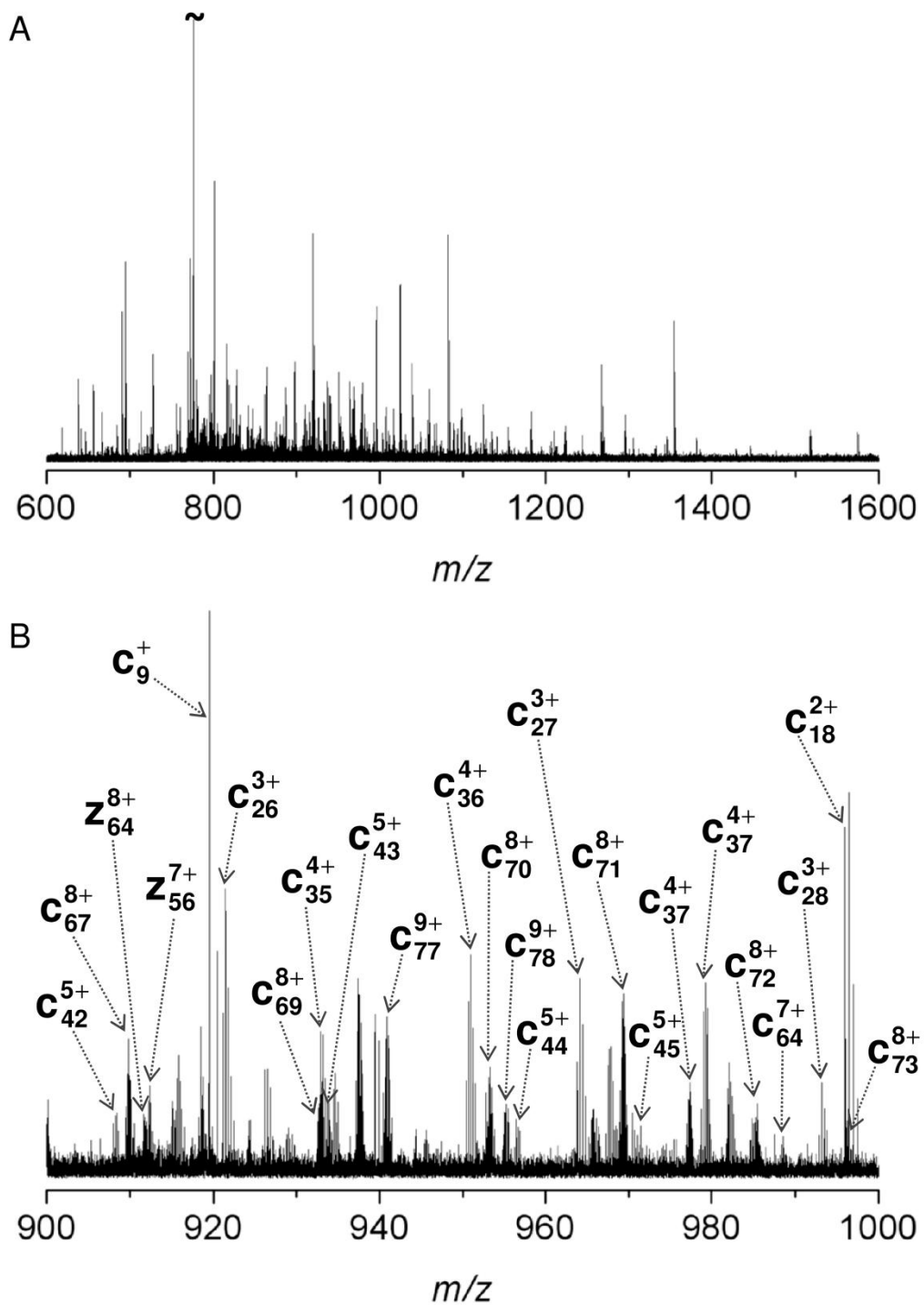


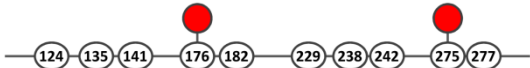


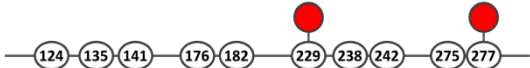
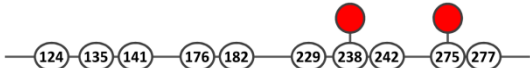


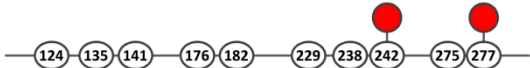


Figure 4.6 Top-down FT-ICR MS of 2NEM-p53 **(A)** ECD mass spectrum of the 32+ charge state (776 m/z) of 2NEM-p53. **(B)** Expansion of the region 900-1000 m/z . Assigned c and z ions are annotated.

Table 4.1 Permutations of 2NEM-p53 that corresponded to the highest number of assigned fragment ions resulting from top-down FT-ICR MS. The red circles indicate the positions of the NEM adducts.

Rank	Permutation	Number of Fragment Ions [†]
1		199
1		199
2		197
2		197
3		181
3		181
4		179
4		179
5		176
5		176

[†]The number of non-redundant *b*, *y*, *c* and *z* ions that corresponded with different permutations of the p53 core domain primary sequence modified with two NEM groups.

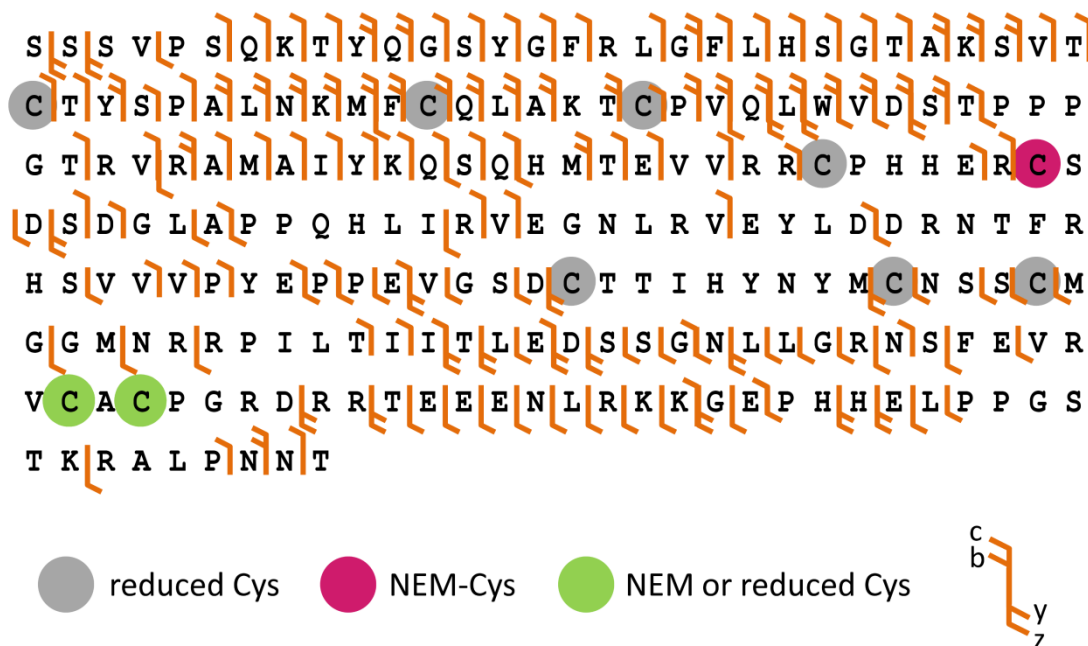


Figure 4.7 The fragment map displays fragment ions resulting from CID and ECD fragmentation of intact p53 core domain (Ser94 - Thr312) modified with two NEM groups. Top-down FT ICR MS of 2NEM-p53 suggested that Cys182 was alkylated and that the second NEM group was located on either Cys275 or Cys277.

The monoisotopic masses of the resulting fragment ions for 2NEM-p53 were searched against theoretical fragment mass lists for each of the 45 permutations of the p53 primary sequence modified with two NEM groups. Permutations of 2NEM-p53 were ranked according to the number of corresponding non-redundant *b*, *y*, *c* and *z* ions. The ten combinations of NEM positions that were associated with the largest numbers of assigned fragment ions are listed in Table 4.1. The highest number of assigned fragment ions (199) corresponded with the two NEM groups located on Cys182 and either Cys275 or Cys277.^{***} Fragment ions associated with this permutation of dialkylated p53 are shown in Figure 4.7. A fragment ion within 10 ppm MME was not observed between Cys275 and Cys277. Therefore, the modification state of these two residues could not be unambiguously determined from top-down MS alone. Taken together, fragments resulting from CID and ECD of

^{***} Mass assignments for fragment ions corresponding to this permutation of 2NEM-p53 are listed in Appendix B.1 (*b* and *y* ions) and B.2 (*c* and *z* ions).

2NEM-p53 resulted in a total protein sequence coverage of 64%, and allowed the modification/oxidation state of eight of the ten Cys residues in p53 to be unambiguously determined.

Of the 340 ions identified in the CID spectrum of the 32+ charge state of 2NEM-p53 (see Figure 4.5), 96 (27%) were assigned as *b* and *y* ions (corresponding with alkylation of Cys182 and Cys275 or Cys277), and of the 219 ions identified in the ECD spectrum of the 32+ charge state (see Figure 4.6), 110 (50%) were assigned as *c* and *z* ions. This observation highlights the increase in side chain losses and internal fragmentation that is typically observed for CID fragmentation of polypeptides when compared to ECD fragmentation (see Chapter 1.5).

As is usual in top-down MS, the majority of fragment ions were observed at the N- and C-termini of the intact protein (Figure 4.7) [135]. In order to increase the number of inter-residue bonds cleaved over the internal region of the p53 core domain and, therefore, to increase confidence in the assignments of Cys alkylation, middle-down MS was performed.

4.3.2 Middle-Down FT-ICR Mass Spectrometry

Lys-C endoproteinase cleaves peptide bonds on the C-terminal side of lysine residues. Cleavage of p53 with Lys-C results in a 127 amino acid peptide from Gln165 to Lys291, containing the seven cysteine residues from Cys176 to Cys277. Dialkylated p53 was incubated with Lys-C for 4 h, after which time a protein precipitate was observed. The precipitated protein was collected by centrifugation, re-suspended in 6 M guanidine supplemented with DTT, desalted and analysed by nESI FT-ICR mass spectrometry. The resulting mass spectrum is shown in Figure 4.8. Comparison of the theoretical isotope distribution for the p53 Lys-C fragment Gln165 – Lys291 modified with two NEM groups (2NEM-p53_{Lys-C}) with the experimental isotope distribution confirmed the presence of 2NEM-p53_{Lys-C}.

The solubility of a protein in an aqueous medium depends on a range of factors, including the concentration of dissolved salts, polarity of the solvent, temperature and pH [237]. A protein is least soluble when its isoelectric point (*pI*) is equivalent to

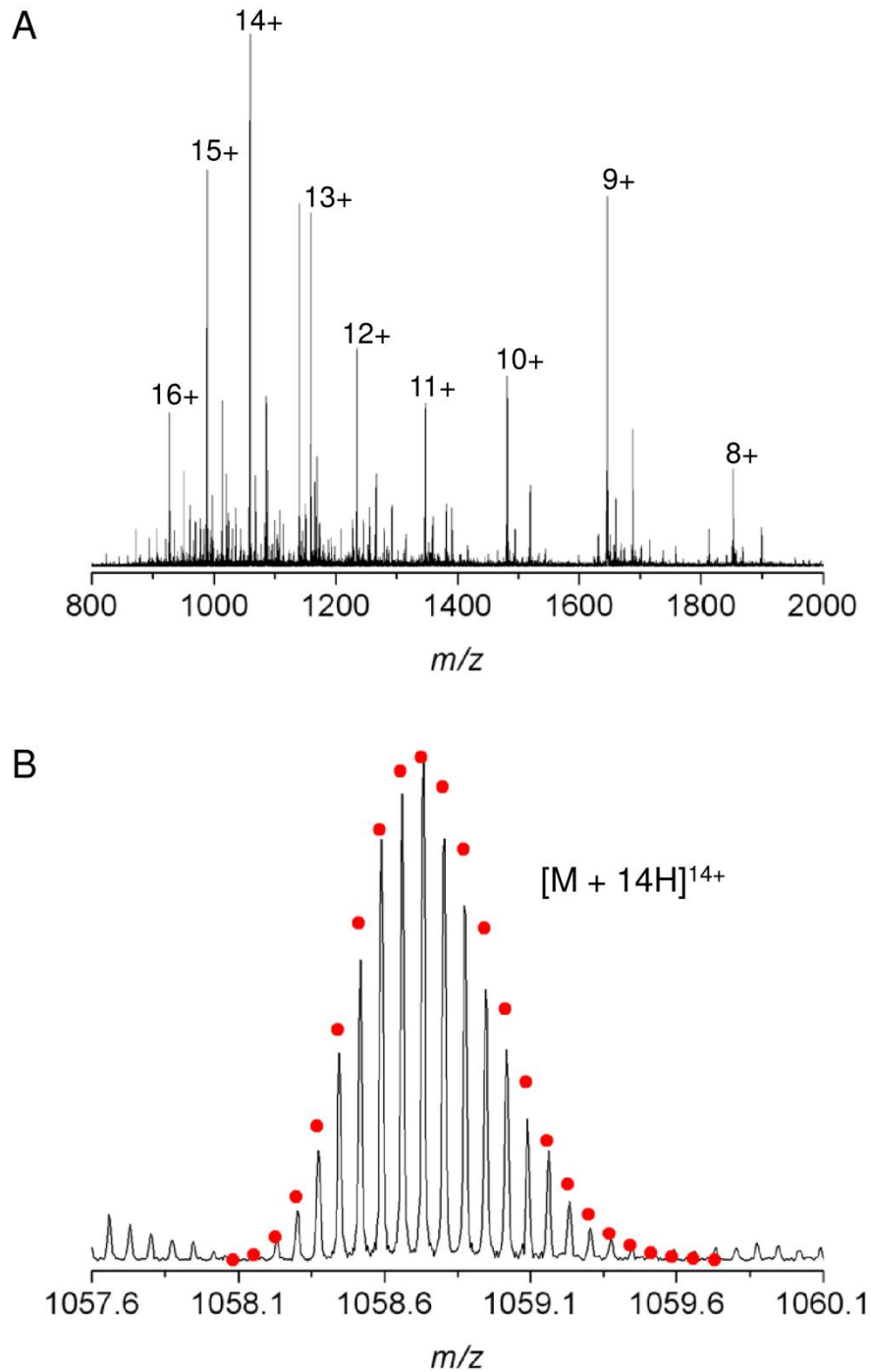


Figure 4.8 Middle-down FT-ICR MS of 2NEM-p53. **(A)** nESI FT-ICR mass spectrum of 2NEM-p53 Lys-C digest precipitate following re-suspension in 6 M guanidine HCl and buffer exchange. **(B)** 14+ charge state. The observed isotope distribution is consistent with the simulated isotope distribution for the p53 Lys-C peptide Gln165-Lys291 modified with two NEM groups (empirical formula $[C_{623}H_{1006}N_{198}O_{200}S_{11}]^{14+}$; \bullet ; 5 ppm MME).

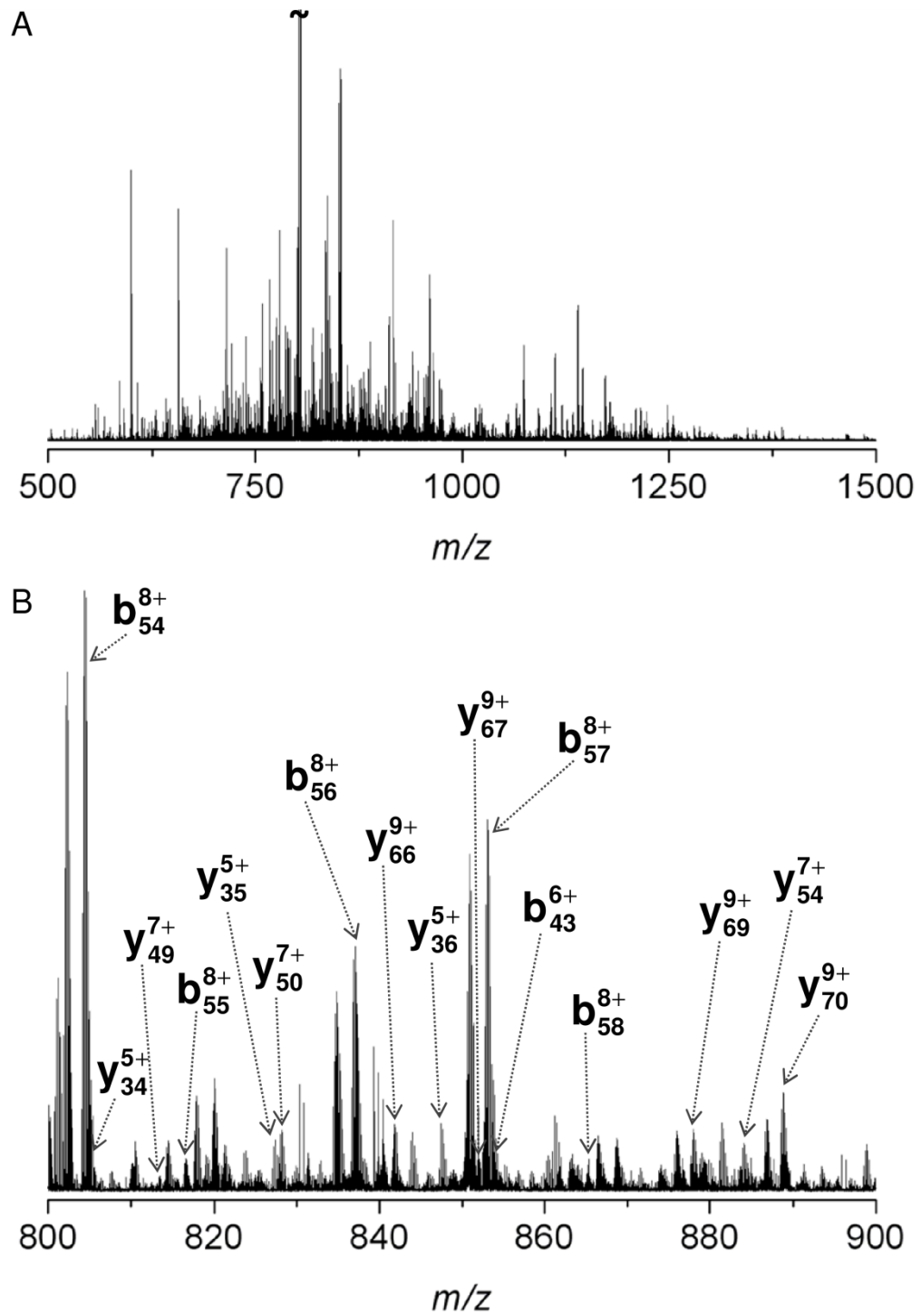


Figure 4.9 Middle-down FT-ICR MS of 2NEM-p53. **(A)** CID mass spectrum of the 21+ charge state (741 m/z) of 2NEM-p53_{Lys-C}. **(B)** Expansion of the region 800-900 m/z . Assigned b and y ions are annotated.

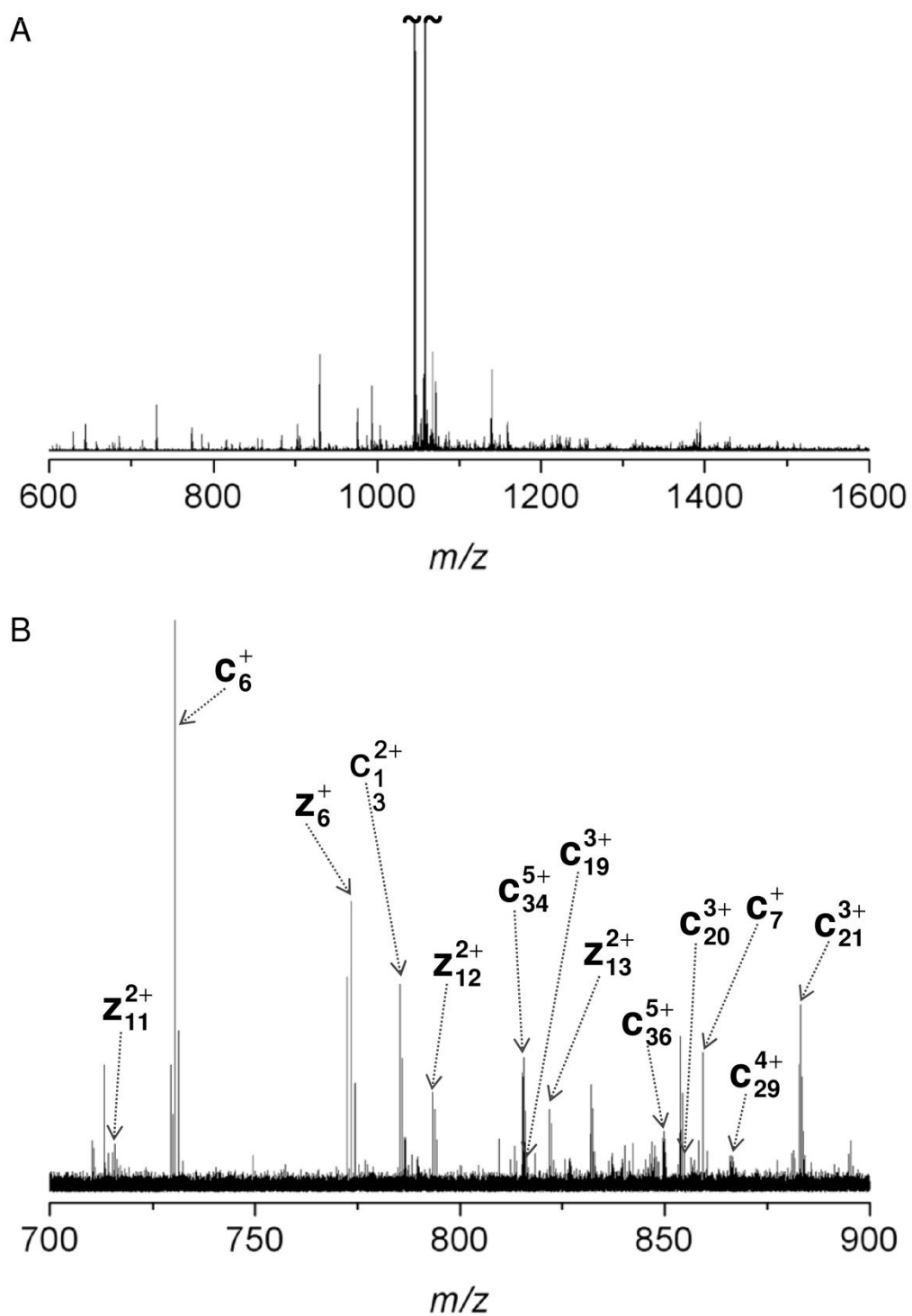
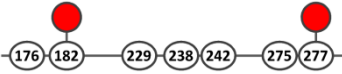




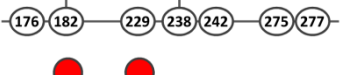

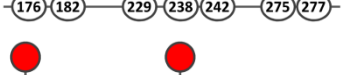

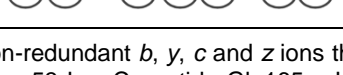


Figure 4.10 Middle-down FT-ICR MS of 2NEM-p53. **(A)** ECD mass spectrum of the 14+ charge state (1058 m/z) of 2NEM-p53_{Lys-C}. **(B)** Expansion of the region 700-900 m/z . Assigned c and z ions are annotated.

Table 4.2 Permutations of 2NEM-p53_{Lys-C} that corresponded to the highest number of assigned fragment ions resulting from middle-down FT-ICR MS. The red circles indicate the positions of the NEM adducts.

Rank	Permutation	Number of Fragment Ions [†]
1		132
2		131
3		125
4		124
5		115
6		112
7		108
7		108
8		105
9		101

[†]The number of non-redundant *b*, *y*, *c* and *z* ions that corresponded with different permutations of the p53 Lys-C peptide Gln165 – Lys291 modified with two NEM groups.

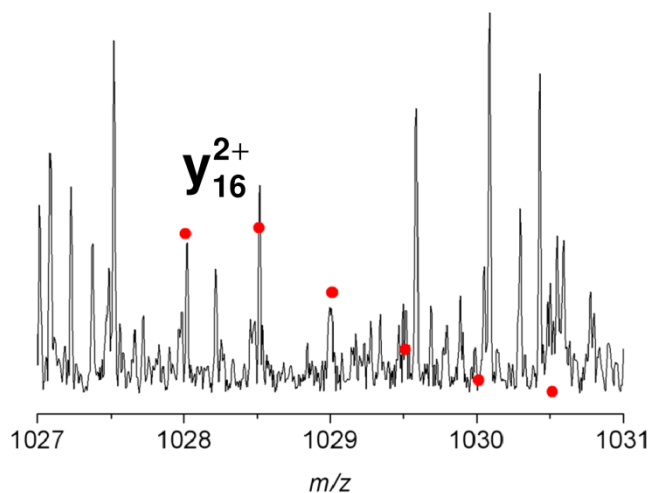


Figure 4.11 Middle-down FT-ICR MS of 2NEM-p53. The fragment ion y_{16}^{2+} (empirical formula $[C_{82}H_{141}N_{31}O_{29}S_1]^{2+}$; •; 2 ppm MME) supports alkylation of Cys277 by NEM.

the pH, i.e. when the net charge on the protein is zero. The estimated pI of the p53 core domain is 8.8, and the estimated pI of the p53 peptide Gln165 – Lys291 is 6.3 (calculated using ExPASy Compute pI/Mw tool). Lys-C digestion of p53 was performed at pH 7.2, which would have resulted in a reduced net charge of 2NEM-p53_{Lys-C} compared to the intact protein. The proximity of the pI of Gln165 – Lys291 to the pH of the buffer was most likely responsible for the observed precipitation of 2NEM-p53_{Lys-C}.

Individual charge states of the dialkylated Gln165 – Lys291 peptide (13+, 14+, 18+, 19+, 20+ and 21+) were isolated and fragmented by either CID or ECD. A typical CID and ECD spectrum of 2NEM-p53_{Lys-C} is shown in Figure 4.9 and Figure 4.10, respectively.

The monoisotopic masses of the resulting fragment ions were searched against theoretical fragment mass lists for each of the 21 permutations of the p53 peptide Gln165 – Lys291 primary sequence, modified with two NEM groups. Table 4.2 shows the ten permutations of 2NEM-p53_{Lys-C} ranked highest, according to the number of assigned fragment ions. As with top-down MS, the highest number of assigned ions (132) corresponded with a NEM group located on Cys182. The number

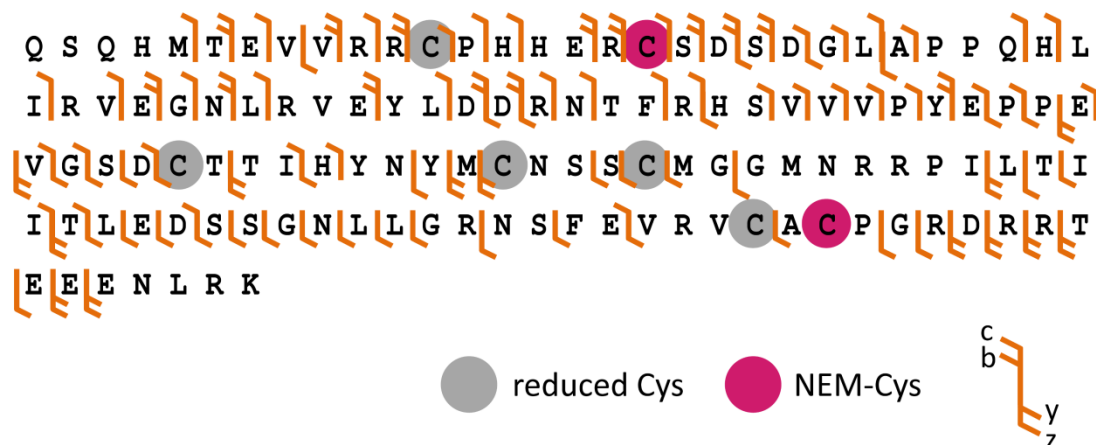


Figure 4.12 Fragment map displaying ions resulting from CID and ECD fragmentation of p53 Lys-C peptide Gln165 - Lys291 modified with two NEM groups. Middle-down FT-ICR MS suggested that Cys277 is alkylated and confirmed the alkylation of Cys182.

of assigned fragments between Cys176 and Cys182 was increased from two (observed in top-down MS) to seven, thus providing confirmation of Cys182 as an alkylated residue. No fragment ions were observed that supported placement of a NEM group on Cys176.

Middle-down FT-ICR MS of 2NEM-p53 resulted in one fragment ion between Cys275 and Cys277, y_{16}^{2+} (see Figure 4.11), which supported placement of the second NEM group on Cys277. Alkylation of Cys182 and Cys277 was the permutation of 2NEM-p53_{Lys-C} with the highest number of assigned *b*, *y*, *c* and *z* ions.^{†††} The assigned ions associated with this permutation are displayed in Figure 4.12. In addition to a diagnostic fragment between Cys275 and Cys277, middle-down FT-ICR MS resulted in an increase in sequence coverage from 53% (achieved for the region Gln165 to Lys291 in intact 2NEM-p53) to 69%, and allowed the oxidation/modification state of each of the seven Cys residues to be unambiguously determined.

In order to verify alkylation of Cys277 by NEM, bottom-up FT-ICR MS was also performed.

^{†††}Mass assignments for fragment ions corresponding to this permutation of 2NEM-p53_{Lys-C} are listed in Appendix B.3 (*b* and *y* ions) and B.4 (*c* and *z* ions).

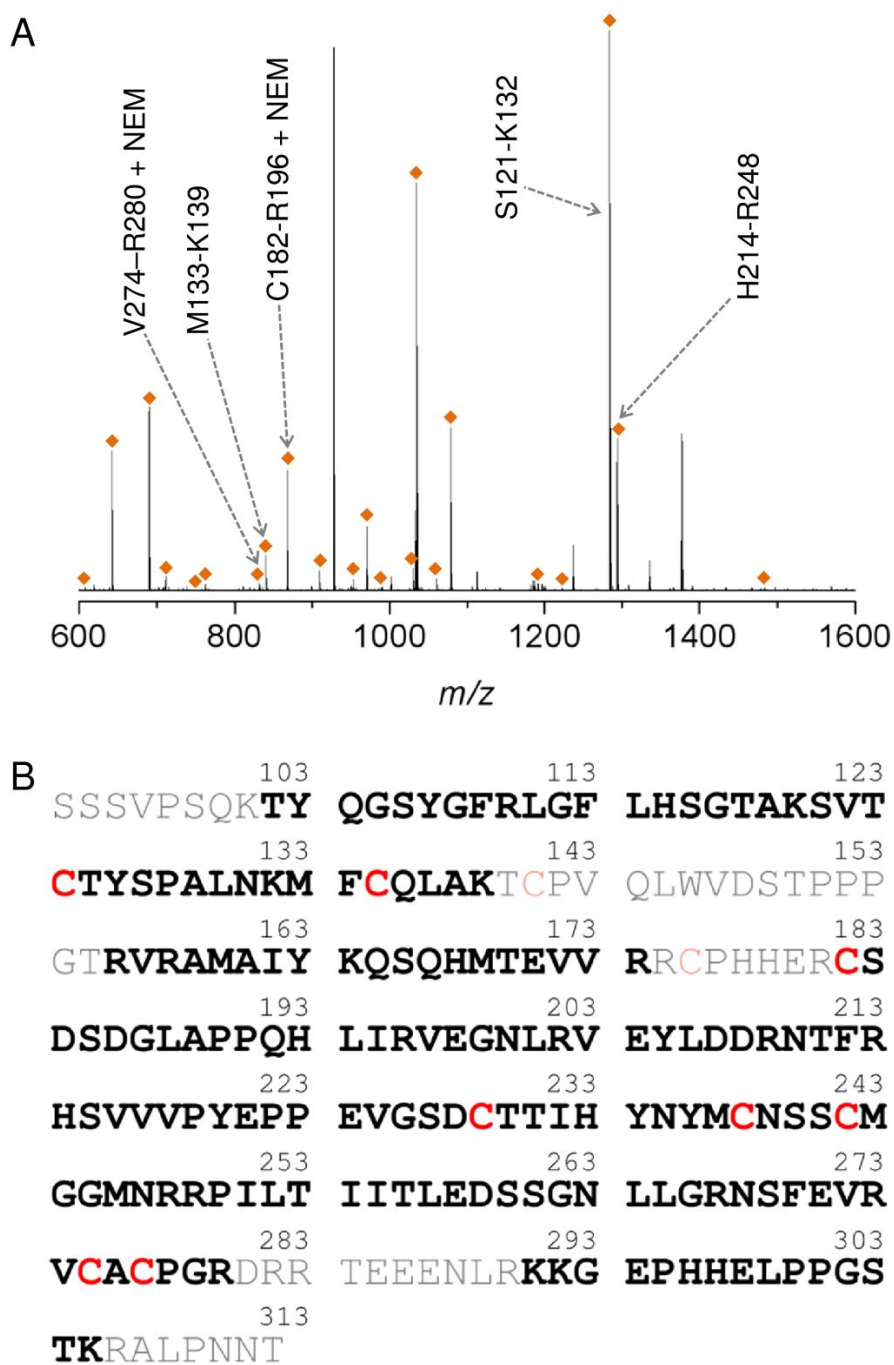


Figure 4.13 Bottom-up FT-ICR MS of 2NEM-p53. **(A)** nESI FT-ICR mass spectrum of 2NEM-p53 following trypsin digest and buffer exchange. Peaks corresponding to p53 tryptic peptides are highlighted by ♦. Cys-containing peptides detected with the highest intensity are annotated. **(B)** Sequence coverage obtained from FT-ICR MS of a tryptic digest of 2NEM-p53 (74%). Identified peptides are shown in bold.

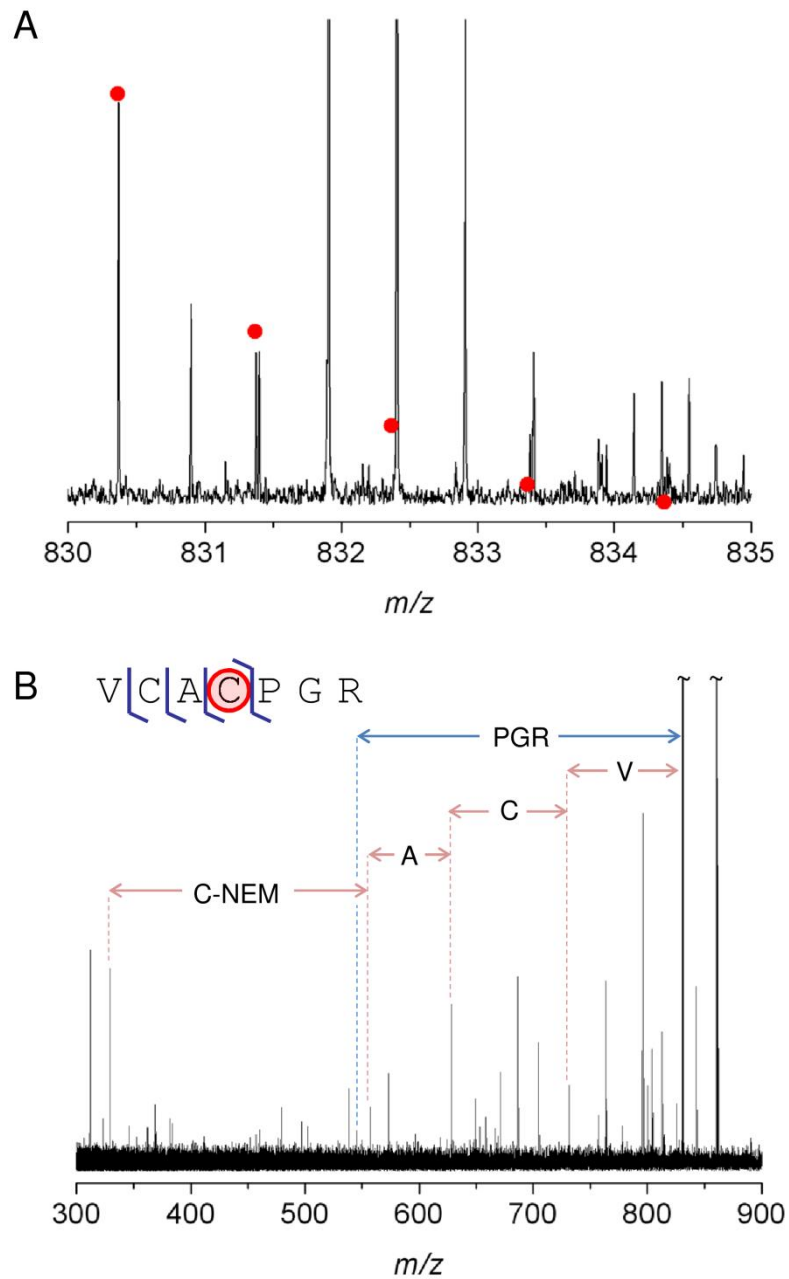


Figure 4.14 Bottom-up FT-ICR MS of 2NEM-p53. **(A)** Isotopic peaks corresponding to tryptic peptide VCACPGR modified with one NEM group. The experimental isotope distribution is consistent with the theoretical isotope distribution for the singly charged modified peptide (empirical formula $[C_{33}H_{56}N_{11}O_{10}S_2]^+$; \bullet ; MME 6 ppm). **(B)** CID mass spectrum of tryptic peptide VCACPGR modified with one NEM group. Four y ions and a complementary b ion confirmed alkylation of Cys277.

4.3.3 Bottom-Up FT-ICR Mass Spectrometry

Cleavage of p53 with trypsin results in the peptide V274 – R280 (VCACPGR), which contains the cysteine residues 275 and 277. Dialkylated p53 core domain was incubated with trypsin and the resulting peptide mixture was desalted and analysed by nESI FT-ICR MS without prior separation. The resulting mass spectrum is shown in Figure 4.13A. A sequence coverage of 74% was achieved (Figure 4.13B) and five out of the seven cysteine-containing tryptic peptides were detected. The absence of Cys-containing peptides in the spectrum illustrates that use of the bottom-up FT-ICR MS approach alone does not allow the oxidation state of each of the 10 Cys residues to be determined. The peptide VCACPGR was detected here, and its mass-to-charge ratio corresponded with the addition of one NEM group (830.370 m/z ; see Figure 4.14A). This peptide was isolated and fragmented using CID. Four *b* ions and one complementary *y* ion was observed that supported placement of the NEM group on Cys277, displayed in Figure 4.14B.^{†††} No fragment ions were observed that supported alkylation of Cys275. Bottom-up FT-ICR MS of 2NEM-p53 confirmed the previous assignment of alkylation of Cys277.

4.4 Alkylation of p53 Cysteine Mutants

In order to verify the preferential cysteine reactivity of Cys182 and Cys277 determined by FT-ICR mass spectrometry on wt p53, alkylation of p53 cysteine to serine mutants C182S, C277S, and the double mutant C182/277S, was performed. Native MS indicated that each of the Cys mutants was correctly folded (see Chapter 3.5). The p53 mutants (35 μ M) were alkylated and analysed following the protocol described for alkylation of wt p53 at 22°C. The resulting neutral mass spectra are shown in Figure 4.15, 4.16 and 4.17.

As expected, only one cysteine residue was preferentially alkylated in C182S and C277S, and no preferential alkylation was observed in C182/277S. In a similar manner to wt p53, at low concentrations of NEM (< 1 mM), one Cys residue was predominately alkylated in the single Cys mutants, and at higher concentrations of

^{†††}Mass assignments for fragment ions corresponding to mono-alkylated peptide VCACPGR are listed in Appendix B.5.

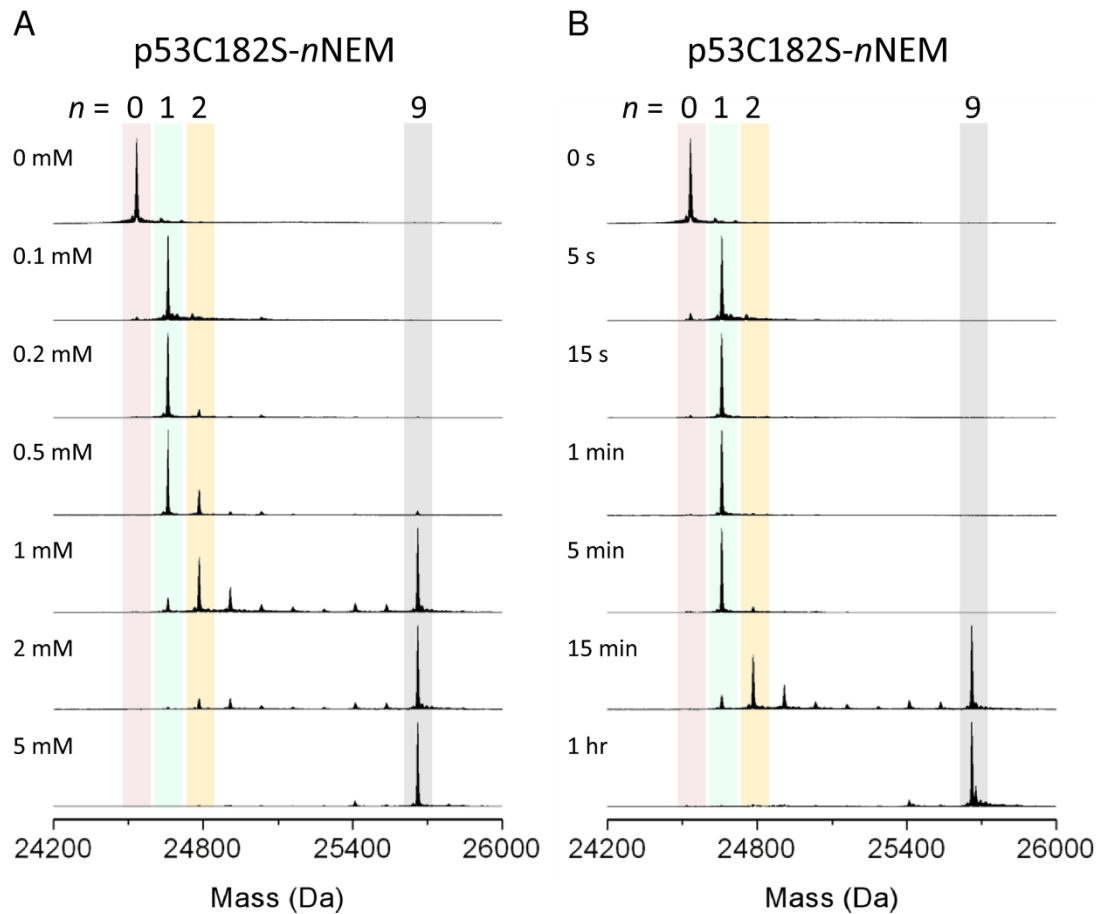


Figure 4.15 Reaction of NEM with the p53 core domain Cys mutant C182S. Reaction conditions used were the same as described for wild type p53. Deconvoluted neutral FT-ICR mass spectra are shown. **(A)** NEM Titration. **(B)** Alkylation over time.

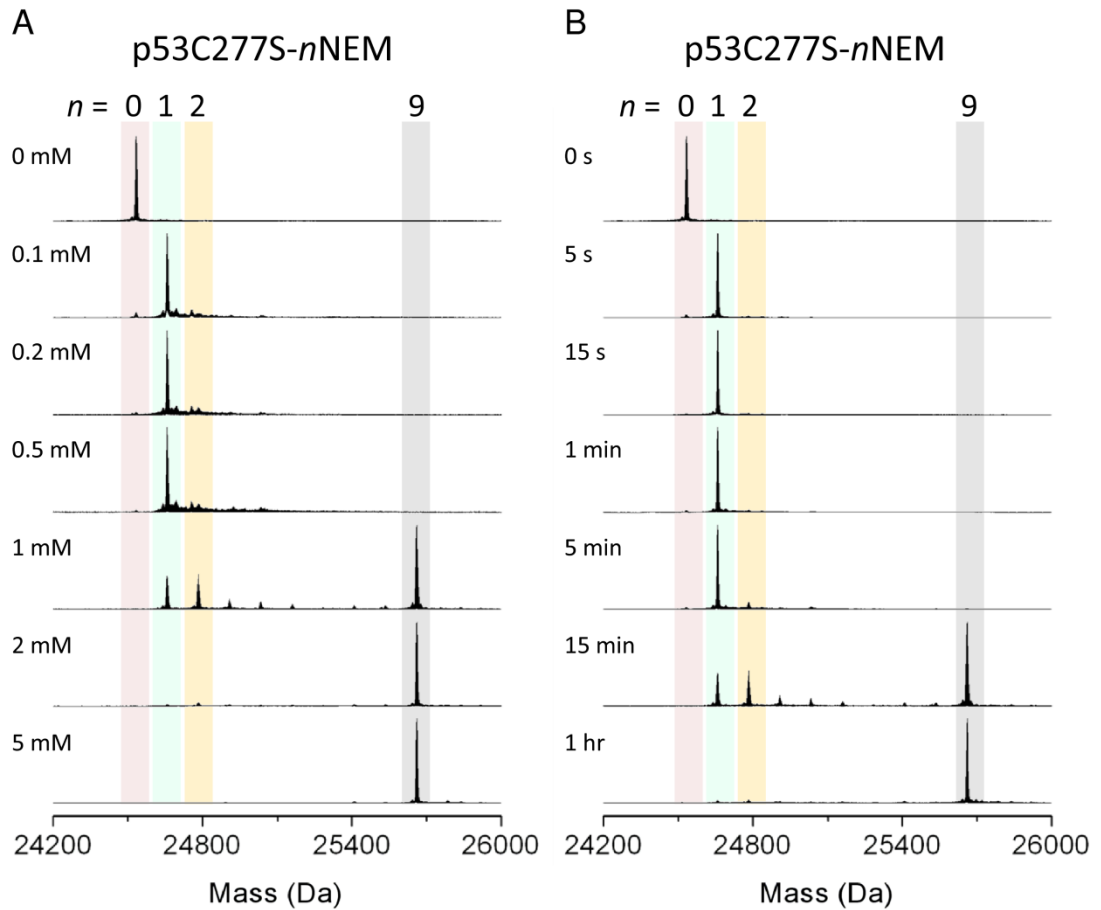


Figure 4.16 Reaction of NEM with the p53 core domain Cys mutant C277S. Reaction conditions used were the same as described for wild type p53. Deconvoluted neutral FT-ICR mass spectra are shown. **(A)** NEM Titration. **(B)** Alkylation over time.

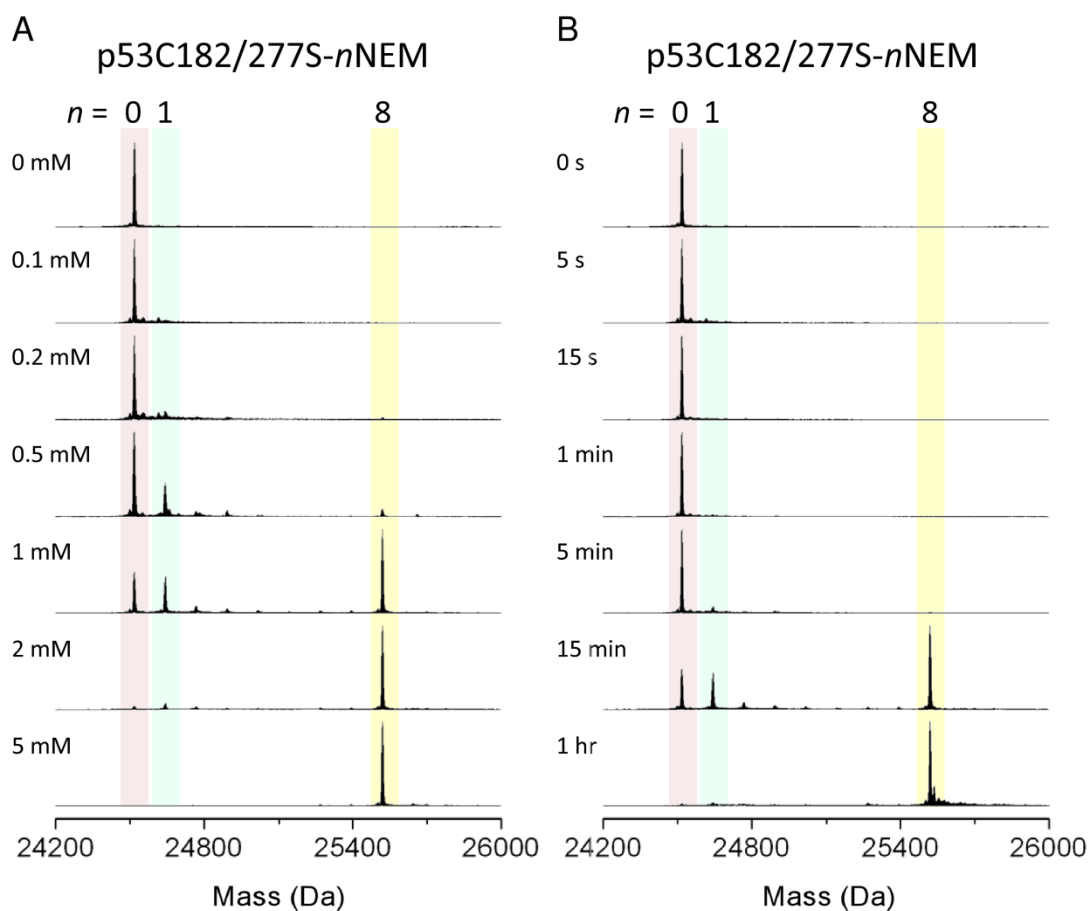


Figure 4.17 Reaction of NEM with the p53 core domain Cys mutant C182/277S. Reaction conditions used were the same as described for wild type p53. Deconvoluted neutral FT-ICR mass spectra are shown. **(A)** NEM Titration. **(B)** Alkylation over time.

NEM (> 1 mM) nine Cys residues were predominately alkylated. C182/277S was predominately unmodified below 1 mM NEM, and fully alkylated, i.e. modified with eight NEM groups, above 1 mM NEM. For both single Cys mutants, approximately 100% of protein was monoalkylated within 5 s with 1 mM NEM, and alkylation beyond one Cys residue was not observed until the 5 min time point. 100% of the double mutant remained unmodified until 5 min, at which point 7% of the protein was monoalkylated. For each p53 mutant, formation of a fully alkylated species became notable with 1 mM NEM for 15 min, similar to wt p53. Relatively small amounts of intermediate stages of alkylation were observed, between dialkylated and fully alkylated C182S and C277S p53, or between monoalkylated and fully alkylated C182/277S p53, providing further evidence that modification of a particular Cys residue in p53 triggers the rapid alkylation of the remaining seven Cys residues. The direct conversion of monoalkylated C182/277S p53 to the fully alkylated form shows that prior alkylation of Cys182 or Cys277 is not required in order to induce the alkylation of a third residue, and the subsequent cascade of Cys alkylation.

4.5 Preferential Alkylation of Cys182 and Cys277

Top-down and middle-down FT-ICR MS identified Cys182 and Cys277 as the sites of preferential alkylation in p53, and these assignments were confirmed by FT-ICR MS analysis of p53 Cys-Ser mutants. Solvent accessibility values for each of the 10 thiol groups in p53 are listed in Table 4.3. These were determined from the X-ray crystal structure of the p53 core domain unbound to DNA (PDB ID 2OCJ) [85] using Accelrys Discovery Studio 2.5 software. Cys182 and Cys277 are the most accessible residues, accounting for their preferential reactivity with alkylating reagent. The sulfur atoms in Cys182 and Cys277 are approximately three times more accessible than the next most exposed sulfur atom, that of Cys229. It can clearly be seen in the surface contour representation of the crystal structure of p53 shown, in Figure 4.18A, that Cys182 and Cys277 are the most accessible cysteine residues on the protein surface.

Table 4.3 Solvent accessibility of thiol groups in p53 core domain unbound to DNA.

Cysteine	Solvent Accessibility [†]
124	6.27
135	0
141	0
176	2.85
182	39.34
229	14.82
238	1.14
242	11.97
275	0
277	43.34

[†]Calculated using Accelrys Discovery Studio 2.5 software.

X-ray crystallography data very recently reported by Karr *et al.* is in agreement with the p53 FT-ICR mass spectrometry results presented here [120]. Stabilised p53 core domain^{§§§} (T-p53C) containing the cancer-derived mutation Y220C was treated with an electrophilic compound, 3-benzoylacrylic acid, identified from a chemical library. This compound was found to increase the thermal stability of T-p53C-Y220C. The resulting crystal structure revealed pronounced electron density surrounding cysteine residues 182, 229 and 277. However, the density was not sufficient to model the modifications unambiguously. Karr *et al.* went on to use a bottom-up MS approach to investigate the order of cysteine reactivity with 3-benzoylacrylic acid. Curiously, they found Cys124 and Cys141 to be the most reactive cysteine residues. This is in direct conflict with their X-ray crystallography data and the MS results described in this thesis. Intriguingly, Velu *et al.* also concluded that Cys141 is the most reactive Cys residue on the p53 surface, after using a bottom-up MS approach to investigate cysteine alkylation [99]. Cys141 has a solvent accessibility value of zero, and the X-ray crystal structure of the p53 core

^{§§§}Fersht and co-workers have designed a quadruple mutant of p53 core domain (M133L/V203A/ N239Y/N268D) which displays increased thermostability compared to the wt protein [238].

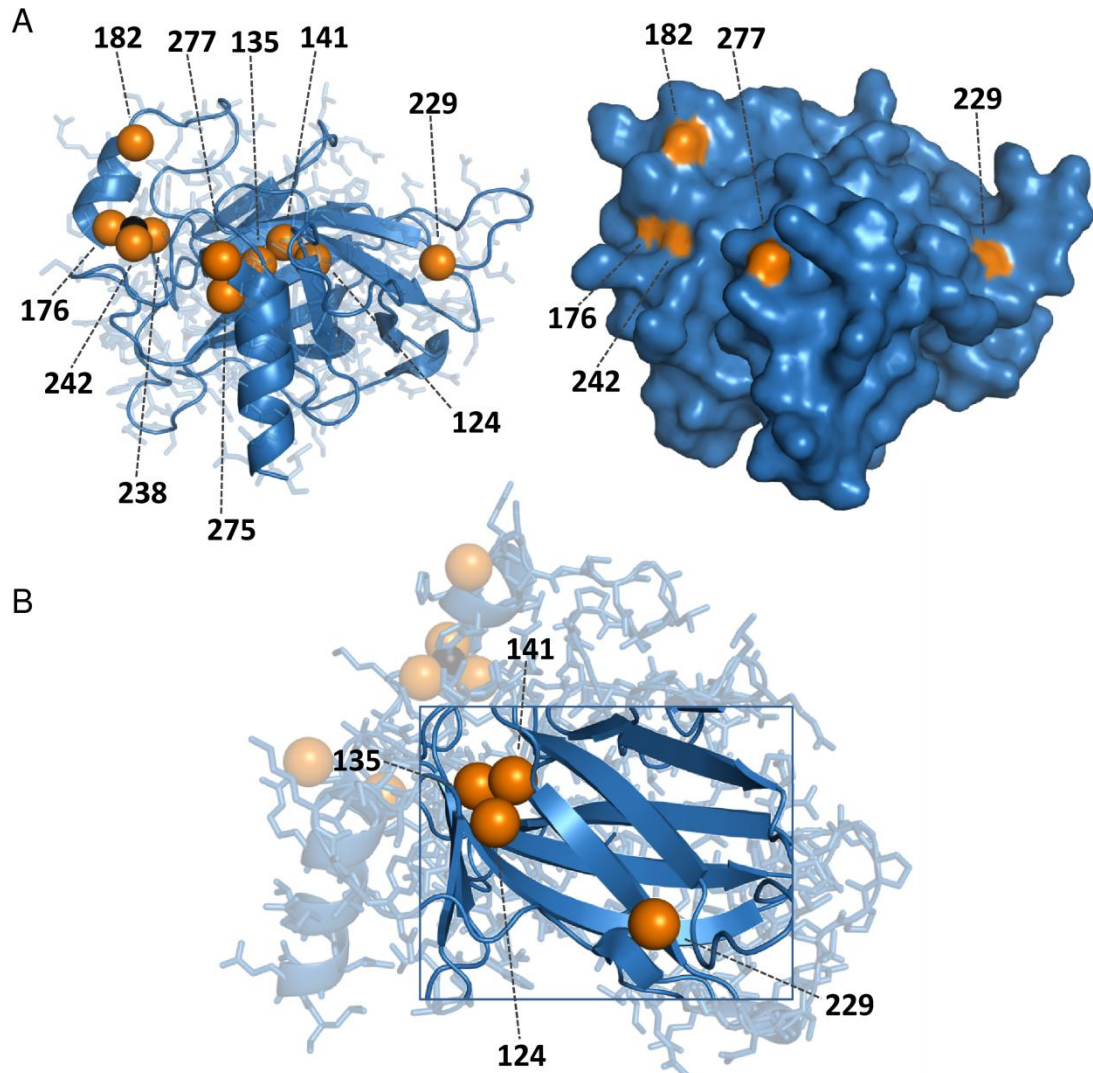


Figure 4.18 X-ray crystal structure of human p53 core domain (PDB ID 2OCJ). **(A, right)** Ribbon diagram highlighting p53 cysteine residues. Sulfur atoms are shown (orange). Cys176, 238 and 242 are involved in the coordination of a zinc ion. **(A, left)** Surface contour of the p53 core domain. The thiol groups of Cys176, 182, 229, 242 and 277 are surface-exposed. **(B)** Alternative orientation of p53 core domain, highlighting the anti-parallel β -sheet sandwich and position of Cys229, 124, 135 and 141.

domain shows that it is buried within two sides of the β -sheet sandwich (see Figure 4.18B).

A major draw-back of bottom-up MS is that, when analysing peptides originating from more than one protein isoform, the 'parent' isoform that a peptide originated from is unknown. Investigating the order of Cys reactivity using a bottom-up approach requires that the modified protein is completely pure prior to proteolytic digestion. It is proposed here that tryptic peptides originating from p53, which was alkylated beyond Cys182, 229 and 277, were present in the peptide samples analysed by Karr *et al.* and Velu *et al.*, and resulted in the misassignment of Cys reactivity.

Both Cys182 and Cys277 have previously been implicated in redox-regulation of p53. Cys277 is a DNA-binding residue [72], and oxidation of this residue has been implicated in differential gene recognition [100]. Cys277 has also been identified as a possible substrate for SeMet-dependent redox-regulation of p53 [102], and it has been postulated that the redox-state of Cys277 serves as a switch to activate DNA repair machinery [65]. Furthermore, the prostaglandin 15-deoxy- $\Delta^{12,14}$ -prostaglandin J₂ (15d-PGJ₂), which is known to covalently modify and regulate the function of the redox-regulated transcription factor NF- κ B, has recently been shown to bind to Cys277 and inhibit specific DNA-binding *in vivo* [119, 121].

p53 contains five highly conserved regions termed 'BOXES' (see Chapter 1.2.2). Cys277 is located in the conserved p53 motif BOX-V (amino acid residues 270 – 286). BOX-V is known to control the specific activity of p53 by binding to enzymes such as the E3 ubiquitin ligase MDM2 which mediates ubiquitination of p53, or the serine/threonine kinase CHK2, that mediates phosphorylation of p53 [239]. Interestingly, redox-regulation of a conserved cysteine in the NF- κ B related protein c-Rel regulates phosphorylation of the protein, which, in turn, regulates its transcriptional activity [240]. It is entirely plausible that redox-regulation of Cys277 modulates binding of p53 to regulatory enzymes, such as MDM2 and CHK2, thereby dictating protein function.

Cys182 has recently been shown to be the most susceptible to diamide oxidation *in vivo*. Held *et al.* used a differential alkylation approach, along with trypsin proteolysis and multiple reaction monitoring (MRM) peptide mass spectrometry, to

identify redox sensitive cysteines in endogenous p53 [103]. Incomplete sequence coverage meant that the oxidation state of each of the 10 Cys residues could not be determined, as the tryptic peptide containing Cys229, 238 and 242 was not detected. Furthermore, top-down FT-ICR MS has been used here to show that Cys182 is susceptible to oxidation in response to hydrogen peroxide treatment (see Chapter 5).

Cysteine alkylation has been identified as a biologically relevant post-translational modification. *S*-methylated cysteine residues are known to occur in human lens proteins, to protect them from detrimental oxidative modifications and to prevent protein aggregation [241, 242]. Endogenous cysteine methylation has also been observed in haemoglobin. However, the reason for its occurrence is unknown [243]. Furthermore, cysteine methylation occurs as part of a methyltransferase DNA repair mechanism, involving the enzyme O(6)-methylguanine-DNA methyltransferase (MGMT), which p53 is known to regulate [244]. Alkylation of p53 Cys residues *in vivo* is yet to be investigated. However, the results described here suggest that Cys182 and Cys277 would be the most likely targets for modification.

4.6 Identification of the Third Site of Alkylation

Since alkylation beyond Cys182 and Cys277 triggers co-operative alkylation of the remaining cysteine residues, top-down FT-ICR MS was used to identify the third site of alkylation in wt p53. p53 core domain was incubated with 1 mM NEM for 15 min, quenched with DTT followed by off-line reverse phase LC, and the p53 containing fraction was manually collected and directly infused into the FT-ICR mass spectrometer. The 23+ and 24+ charge states of trialkylated p53 were sequentially isolated and fragmented using CID. The CID spectrum of the 24+ charge state of 3NEM-p53 is shown in Figure 4.19. Relatively low charge states were selected for fragmentation, compared to top-down and middle down FT-ICR MS of the dialkylated species, due to overlapping charge states of 3NEM-p53 and 10NEM-p53 at higher m/z values. The monoisotopic masses of the resulting fragment ions were searched against theoretical fragment mass lists for each permutation of p53 core domain, modified with a NEM group at Cys182 and Cys277, and one NEM group

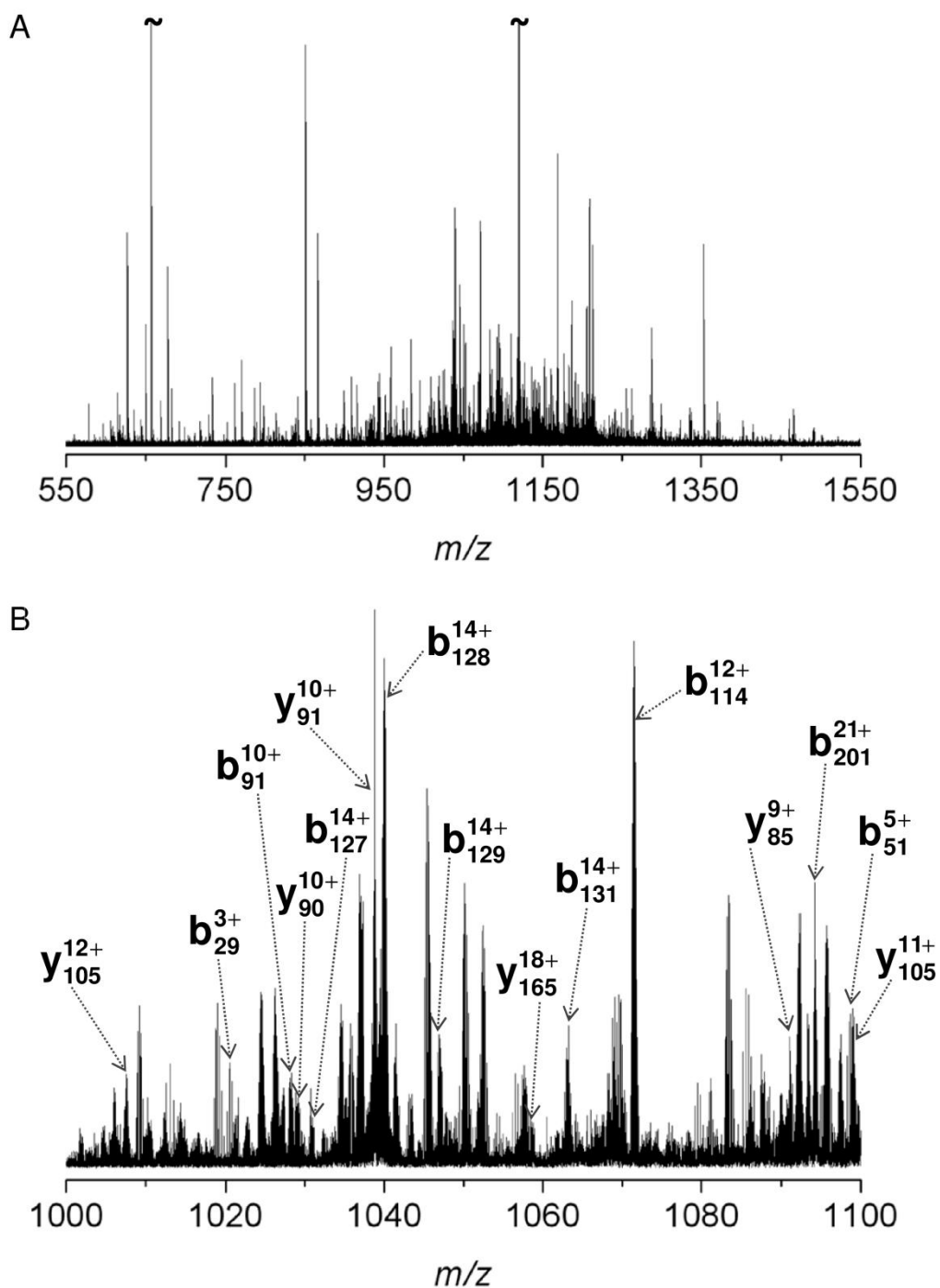










Figure 4.19 Top-down FT-ICR MS of 3NEM-p53. **(A)** CID mass spectrum of the 24+ charge state (1040 m/z) of 3NEM-p53. **(B)** Expansion of the region 1000-1100 m/z . Assigned *b* and *y* ions are annotated.

Table 4.4 Permutations of 3NEM-p53, ranked according to the highest number of assigned fragment ions resulting from top-down FT-ICR MS. The red circles indicate the positions of the NEM adducts.

Rank	Permutation	Number of Fragment Ions [†]
1		42
1		42
1		42
2		41
3		38
4		33
5		29
6		24

[†]The number of non-redundant *b* and *y* ions that corresponded with the possible locations of the third NEM group.

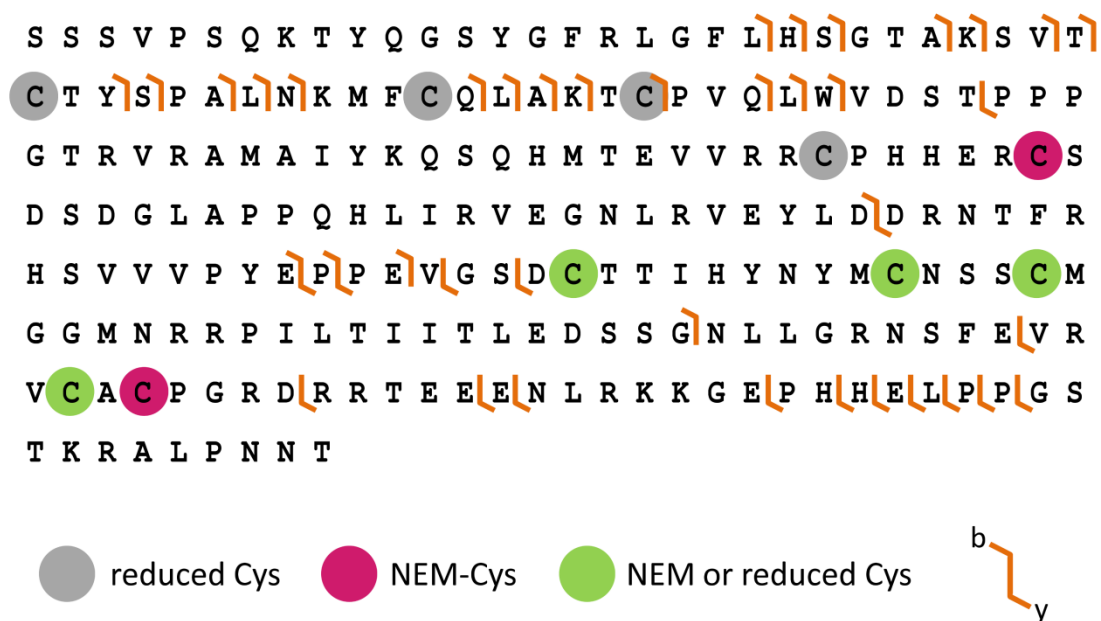


Figure 4.20 Fragment map displaying *b* and *y* ions resulting from CID fragmentation of intact p53 core domain modified with three NEM groups. Top-down FT-ICR MS of 3NEM-p53 suggested that Cys229, Cys238 or Cys242 was alkylated.

located on one of the remaining 8 Cys residues. Table 4.4 shows the 8 possible locations of the third NEM group, ranked according to the number of corresponding non-redundant *b* and *y* ions. The highest number of assigned fragment ions (42) corresponded with the third Cys residue on Cys229, Cys238 or Cys242.^{****} The assigned *b* and *y* ions are shown in the fragment map in Figure 4.20. One *b* ion (b_{169}^{16+} ; see Figure 4.21A) was observed that supported placement of the third NEM group on Cys229, 238 or 242. However, one *y* ion (y_{41}^{5+} ; Figure 4.21B) was also observed that supported placement of the third NEM group on Cys275. No ions were observed that supported placement of a NEM group on the remaining Cys residues Cys124, 135, 141 or 182.

According to the X-ray crystal structure of p53 (see Figure 4.18), Cys229 is the third most accessible thiol group in p53, and the thiol group of Cys275 is completely buried (see Table 4.3). In addition, Cys238 and Cys242 are zinc-binding residues. Hence, it seems unlikely that either of these residues is the third site of alkylation.

^{****} Mass assignments for fragment ions corresponding to these permutations of 3NEM-p53 are listed in Appendix B.6.

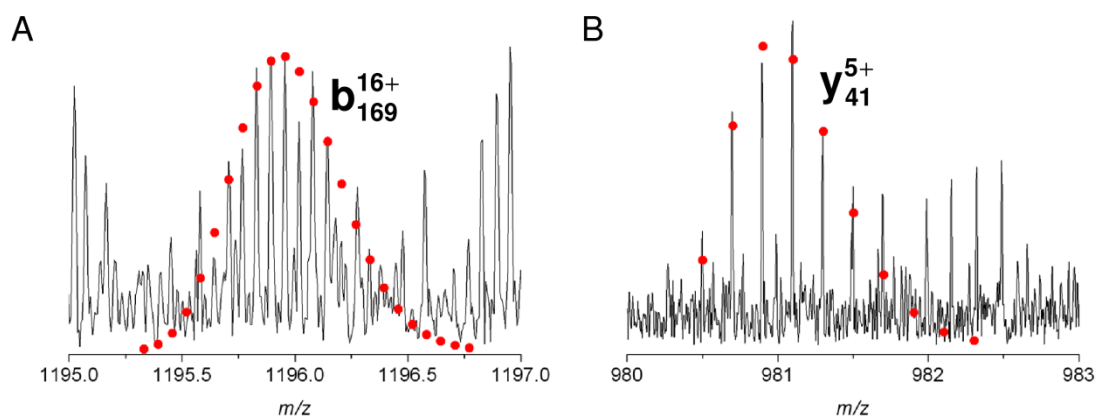


Figure 4.21 Top-down MS of 3NEM-p53. **(A)** The fragment ion b_{169}^{16+} (empirical formula $[C_{829}H_{1310}N_{240}O_{253}S_{14}]^{16+}$; •; 3 ppm MME) supported placement of the third NEM group on Cys229, Cys238 or Cys242. **(B)** The fragment ion y_{41}^{5+} (empirical formula $[C_{205}H_{342}N_{71}O_{65}S_2]^{5+}$; •; 5 ppm MME) supported placement of the third NEM group on Cys275.

Cys229 is the most likely candidate for alkylation. However, alkylation of Cys275, 238 and 242 cannot be ruled out. In order to increase the number of fragments between Cys229, 238, 242 and 275 and, therefore, unambiguously determine the third site(s) of alkylation, higher charge states could be selected for fragmentation or middle-down FT-ICR MS could be performed. However, different forms of alkylated p53 would require separation prior to top-down FT-ICR MS or proteolytic digestion.

4.7 Disruption of Secondary Structure and Protein Unfolding

Alkylation of a third Cys residue in wt p53 core domain (or a second Cys in the mutants C182S and C277S, or the first Cys in C182/277S) triggers rapid modification of the remaining thiol groups. Based on the results from top-down FT-ICR MS of trialkylated p53, and the solvent accessibility of p53 thiol groups (see Table 4.3), the most likely candidate for the third site of alkylation is Cys229. However, alkylation of Cys238, 242 and 275 cannot be ruled out at this stage.

According to crystallography data, Cys229 is surface exposed, and is located adjacent to the N-terminal end of a strand of β -sheet from the anti-parallel β -sheet sandwich, and Cys275 is located adjacent to the C-terminal end of a strand of β -

sheet (see Figure 1.6). The β -sheet sandwich is the main structural feature of the p53 core domain, and acts as a scaffold for the loop-sheet-helix motif, and for the two large loops (L2 and L3) which make up the DNA-binding surface of the protein (see Chapter 1.2.3) [72]. It is predicted that alkylation of Cys229 disrupts this stabilising structural feature, therefore, allowing access of NEM to the cluster of cysteines 124, 135 and 141, which are located in between the two sides of the β -sandwich (see Figure 4.18B). An appreciable energy barrier would be associated with disruption of the β -sheet sandwich (due to disruption of H-bonding and possibly hydrophobic interactions [245]), thus providing an explanation for the observed delay in alkylation of the third Cys residue, compared with alkylation of Cys182 and Cys277. Furthermore, Cys124, 135 and 141 are all located at the beginning or end of β -strands. Alkylation of any one of these cysteines may result in severe disruption of p53 secondary structure, and is likely to be responsible for the observed rapid alkylation of the remaining Cys residues.

Prior alkylation of Cys182 or Cys277 is not required in order to induce alkylation of Cys229 (or Cys 238, 242 or 275), illustrated by the rapid conversion of monoalkylated C182/277S p53 to the fully alkylated form. The removal of Cys182 and Cys277 had no detectable effects on alkylation of the remaining thiol groups, suggesting that modification of these two residues by NEM does not significantly affect p53 core domain tertiary structure. Significant conformational changes do not need to accompany Cys oxidation/reduction, in order for a protein to take part in redox-signalling. For example, high resolution NMR structures of human and *E. coli* thioredoxin have shown that there is very little difference between the reduced (Trx-(SH)₂) and oxidised (Trx-S₂) forms of the protein. Yet, Trx-(SH)₂ and Trx-S₂ display radically different binding affinities for the same target protein [246]. Subtle changes to p53 surface chemistry, via modification of Cys182 or Cys277, may be enough to radically alter binding specificity of p53 to its target proteins.

Zn²⁺ is required for the correct folding and specific DNA-binding activity of p53 [90, 91, 247]. Notably, the rapid alkylation of p53 Cys residues observed here includes alkylation of all three zinc-binding Cys residues, indicating that hyper-alkylation of p53 causes detrimental structural distortion of the core domain. This has

implications for the re-activation of mutant p53, with anti-tumour compounds that covalently bind to Cys residues such as MIRA-1, PRIMA-1 and STIMA-1 [115-117]. Indeed, MIRA-1 is known to increase DNA-binding of certain p53 mutants at low concentrations, and to decrease DNA-binding at higher concentrations. A similar effect has also been observed for alkylation of wt p53 with NEM [115]. Based on the results described here, it is hypothesised that dialkylated p53 is responsible for the observed increase in DNA-binding. Above a certain concentration of MIRA-1 or NEM, hyper-alkylation of p53 probably occurs, causing unfolding of the protein thus resulting in decreased DNA-binding. X-ray crystallography could be employed to determine the specific affect that alkylation of Cys182 and Cys277 has on p53-DNA interactions.

4.8 Conclusion

FT-ICR mass spectrometry of p53 core domain, incubated with the alkylating reagent NEM under various conditions, has revealed that alkylation of p53 cysteine residues proceeds in distinct steps. Initially, two Cys residues are rapidly alkylated to form a stable dialkylated species. An increase in NEM concentration or time leads to alkylation of a third Cys residue, which initiates rapid alkylation of the remaining seven Cys residues. Alkylation of wt p53 was repeated at 37°C and the same trend was observed, albeit it at a faster rate.

Top-down FT-ICR MS allowed the oxidation/modification state of eight out of the ten Cys residues to be determined unambiguously, and identified Cys182 and either Cys275 or Cys277 as the sites of preferential alkylation. Middle-down FT-ICR MS allowed the oxidation/modification state of each of the seven Cys residues, from Cys176 to Cys277, to be determined unambiguously, and identified Cys277 as the second site of preferential alkylation. This result was confirmed by bottom-up FT-ICR MS. FT-ICR mass spectrometry of the p53 cysteine to serine mutants C182S, C277S and C182/277S, incubated with NEM under various conditions, verified that Cys182 and Cys277 are the fast-reacting Cys residues on the p53 surface.

Alkylation of a third Cys residue in p53 appears to result in unfolding of the protein, suggesting that this cysteine is crucial for the structural integrity of p53 core domain. Top-down FT-ICR MS of trialkylated p53, together with what is known about solvent accessibility of p53 thiol groups and the zinc-binding properties of p53, suggested that Cys229 is the most likely candidate for the third site of alkylation. However, further experiments are required in order to verify this.

Selective modification of cysteine residues is a fundamental requirement in cellular redox-signalling. Here, it has clearly and unambiguously been shown that Cys182 and Cys277 are selectively alkylated in p53, and that modification beyond these two residues has a detrimental effect on p53 tertiary structure. Cys182 and Cys277 have previously been implicated in redox-regulation of p53, and the results described here provide striking evidence supporting this notion. Furthermore, these findings will allow a more targeted and focused approach for investigating cysteine modulated control of p53 function.

4.9 Future Work

To further this study on the reactivity of Cys residues in p53, the pK_a values of Cys182 and Cys277, and possibly the remaining Cys residues, could be determined. This would involve treating p53 with NEM (or an alternative cysteine derivatising reagent) at different pH values, and measuring the degree of alkylation (which could be done using MS, as described here) [248, 249] The pH at which 50% of a Cys residue is modified would equate to the pK_a of that Cys residue. Determining pK_a values of Cys182 and Cys277 would be a useful way of standardising their reactivity, and for comparing them to reactive Cys residues in other proteins.

The FT-ICR MS techniques used here could also be employed to investigate alkylation of p53 cancer hot spot mutants that frequently occur in tumours (see Chapter 1.2.3; Figure 1.3). p53 hot spot mutations are classified as either contact or structural mutants. Contact mutants are those where an essential DNA-contact residue is removed, such as R273H and R248W, and structural mutants containing a mutation which affects the overall structure of the DNA-binding surface, such as R175H and R249S [73]. It is expected that alkylation of contact mutants would occur

in a similar manner to alkylation of wt p53. These mutations do not generally affect protein stability and alkylation of structural mutants would result in an increased rate of Cys-modification because these mutations typically cause thermodynamic destabilisation of p53, and increased protein unfolding [212].

Alkylation of cysteine residues in p53 hot spot mutants results in the death of tumour cells [118]. However, the specific binding sites and mechanism of action of these anti-cancer compounds are unknown. The FT-ICR MS methods that have been described here can be utilised to determine which Cys residues are modified by anti-tumour alkylating compounds, therefore shedding light on their role in apoptosis of cancerous cells.

In order to test whether dialkylated forms of wt or mutant p53 are responsible for the increase in DNA-binding that is observed upon treatment with NEM or MIRA-1, DNA-binding assays could be performed by electromobility shift assays following the same protocol described in Chapter 2.2.9, using unmodified, dialkylated and fully alkylated p53. Alternatively, fluorescence anisotropy or mass spectrometry could be used to measure DNA-binding. Fluorescence anisotropy and mass spectrometry have both previously been used to measure dissociation constants (K_D) for p53 core domain, as well as the tetramerization domain (p53CT) bound to consensus DNA [250, 251]. Understanding how and why alkylation of p53 Cys residues increases p53 DNA-binding, and promotes the death of tumour cells, will accelerate the development of effective chemotherapeutics.

Chapter 5: Oxidation of p53 by Hydrogen Peroxide

5.1 Introduction

The effects of common post-translational modifications (PTMs) such as phosphorylation, acetylation, ubiquitination and methylation on p53 activity and stability have been well documented [252-255]. In contrast, little attention has been paid to the role of redox-modifications of highly conserved cysteine residues in p53. However, the recent discovery of p53 thiol-targeting anti-tumour compounds [118], and increasing evidence linking reactive oxygen species (ROS) with p53 function [104-106], has emphasised the importance of p53 cysteines and is leading to wider recognition of their fundamental role in regulation of p53 activity.

Basal physiological levels of the ROS hydrogen peroxide (H_2O_2) are known to correlate with p53-mediated transcription of antioxidant genes such as glutathione peroxidase-1 (GPX1) and mammalian sestrin homologue (SESN1), whereas hyperphysiological levels of H_2O_2 induce p53-mediated transcription of pro-oxidant genes, such as quinone oxidoreductase (NQO1) and proline oxidase (POX) [104, 106]. However, the direct result of the interaction between H_2O_2 and p53 on protein redox-state, structure and function is unknown.

In this Chapter, the *in vitro* oxidation of the p53 core domain by the ROS signalling molecule hydrogen peroxide is described. An affinity purification strategy was developed in order to purify oxidised p53, and the analytical power of FT-ICR mass spectrometry was utilised to unambiguously identify the oxidation state of each Cys residue. It was found that oxidation of p53 by H_2O_2 proceeds via an ordered oxidation pathway, and that oxidation via an alternative route results in indiscriminate over oxidation of the protein. Furthermore, oxidation in the presence of intracellular redox factors Zn^{2+} and glutathione (GSH) was investigated. The results discussed here provide insights into the signalling mechanisms between cellular ROS and p53.

5.2 Air Oxidation

Prior to investigating H_2O_2 -mediated oxidation of p53, it was noticed that low levels of p53 oxidation occur when the protein is stored in the absence of reducing agent. The mass spectrum of p53 core domain displayed in Figure 3.3 (see Chapter 3.3)

suggested that each cysteine residue was in its reduced form. This spectrum was recorded immediately after buffer exchange from storage buffer (containing reducing agent) into ammonium acetate followed by the addition of acid for denaturing electrospray ionisation (ESI) conditions (low pH prevents cysteine oxidation due to protonation of the thiol groups). The spectrum shown in Figure 5.1A was recorded from p53 core domain stored in ammonium acetate in the absence of reducing agent for > 1 h. The experimental isotope distribution of p53 stored in the absence of reducing agent lies between the theoretical isotope distributions for fully reduced p53 core domain and for p53 with one disulfide bond (i.e. with a 2 Da mass decrease corresponding to the loss of two hydrogen atoms). This suggests that a mixture of reduced and oxidised species were present in solution. Correspondingly, the mass spectrum of p53 treated with an excess of alkylating reagent (see Figure 3.5) revealed the presence of p53 modified with only 8 NEM groups, suggesting that a proportion of the protein had formed one intramolecular disulfide bond. The thiol groups were presumably oxidised by soluble oxygen. Interestingly, when the p53 Cys-Ser mutant C277S was treated with an excess of alkylating reagent (see Chapter 4.4), this low level oxidation of p53 was not observed (see Figure 4.16), suggesting that Cys277 is susceptible to air oxidation in the absence of reducing agent.

Delphin *et al.* analysed ^{14}C -iodoacetamide labelled p53, which had been stored in the absence of DTT by SDS-PAGE, followed by autoradiography [94]. They estimated that p53 lost an average of three or four free thiol groups after three weeks in the absence of reducing agent. Momand *et al.* analysed p53 using Ellman's reagent (which absorbs at 412 nm upon binding to thiol groups) and found that p53 loses one free thiol group when stored in the absence of reducing agent for 1 h [97]. Both studies showed that the presence of oxidised p53 correlated with inhibition of specific DNA-binding. However, neither Delphin *et al.* nor Momand *et al.* were able to identify which Cys residues were responsible for regulating p53 DNA-binding activity *in vitro*.

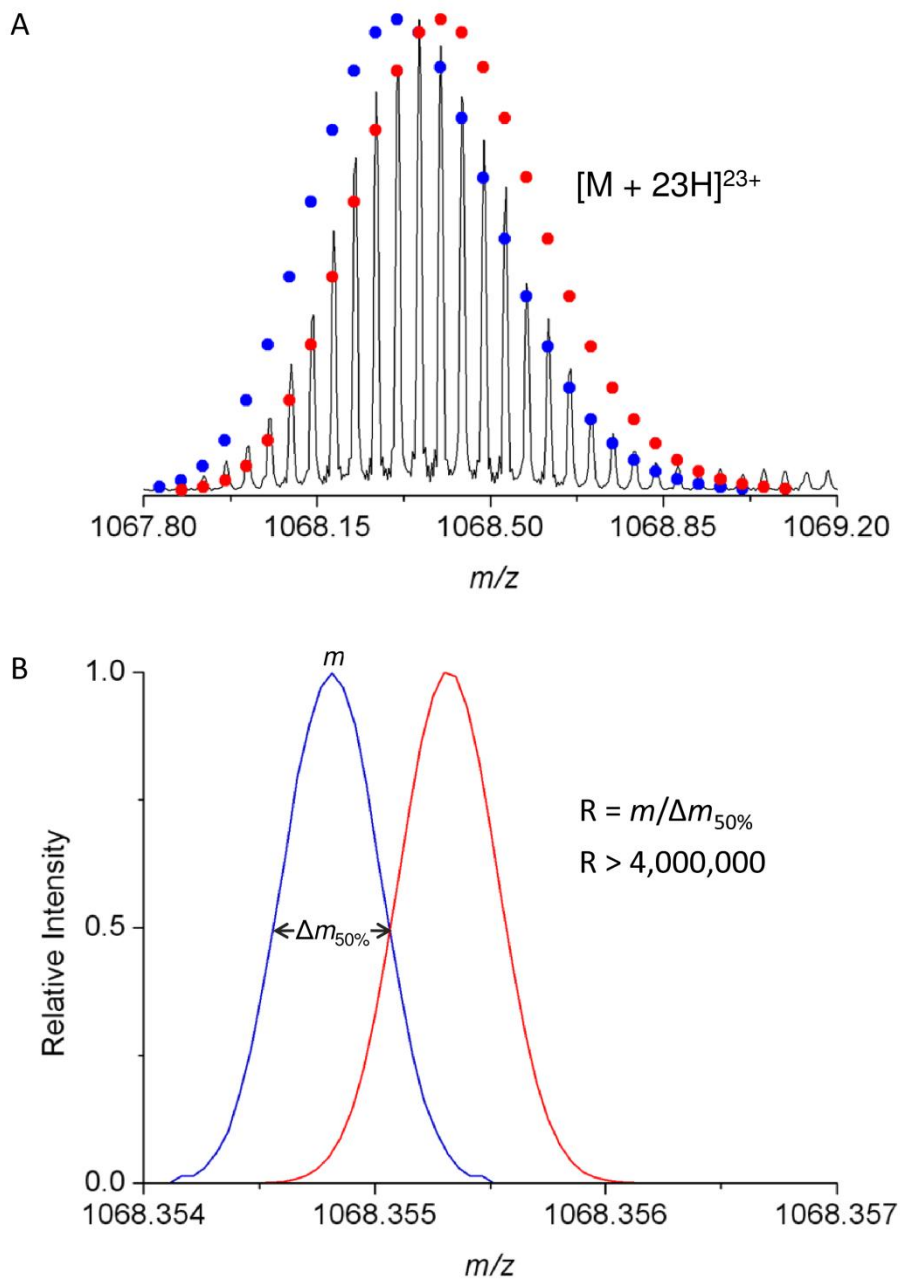


Figure 5.1 Air oxidation of p53. **(A)** The experimental isotope distribution of the 23+ charge state of p53 core domain stored in the absence of reducing agent lies in between the simulated isotope distributions for reduced p53 and p53 with one disulfide bond (empirical formulae $[C_{1055}H_{1696}N_{321}O_{324}S_{16}]^{23+}$; \bullet ; and $[C_{1055}H_{1694}N_{321}O_{324}S_{16}]^{23+}$; \circ ; respectively). **(B)** Simulated individual isotope peaks for reduced p53 and p53 with one disulfide bond. The resolving power required to distinguish the reduced and oxidised form of p53 from each other is $> 2,000,000$ at m/z 1068.

5.3 Mixtures of Oxidised and Reduced p53

At 25 kDa, the p53 core domain has a relatively broad isotope distribution. Hence, when a species is present that only differs in mass by 2 Da (i.e. p53 with a disulfide bond), the isotope peaks from the different species overlap and contribute to an observed isotope distribution which is the sum of the distributions for the different species, as shown in Figure 5.1A. The overlapping isotope peaks do in fact differ in mass due to the mass of hydrogen not being exactly 1 Da. However, the resolving power needed to distinguish the peaks from each other is exceptionally high. Figure 5.1B shows two simulated isotope peaks for the 23+ charge state of reduced p53, and for p53 with one disulfide bond. The resolution in terms of FWHM ($\Delta m_{50\%}$) required to resolve these two peaks is 0.0005 Da, corresponding to a resolving power (R) in excess of 2,000,000 at 1068 m/z . The resolving power achieved in the mass spectrum of p53 shown in Figure 5.1A is 100,000 at m/z 1068. Heterodyne detection (narrow band mode) and tuning of instrument parameters can be performed in order to maximise resolving power, which is limited by many factors including magnetic field strength and vacuum pressure [163, 166]. However, achieving the high resolving power required for separation of reduced and oxidised forms of p53 during routine analysis is difficult, and labelling of free thiol groups provides a simple means of identifying the oxidation states present in the mixture. For example, for each disulfide bond that is present, labelling of free thiol groups with NEM (125 Da) will result in a mass decrease of 250 Da. Providing that the mass range is sufficient, determining the number of oxidised and reduced cysteine residues in an intact protein can, therefore, be achieved using relatively inexpensive low resolution mass spectrometers, such as linear quadrupole or TOF instruments [144, 149].

5.4 H₂O₂ Oxidation

5.4.1 Disulfide Bond Formation

p53 core domain (15 μ M) in ammonium acetate buffer was treated with increasing concentrations of H₂O₂ for 1 min at room temperature. Oxidation was quenched by lowering the pH with the addition of denaturing ESI-MS solution (50% MeOH and

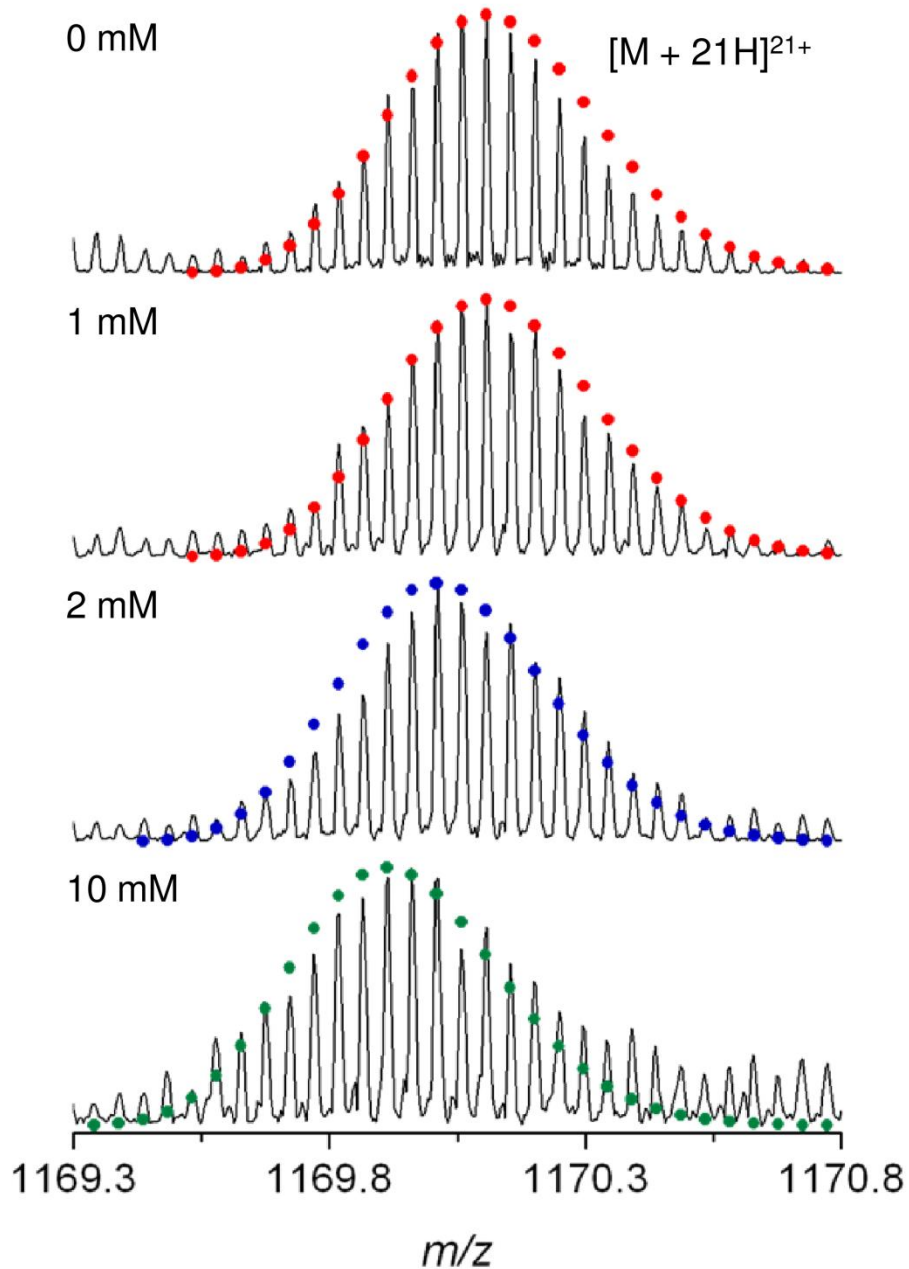


Figure 5.2 Isotope distributions of p53 core domain treated with increasing concentrations of H_2O_2 for 1 min. The 21+ charge states are shown. Experimental distributions that lie in between simulated isotope distributions for reduced p53, p53 with one disulfide bond or p53 with two disulfide bonds (empirical formulae $[C_{1055}H_{1694}N_{321}O_{324}S_{16}]^{21+}$; •; $[C_{1055}H_{1692}N_{321}O_{324}S_{16}]^{21+}$; •; and $[C_{1055}H_{1690}N_{321}O_{324}S_{16}]^{21+}$; •; respectively) suggest a mixture of reduced and oxidised species was present.

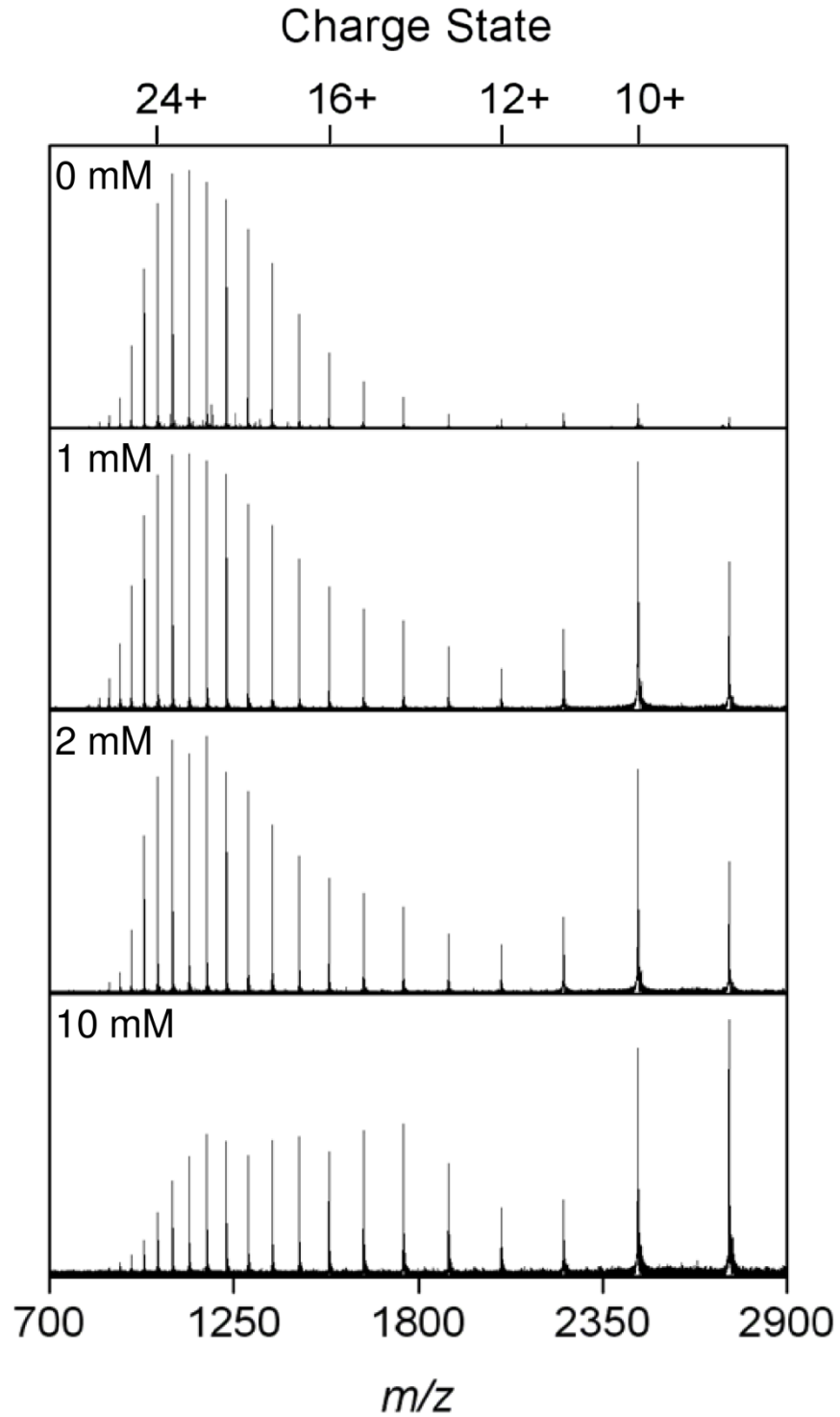


Figure 5.3 Charge state distributions of p53 core domain treated with increasing concentrations of H₂O₂ for 1 min. FT-ICR mass spectra were recorded under denaturing conditions. The addition of H₂O₂ results in an increase in the relative abundance of lower charge states such as [M + 10H]¹⁰⁺ and [M + 9H]⁹⁺.

0.1% formic acid). nESI FT-ICR mass spectra were recorded and the resulting isotope distributions for the 21+ charge states are shown in Figure 5.2.

As H_2O_2 concentration increases, the isotope distributions shift to lower m/z values indicating disulfide bond formation. However, the experimental isotope distributions for p53 at 2 mM and 10 mM H_2O_2 lie in between theoretical distributions for p53 core domain with one or two disulfide bonds. As described above, this indicates that a mixture of species was present and labelling of the free thiol groups was carried out in order to identify the oxidised forms present.

5.4.2 Effect on Protein Structure

The charge state distributions of p53 treated with increasing concentrations of H_2O_2 for 1 min are shown in Figure 5.3. The charge state distribution of p53 prior to the addition of oxidising agent is typical of denatured p53, with the predominate distribution ranging over relatively high charge states, predominately from 14+ to 30+. Interestingly, upon addition of H_2O_2 , the relative abundance of the lower 9+ and 10+ charge states dramatically increased, suggesting that some degree of p53 was present in a folded conformation.

Lower charge states are associated with folded, more compact forms of a protein's tertiary structure. The predominate charge states in the mass spectrum of folded, Zn^{2+} -bound p53 core domain recorded under native conditions (see Chapter 3; Figure 3.4) were 9+ and 10+. Despite the denaturing conditions used here, FT-ICR mass spectra of p53 treated with H_2O_2 suggest that some degree of p53 was present in a more compact conformation, which has many of its protonation sites protected. This observation is consistent with the formation of disulfide bonds. Reduction of disulfide bonds in the proteins lysozyme and bovine serum albumin is known to result in higher charge states, due to the exposure of the buried basic residues Arg, Lys and His [256]. A disulfide bond formed between two Cys residues in p53 could have effectively 'locked' the protein in a particular folded conformation, therefore, preventing the protein from unfolding and exposing the side chains of buried basic amino acids.

5.4.3 Labelling of Free Thiol Groups

p53 core domain (130 μ M) was incubated with 4 mM H₂O₂ on ice and the reaction was quenched at various time points by TCA precipitation. The protein was re-suspended in 6 M guanidine supplemented with 10 mM NEM and the alkylated protein was analysed by on-line reverse phase LC FT-ICR MS. The resulting deconvoluted neutral mass spectra are shown in Figure 5.4.

The spectrum recorded for the 0 min time point (i.e. prior to addition of H₂O₂) shows that a small fraction (5%) of p53 was modified with 8 NEM groups, indicating that a small degree of air oxidation occurred prior to oxidation with hydrogen peroxide.

At the 15 min time point, the presence of p53 modified with 6 NEM groups was apparent, indicating the formation of 2 disulfide bonds. By 30 min, the relative abundance of the 6 NEM, 2-disulfide species had increased from to 34%, and the appearance of p53 modified with 4 NEM groups was observed, indicating formation of 3 disulfide bonds. By 60 min, 40% of p53 present had 2 disulfide bonds and 21% of p53 had 3 disulfide bonds. After 4 h, 59% of p53 contained 3 disulfide bonds, 21% of p53 contained 2 disulfide bonds and the appearance of p53 with 4 disulfide bonds was observed. Comparison of theoretical isotope distributions with experimental isotope distributions observed in the undeconvoluted spectra of p53 treated with H₂O₂ (see Figure 5.5) confirmed the presence of fully alkylated p53, the 6 NEM, 2-disulfide species and the 4 NEM, 3-disulfide species. The MME for each species was < 10 ppm.

The relative abundance of the 8 NEM, 1-disulfide species was ~15% at the 15, 30 and 60 min time points. At this stage it is unknown if oxidation of p53, resulting in the 2-disulfide species, occurred in a sequential or concerted manner. The 1-disulfide species may be an intermediate oxidised form of the protein, which occurred prior to oxidation of the second disulfide bond. Alternatively, this species may represent p53 oxidised via an alternative pathway.

Adducts of 16 Da were observed after H₂O₂ treatment, corresponding to the addition of one oxygen atom. It is likely that the thioether group in a methionine

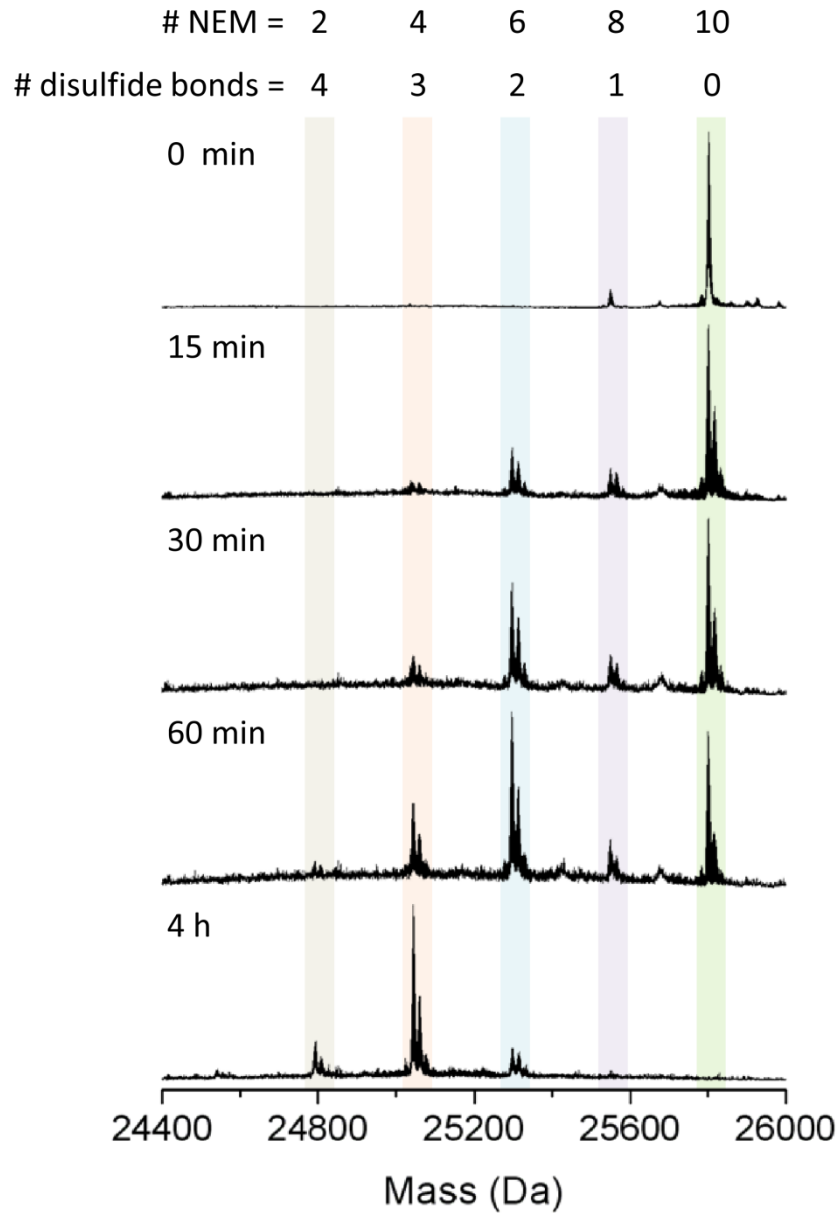


Figure 5.4 Oxidation of the p53 core domain over time. p53 was incubated with 4 mM H_2O_2 on ice for increasing times followed by alkylation of free thiols with NEM and analysis by LC FT-ICR MS. Deconvoluted neutral mass spectra are shown. The number of disulfide bonds present in p53, as determined from the number of NEM adducts, are indicated.

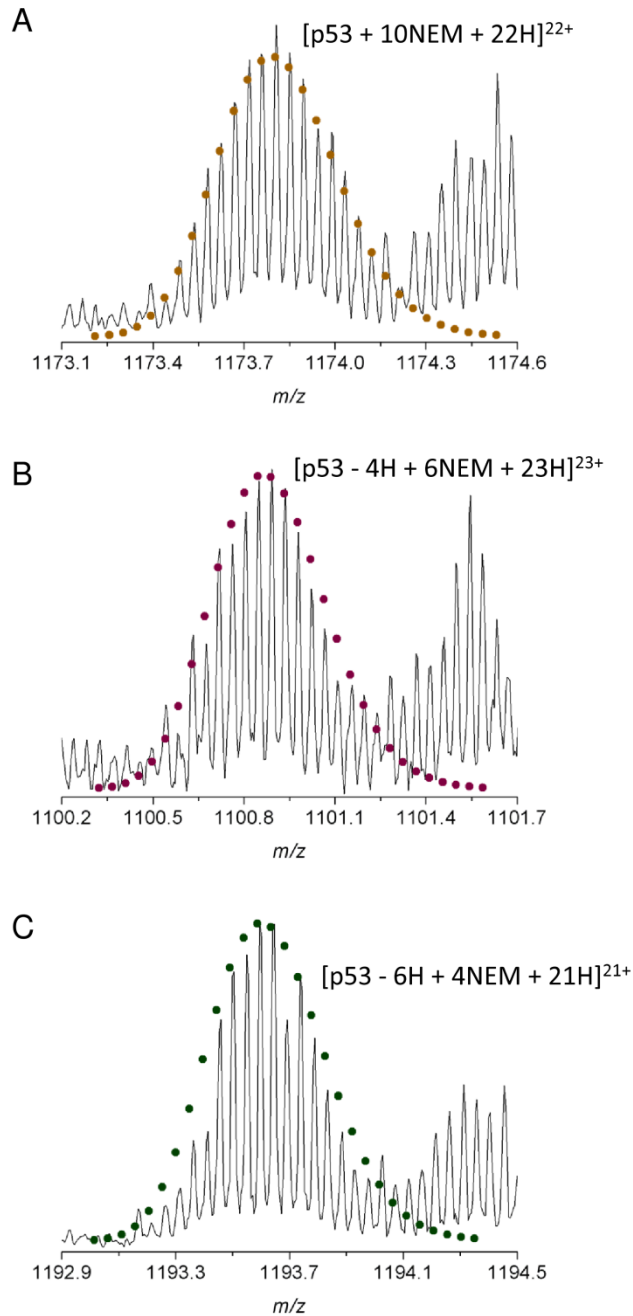


Figure 5.5 Isotope distributions of p53 core domain treated with H₂O₂ and alkylated with NEM. Theoretical isotope distributions are consistent with the experimental isotope distributions for **(A)** p53 modified with 10 NEM groups (22+ charge state; empirical formula [C₁₁₁₅H₁₇₆₅N₃₃₁O₃₄₄S₁₆]²²⁺; •; 4 ppm MME) **(B)** p53 with 2 disulfide bonds and 6 alkylated Cys residues (23+ charge state; empirical formula [C₁₀₉₁H₁₇₃₄N₃₂₇O₃₃₆S₁₆]²³⁺; •; 3 ppm MME) and **(C)** p53 with 3 disulfide bonds and 4 alkylated Cys residues (21+ charge state; empirical formula [C₁₀₇₉H₁₇₁₆N₃₂₅O₃₃₂S₁₆]²¹⁺; •; 9 ppm MME).

residue was oxidised to a sulfoxide ($R_2S=O$). Surprisingly, the level of oxygen incorporation did not increase, even after 4 h of incubation with an excess of peroxide.

As with alkylation of p53 Cys residues, oxidation of p53 by the reactive oxygen species hydrogen peroxide seems to proceed in distinct steps. Initially, the majority of p53 forms two disulfide bonds, resulting in a stable oxidised species. It is unknown if these disulfide linkages are formed sequentially or in a concerted manner. Further oxidation results in the formation of a third disulfide bond, again resulting in a stable oxidised species. Oxidation of a p53 cysteine residue to sulfinic or sulfonic acid was not detected. It is expected that continued incubation with H_2O_2 would have resulted in the formation of 5 disulfide bonds. However, it seems unlikely that p53 is oxidised to this extent *in vivo*.

Top-down mass spectrometry can be performed to identify which Cys residues were oxidised by H_2O_2 . However, separation of the reduced and oxidised forms of p53 is desirable in order to maximise the potential for extensive fragmentation of the protein.

5.5 Affinity Purification of Oxidised p53

5.5.1 Methodology

As described above, oxidation of p53 core domain by H_2O_2 does not result in a single species. As the heterogeneity of a sample increases, the signal to noise ratio in the resulting mass spectrum decreases. In order to achieve extensive fragmentation over the entire length of an intact protein, a relatively high abundance of the parent ion is required, especially when fragmentation techniques such as ECD are employed. In addition to improving the potential for high sequence coverage, purification of oxidised forms of p53 would also be beneficial for investigating functional properties such as specific DNA-binding activity, or testing recognition by p53 conformation-specific antibodies [93].

Neither reverse phase nor ion exchange liquid chromatography performed under a range of conditions resulted in separation of the NEM-labelled reduced and oxidised forms of p53 core domain. Hence, a purification method was developed

based on the presence of free thiol groups and the ultra-strong non-covalent interaction ($K_D = 10^{-15}$ M) between biotin and avidin [257]. Free thiol groups can be reversibly biotinylated via a thiol-disulfide exchange mechanism using the reagent EZ-Link Biotin-HPDP (N-[6-(Biotinamido)hexyl]-3'-(2'-pyridyldithio) propionamide; Pierce) shown in Figure 5.6. The addition of one Biotin-HPDP group corresponds with a monoisotopic mass increase of 428.1916 Da. Furthermore, the pyridine-2-thione by-product absorbs at 343 nm, hence, incorporation of the Biotin-HPDP group can also be monitored by UV-Vis spectroscopy in addition to MS [258].

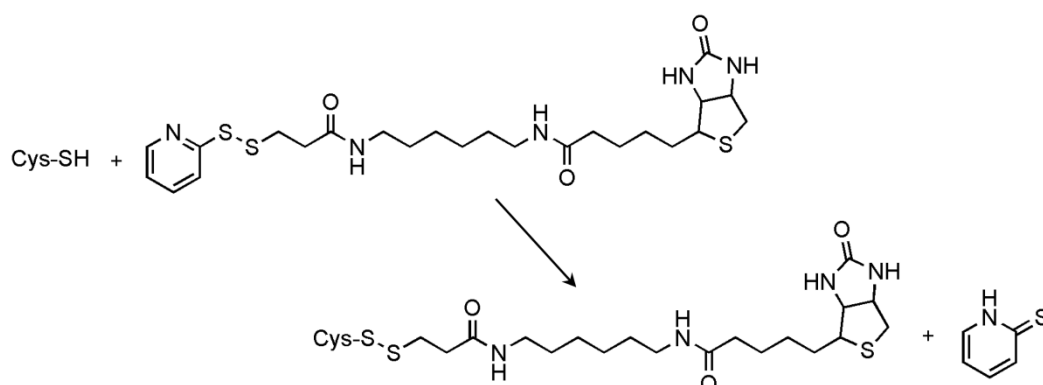


Figure 5.6 Biotinylation of cysteine using the free thiol-labelling reagent EZ-Link Biotin-HPDP (Pierce).

A schematic diagram illustrating separation of oxidised p53 from reduced p53 is shown in Figure 5.7. Following oxidation and irreversible alkylation of free thiol groups with NEM, the mixture of species is treated with reducing agent leading to reduction of the disulfide bonds in oxidised p53. The resulting free thiol groups are biotinylated using the Biotin-HPDP reagent and biotinylated-p53 is captured by immobilised avidin. Fully NEM-labelled p53 (corresponding to reduced p53) is then removed by washing steps. Partially NEM-labelled p53 (corresponding to oxidised p53) is eluted from immobilised avidin by reduction of the disulfide bond between p53 and Biotin-HDPD.

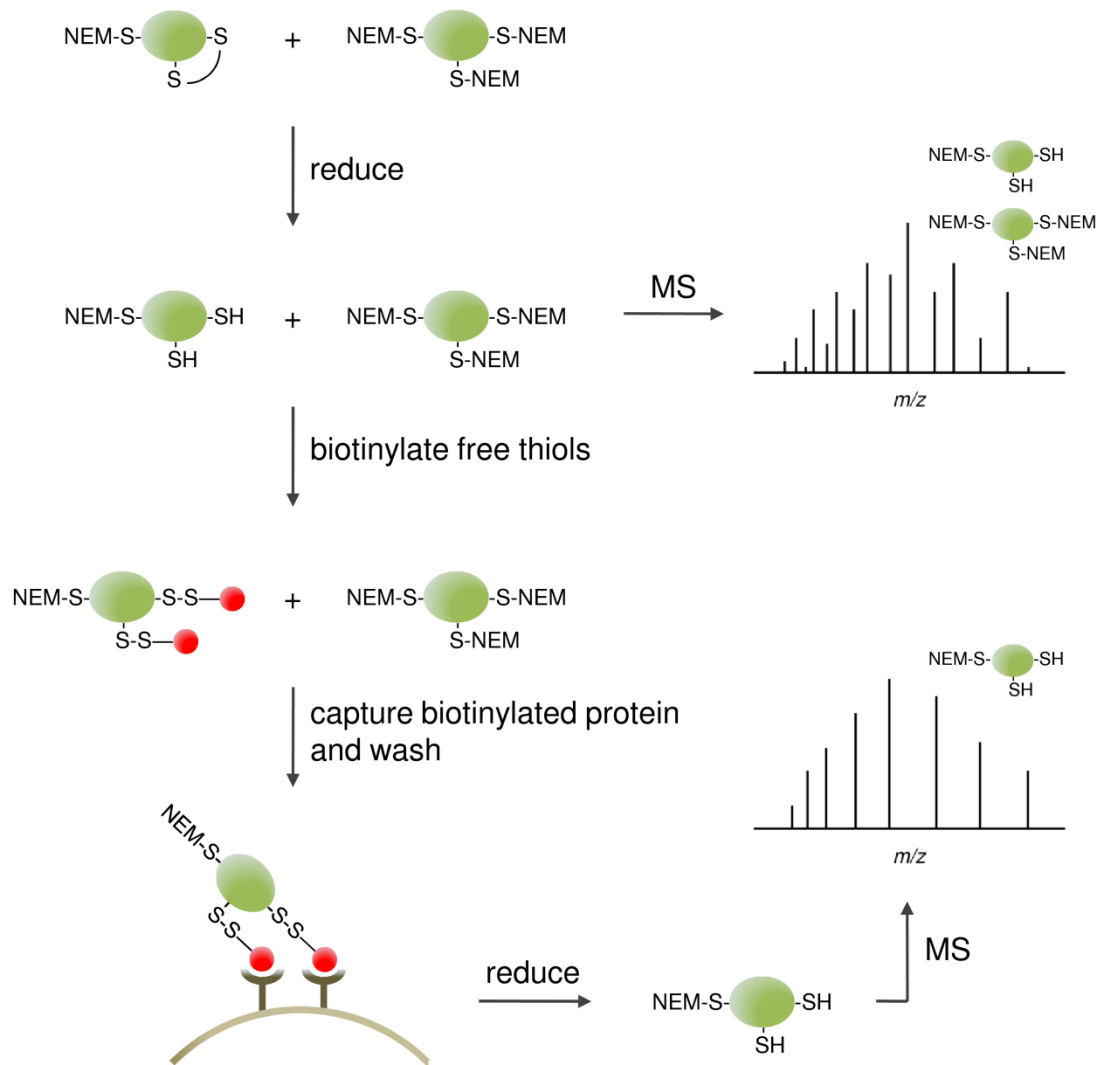


Figure 5.7 Affinity enrichment of oxidised p53. Schematic diagram illustrating the separation of oxidised protein from reduced protein using the free thiol labelling reagent Biotin-HPDP.

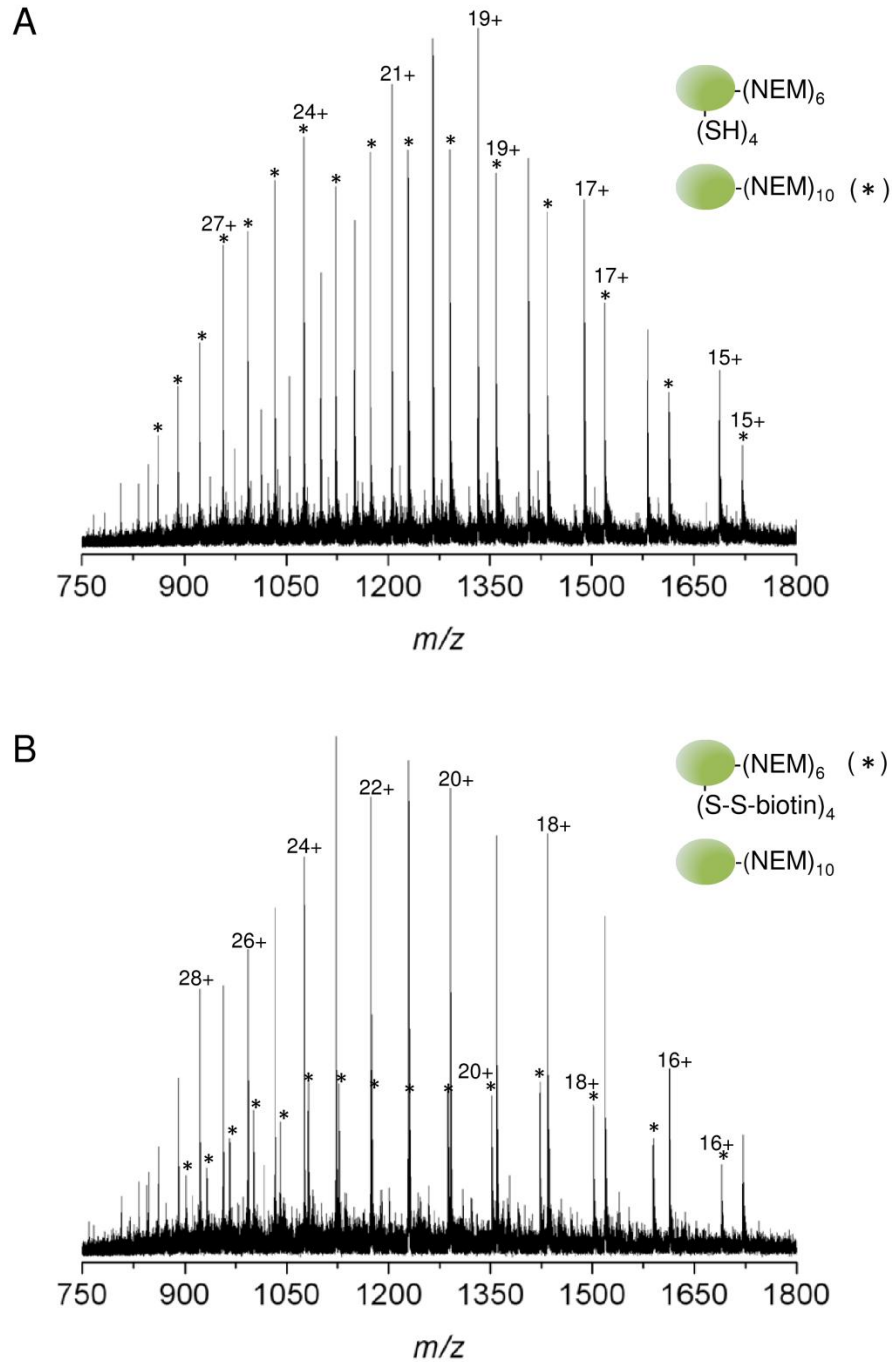


Figure 5.8 Affinity enrichment of oxidised p53. **(A)** FT-ICR mass spectrum of p53 following H_2O_2 and NEM treatment. Two main charge state distributions are apparent, corresponding to p53 with 10 alkylated Cys residues (reduced) (indicated with an asterisk) and p53 with 2 disulfide bonds and 6 alkylated Cys residues (oxidised). **(B)** FT-ICR mass spectrum of p53 following H_2O_2 , NEM and Biotin-HPDP treatment. The low abundance charge-state distribution corresponds to p53 modified with 6 NEM groups and 4 Biotin-HPDP groups (indicated with an asterisk).

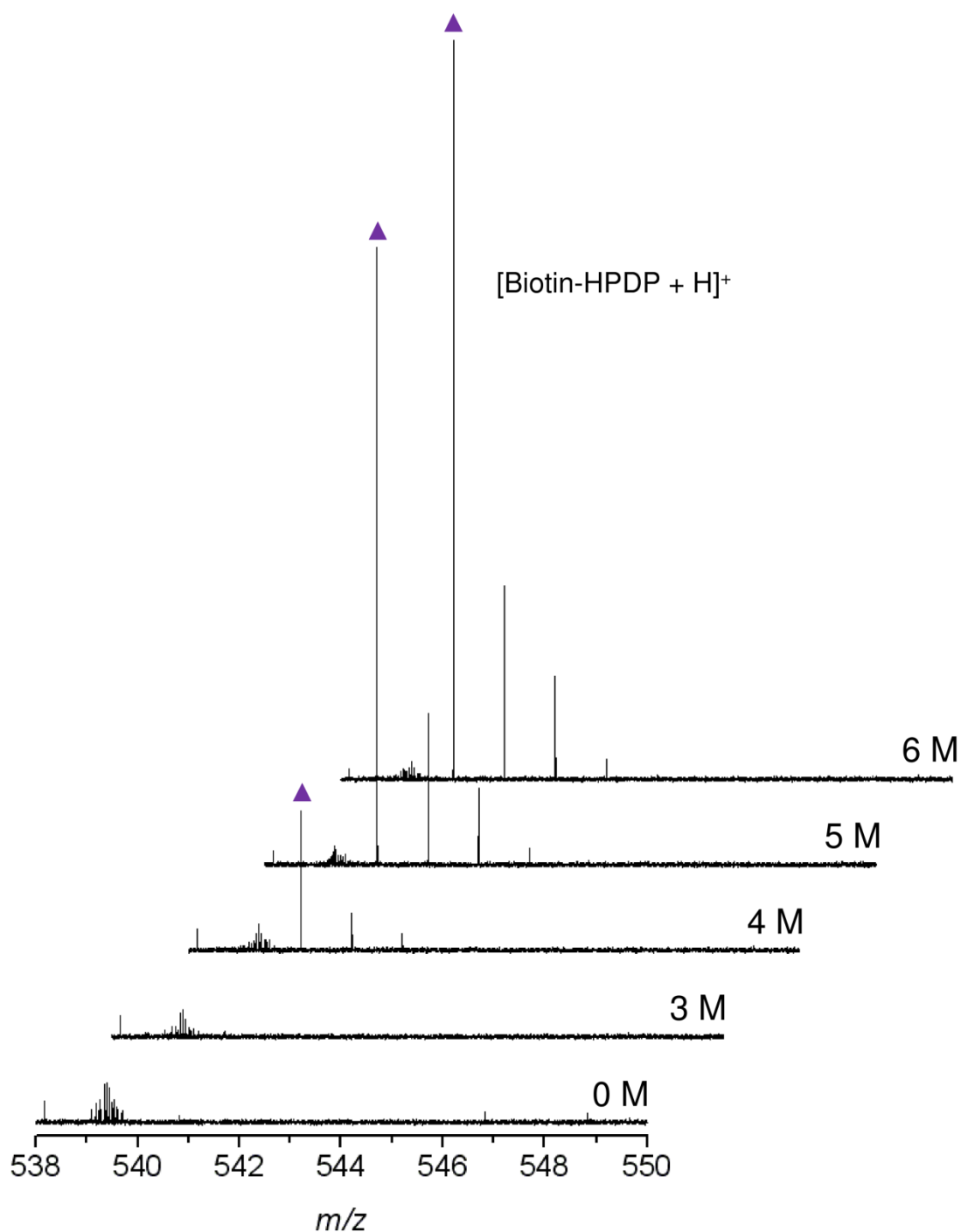


Figure 5.9 Determination of the tolerance of the monomeric avidin–biotin complex to guanidine. Biotin-HPDP was incubated with immobilised monomeric avidin in increasing concentrations of guanidine.HCL and the supernatant was analysed by LC FT-ICR MS. Biotin-HPDP ions (m/z 540.21; \blacktriangle) were observed at a concentration of 4 M guanidine and higher concentrations.

5.5.2 Biotinylation

p53 core domain (130 μ M) was oxidised for 15 min and alkylated as described previously. Figure 5.8A shows the resulting mass spectrum. Two charge states are apparent; one corresponding to p53 with 10 alkylated Cys residues (indicated with an asterisk) and the other corresponding to p53 with 6 alkylated Cys residues, indicating the formation of 2 disulfide bonds. The alkylated p53 mixture was incubated with an excess of DTT (25 mM) followed by TCA precipitation, re-suspension in 6 M guanidine supplemented with 0.4 mM Biotin-HPDP and analysis by FT-ICR MS. Two charge state distributions are again observed in the resulting mass spectrum (see Figure 5.8B); one corresponding to p53 with 10 NEM adducts and one corresponding to p53 modified with 6 NEM adducts and 4 Biotin-HPDP adducts (indicated with an asterisk).

5.5.3 Capture

The biotinylated p53 species was found to be prone to precipitation. Hence, the biotinylation reaction was performed in 6 M guanidine solution. However, in order for the non-covalent interaction between biotin and avidin to be retained, such harsh denaturing conditions cannot be used for the capture of biotinylated p53. A titration was performed in order to determine the maximum concentration of guanidine that the biotin-avidin complex could withstand. Biotin-HPDP was incubated with monomeric avidin agarose in increasing concentrations of guanidine-HCl, and the supernatants were analysed by LC FT-ICR MS (see Figure 5.9). Biotin-HPDP ions (m/z 540.21) were detected at a concentration of 4 M guanidine and at higher concentrations, indicating denaturation of avidin at these higher concentrations. However, only a relatively small degree of avidin-biotin dissociation was observed at a concentration of 4 M guanidine. Hence, capture of biotinylated p53 was performed at this concentration in order to maximise the solubility of p53.

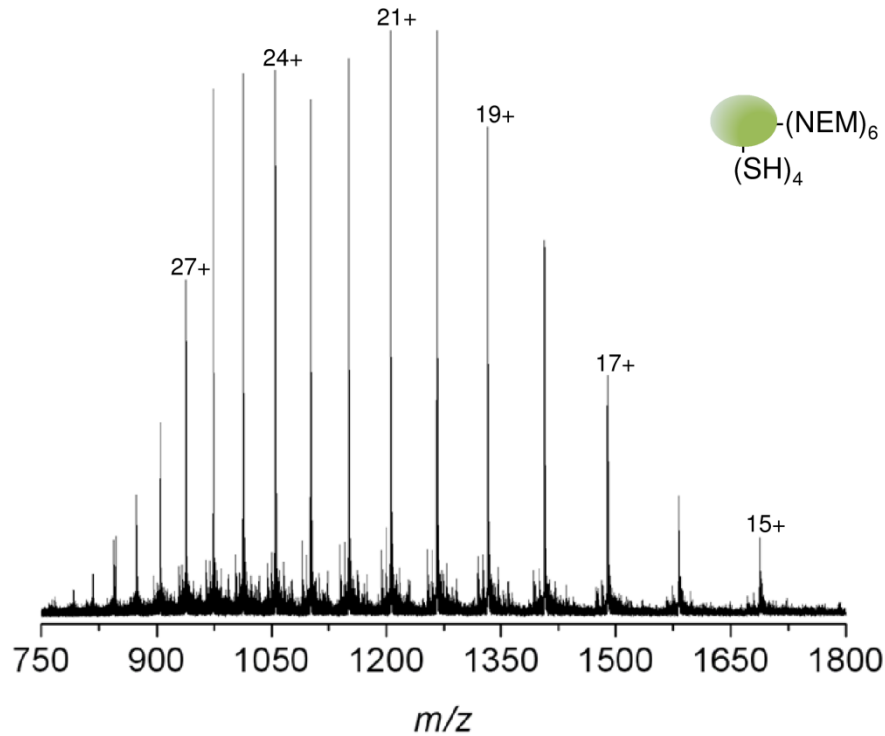


Figure 5.10 Affinity enrichment of oxidised p53. FT-ICR mass spectrum of p53 following affinity enrichment steps illustrated in Figure 5.7. The predominating charge state distribution corresponds to oxidised p53 (6NEM-p53).

5.5.4 Elution

Following capture of biotinylated-p53 with immobilised monomeric avidin, the beads were washed and supernatant containing 10NEM-p53 was removed. Elution of partially alkylated p53 was achieved by incubation of the captured protein with an excess of DTT (50 mM). The FT-ICR mass spectrum of the eluent is shown in Figure 5.10. One charge state distribution is present which corresponds to 6NEM-p53, demonstrating the successful purification of p53 which had been oxidised by H_2O_2 .

5.6 Identification of Oxidised Cysteine Residues

Top-down FT-ICR MS was used to identify the NEM-labelled and reduced Cys residues in 6NEM-p53, in order to identify the four Cys residues that were initially

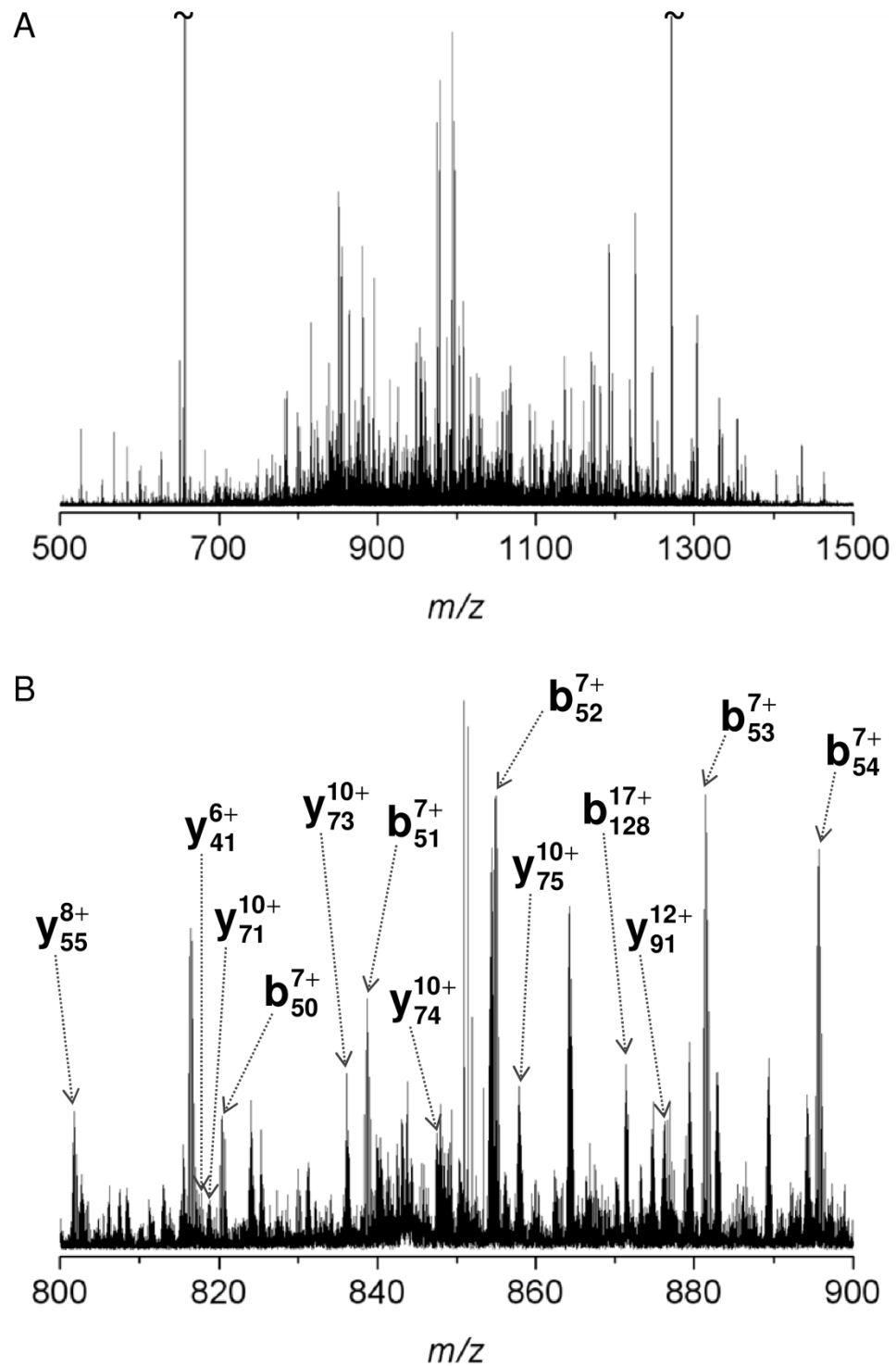












Figure 5.11 Top-down FT-ICR MS of 6NEM-p53. **(A)** CID mass spectrum of the 30+ charge state (844 m/z) of 6NEM-p53. **(B)** Expansion of the region 800-900 m/z . Assigned b and y ions are annotated.

Table 5.1 Permutations of 6NEM-p53 that corresponded with the highest number of assigned fragment ions resulting from top-down FT-ICR MS. The red circles indicate the positions of the NEM adducts.

Rank	Permutation	Number of Fragment Ions [†]
1		69
2		68
3		66
4		60
4		60
5		59
5		59
6		59
6		59
7		58

[†]The number of non-redundant *b* and *y* ions that corresponded with different permutations of the p53 core domain primary sequence modified with six NEM groups.

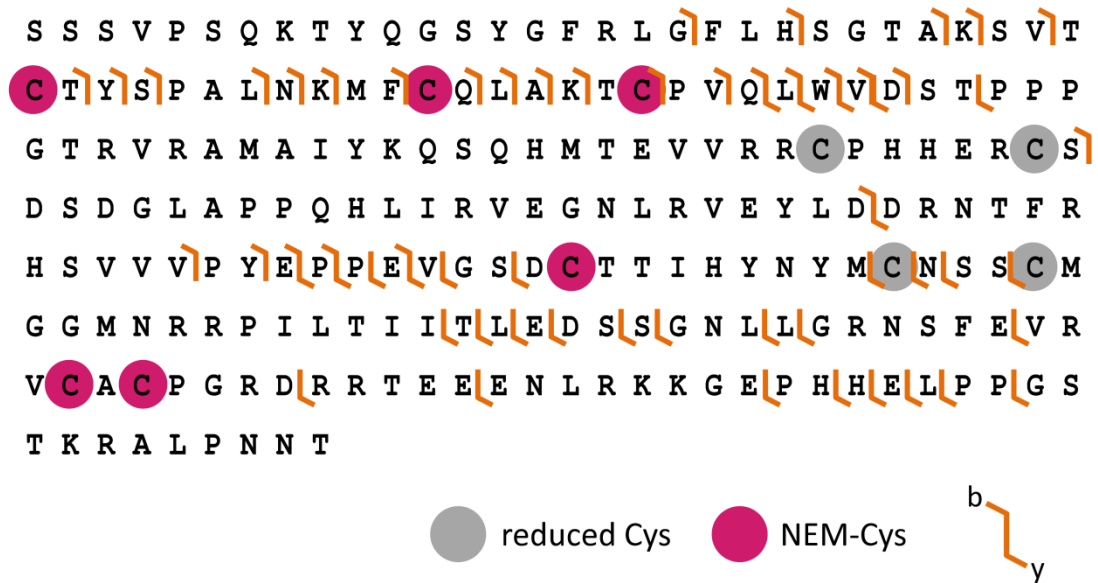


Figure 5.12 The fragment map displays ions resulting from CID fragmentation of intact p53 core domain (Ser94 - Thr312) modified with six NEM groups. Top-down FT ICR MS of 6NEM-p53 suggested that Cys124, 135, 141, 229, 275 and 277 were alkylated therefore Cys176, 182, 238 and 242 were the oxidised residues.

oxidised by H_2O_2 . The purified 6NEM-p53 species was desalted by off-line reverse-phase liquid chromatography and the p53-containing fraction was manually collected and directly infused into the FT-ICR mass spectrometer. Individual charge states (24+, 16+ and 30+) were sequentially isolated and fragmented using collision-induced dissociation (CID). A typical CID spectrum of 6NEM-p53 is shown in Figure 5.11.

The monoisotopic masses of the resulting fragment ions were searched against theoretical fragment mass lists for each of the 210 permutations of the p53 core domain primary sequence, modified with six NEM groups. Permutations of 6NEM-p53 were ranked according to the number of corresponding non-redundant *b* and *y* ions. The ten combinations of NEM positions that were associated with the number of assigned fragment ions (69) corresponded with the six NEM groups

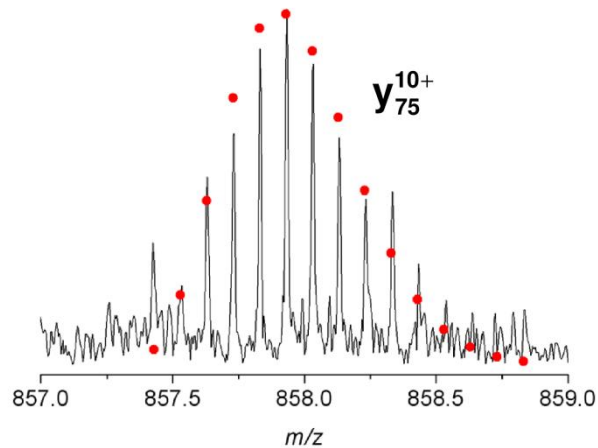


Figure 5.13 The fragment ion y_{75}^{10+} (empirical formula $[C_{356}H_{598}N_{118}O_{116}S_6]^{10+}$; •; 3 ppm MME) supports the assignment of oxidation of Cys238.

located on Cys124, 135, 141, 229, 275 and 277.^{†††} The fragment ions associated with this permutation of 6NEM-p53 are shown in Figure 5.12. Cys176, 182, 238 and 242 were not found to be alkylated. Therefore, revealing that they were the residues involved in disulfide bond formation. Interestingly, Cys176, 238 and 242 are zinc binding residues.

Taken together, the fragments resulting from CID of 6NEM-p53 resulted in 25% protein sequence coverage. Fragment ions were not observed between each Cys residue yet, due to the positions of the NEM groups, the oxidation/modification state of each of the 10 Cys residues in p53 core domain was unambiguously determined. For example, both Cys275 and Cys277 were alkylated therefore a diagnostic *b* or *y* ion located in between these two Cys residues was not required in order to determine their oxidation states.

One fragment ion which is shown in Figure 5.13, y_{75}^{10+} , was observed between Cys229 and Cys238 which supported placement of the NEM group on Cys238. In order to increase the number of inter-residue bonds cleaved over the internal region of the protein, therefore increasing confidence in the assignment of Cys oxidation

^{†††}Mass assignments for fragment ions corresponding to this permutation of 6NEM-p53 are listed in Appendix B.7.

Table 5.2 Possible combinations of cross-linked tryptic peptides from 6NEM-p53 with two intramolecular disulfide bonds involving Cys176, 182, 238 and 242 and their associated monoisotopic masses. The red dots indicate the position of NEM adducts.

Peptides	Connectivity	Mass / Da
C176 – R181 C182 – R196		3051.45
H214 – R196		3999.65
C176 – R181 C182 – R196 H214 – R248		7051.10
C176 – R181 C182 – R196 H214 – R248		7051.10

states, middle-down MS could be performed on the purified 6NEM-p53 species, as described in Chapter 4.3.2.

5.7 Cysteine Connectivity

Bottom-up FT-ICR mass spectrometry of oxidised p53 was performed in order to determine the connectivity of the disulfide bonds involving Cys176, 182, 238 and 242. p53 treated with H₂O₂ and alkylated with NEM was incubated with trypsin and the resulting peptide mixture was desalted and analysed by nESI FT-ICR MS, without prior separation. Table 5.2 shows the possible combinations of crosslinked peptides that could arise from tryptic digestion of 6NEM-p53 with 2 disulfide bonds involving Cys176, 182, 238 and 242, and their associated monoisotopic masses. Cysteines 238 and 242 are located in the same tryptic peptide. Hence, if either of these residues were linked to Cys176 or Cys182, fragmentation would be required in order to determine their connectivity.

Unfortunately, no tryptic peptides containing cross-linked Cys residues were detected in the bottom up FT-ICR mass spectrum of H₂O₂-treated p53 (data not

shown). Peptides were detected that showed NEM alkylation of each of the 10 Cys residues in p53, presumably originating from the 10NEM-p53 species corresponding to reduced p53. Bottom-up FT-ICR MS should be performed on the purified 6NEM-p53, 2-disulfide species in order to increase the probability of detecting the crosslinked peptides. In addition, peptides of interest could be purified by high performance liquid chromatography (HPLC), as described by Campopiano *et al.* [259]. As previously discussed, incomplete sequence coverage is a problem common to peptide based proteomic strategies for mapping PTMs.

5.8 Oxidation of Zinc-Binding Cysteines

Oxidation of p53 by hydrogen peroxide results in the initial formation of two disulfide bonds involving Cys176, 182, 238 and 242. Interestingly, Cys176, 238 and 242 are the three Zn²⁺ binding cysteine residues in p53. The zinc ion is presumably displaced upon oxidation of these residues. This could be verified by FT-ICR MS of oxidised p53 under native conditions, or by using the Zn²⁺ chelating dye 4-(2-pyridylazo) resorcinol (PAR), which absorbs strongly at 500 nm upon formation of the Zn(PAR)₂ complex (66,000 M⁻¹) [260].

Formation of disulfide linkages between zinc-binding Cys residues correlates well with the charge state distributions observed in mass spectra of p53 treated with H₂O₂ for 1 min (see Section 5.4.2; Figure 5.3). The appearance of lower charge states, which normally predominate in native spectra of p53, suggested that p53 adopts a native-like conformation when oxidised by H₂O₂. Formation of a disulfide bond between Cys176 or Cys182 and Cys 238 or Cys242 would indeed ‘lock’ p53 in a native-like fold, therefore, preventing unfolding despite the denaturing conditions used for FT-ICR MS. In agreement with these FT-ICR MS measurements, the solution and crystal structures of the zinc-free p53 core domain show that the overall fold of *apo*-p53 (i.e. the anti-parallel β -sandwich and the secondary structural elements) is the same as that in zinc-bound p53 [91, 261]. However, the NMR and X-ray structures show that the L3 loop is displaced in *apo*-p53 with respect to *holo*-p53. Interestingly, the L3 loop is responsible for p53 binding to the minor groove of DNA and contains Cys238 and Cys242 (see Chapter 1.2; Figure 1.6) [72]. Moreover,

the highly conserved p53 sequence Cys242X₄NRRX₂LTX₂TLX₆L is homologous to the sequence Cys154X₁NRRX₂LTX₁TLX₆L in the redox-regulated transcription factor c-Fos [95]. Transcriptional activity of c-Fos is controlled via redox-modification of the critical cysteine residue Cys154 [35, 262, 263], suggesting that Cys242 plays a similar regulatory role in p53.

p53 positively and negatively regulates the transcription of a large and disparate group of genes [69]. Oxidation of the zinc-binding cysteines in p53 may serve as a redox-switch which regulates the transcriptional activity of p53 by directly influencing p53-DNA binding via the L3 loop-minor groove interaction. Furthermore, ROS are known to induce translocation of p53 to the mitochondria resulting in transcription-independent p53-induced apoptosis [264, 265]. Oxidation of the zinc-binding domain may represent the ROS-induced redox-signalling event that activates the transcriptional-independent apoptotic activity of p53. As discussed in Chapter 1.1.3, a growing number of proteins including Hsp33, RsrA, protein kinase C and numerous zinc-containing transcription factors are known to have their function controlled via zinc-redox switches [49, 50, 53].

Rainwater *et al.* have postulated that p53 is under different levels of redox-control due to their observation that separate clusters of Cys-Ser mutations resulted in the presence of two distinct phenotypes [95]. Cys277 has previously been implicated in redox-regulation of p53 [100, 102] and the results presented in Chapter 4 also suggest a role for this residue in modulation of p53 activity. Oxidation of Cys277 and the zinc-binding Cys residues, along with Cys182, probably occurs via separate signalling pathways under different cellular conditions, and represents two discrete redox-mechanisms by which p53 function may be regulated.

The correlation between intracellular H₂O₂ levels and p53-mediated transcription of antioxidant or pro-oxidant genes is of current interest [105, 106]. It has been demonstrated here that the interaction between H₂O₂ and p53 *in vitro* is well defined, resulting in oxidation of the zinc-binding Cys residues, most probably accompanied by displacement of the Zn²⁺ ion. It is exciting to speculate that, at low basal levels of intracellular ROS *in vivo*, p53 is in its reduced *holo* form, in a conformation specific

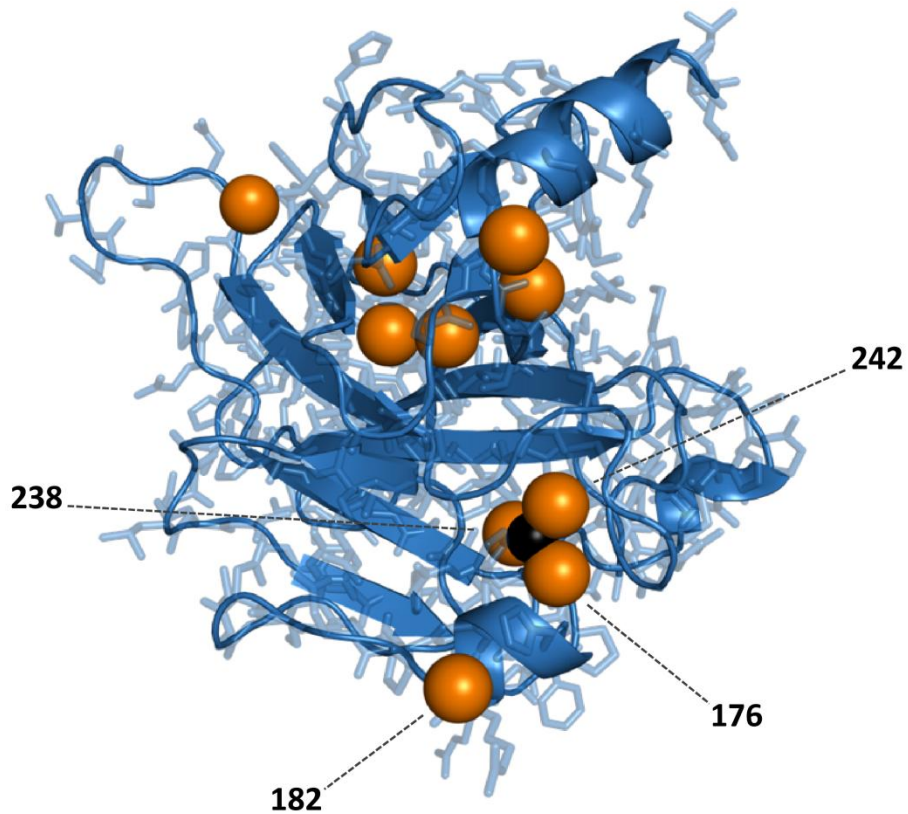


Figure 5.14 X-ray crystal structure of human p53 core domain (PDB ID 2OCJ), highlighting Cys182 and the zinc-binding Cys residues. It is proposed that formation of a sulfenic acid on Cys182 is the first step in the mechanism of H_2O_2 oxidation of p53, followed by oxidation of the zinc-binding Cys.

for activating transcription of antioxidant genes such as GPX1 and SESN1, and at elevated levels of ROS, e.g. during oxidative stress, p53 interacts with H_2O_2 to form zinc-free *apo*-p53 in a conformation specific for transactivation of ROS producing enzymes such as NQO1 and POX. The pro-oxidant function of p53 is associated with induction of p53-mediated apoptosis [266]. p53 cancer-associated mutants with low thermodynamic stability such as R175H and R249S are known to unfold *in vitro* and *in vivo* [212, 227, 267]. This may result in preferential oxidation of the ‘wrong’ Cys residues, therefore, resulting in inhibition of ROS-induced p53-mediated apoptosis and the onset of tumourigenesis. Alkylation of the Cys residues which are not involved in this response, i.e. by the anti-tumour compounds PRIMA-1 and MIRA-1

(see Chapter 1.2.4), would exclude them as ROS-targets, therefore, promoting preferential oxidation of the zinc-binding Cys residues, induction of p53-mediated apoptosis and the subsequent death of tumour cells. Based on the results presented in Chapter 4, Cys182 is one of the highly reactive cysteine residues located on the p53 surface (along with Cys277). Figure 5.14 highlights the position of Cys182 and the zinc-binding Cys residues in the X-ray crystal structure of p53core domain (PDB ID 2OCJ). It is proposed here that the initial step in the mechanism of oxidation of p53 by H₂O₂ is the formation of a sulfenic acid (–SOH) on Cys182, which is rapidly condensed by the thiol group of either Cys238 or Cys242.

5.9 Trapping of Sulfenic Acid

In order to test the hypothesis of the formation of a sulfenic acid on Cys182 as the initial step in H₂O₂-mediated oxidation of p53, oxidation was performed in the presence of the sulfenic trapping reagent dimedone (5,5-dimethyl-1,3-cyclohexanedione). Nucleophilic dimedone reacts with the electrophilic sulfur atom of sulfenic acid to form a covalent thioether bond as shown in Figure 5.15 [268, 269]. The addition of a dimedone group results in a monoisotopic mass increase of 139.0760 Da.

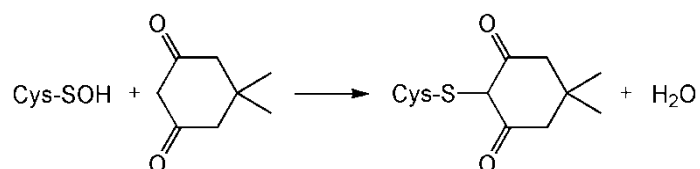


Figure 5.15 The reaction of cysteine sulfenic acid with dimedone.

p53 core domain was oxidised under conditions previously described with the addition of dimedone (5 mM) for 1 h, followed by alkylation of free thiol groups and LC FT-ICR MS. No dimedone adducts were detected, and oxidation of p53 proceeded to form 2 disulfide bonds in the manner observed previously. The rate constant for the reaction between human serum albumin sulfenic acid (HSA-SOH) and dimedone is lower than the rate constant for the reaction between HSA-SOH and

free cysteine ($0.027 \pm 0.009 \text{ M}^{-1} \text{ s}^{-1}$ at 37°C and $21.6 \pm 0.2 \text{ M}^{-1} \text{ s}^{-1}$ at 25°C respectively) [269]. The absence of p53-dimedone adducts was probably due to a sulfenic acid on Cys182 reacting faster with an adjacent zinc-binding Cys residue than with dimedone.

An alternative sulfenic trapping agent is thionitrobenzoate (TNB; the reduced form of Ellman's reagent). TNB reacts faster with HAS-SOH than cysteine ($105 \pm 11 \text{ M}^{-1} \text{ s}^{-1}$ at 25°C). Therefore, this reagent should be used in future attempts to trap p53 sulfenic acids. However, several TNB synthesis and purification steps are required prior to sulfenic trapping [269, 270].

5.10 Oxidation of p53 Cysteine Mutant C182S

Hydrogen peroxide oxidation of the p53 cysteine-to-serine mutant C182S was performed in order to investigate the mechanism of p53 oxidation. Wild type and mutant p53 core domain ($115 \mu\text{M}$) were incubated with $4 \text{ mM H}_2\text{O}_2$, in parallel, on ice and the reactions were quenched by TCA precipitation at various time points. Free thiol groups were alkylated by NEM as described previously. The resulting deconvoluted neutral mass spectra are shown in Figure 5.16.

H_2O_2 treatment of wt p53 resulted in a similar pattern of oxidation as observed previously, i.e. the predominate formation of 2 disulfide bonds at 60 min and 3 disulfide bonds at 4 h. In contrast, oxidation of p53C182S did not occur in such a well defined fashion. At 60 min, a particular oxidised form of mutant p53 did not predominate, and each alkylated form of the protein from 1NEM-p53C182S to 8NEM-p53C182S was detected, indicating that up to 8 of the 9 Cys residues had been oxidised. The observation of even numbers of NEM adducts suggests that H_2O_2 -mediated oxidation of the C182S mutant does not proceed solely via intramolecular disulfide bond formation. Oxidative-modifications to individual Cys residues such as sulfinic and sulfonic acid may have occurred as well as intermolecular disulfide linkages. The wide range of oxidation states present and the absence of a predominating oxidised species suggests that oxidation of the p53 mutant C182S is non-specific. Moreover, oxidation in the absence of Cys182 leads to extensive over-oxidation of p53. After 4 h, the FT-ICR mass spectra show that

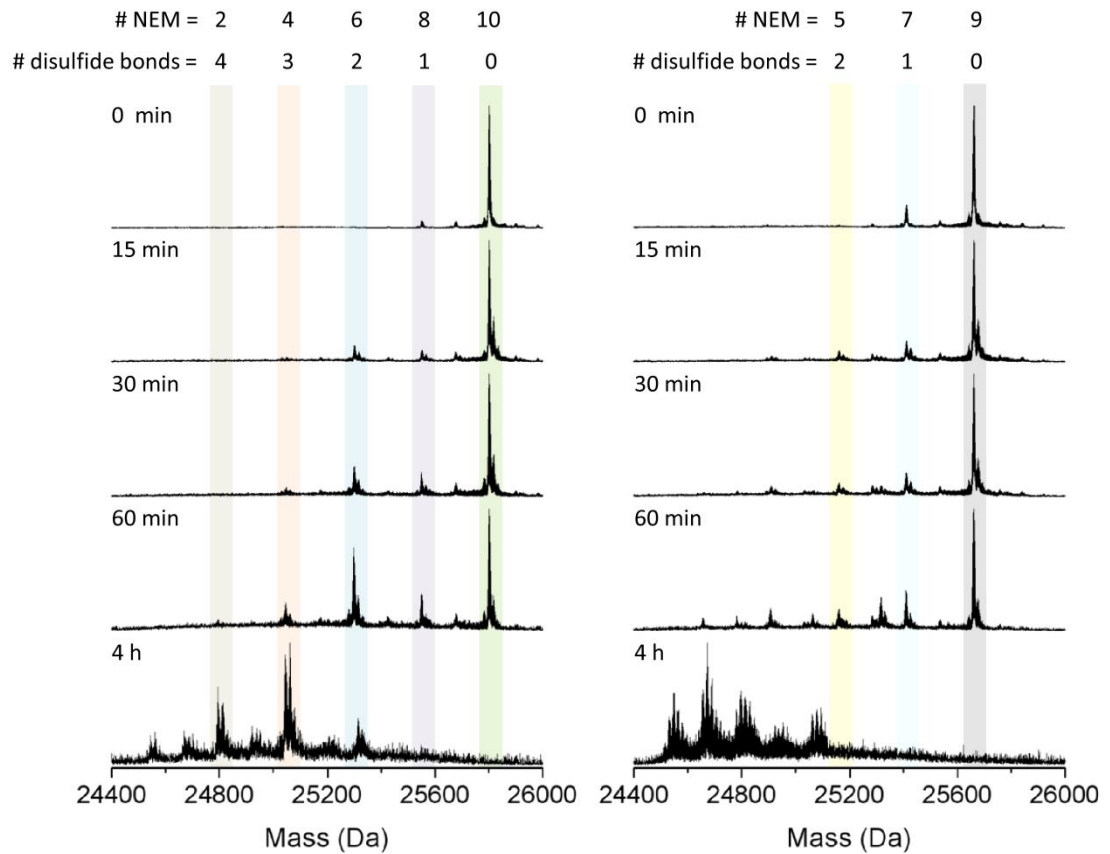


Figure 5.16 Oxidation of p53 cysteine to serine mutant C182S over time. Wild type and mutant p53 core domain was incubated with 4 mM H_2O_2 at 0°C for increasing times followed by alkylation of free thiols with NEM and analysis by LC FT-ICR MS. Deconvoluted neutral FT-ICR mass spectra are shown.

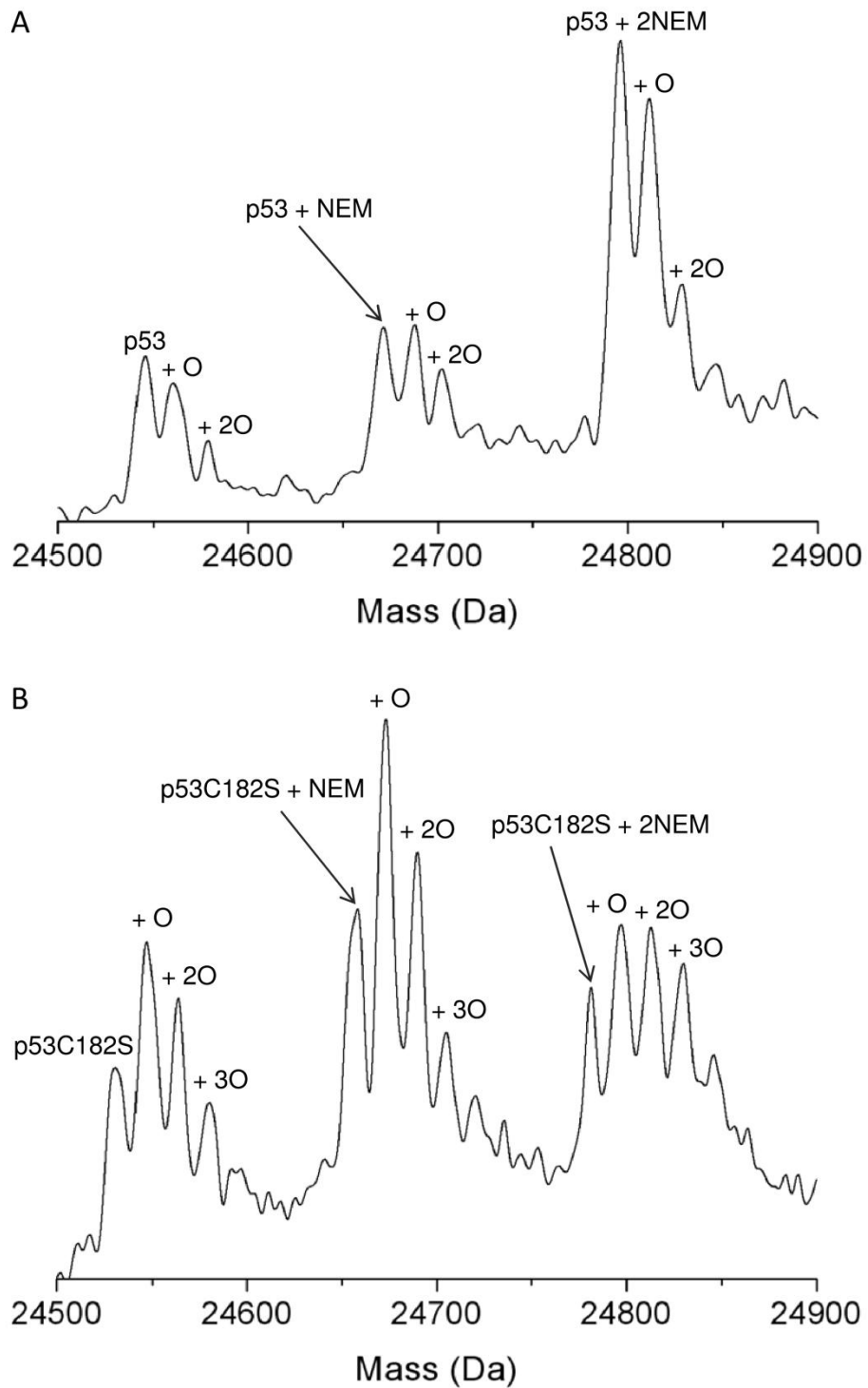


Figure 5.17 Extensive oxidation of p53 mutant C182S. The smoothed neutral FT-ICR mass spectra of **(A)** wt and **(B)** mutant p53 incubated with H_2O_2 for 4 h show the increased level of oxygen incorporation into p53C182S compared to wt p53.

between 7 and 9 Cys residues had been oxidised in the majority of mutant p53 present, compared to 6 Cys residues in wt p53, and an increase in the incorporation of oxygen atoms was observed for p53C182S compared to wt p53 (see Figure 5.17).

The stark contrast observed in the oxidation patterns of wt and C182S p53 confirms the involvement of Cys182 in the mechanism of p53 oxidation by H₂O₂. Furthermore, the non-specific over-oxidation of p53C182S suggests that oxidation via an alternative pathway, which does not involve Cys182, is not a viable option in p53 redox-signalling.

5.11 Effect of Zn²⁺ on Oxidation of p53

Zinc is known to rapidly dissociate from p53 at physiological temperature [91]. This observation is in agreement with the zinc-sulfur centre in p53 serving as a regulatory zinc-redox switch. Despite the high thermodynamic stability of eukaryotic protein zinc-complexes (pK_D 's generally in the region of 10-12), zinc-exchange rates can vary dramatically (from seconds to years). Fast Zn²⁺-exchange rates at zinc-sulfur centres are often associated with ligand-centred redox-chemistry [49, 53, 271].

p53 core domain was oxidised in the presence of excess Zn²⁺ in order to further investigate the mechanism of oxidation by H₂O₂. It was hypothesised that, if formation of a sulfenic acid on Cys182 is indeed the first step in the mechanism, then according to Le Chatelier's principle, oxidation in the presence of excess Zn²⁺ should slow the subsequent oxidation of either Cys176, 238 or 242, therefore, stabilising the sulfenic acid and increasing the chances of its detection [272].

Zinc salts are known to cause protein precipitation. Therefore, oxidation of p53 (100 μM), in the presence and absence of Zn²⁺ (2 mM), was performed in parallel for 1 h followed by determination of soluble protein concentration [273]. Both samples lost 25% of soluble protein, indicating that Zn²⁺ did not result in p53 precipitation during this time. Free thiol groups were alkylated as described previously and the resulting deconvoluted neutral mass spectra are shown in Figure 5.18.

It is clear that H₂O₂ oxidation in the presence of excess Zn²⁺ significantly slowed the rate of disulfide bond formation. After 1 h, the majority of p53 incubated with

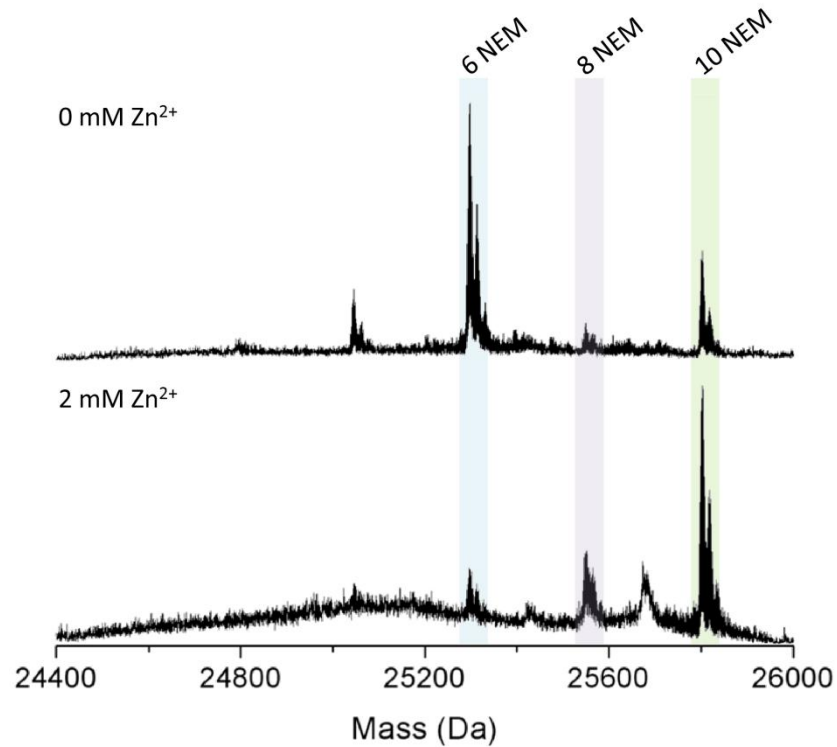


Figure 5.18 Effect of zinc on oxidation of wt p53 core domain. p53 was incubated with 4 mM H₂O₂ at 0°C for 1 h in the presence or absence of 2 mM Zn²⁺ followed by alkylation of free thiols with NEM and analysis by LC FT-ICR MS. Deconvoluted neutral mass spectra are shown.

H₂O₂ in the absence of excess Zn²⁺ had formed 2 disulfide bonds. The formation of 2 disulfide bonds was apparent for p53 incubated in the presence of Zn²⁺. However, the majority of protein still contained 10 free thiol groups, even after 1 h. A p53 species with 9 alkylated Cys residues was detected in the mass spectrum of p53 oxidised in the presence of Zn²⁺. This species may have corresponded to p53 with a stabilised sulfenic acid. However, its ion abundance was too low to confirm this by top-down FT-ICR MS.

These results do not allow the confirmation of formation of a sulfenic acid on Cys182. However, they do suggest that the dissociated thiolate (-S⁻) of either Cys176, 238 or 242 acts as a nucleophile in the mechanism of p53 oxidation by H₂O₂. If oxidation proceeded via an associative mechanism (i.e. a Zn²⁺-bound

thiolate acts as the nucleophile), then the presence of excess Zn^{2+} ions would not have affected the rate of disulfide bond formation.

5.12 Effect of GSH on Oxidation of p53

The tripeptide glutathione (L- γ -glutamyl-L-cysteinylglycine; GSH) is the most abundant low-molecular-weight thiol present in eukaryotic cells, and has an essential role in maintaining the intracellular redox-potential [15, 274, 275]. The formation of an intermolecular disulfide bond between a protein cysteine residue and GSH, known as S-glutathionylation, is a post-translational modification involved in redox-signalling (Figure 5.19). The concentration of GSH in mammalian cells ranges from 1-10 mM, depending on cell type and localisation. Interestingly, p53 S-glutathionylation has previously been observed *in vivo* and the level of modification was found to increase upon addition of oxidising agents [99]. Here, H_2O_2 oxidation of p53 in the presence of an excess of the intracellular antioxidant GSH was investigated *in vitro* [124].

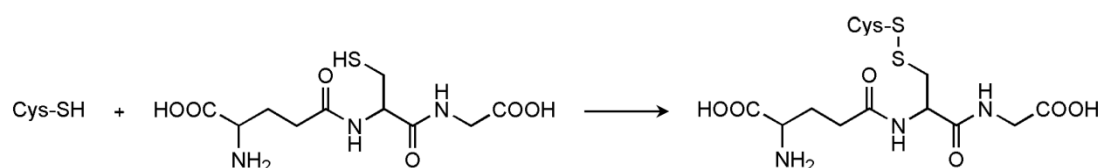


Figure 5.19 Formation of a disulfide bond between cysteine and glutathione.

p53 core domain (150 μM) was incubated with 0 mM or 4 mM H_2O_2 in the presence of 2 mM GSH for 1 h on ice. The reactions were quenched and free thiol groups alkylated as previously described. The resulting deconvoluted neutral mass spectra are shown in Figure 5.20.

After 1 h incubation in the presence of GSH alone, a small proportion of p53 (4%) had formed 1 disulfide bond with GSH. Oxidation presumably occurred via thiol/disulfide exchange, or with dissolved oxygen acting as the oxidising agent. After 1 h incubation in the presence of both GSH and H_2O_2 , an increase in the level of

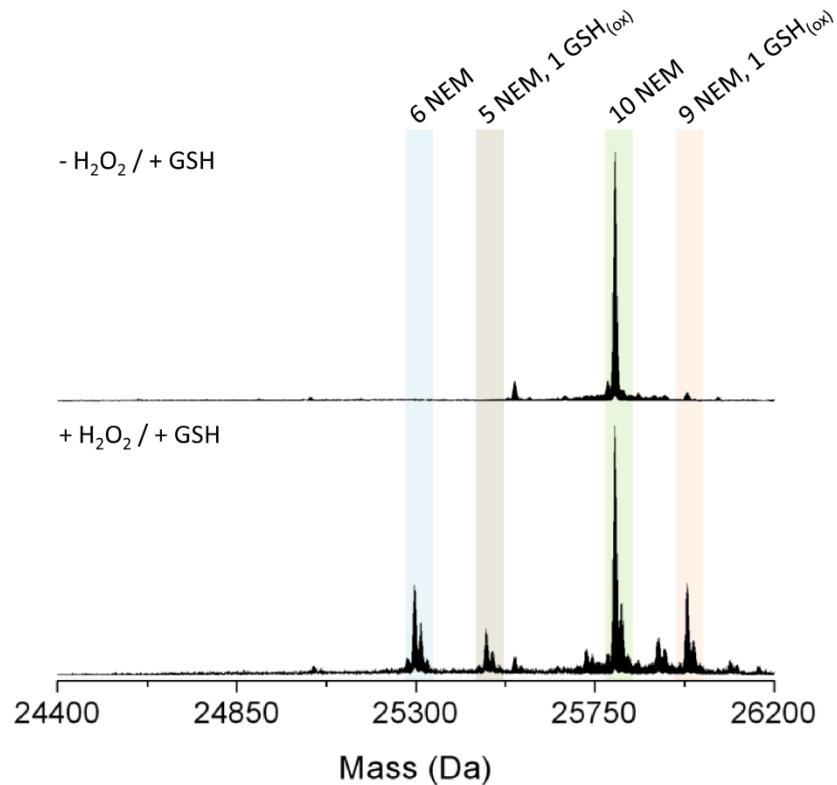


Figure 5.20 Effect of glutathione on oxidation of wt p53 core domain. p53 was incubated with 0 mM or 4 mM H_2O_2 and 2 mM GSH at 0°C for 1 h followed by alkylation of free thiols with NEM and analysis by LC FT-ICR MS. Deconvoluted neutral mass spectra are shown. GSH_{ox} refers to S-glutathionylation.

S-glutathionylation was observed. 32% of p53 had formed 1 intermolecular disulfide bond with GSH, and 25% of S-glutathionylated protein also contained 2 intramolecular disulfide bonds. The identities of the S-glutathionylated p53 species were confirmed by comparison of the theoretical isotope distributions with the experimental isotope distributions (see Figure 5.21). Despite the presence of an excess of free GSH, 19% of p53 formed 2 disulfide bonds without S-glutathionylation.

The presence of 2 disulfide bonds in addition to a GSH adduct (GSH_{ox}) suggests that Cys176, 182, 238 or 242 were not S-glutathionylated, due to the previous assignment of their involvement in intramolecular disulfide bond formation. Based on the results presented in Chapter 4, Cys277 may be the residue susceptible to

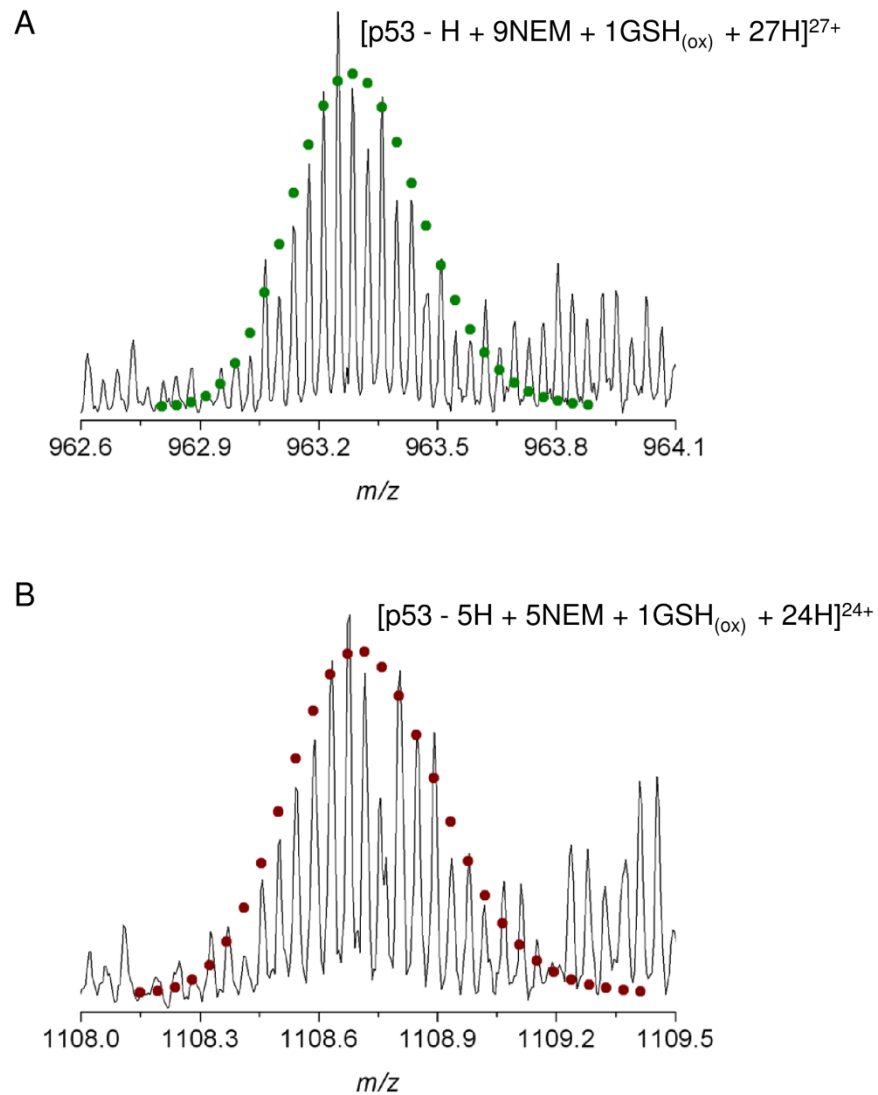


Figure 5.21 Isotope distributions of p53 core domain treated with H_2O_2 in the presence of GSH and alkylated with NEM. Theoretical isotope distributions are consistent with the experimental isotope distributions for **(A)** p53 with an intermolecular disulfide bond to GSH and 9 alkylated Cys residues ($27+$ charge state; empirical formula $[C_{1119}H_{1778}N_{333}O_{348}S_{17}]^{27+}$; \bullet ; MME < 1 ppm) and **(B)** p53 with 2 intramolecular disulfide bonds and 1 intermolecular disulfide bond to GSH and 5 alkylated Cys residues ($24+$ charge state; empirical formula $[C_{1095}H_{1742}N_{329}O_{340}S_{17}]^{24+}$; \bullet ; MME < 1 ppm)

S-glutathionylation. Top-down FT-ICR MS could be performed in order to investigate the sites of *S*-glutathionylation.

Importantly, these results suggest that an excess of GSH does not protect the zinc-binding Cys residues from oxidation, thus providing further evidence for their role in redox-regulation of p53. However, a more comprehensive investigation into H₂O₂ oxidation of p53 in the presence of GSH is required in order to check this. A wider range of GSH concentrations should be used, and the reaction should also be monitored over time. In addition, cellular redox-potentials could be mimicked by the addition of glutathione disulfide (GSSG) to give the appropriate ratio of GSH:GSSG. Measuring the degree of oxidation over a range of ambient redox-potentials allows the equilibrium midpoint potential of disulfide bonds to be determined [276, 277].

5.13 Conclusion

Hydrogen peroxide oxidation of p53 has been investigated *in vitro* using FT-ICR mass spectrometry. H₂O₂ treatment resulted in overlapping p53 isotope distributions suggesting that a mixture of species was present. Alkylation of free thiol groups allowed identification of cysteine oxidation states and showed that H₂O₂ oxidation of p53 proceeds via a distinct pathway, involving the initial formation of a stable 2-disulfide species. Further oxidation results in the formation of additional disulfide bonds.

p53 containing two disulfide bonds was purified using an affinity purification strategy based on the presence of free thiol groups. Top-down FT-ICR mass spectrometry identified unambiguously the oxidation state of each of the 10 Cys residues in p53, revealing that Cys176, 182, 238 and 242 are selectively oxidised in response to H₂O₂. Interestingly, Cys176, 238 and 242 are the Zn²⁺-binding residues. Cysteine connectivity could not be determined from bottom-up FT-ICR mass spectrometry. However, charge-state distributions of oxidised p53 were consistent with disulfide linkages between either Cys176 or Cys182 and Cys238 or Cys242.

The mechanism of H₂O₂-mediated oxidation of p53 was investigated by oxidation the p53 Cys-Ser mutant C182S. H₂O₂ treatment in the absence of Cys182 resulted in non-specific over-oxidation of p53, providing further evidence for its role

in p53 redox-signalling mechanisms. Furthermore, the rate of wt p53 oxidation in the presence of excess Zn^{2+} was substantially decreased, suggesting that the thiolate of a zinc-binding Cys residue serves as a nucleophile in p53. Additional evidence supporting a role for zinc-ligand redox-chemistry in p53 regulation is provided by the observation that excess glutathione does not protect the zinc-binding Cys residues from oxidation.

This investigation has revealed hitherto unknown molecular details regarding the interaction between the biological ROS signalling molecule H_2O_2 and the redox-regulated tumour-suppressor p53. It is proposed that selective H_2O_2 oxidation of Cys182 followed by specific disulfide bond formation between the zinc-binding cysteine residues represents a biologically relevant redox-signalling event that contributes to regulation of p53 activity *in vivo*.

5.14 Future Work

The ultimate goal of this research is to identify the redox-states of p53 cysteine residues *in vivo*. A major challenge associated with this endeavour is the acquisition of sufficient amounts of protein in order to carry out an extensive FT-ICR MS study. Other more sensitive MS techniques, such as multiple reaction monitoring (MRM), could be utilised [103]. However, these techniques would require cleavage of p53 into peptides. The limitations of the bottom-up MS approach, such as incomplete sequence coverage, have been demonstrated in this thesis.

An *in vivo* study of intact p53 would involve the analysis of the full length 46 kDa protein purified from a tissue culture. Sensitivity in FT-ICR MS decreases as protein size increases. Therefore, to increase the potential for detection, the 14.5 kDa peptide Gln165-Lys291 could be excised from full length p53 using the protease Lys-C (as described in Chapter 4.3.2). This peptide contains seven of the ten cysteine residues in p53, including each of the Cys residues shown in this thesis to be of significance (i.e. Cys176, 182, 238, 242 and 277). This middle-down approach is recommended for the unambiguous assignment of p53 cysteine redox-states *in vivo*.

References

1. Fridovich I (1978) The biology of oxygen radicals. *Science* 201: 875-80.
2. Halliwell B and Gutteridge JMC (1999) *Free radicals in biology and medicine* (Oxford University Press, Oxford).
3. Droge W (2002) Free radicals in the physiological control of cell function. *Physiol Rev* 82: 47-95.
4. Nathan C (2003) Specificity of a third kind: reactive oxygen and nitrogen intermediates in cell signaling. *J Clin Invest* 111: 769-78.
5. D'Autreaux B and Toledano MB (2007) ROS as signalling molecules: mechanisms that generate specificity in ROS homeostasis. *Nature Rev Mol Cell Biol* 8: 813-824.
6. Wentworth P, Jr., McDunn JE, Wentworth AD, Takeuchi C, Nieva J, Jones T, Bautista C, Ruedi JM, Gutierrez A, Janda KD, Babior BM, Eschenmoser A and Lerner RA (2002) Evidence for antibody-catalyzed ozone formation in bacterial killing and inflammation. *Science* 298: 2195-9.
7. Wardman P and Candeias LP (1996) Fenton chemistry: an introduction. *Radiat Res* 145: 523-31.
8. Patten DA, Germain M, Kelly MA and Slack RS (2010) Reactive oxygen species: stuck in the middle of neurodegeneration. *J Alzheimers Dis* 20 Suppl 2: S357-67.
9. Schumacker PT (2006) Reactive oxygen species in cancer cells: live by the sword, die by the sword. *Cancer Cell* 10: 175-6.

10. Arora S, Vaishya R, Dabla PK and Singh B (2010) NAD(P)H oxidases in coronary artery disease. *Adv Clin Chem* 50: 65-86.
11. Kaneto H, Katakami N, Matsuhisa M and Matsuoka TA (2010) Role of reactive oxygen species in the progression of type 2 diabetes and atherosclerosis. *Mediators Inflamm* 2010: 453892.
12. Paulsen CE and Carroll KS (2010) Orchestrating redox signaling networks through regulatory cysteine switches. *ACS Chem Biol* 5: 47-62.
13. Finkel T (2000) Redox-dependent signal transduction. *FEBS Lett* 476: 52-4.
14. Jacob C, Giles GI, Giles NM and Sies H (2003) Sulfur and selenium: the role of oxidation state in protein structure and function. *Angew Chem Int Ed Engl* 42: 4742-58.
15. Circu ML and Aw TY (2010) Reactive oxygen species, cellular redox systems, and apoptosis. *Free Radic Biol Med* 48: 749-62.
16. Forman HJ, Fukuto JM and Torres M (2004) Redox signaling: thiol chemistry defines which reactive oxygen and nitrogen species can act as second messengers. *Am J Physiol Cell Physiol* 287: C246-56.
17. Winterbourn CC and Hampton MB (2008) Thiol chemistry and specificity in redox signaling. *Free Radic Biol Med* 45: 549-61.
18. Walsh C (2006) *Posttranslational modification of proteins: expanding nature's inventory* (Roberts and Co., Eaglewood, Colorado), pp. 95-119.

19. Harris TK and Turner GJ (2002) Structural basis of perturbed pKa values of catalytic groups in enzyme active sites. *IUBMB Life* 53: 85-98.
20. Schirra HJ, Renner C, Czisch M, Huber-Wunderlich M, Holak TA and Glockshuber R (1998) Structure of reduced DsbA from *Escherichia coli* in solution. *Biochemistry* 37: 6263-76.
21. Clayden J, Greeves N, Warren S and Wothers P (2001) *Organic chemistry* (Oxford University Press, Oxford), pp. 1247-1275.
22. Biteau B, Labarre J and Toledano MB (2003) ATP-dependent reduction of cysteine-sulphinic acid by *S-cerevisiae* sulphiredoxin. *Nature* 425: 980-984.
23. Weissbach H, Resnick L and Brot N (2005) Methionine sulfoxide reductases: history and cellular role in protecting against oxidative damage. *Biochim Biophys Acta* 1703: 203-12.
24. Sohn J and Rudolph J (2003) Catalytic and chemical competence of regulation of cdc25 phosphatase by oxidation/reduction. *Biochemistry* 42: 10060-70.
25. Chiarugi P (2001) The redox regulation of LMW-PTP during cell proliferation or growth inhibition. *IUBMB Life* 52: 55-9.
26. Kwon J, Lee SR, Yang KS, Ahn Y, Kim YJ, Stadtman ER and Rhee SG (2004) Reversible oxidation and inactivation of the tumor suppressor PTEN in cells stimulated with peptide growth factors. *Proc Natl Acad Sci USA* 101: 16419-24.

27. Salmeen A, Andersen JN, Myers MP, Meng TC, Hinks JA, Tonks NK and Barford D (2003) Redox regulation of protein tyrosine phosphatase 1B involves a sulphenyl-amide intermediate. *Nature* 423: 769-773.
28. Yang J, Groen A, Lemeer S, Jans A, Slijper M, Roe SM, den Hertog J and Barford D (2007) Reversible oxidation of the membrane distal domain of receptor PTPalpha is mediated by a cyclic sulfenamide. *Biochemistry* 46: 709-19.
29. Chen CY, Willard D and Rudolph J (2009) Redox regulation of SH2-domain-containing protein tyrosine phosphatases by two backdoor cysteines. *Biochemistry* 48: 1399-409.
30. Nadeau PJ, Charette SJ, Toledano MB and Landry J (2007) Disulfide Bond-mediated multimerization of Ask1 and its reduction by thioredoxin-1 regulate H₂O₂-induced c-Jun NH₂-terminal kinase activation and apoptosis. *Mol Biol Cell* 18: 3903-13.
31. Brennan JP, Bardswell SC, Burgoyne JR, Fuller W, Schroder E, Wait R, Begum S, Kentish JC and Eaton P (2006) Oxidant-induced activation of type I protein kinase A is mediated by RI subunit interprotein disulfide bond formation. *J Biol Chem* 281: 21827-36.
32. Burgoyne JR, Madhani M, Cuello F, Charles RL, Brennan JP, Schroder E, Browning DD and Eaton P (2007) Cysteine redox sensor in PKGla enables oxidant-induced activation. *Science* 317: 1393-7.
33. Kemble DJ and Sun G (2009) Direct and specific inactivation of protein tyrosine kinases in the Src and FGFR families by reversible cysteine oxidation. *Proc Natl Acad Sci USA* 106: 5070-5.

34. Veal EA, Findlay VJ, Day AM, Bozonet SM, Evans JM, Quinn J and Morgan BA (2004) A 2-Cys peroxiredoxin regulates peroxide-induced oxidation and activation of a stress-activated MAP kinase. *Mol Cell* 15: 129-39.
35. Abate C, Patel L, Rauscher FJ and Curran T (1990) Redox Regulation of Fos and Jun DNA-Binding Activity In vitro. *Science* 249: 1157-1161.
36. Dansen TB, Smits LM, van Triest MH, de Keizer PL, van Leenen D, Koerkamp MG, Szypowska A, Meppelink A, Brenkman AB, Yodoi J, Holstege FC and Burgering BM (2009) Redox-sensitive cysteines bridge p300/CBP-mediated acetylation and FoxO4 activity. *Nat Chem Biol* 5: 664-72.
37. Ahn SG and Thiele DJ (2003) Redox regulation of mammalian heat shock factor 1 is essential for Hsp gene activation and protection from stress. *Genes Dev* 17: 516-28.
38. Fourquet S, Guerois R, Biard D and Toledano MB (2010) Activation of NRF2 by nitrosative agents and H₂O₂ involves KEAP1 disulfide formation. *J Biol Chem* 285: 8463-71.
39. Lee JW, Soonsanga S and Helmann JD (2007) A complex thiolate switch regulates the *Bacillus subtilis* organic peroxide sensor OhrR. *Proc Natl Acad Sci USA* 104: 8743-8.
40. Storz G, Tartaglia LA and Ames BN (1990) Transcriptional regulator of oxidative stress-inducible genes: direct activation by oxidation. *Science* 248: 189-94.
41. Poor CB, Chen PR, Duguid E, Rice PA and He C (2009) Crystal structures of the reduced, sulfenic acid, and mixed disulfide forms of

- SarZ, a redox active global regulator in *Staphylococcus aureus*. *J Biol Chem* 284: 23517-24.
42. Paulsen CE and Carroll KS (2009) Chemical dissection of an essential redox switch in yeast. *Chem Biol* 16: 217-25.
 43. Blackinton J, Lakshminarasimhan M, Thomas KJ, Ahmad R, Greggio E, Raza AS, Cookson MR and Wilson MA (2009) Formation of a stabilized cysteine sulfinic acid is critical for the mitochondrial function of the parkinsonism protein DJ-1. *J Biol Chem* 284: 6476-85.
 44. Yan Y, Sabharwal P, Rao M and Sockanathan S (2009) The antioxidant enzyme Prdx1 controls neuronal differentiation by thiol-redox-dependent activation of GDE2. *Cell* 138: 1209-21.
 45. Ago T, Liu T, Zhai P, Chen W, Li H, Molkentin JD, Vatner SF and Sadoshima J (2008) A redox-dependent pathway for regulating class II HDACs and cardiac hypertrophy. *Cell* 133: 978-93.
 46. Ilbert M, Horst J, Ahrens S, Winter J, Graf PC, Lilie H and Jakob U (2007) The redox-switch domain of Hsp33 functions as dual stress sensor. *Nat Struct Mol Biol* 14: 556-63.
 47. Fu X, Kassim SY, Parks WC and Heinecke JW (2001) Hypochlorous acid oxygenates the cysteine switch domain of pro-matrilysin (MMP-7). A mechanism for matrix metalloproteinase activation and atherosclerotic plaque rupture by myeloperoxidase. *J Biol Chem* 276: 41279-87.
 48. Dinkova-Kostova AT, Holtzclaw WD and Kensler TW (2005) The role of Keap1 in cellular protective responses. *Chem Res Toxicol* 18: 1779-91.

49. Maret W (2005) Zinc coordination environments in proteins determine zinc functions. *J Trace Elem Med Biol* 19: 7-12.
50. Ilbert M, Graf PC and Jakob U (2006) Zinc center as redox switch--new function for an old motif. *Antioxid Redox Signal* 8: 835-46.
51. Maret W (2003) Cellular zinc and redox states converge in the metallothionein/thionein pair. *J Nutr* 133: 1460S-2S.
52. Maret W (2009) Molecular aspects of human cellular zinc homeostasis: redox control of zinc potentials and zinc signals. *Biomaterials* 22: 149-57.
53. Maret W and Li Y (2009) Coordination dynamics of zinc in proteins. *Chem Rev* 109: 4682-707.
54. Neculai AM, Neculai D, Griesinger C, Vorholt JA and Becker S (2005) A dynamic zinc redox switch. *J Biol Chem* 280: 2826-30.
55. Wedemeyer WJ, Welker E, Narayan M and Scheraga HA (2000) Disulfide bonds and protein folding. *Biochemistry* 39: 7032.
56. Faratian D, Goltsov A, Lebedeva G, Sorokin A, Moodie S, Mullen P, Kay C, Um IH, Langdon S, Goryanin I and Harrison DJ (2009) Systems biology reveals new strategies for personalizing cancer medicine and confirms the role of PTEN in resistance to trastuzumab. *Cancer Res* 69: 6713-20.
57. Lee SR, Yang KS, Kwon J, Lee C, Jeong W and Rhee SG (2002) Reversible inactivation of the tumor suppressor PTEN by H₂O₂. *J Biol Chem* 277: 20336-42.

58. Kim Y, Song YB, Kim TY, Kim I, Han SJ, Ahn Y, Cho SH, Choi CY, Chay KO, Yang SY, Ahn BW, Huh WK and Lee SR (2010) Redox regulation of the tumor suppressor PTEN by glutathione. *FEBS Lett* 584: 3550-6.
59. Vogelstein B, Lane D and Levine AJ (2000) Surfing the p53 network. *Nature* 408: 307-10.
60. Laptenko O and Prives C (2006) Transcriptional regulation by p53: one protein, many possibilities. *Cell Death Differ* 13: 951-961.
61. Lane DP and Crawford LV (1979) T-Antigen Is Bound to a Host Protein in Sv40-Transformed Cells. *Nature* 278: 261-263.
62. Linzer DIH and Levine AJ (1979) Characterization of a 54k Dalton Cellular Sv40 Tumor-Antigen Present in Sv40-Transformed Cells and Uninfected Embryonal Carcinoma-Cells. *Cell* 17: 43-52.
63. Levine AJ and Oren M (2009) The first 30 years of p53: growing ever more complex. *Nat Rev Cancer* 9: 749-758.
64. Smith ML and Seo YR (2002) p53 regulation of DNA excision repair pathways. *Mutagenesis* 17: 149-56.
65. Haupt S, Berger M, Goldberg Z and Haupt Y (2003) Apoptosis - the p53 network. *J Cell Sci* 116: 4077-85.
66. Hollstein M, Sidransky D, Vogelstein B and Harris CC (1991) p53 mutations in human cancers. *Science* 253: 49-53.
67. Royds JA and Iacopetta B (2006) p53 and disease: when the guardian angel fails. *Cell Death Differ* 13: 1017-1026.

68. Olivier M, Hollstein M and Hainaut P (2010) TP53 Mutations in Human Cancers: Origins, Consequences, and Clinical Use. *Cold Spring Harb Perspect Biol* 2: a001008.
69. Vousden KH and Lane DP (2007) p53 in health and disease. *Nat Rev Mol Cell Biol* 8: 275-283.
70. Vousden KH and Prives C (2009) Blinded by the Light: The Growing Complexity of p53. *Cell* 137: 413-31.
71. Yee KS and Vousden KH (2005) Complicating the complexity of p53. *Carcinogenesis* 26: 1317-22.
72. Cho YJ, Gorina S, Jeffrey PD and Pavletich NP (1994) Crystal-Structure of a P53 Tumor-Suppressor DNA Complex - Understanding Tumorigenic Mutations. *Science* 265: 346-355.
73. Joerger AC and Fersht AR (2008) Structural biology of the tumor suppressor p53. *Annu Rev Biochem* 77: 557-582.
74. Gomes NP and Espinosa JM (2010) Differential regulation of p53 target genes: it's (core promoter) elementary. *Genes Dev* 24: 111-4.
75. Romer L, Klein C, Dehner A, Kessler H and Buchner J (2006) p53 - A natural cancer killer: Structural insights and therapeutic concepts. *Angew Chem, Int Ed Engl* 45: 6440-6460.
76. Brown CJ, Lain S, Verma CS, Fersht AR and Lane DP (2009) Awakening guardian angels: drugging the p53 pathway. *Nat Rev Cancer* 9: 862-873.
77. Wiman KG (2010) Pharmacological reactivation of mutant p53: from protein structure to the cancer patient. *Oncogene* 29: 4245-52.

78. Petitjean A, Mathe E, Kato S, Ishioka C, Tavtigian SV, Hainaut P and Olivier M (2007) Impact of mutant p53 functional properties on TP53 mutation patterns and tumor phenotype: lessons from recent developments in the IARC TP53 database. *Hum Mutat* 28: 622-9.
79. Soussi T, Defromental CC and May P (1990) Structural Aspects of the P53 Protein in Relation to Gene Evolution. *Oncogene* 5: 945-952.
80. Fink AL (2005) Natively unfolded proteins. *Curr Opin Struct Biol* 15: 35-41.
81. Pavletich NP, Chambers KA and Pabo CO (1993) The DNA-binding domain of p53 contains the four conserved regions and the major mutation hot spots. *Genes Dev* 7: 2556-64.
82. Ho WC, Fitzgerald MX and Marmorstein R (2006) Structure of the p53 core domain dimer bound to DNA. *J Biol Chem* 281: 20494-20502.
83. Malecka KA, Ho WC and Marmorstein R (2009) Crystal structure of a p53 core tetramer bound to DNA. *Oncogene* 28: 325-33.
84. Joerger AC, Ang HC and Fersht AR (2006) Structural basis for understanding oncogenic p53 mutations and designing rescue drugs. *Proc Natl Acad Sci USA* 103: 15056-15061.
85. Wang Y, Rosengarth A and Luecke H (2007) Structure of the human p53 core domain in the absence of DNA. *Acta Crystallogr, Sect D: Biol Crystallogr* 63: 276-281.
86. Kitayner M, Rozenberg H, Kessler N, Rabinovich D, Shaulov L, Haran TE and Shakked Z (2006) Structural basis of DNA recognition by p53 tetramers. *Mol Cell* 22: 741-53.

87. Derbyshire DJ, Basu BP, Serpell LC, Joo WS, Date T, Iwabuchi K and Doherty AJ (2002) Crystal structure of human 53BP1 BRCT domains bound to p53 tumour suppressor. *EMBO J* 21: 3863-72.
88. Frausto da Silva JJR and Williams RJP (2001) *The biological chemistry of the elements: the inorganic chemistry of life* (Oxford University Press, Oxford), pp. 315-339.
89. Verhaegh GW, Parat MO, Richard MJ and Hainaut P (1998) Modulation of p53 protein conformation and DNA-binding activity by intracellular chelation of zinc. *Mol Carcinog* 21: 205-214.
90. Meplan C, Richard MJ and Hainaut P (2000) Metalloregulation of the tumor suppressor protein p53: zinc mediates the renaturation of p53 after exposure to metal chelators in vitro and in intact cells. *Oncogene* 19: 5227-5236.
91. Butler JS and Loh SN (2003) Structure, function, and aggregation of the zinc-free form of the p53 DNA binding domain. *Biochemistry* 42: 2396-2403.
92. Hupp TR, Meek DW, Midgley CA and Lane DP (1993) Activation of the cryptic DNA binding function of mutant forms of p53. *Nucleic Acids Res* 21: 3167-74.
93. Hainaut P and Milner J (1993) Redox modulation of p53 conformation and sequence-specific DNA binding in vitro. *Cancer Res* 53: 4469-73.
94. Delphin C, Cahen P, Lawrence JJ and Baudier J (1994) Characterization of Baculovirus Recombinant Wild-Type P53 - Dimerization of P53 Is Required for High-Affinity DNA-Binding and

- Cysteine Oxidation Inhibits P53 DNA-Binding. *Eur J Biochem* 223: 683-692.
95. Rainwater R, Parks D, Anderson ME, Tegtmeyer P and Mann K (1995) Role of Cysteine Residues in Regulation of P53 Function. *Mol Cell Biol* 15: 3892-3903.
 96. Parks D, Bolinger R and Mann K (1997) Redox state regulates binding of p53 to sequence-specific DNA, but not to non-specific or mismatched DNA. *Nucleic Acids Res* 25: 1289-1295.
 97. Sun XZ, Vinci C, Makmura L, Han SB, Tran D, Nguyen J, Hamann M, Grazziani S, Sheppard S, Gutova M, Zhou FM, Thomas J and Momand J (2003) Formation of disulfide bond in p53 correlates with inhibition of DNA binding and tetramerization. *Antioxid Redox Signal* 5: 655-665.
 98. Augustyn KE, Merino EJ and Barton JK (2007) A role for DNA-mediated charge transport in regulating p53: Oxidation of the DNA-bound protein from a distance. *Proc Natl Acad Sci USA* 104: 18907-18912.
 99. Velu CS, Niture SK, Doneanu CE, Pattabiraman N and Srivenugopal KS (2007) Human p53 is inhibited by glutathionylation of cysteines present in the proximal DNA-Binding domain during oxidative stress. *Biochemistry* 46: 7765-7780.
 100. Buzek J, Latonen L, Kurki S, Peltonen K and Laiho M (2002) Redox state of tumor suppressor p53 regulates its sequence-specific DNA binding in DNA-damaged cells by cysteine 277. *Nucleic Acids Res* 30: 2340-2348.

101. Wu HH and Momand J (1998) Pyrrolidine dithiocarbamate prevents p53 activation and promotes p53 cysteine residue oxidation. *J Biol Chem* 273: 18898-18905.
102. Seo YR, Kelley MR and Smith ML (2002) Selenomethionine regulation of p53 by a ref1-dependent redox mechanism. *Proc Natl Acad Sci USA* 99: 14548-14553.
103. Held JM, Danielson SR, Behring JB, Atsriku C, Britton DJ, Puckett RL, Schilling B, Campisi J, Benz CC and Gibson BW (2010) Targeted quantitation of site-specific cysteine oxidation in endogenous proteins using a differential alkylation and multiple reaction monitoring mass spectrometry approach. *Mol Cell Proteomics* 9: 1400-10.
104. Liu B, Chen YM and Clair DKS (2008) ROS and p53: A versatile partnership. *Free Radical Biol Med* 44: 1529-1535.
105. Veal EA, Day AM and Morgan BA (2007) Hydrogen peroxide sensing and signaling. *Mol Cell* 26: 1-14.
106. Sablina AA, Budanov AV, Ilyinskaya GV, Agapova LS, Kravchenko JE and Chumakov PM (2005) The antioxidant function of the p53 tumor suppressor. *Nat Med* 11: 1306-13.
107. Jayaraman L, Murthy KGK, Zhu C, Curran T, Xanthoudakis S and Prives C (1997) Identification of redox/repair protein Ref-1 as a potent activator of p53. *Genes Dev* 11: 558-570.
108. Ueno M, Masutani H, Arai RJ, Yamauchi A, Hirota K, Sakai T, Inamoto T, Yamaoka Y, Yodoi J and Nikaido T (1999) Thioredoxin-dependent redox regulation of p53-mediated p21 activation. *J Biol Chem* 274: 35809-35815.

109. Hanson S, Kim E and Deppert W (2005) Redox factor 1 (Ref-1) enhances specific DNA binding of p53 by promoting p53 tetramerization. *Oncogene* 24: 1641-7.
110. Seemann S and Hainaut P (2005) Roles of thioredoxin reductase 1 and APE/Ref-1 in the control of basal p53 stability and activity. *Oncogene* 24: 3853-3863.
111. Stoner CS, Pearson GD, Koc A, Merwin JR, Lopez NI and Merrill GF (2009) Effect of Thioredoxin Deletion and p53 Cysteine Replacement on Human p53 Activity in Wild-Type and Thioredoxin Reductase Null Yeast. *Biochemistry* 48: 9156-9169.
112. Fritz G, Grosch S, Tomicic M and Kaina B (2003) APE/Ref-1 and the mammalian response to genotoxic stress. *Toxicology* 193: 67-78.
113. Nishiyama A, Masutani H, Nakamura H, Nishinaka Y and Yodoi J (2001) Redox regulation by thioredoxin and thioredoxin-binding proteins. *IUBMB Life* 52: 29-33.
114. Bykov VJ, Issaeva N, Shilov A, Hultcrantz M, Pugacheva E, Chumakov P, Bergman J, Wiman KG and Selivanova G (2002) Restoration of the tumor suppressor function to mutant p53 by a low-molecular-weight compound. *Nat Med* 8: 282-8.
115. Bykov VJN, Issaeva N, Zache N, Shilov A, Hultcrantz M, Bergman J, Selivanova G and Wiman KG (2005) Reactivation of mutant p53 and induction of apoptosis in human tumor cells by maleimide analogs. *J Biol Chem* 280: 30384-30391.

116. Zache N, Lambert JM, Rokaeus N, Shen J, Hainaut P, Bergman J, Wiman KG and Bykov VJ (2008) Mutant p53 targeting by the low molecular weight compound STIMA-1. *Mol Oncol* 2: 70-80.
117. Lambert JMR, Gorzov P, Veprintsev DB, Soderqvist M, Segerback D, Bergman J, Fersht AR, Hainaut P, Wiman KG and Bykov VJN (2009) PRIMA-1 Reactivates Mutant p53 by Covalent Binding to the Core Domain. *Cancer Cell* 15: 376-388.
118. Bykov VJN, Lambert JMR, Hainaut P and Wiman KG (2009) Mutant p53 rescue and modulation of p53 redox state. *Cell Cycle* 8: 2509-2517.
119. Kim DH, Kim EH, Na HK, Sun Y and Surh YJ (2010) 15-Deoxy-Delta(12,14)-prostaglandin J(2) stabilizes, but functionally inactivates p53 by binding to the cysteine 277 residue. *Oncogene* 29: 2560-76.
120. Kaar JL, Basse N, Joerger AC, Stephens E, Rutherford TJ and Fersht AR (2010) Stabilization of mutant p53 via alkylation of cysteines and effects on DNA binding. *Protein Sci* Epub ahead of print.
121. Straus DS and Glass CK (2001) Cyclopentenone prostaglandins: new insights on biological activities and cellular targets. *Med Res Rev* 21: 185-210.
122. Kondo M, Shibata T, Kumagai T, Osawa T, Shibata N, Kobayashi M, Sasaki S, Iwata M, Noguchi N and Uchida K (2002) 15-Deoxy-Delta(12,14)-prostaglandin J(2): the endogenous electrophile that induces neuronal apoptosis. *Proc Natl Acad Sci USA* 99: 7367-72.

123. Eaton P (2006) Protein thiol oxidation in health and disease: Techniques for measuring disulfides and related modifications in complex protein mixtures. *Free Radical Biol Med* 40: 1889-1899.
124. Zhao C, Sethuraman M, Clavreul N, Kaur P, Cohen RA and O'Connor PB (2006) Detailed map of oxidative post-translational modifications of human p21ras using Fourier transform mass spectrometry. *Anal Chem* 78: 5134-42.
125. van Montfort RL, Congreve M, Tisi D, Carr R and Jhoti H (2003) Oxidation state of the active-site cysteine in protein tyrosine phosphatase 1B. *Nature* 423: 773-7.
126. Tanaka K, Waki H, Ido Y, Akita S, Yoshida Y, Yoshida T and Matsuo T (1988) Protein and polymer analyses up to m/z 100 000 by laser ionization time-of-flight mass spectrometry. *Rapid Commun Mass Spectrom* 2: 151-153.
127. Fenn JB, Mann M, Meng CK, Wong SF and Whitehouse CM (1989) Electrospray ionization for mass spectrometry of large biomolecules. *Science* 246: 64-71.
128. Domon B and Aebersold R (2006) Mass spectrometry and protein analysis. *Science* 312: 212-7.
129. Khalsa-Moyers G and McDonald WH (2006) Developments in mass spectrometry for the analysis of complex protein mixtures. *Brief Funct Genomic Proteomic* 5: 98-111.
130. Seidler J, Zinn N, Boehm ME and Lehmann WD (2010) De novo sequencing of peptides by MS/MS. *Proteomics* 10: 634-49.

131. Bogdanov B and Smith RD (2005) Proteomics by FTICR mass spectrometry: Top down and bottom up. *Mass Spectrom Rev* 24: 168-200.
132. Woods AS and Ferre S (2005) Amazing stability of the arginine-phosphate electrostatic interaction. *J Proteome Res* 4: 1397-402.
133. van den Heuvel RH and Heck AJ (2004) Native protein mass spectrometry: from intact oligomers to functional machineries. *Curr Opin Chem Biol* 8: 519-26.
134. Boivin B, Zhangt S, Arbiser JL, Zhang ZY and Tonks NK (2008) A modified cysteinyl-labeling assay reveals reversible oxidation of protein tyrosine phosphatases in angiomyolipoma cells. *Proc Natl Acad Sci USA* 105: 9959-9964.
135. Macht M (2009) Mass spectrometric top-down analysis of proteins. *Bioanalysis* 1: 1131-1148.
136. Boyne MT, Garcia BA, Li MX, Zamdborg L, Wenger CD, Babai S and Kelleher NL (2009) Tandem Mass Spectrometry with Ultrahigh Mass Accuracy Clarifies Peptide Identification by Database Retrieval. *J Proteome Res* 8: 374-379.
137. Reid GE and McLuckey SA (2002) 'Top down' protein characterization via tandem mass spectrometry. *J Mass Spectrom* 37: 663-75.
138. Siuti N and Kelleher NL (2007) Decoding protein modifications using top-down mass spectrometry. *Nat Methods* 4: 817-821.

139. Han X, Jin M, Breuker K and McLafferty FW (2006) Extending top-down mass spectrometry to proteins with masses greater than 200 kilodaltons. *Science* 314: 109-12.
140. Vestling MM, Kelly MA, Fenselau C and Costello CE (1994) Optimization by mass spectrometry of a tryptophan-specific protein cleavage reaction. *Rapid Communications in Mass Spectrometry* 8: 786-790.
141. Karas M, Bachmann D and Hillenkamp F (1985) Influence of the Wavelength in High-Irradiance Ultraviolet-Laser Desorption Mass-Spectrometry of Organic-Molecules. *Anal Chem* 57: 2935-2939.
142. Tanaka K (2003) The origin of macromolecule ionization by laser irradiation (Nobel lecture). *Angew Chem Int Ed Engl* 42: 3860-70.
143. Fenn JB (2003) Electrospray wings for molecular elephants (Nobel lecture). *Angew Chem Int Ed Engl* 42: 3871-94.
144. Gross JH (2004) *Mass spectrometry: a textbook* (Springer, Berlin; London).
145. Gaskell SJ (1997) Electrospray: Principles and practice. *J Mass Spectrom* 32: 677-688.
146. Hendrickson CL and Emmett MR (1999) Electrospray ionization Fourier transform ion cyclotron resonance mass spectrometry. *Annu Rev Phys Chem* 50: 517-36.
147. Kebarle P (2000) A brief overview of the present status of the mechanisms involved in electrospray mass spectrometry. *J Mass Spectrom* 35: 804-17.

148. Wilm MS and Mann M (1994) Electrospray and Taylor-Cone Theory, Doles Beam of Macromolecules at Last. *Int J Mass spectrom* 136: 167-180.
149. Hoffmann Ed and Stroobant V (2007) *Mass spectrometry: principles and applications* (Wiley; Chichester, Hoboken, N.J.).
150. Pasa-Tolic L, Masselon C, Barry RC, Shen YF and Smith RD (2004) Proteomic analyses using an accurate mass and time tag strategy. *Biotechniques* 37: 621-639.
151. Konermann L and Douglas DJ (1998) Equilibrium unfolding of proteins monitored by electrospray ionization mass spectrometry: distinguishing two-state from multi-state transitions. *Rapid Commun Mass Spectrom* 12: 435-42.
152. Dobo A and Kaltashov IA (2001) Detection of multiple protein conformational ensembles in solution via deconvolution of charge-state distributions in ESI MS. *Anal Chem* 73: 4763-73.
153. Kaltashov IA and Eyles SJ (2002) Studies of biomolecular conformations and conformational dynamics by mass spectrometry. *Mass Spectrom Rev* 21: 37-71.
154. Marshall AG, Hendrickson CL and Jackson GS (1998) Fourier transform ion cyclotron resonance mass spectrometry: a primer. *Mass Spectrom Rev* 17: 1-35.
155. Loo JA (1997) Studying noncovalent protein complexes by electrospray ionization mass spectrometry. *Mass Spectrom Rev* 16: 1-23.

156. Beck JL, Colgrave ML, Ralph SF and Sheil MM (2001) Electrospray ionization mass spectrometry of oligonucleotide complexes with drugs, metals, and proteins. *Mass Spectrom Rev* 20: 61-87.
157. Robinson NE, Zabrouskov V, Zhang J, Lampi KJ and Robinson AB (2006) Measurement of deamidation of intact proteins by isotopic envelope and mass defect with ion cyclotron resonance Fourier transform mass spectrometry. *Rapid Commun Mass Spectrom* 20: 3535-41.
158. Clarke DJ, Mackay CL, Campopiano DJ, Langridge-Smith P and Brown AR (2009) Interrogating the molecular details of the peroxiredoxin activity of the Escherichia coli bacterioferritin comigratory protein using high-resolution mass spectrometry. *Biochemistry* 48: 3904-14.
159. Li X, Lin C and O'Connor PB (2010) Glutamine deamidation: differentiation of glutamic acid and gamma-glutamic acid in peptides by electron capture dissociation. *Anal Chem* 82: 3606-15.
160. Clauser KR, Baker P and Burlingame AL (1999) Role of accurate mass measurement (+/- 10 ppm) in protein identification strategies employing MS or MS/MS and database searching. *Anal Chem* 71: 2871-82.
161. Loo JA, Quinn JP, Ryu SI, Henry KD, Senko MW and McLafferty FW (1992) High-resolution tandem mass spectrometry of large biomolecules. *Proc Natl Acad Sci USA* 89: 286-9.
162. Robertson DH, Wong SC, Beynon RJ, Hurst JL and Gaskell SJ (2008) Observation of heterogeneous gene products by FT-ICR MS. *J Am Soc Mass Spectrom* 19: 103-10.

163. Amster IJ (1996) Fourier transform mass spectrometry. *J Mass Spectrom* 31: 1325-1337.
164. Meng FY, Forbes AJ, Miller LM and Kelleher NL (2005) Detection and localization of protein modifications by high resolution tandem mass spectrometry. *Mass Spectrom Rev* 24: 126-134.
165. McLafferty FW, Breuker K, Jin M, Han X, Infusini G, Jiang H, Kong X and Begley TP (2007) Top-down MS, a powerful complement to the high capabilities of proteolysis proteomics. *Febs J* 274: 6256-68.
166. Marshall AG, Hendrickson CL and Jackson GS (1998) Fourier transform ion cyclotron resonance mass spectrometry: A primer. *Mass Spectrom Rev* 17: 1-35.
167. Heeren RM, Kleinnijenhuis AJ, McDonnell LA and Mize TH (2004) A mini-review of mass spectrometry using high-performance FTICR-MS methods. *Anal Bioanal Chem* 378: 1048-58.
168. Marshall AG (2000) Milestones in Fourier transform ion cyclotron resonance mass spectrometry technique development. *Int J Mass spectrom* 200: 331-356.
169. Zhang LK, Rempel D, Pramanik BN and Gross ML (2005) Accurate mass measurements by Fourier transform mass spectrometry. *Mass Spectrom Rev* 24: 286-309.
170. Barlow SE and Tinkle MD (2002) "Linearizing" an ion cyclotron resonance cell. *Rev Sci Instrum* 73: 4185-4200.

171. Cooper HJ, Hakansson K and Marshall AG (2005) The role of electron capture dissociation in biomolecular analysis. *Mass Spectrom Rev* 24: 201-22.
172. Marshall AG, Wang TCL and Ricca TL (1985) Tailored Excitation for Fourier-Transform Ion-Cyclotron Resonance Mass-Spectrometry. *J Am Chem Soc* 107: 7893-7897.
173. de Koning LJ, Nibbering NMM, van Orden SL and Laukien FH (1997) Mass selection of ions in a Fourier transform ion cyclotron resonance trap using correlated harmonic excitation fields (CHEF). *Int J Mass spectrom* 165: 209-219.
174. Zubarev RA, Kelleher NL and McLafferty FW (1998) Electron capture dissociation of multiply charged protein cations. A nonergodic process. *J Am Chem Soc* 120: 3265-3266.
175. Little DP, Speir JP, Senko MW, Oconnor PB and Mclafferty FW (1994) Infrared Multiphoton Dissociation of Large Multiply-Charged Ions for Biomolecule Sequencing. *Anal Chem* 66: 2809-2815.
176. Gauthier JW, Trautman TR and Jacobson DB (1991) Sustained Off-Resonance Irradiation for Collision-Activated Dissociation Involving Fourier-Transform Mass-Spectrometry - Collision-Activated Dissociation Technique That Emulates Infrared Multiphoton Dissociation. *Anal Chim Acta* 246: 211-225.
177. Price WD, Schnier PD and Williams ER (1996) Tandem mass spectrometry of large biomolecule ions by blackbody infrared radiative dissociation. *Anal Chem* 68: 859-866.

178. Mabud MDA, Dekrey MJ and Cooks RG (1985) Surface-Induced Dissociation of Molecular-Ions. *Int J Mass Spectrom Ion Processes* 67: 285-294.
179. Syka JE, Coon JJ, Schroeder MJ, Shabanowitz J and Hunt DF (2004) Peptide and protein sequence analysis by electron transfer dissociation mass spectrometry. *Proc Natl Acad Sci USA* 101: 9528-33.
180. Coon JJ, Shabanowitz J, Hunt DF and Syka JE (2005) Electron transfer dissociation of peptide anions. *J Am Soc Mass Spectrom* 16: 880-2.
181. Roepstorff P and Fohlman J (1984) Proposal for a common nomenclature for sequence ions in mass spectra of peptides. *Biomed Mass Spectrom* 11: 601.
182. Biemann K (1990) Appendix 5. Nomenclature for peptide fragment ions (positive ions). *Methods Enzymol* 193: 886-7.
183. Hayes RN and Gross ML (1990) Collision-induced dissociation. *Methods Enzymol* 193: 237-63.
184. Shukla AK and Futrell JH (2000) Tandem mass spectrometry: dissociation of ions by collisional activation. *J Mass Spectrom* 35: 1069-90.
185. Sleno L and Volmer DA (2004) Ion activation methods for tandem mass spectrometry. *J Mass Spectrom* 39: 1091-112.
186. Wells JM and McLuckey SA (2005) Collision-induced dissociation (CID) of peptides and proteins. *Methods Enzymol* 402: 148-85.

187. McLuckey SA and Goeringer DE (1997) Slow heating methods in tandem mass spectrometry. *J Mass Spectrom* 32: 461-474.
188. Biemann K (1990) Sequencing of peptides by tandem mass spectrometry and high-energy collision-induced dissociation. *Methods Enzymol* 193: 455-79.
189. van der Burgt YEM, Palmblad M, Dalebout H, Heeren RMA and Deelder AM (2009) Electron capture dissociation of peptide hormone changes upon opening of the tocin ring and complexation with transition metal cations. *Rapid Commun Mass Spectrom* 23: 31-38.
190. Zubarev RA, Haselmann KF, Budnik B, Kjeldsen F and Jensen F (2002) Towards an understanding of the mechanism of electron-capture dissociation: a historical perspective and modern ideas. *Eur J Mass Spectrom* 8: 337-349.
191. Zubarev RA (2003) Reactions of polypeptide ions with electrons in the gas phase. *Mass Spectrom Rev* 22: 57-77.
192. Leymarie N, Costello CE and O'Connor PB (2003) Electron capture dissociation initiates a free radical reaction cascade. *J Am Chem Soc* 125: 8949-58.
193. Syrstad EA and Turecek F (2005) Toward a general mechanism of electron capture dissociation. *J Am Soc Mass Spectrom* 16: 208-24.
194. Sohn CH, Chung CK, Yin S, Ramachandran P, Loo JA and Beauchamp JL (2009) Probing the mechanism of electron capture and electron transfer dissociation using tags with variable electron affinity. *J Am Chem Soc* 131: 5444-59.

195. Creese AJ and Cooper HJ (2008) The effect of phosphorylation on the electron capture dissociation of peptide ions. *J Am Soc Mass Spectrom* 19: 1263-1274.
196. Breuker K, Oh HB, Lin C, Carpenter BK and McLafferty FW (2004) Nonergodic and conformational control of the electron capture dissociation of protein cations. *Proc Natl Acad Sci USA* 101: 14011-14016.
197. Ben Hamidane H, Vorobyev A, Larregola M, Lukaszuk A, Tourwe D, Lavielle S, Karoyan P and Tsybin YO (2010) Radical Stability Directs Electron Capture and Transfer Dissociation of beta-Amino Acids in Peptides. *Chemistry-a European Journal* 16: 4612-4622.
198. Kalli A and Hakansson K (2008) Comparison of the electron capture dissociation fragmentation behavior of doubly and triply protonated peptides from trypsin, Glu-C, and chymotrypsin digestion. *J Proteome Res* 7: 2834-2844.
199. McLafferty FW, Horn DM, Breuker K, Ge Y, Lewis MA, Cerda B, Zubarev RA and Carpenter BK (2001) Electron capture dissociation of gaseous multiply charged ions by Fourier-transform ion cyclotron resonance. *J Am Soc Mass Spectrom* 12: 245-9.
200. Zubarev RA (2004) Electron-capture dissociation tandem mass spectrometry. *Curr Opin Biotechnol* 15: 12-6.
201. Silivra OA, Kjeldsen F, Ivonin IA and Zubarev RA (2005) Electron capture dissociation of polypeptides in a three-dimensional quadrupole ion trap: Implementation and first results. *J Am Soc Mass Spectrom* 16: 22-7.

202. Satake H, Hasegawa H, Hirabayashi A, Hashimoto Y, Baba T and Masuda K (2007) Fast multiple electron capture dissociation in a linear radio frequency quadrupole ion trap. *Anal Chem* 79: 8755-61.
203. Sweet SM and Cooper HJ (2007) Electron capture dissociation in the analysis of protein phosphorylation. *Expert Rev Proteomics* 4: 149-59.
204. Kelleher RL, Zubarev RA, Bush K, Furie B, Furie BC, McLafferty FW and Walsh CT (1999) Localization of labile posttranslational modifications by electron capture dissociation: The case of gamma-carboxyglutamic acid. *Anal Chem* 71: 4250-4253.
205. Xie Y, Zhang J, Yin S and Loo JA (2006) Top-down ESI-ECD-FT-ICR mass spectrometry localizes noncovalent protein-ligand binding sites. *J Am Chem Soc* 128: 14432-3.
206. Horn DM, Ge Y and McLafferty FW (2000) Activated ion electron capture dissociation for mass spectral sequencing of larger (42 kDa) proteins. *Anal Chem* 72: 4778-84.
207. Zubarev RA, Kruger NA, Fridriksson EK, Lewis MA, Horn DM, Carpenter BK and McLafferty FW (1999) Electron capture dissociation of gaseous multiply-charged proteins is favored at disulfide bonds and other sites of high hydrogen atom affinity. *J Am Chem Soc* 121: 2857-2862.
208. Clarke DJ, Stokes AA, Langridge-Smith P and Mackay CL (2010) Online quench-flow electrospray ionization Fourier transform ion cyclotron resonance mass spectrometry for elucidating kinetic and chemical enzymatic reaction mechanisms. *Anal Chem* 82: 1897-904.

209. Tsybin YO, Witt M, Baykut G, Kjeldsen F and Håkansson P (2003) Combined infrared multiphoton dissociation and electron capture dissociation with a hollow electron beam in Fourier transform ion cyclotron resonance mass spectrometry. *Rapid Commun Mass Spectrom* 17: 1759-1768.
210. Sambrook J and Russell DW (2001) *Molecular cloning: a laboratory manual* (Cold Spring Harbor Laboratory Press, Cold Spring Harbor, N.Y.).
211. Walerych D, Kudla G, Gutkowska M, Wawrzynow B, Muller L, King FW, Helwak A, Boros J, Zylicz A and Zylicz M (2004) Hsp90 chaperones wild-type p53 tumor suppressor protein. *J Biol Chem* 279: 48836-45.
212. Bullock AN, Henckel J, DeDecker BS, Johnson CM, Nikolova PV, Proctor MR, Lane DP and Fersht AR (1997) Thermodynamic stability of wild-type and mutant p53 core domain. *Proc Natl Acad Sci USA* 94: 14338-14342.
213. Brenton AG and Godfrey AR (2010) Accurate Mass Measurement: Terminology and Treatment of Data. *J Am Soc Mass Spectrom* Epub ahead of print.
214. Pesavento JJ, Mizzen CA and Kelleher NL (2006) Quantitative analysis of modified proteins and their positional isomers by tandem mass spectrometry: Human histone H4. *Anal Chem* 78: 4271-4280.
215. LeDuc RD, Taylor GK, Kim YB, Januszyk TE, Bynum LH, Sola JV, Garavelli JS and Kelleher NL (2004) ProSight PTM: an integrated environment for protein identification and characterization by top-down mass spectrometry. *Nucleic Acids Res* 32: W340-W345.

216. Hansen S, Hupp TR and Lane DP (1996) Allosteric regulation of the thermostability and DNA binding activity of human p53 by specific interacting proteins. *J Biol Chem* 271: 3917-3924.
217. Bell S, Klein C, Muller L, Hansen S and Buchner J (2002) p53 contains large unstructured regions in its native state. *J Mol Biol* 322: 917-27.
218. Bell S, Hansen S and Buchner J (2002) Refolding and structural characterization of the human p53 tumor suppressor protein. *Biophys Chem* 96: 243-57.
219. Zhao X, Liu M, Wu N, Ding L, Liu H and Lin X (2010) Recovery of recombinant zebrafish p53 protein from inclusion bodies and its binding activity to p53 mRNA in vitro. *Protein Expr Purif* 72: 262-6.
220. Deb S and Deb SP (2003) *p53 protocols* (Humana Press, Totowa, N.J.), pp. 17-28.
221. Miroux B and Walker JE (1996) Over-production of proteins in *Escherichia coli*: Mutant hosts that allow synthesis of some membrane proteins and globular proteins at high levels. *J Mol Biol* 260: 289-298.
222. Dumon-Seignovert L, Cariot G and Vuillard L (2004) The toxicity of recombinant proteins in *Escherichia coli*: a comparison of overexpression in BL21(DE3), C41(DE3), and C43(DE3). *Protein Expr Purif* 37: 203-6.
223. Scopes RK (1993) *Protein purification: principles and practice* (Springer-Verlag, New York; London).

224. Butler JS and Loh SN (2006) Folding and misfolding mechanisms of the p53 DNA binding domain at physiological temperature. *Protein Sci* 15: 2457-65.
225. Butler JS and Loh SN (2005) Kinetic partitioning during folding of the p53 DNA binding domain. *J Mol Biol* 350: 906-18.
226. Walker DR, Bond JP, Tarone RE, Harris CC, Makalowski W, Boguski MS and Greenblatt MS (1999) Evolutionary conservation and somatic mutation hotspot maps of p53: correlation with p53 protein structural and functional features. *Oncogene* 18: 211-8.
227. Bullock AN, Henckel J and Fersht AR (2000) Quantitative analysis of residual folding and DNA binding in mutant p53 core domain: definition of mutant states for rescue in cancer therapy. *Oncogene* 19: 1245-56.
228. Grunberg-Manago M (1999) Messenger RNA stability and its role in control of gene expression in bacteria and phages. *Annu Rev Genet* 33: 193-227.
229. Kallis GB and Holmgren A (1980) Differential reactivity of the functional sulfhydryl groups of cysteine-32 and cysteine-35 present in the reduced form of thioredoxin from *Escherichia coli*. *J Biol Chem* 255: 10261-5.
230. Smyth DG, Blumenfeld OO and Konigsberg W (1964) Reactions of N-ethylmaleimide with peptides and amino acids. *Biochem J* 91: 589-95.
231. Clayden J, Greeves N, Warren S and Wothers P (2001) *Organic chemistry* (Oxford University Press, Oxford), pp. 227-242.

232. Bhanoori M, Yellaturu CR, Ghosh SK, Hassid A, Jennings LK and Rao GN (2003) Thiol alkylation inhibits the mitogenic effects of platelet-derived growth factor and renders it proapoptotic via activation of STATs and p53 and induction of expression of caspase1 and p21(waf1/cip1). *Oncogene* 22: 117-130.
233. Pesavento JJ, Mizzen CA and Kelleher NL (2006) Quantitative analysis of modified proteins and their positional isomers by tandem mass spectrometry: human histone H4. *Anal Chem* 78: 4271-80.
234. Gordon EF, Mansoori BA, Carroll CF and Muddiman DC (1999) Hydrophobic influences on the quantification of equine heart cytochrome c using relative ion abundance measurements by electrospray ionization fourier transform ion cyclotron resonance mass spectrometry. *J Mass Spectrom* 34: 1055-62.
235. Khoo KH, Mayer S and Fersht AR (2009) Effects of stability on the biological function of p53. *J Biol Chem* 284: 30974-80.
236. Friedler A, Veprintsev DB, Hansson LO and Fersht AR (2003) Kinetic instability of p53 core domain mutants: implications for rescue by small molecules. *J Biol Chem* 278: 24108-12.
237. Voet D, Voet JG and Pratt CW (2005) *Fundamentals of Biochemistry 2nd Edition* (Wiley, New York), pp. 101-102.
238. Joerger AC, Allen MD and Fersht AR (2004) Crystal structure of a superstable mutant of human p53 core domain. Insights into the mechanism of rescuing oncogenic mutations. *J Biol Chem* 279: 1291-6.

239. Craig AL, Chrystal JA, Fraser JA, Sphyris N, Lin Y, Harrison BJ, Scott MT, Dornreiter I and Hupp TR (2007) The MDM2 ubiquitination signal in the DNA-binding domain of p53 forms a docking site for calcium calmodulin kinase superfamily members. *Mol Cell Biol* 27: 3542-3555.
240. Glineur C, Davioud-Charvet E and Vandebunder B (2000) The conserved redox-sensitive cysteine residue of the DNA-binding region in the c-Rel protein is involved in the regulation of the phosphorylation of the protein. *Biochem J* 352: 583-591.
241. Lapko VN, Smith DL and Smith JB (2002) S-methylated cysteines in human lens gamma S-crystallins. *Biochemistry* 41: 14645-51.
242. Lapko VN, Cerny RL, Smith DL and Smith JB (2005) Modifications of human betaA1/betaA3-crystallins include S-methylation, glutathiolation, and truncation. *Protein Sci* 14: 45-54.
243. Bailey E, Connors TA, Farmer PB, Gorf SM and Rickard J (1981) Methylation of cysteine in hemoglobin following exposure to methylating agents. *Cancer Res* 41: 2514-7.
244. Grombacher T, Eichhorn U and Kaina B (1998) P53 is involved in regulation of the DNA repair gene O-6-methylguanine-DNA methyltransferase (MGMT) by DNA damaging agents. *Oncogene* 17: 845-851.
245. Voet D, Voet JG and Pratt CW (2005) *Fundamentals of Biochemistry 2nd Edition* (Wiley, New York), pp. 156-161.
246. Holmgren A (1995) Thioredoxin structure and mechanism: conformational changes on oxidation of the active-site sulfhydryls to a disulfide. *Structure* 3: 239-43.

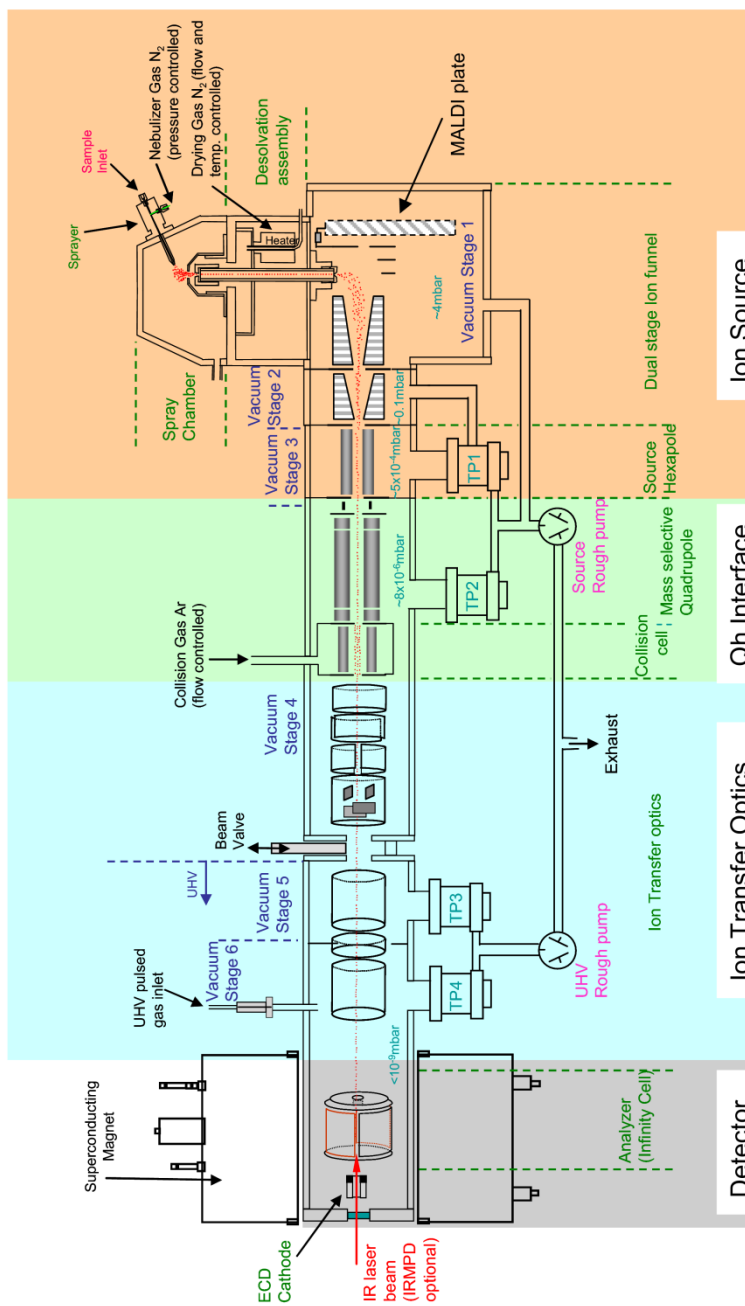
247. Hainaut P and Mann K (2001) Zinc binding and redox control of p53 structure and function. *Antioxid Redox Signal* 3: 611-623.
248. Nelson KJ, Day AE, Zeng BB, King SB and Poole LB (2008) Isotope-coded, iodoacetamide-based reagent to determine individual cysteine pK(a) values by matrix-assisted laser desorption/ionization time-of-flight mass spectrometry. *Anal Biochem* 375: 187-95.
249. Nelson KJ, Parsonage D, Hall A, Karplus PA and Poole LB (2008) Cysteine pK(a) values for the bacterial peroxiredoxin AhpC. *Biochemistry* 47: 12860-8.
250. Weinberg RL, Veprintsev DB and Fersht AR (2004) Cooperative binding of tetrameric p53 to DNA. *J Mol Biol* 341: 1145-59.
251. Natan E, Hirschberg D, Morgner N, Robinson CV and Fersht AR (2009) Ultraslow oligomerization equilibria of p53 and its implications. *Proc Natl Acad Sci USA* 106: 14327-32.
252. Bode AM and Dong Z (2004) Post-translational modification of p53 in tumorigenesis. *Nat Rev Cancer* 4: 793-805.
253. Meek DW and Anderson CW (2009) Posttranslational modification of p53: cooperative integrators of function. *Cold Spring Harb Perspect Biol* 1: a000950.
254. Lee JT and Gu W (2010) The multiple levels of regulation by p53 ubiquitination. *Cell Death Differ* 17: 86-92.
255. Scoumanne A and Chen X (2008) Protein methylation: a new mechanism of p53 tumor suppressor regulation. *Histol Histopathol* 23: 1143-9.

256. Loo JA, Edmonds CG, Udseth HR and Smith RD (1990) Effect of reducing disulfide-containing proteins on electrospray ionization mass spectra. *Anal Chem* 62: 693-8.
257. Green NM (1966) Thermodynamics of the binding of biotin and some analogues by avidin. *Biochem J* 101: 774-80.
258. Carlsson J, Drevin H and Axen R (1978) Protein thiolation and reversible protein-protein conjugation. N-Succinimidyl 3-(2-pyridyldithio)propionate, a new heterobifunctional reagent. *Biochem J* 173: 723-37.
259. Campopiano DJ, Clarke DJ, Polfer NC, Barran PE, Langley RJ, Govan JR, Maxwell A and Dorin JR (2004) Structure-activity relationships in defensin dimers: a novel link between beta-defensin tertiary structure and antimicrobial activity. *J Biol Chem* 279: 48671-9.
260. Collet JF, D'Souza JC, Jakob U and Bardwell JC (2003) Thioredoxin 2, an oxidative stress-induced protein, contains a high affinity zinc binding site. *J Biol Chem* 278: 45325-32.
261. Kwon E, Kim DY, Suh SW and Kim KK (2008) Crystal structure of the mouse p53 core domain in zinc-free state. *Proteins* 70: 280-3.
262. Nikitovic D, Holmgren A and Spyrou G (1998) Inhibition of AP-1 DNA binding by nitric oxide involving conserved cysteine residues in Jun and Fos. *Biochem Biophys Res Commun* 242: 109-12.
263. Sun Y and Oberley LW (1996) Redox regulation of transcriptional activators. *Free Radic Biol Med* 21: 335-48.

264. Erster S, Mihara M, Kim RH, Petrenko O and Moll UM (2004) In vivo mitochondrial p53 translocation triggers a rapid first wave of cell death in response to DNA damage that can precede p53 target gene activation. *Mol Cell Biol* 24: 6728-41.
265. Galluzzi L, Morselli E, Kepp O, Vitale I, Pinti M and Kroemer G (2010) Mitochondrial liaisons of p53. *Antioxid Redox Signal* Epub ahead of print.
266. Polyak K, Xia Y, Zweier JL, Kinzler KW and Vogelstein B (1997) A model for p53-induced apoptosis. *Nature* 389: 300-5.
267. Mayer S, Rudiger S, Ang HC, Joerger AC and Fersht AR (2007) Correlation of levels of folded recombinant p53 in escherichia coli with thermodynamic stability in vitro. *J Mol Biol* 372: 268-76.
268. Allison WS (1976) Formation and Reactions of Sulfenic Acids in Proteins. *Acc Chem Res* 9: 293-299.
269. Turell L, Botti H, Carballal S, Ferrer-Sueta G, Souza JM, Duran R, Freeman BA, Radi R and Alvarez B (2008) Reactivity of sulfenic acid in human serum albumin. *Biochemistry* 47: 358-67.
270. Rehder DS and Borges CR (2010) Possibilities and pitfalls in quantifying the extent of cysteine sulfenic acid modification of specific proteins within complex biofluids. *BMC Biochem* 11: 25.
271. Maret W (2004) Zinc and sulfur: a critical biological partnership. *Biochemistry* 43: 3301-9.
272. Le Chatelier HL (1884) Sur un énoncé général des lois des équilibres chimiques. *Comptes Rendus Académie des Sciences* 99: 786-789.

273. Polson C, Sarkar P, Incledon B, Raguvaran V and Grant R (2003) Optimization of protein precipitation based upon effectiveness of protein removal and ionization effect in liquid chromatography-tandem mass spectrometry. *J Chromatogr B Analyt Technol Biomed Life Sci* 785: 263-75.
274. Sies H (1999) Glutathione and its role in cellular functions. *Free Radic Biol Med* 27: 916-21.
275. Dalle-Donne I, Rossi R, Colombo G, Giustarini D and Milzani A (2009) Protein S-glutathionylation: a regulatory device from bacteria to humans. *Trends Biochem Sci* 34: 85-96.
276. Hutchison RS and Ort DR (1995) Measurement of equilibrium midpoint potentials of thiol/disulfide regulatory groups on thioredoxin-activated chloroplast enzymes. *Methods Enzymol* 252: 220-8.
277. Setterdahl AT, Goldman BS, Hirasawa M, Jacquot P, Smith AJ, Kranz RG and Knaff DB (2000) Oxidation-reduction properties of disulfide-containing proteins of the *Rhodobacter capsulatus* cytochrome c biogenesis system. *Biochemistry* 39: 10172-6.

Appendix A: FT-ICR MS Instrumentation



Overview of the Bruker Daltonics apex-Qe FT-ICR mass spectrometer used extensively for the work presented in this thesis.

Appendix B: Mass Assignments for Fragment Ions

B.1 CID of 2NEM-p53

Assigned *b* and *y* fragment ions corresponding to p53 core domain alkylated at residues Cys182 and Cys275 or Cys277.

Fragment Ion	Observed Monoisotopic Mass (Da)	Theoretical Monoisotopic Mass (Da)	MME (ppm)
b10	1064.520	1064.514	5.50
b11	1192.581	1192.572	7.19
b19	2029.979	2029.986	-3.57
b26	2743.348	2743.335	4.74
b27	2871.447	2871.430	5.66
b28	2958.490	2958.462	9.37
b33	3525.708	3525.699	2.50
b34	3612.741	3612.731	2.82
b36	3780.828	3780.821	1.99
b37	3893.919	3893.905	3.76
b38	4007.961	4007.948	3.25
b39	4136.057	4136.043	3.38
b40	4267.084	4267.083	0.21
b41	4414.150	4414.151	-0.39
b42	4517.154	4517.161	-1.58
b43	4645.229	4645.219	2.05
b44	4758.312	4758.303	1.77
b45	4829.350	4829.340	2.04
b47	5058.490	5058.483	1.36
b48	5161.500	5161.492	1.45
b49	5258.552	5258.545	1.36
b50	5357.610	5357.613	-0.67
b51	5485.679	5485.672	1.25
b52	5598.758	5598.756	0.43
b53	5784.840	5784.835	0.83
b54	5883.904	5883.904	0.01
b55	5998.948	5998.931	2.96
b56	6085.966	6085.963	0.56
b57	6187.007	6187.010	-0.53
b65	7047.534	7047.508	3.59
b76	8336.159	8336.114	5.41
b82	9076.532	9076.543	-1.23
b87	9679.736	9679.766	-3.07
b93	10468.093	10468.041	4.97
b96	10709.244	10709.184	5.68
b114	12838.333	12838.322	0.86
b124	14050.008	14049.938	5.03
b125	14149.020	14149.006	0.96
b126	14246.140	14246.059	5.69
b128	14538.170	14538.165	0.32
b129	14635.232	14635.218	1.01
b131	14861.322	14861.313	0.63

b160	18066.817	18066.682	7.46
b161	18179.802	18179.766	1.97
b162	18292.674	18292.850	-9.64
b165	18636.102	18636.025	4.12
b169	18982.222	18982.137	4.47
b175	19649.395	19649.514	-6.06
b199	22633.882	22633.995	-5.02
b201	22820.146	22820.059	3.79
b216	24437.960	24437.933	1.09
b217	24552.065	24551.976	3.63
y13	1351.730	1351.723	5.08
y15	1593.855	1593.849	3.65
y16	1730.913	1730.908	2.49
y18	1965.025	1965.020	2.36
y20	2151.070	2151.084	-6.56
y29	3278.681	3278.678	1.01
y31	3590.887	3590.880	2.14
y41	4772.427	4772.422	1.01
y46	5405.697	5405.710	-2.30
y47	5462.743	5462.731	2.14
y48	5575.827	5575.815	2.12
y49	5688.890	5688.899	-1.55
y50	5802.957	5802.942	2.64
y51	5859.960	5859.963	-0.62
y52	5947.002	5946.996	1.15
y53	6034.034	6034.028	1.11
y54	6149.062	6149.054	1.23
y55	6278.098	6278.097	0.09
y56	6391.187	6391.181	0.93
y57	6492.236	6492.229	1.12
y70	7945.055	7945.035	2.56
y71	8048.043	8048.044	-0.06
y72	8135.080	8135.076	0.58
y74	8336.159	8336.151	1.02
y75	8439.168	8439.160	0.94
y84	9565.630	9565.618	1.34
y85	9680.733	9680.644	9.16
y87	9824.704	9824.698	0.66
y88	9923.773	9923.766	0.70
y89	10052.830	10052.809	2.11
y90	10149.857	10149.862	-0.47
y91	10246.914	10246.914	-0.02
y97	10933.314	10933.278	3.25
y105	11946.782	11946.757	2.06
y123	14075.922	14075.896	1.89
y124	14146.795	14146.933	-9.70
y128	14519.197	14519.097	6.85
y129	14634.184	14634.124	4.07
y145	16717.104	16717.065	2.36
y147	16932.116	16932.155	-2.32
y162	18598.075	18598.069	0.34

y164	18786.227	18786.149	4.19
y165	18901.181	18901.176	0.31
y166	19000.255	19000.244	0.60
y167	19186.341	19186.323	0.93
y168	19299.431	19299.407	1.23
y215	24424.985	24424.915	2.89
y217	24611.058	24611.015	1.74
y218	24698.051	24698.047	0.16

B.2 ECD of 2NEM-p53

Assigned *c* and *z* fragment ions corresponding to p53 core domain alkylated at residues Cys182 and Cys275 or Cys277.

Fragment Ion	Observed Monoisotopic Mass (Da)	Theoretical Monoisotopic Mass (Da)	MME (ppm)
c6	561.281	561.276	8.84
c7	689.338	689.334	5.63
c8	817.432	817.429	3.33
c9	918.478	918.477	1.02
c10	1081.539	1081.540	-1.01
c11	1209.604	1209.599	4.66
c12	1266.626	1266.620	4.16
c13	1353.659	1353.652	5.13
c14	1516.722	1516.716	4.16
c15	1573.742	1573.737	3.21
c16	1720.810	1720.806	2.52
c18	1989.997	1989.991	3.35
c19	2047.019	2047.012	3.13
c20	2194.088	2194.081	3.51
c21	2307.171	2307.165	2.75
c22	2444.231	2444.224	3.24
c23	2531.258	2531.256	0.95
c24	2588.282	2588.277	1.79
c25	2689.329	2689.325	1.70
c26	2760.366	2760.362	1.58
c27	2888.461	2888.457	1.45
c28	2975.493	2975.489	1.43
c29	3074.563	3074.557	1.94
c30	3175.608	3175.605	0.97
c31	3278.626	3278.614	3.68
c33	3542.728	3542.725	0.81
c35	3726.813	3726.810	0.85
c36	3797.851	3797.847	1.05
c37	3910.934	3910.931	0.87
c38	4024.977	4024.974	0.64
c39	4153.075	4153.069	1.38
c40	4284.116	4284.109	1.43
c41	4431.182	4431.178	0.84
c42	4534.188	4534.187	0.16
c43	4662.250	4662.246	0.98
c44	4775.329	4775.330	-0.04
c45	4846.368	4846.367	0.22
c47	5075.510	5075.509	0.15
c49	5275.581	5275.571	1.89
c50	5374.639	5374.640	-0.21
c51	5502.700	5502.698	0.33
c52	5615.782	5615.782	-0.12

c53	5801.878	5801.862	2.85
c54	5900.930	5900.930	0.02
c55	6015.955	6015.957	-0.37
c56	6102.989	6102.989	-0.09
c62	6653.234	6653.264	-4.50
c64	6908.439	6908.434	0.76
c65	7064.537	7064.535	0.26
c66	7135.589	7135.572	2.33
c67	7266.613	7266.612	0.02
c68	7337.653	7337.650	0.44
c69	7450.736	7450.734	0.38
c70	7613.798	7613.797	0.19
c71	7741.891	7741.892	-0.12
c72	7869.951	7869.950	0.02
c73	7956.984	7956.982	0.23
c74	8085.041	8085.041	-0.04
c76	8353.123	8353.140	-2.13
c77	8454.188	8454.188	0.02
c78	8583.231	8583.231	0.08
c80	8781.369	8781.368	0.19
c88	9852.872	9852.893	-2.20
c92	10369.976	10370.040	-6.25
c103	11567.687	11567.702	-1.34
c104	11666.773	11666.771	0.20
c110	12335.164	12335.131	2.62
c217	24569.021	24569.002	0.76
c218	24683.079	24683.045	1.35
z7	768.403	768.400	3.49
z14	1448.786	1448.786	-0.44
z15	1577.827	1577.829	-1.41
z16	1714.884	1714.888	-2.06
z20	2135.070	2135.063	3.02
z21	2263.153	2263.158	-2.52
z22	2391.263	2391.253	4.03
z23	2547.360	2547.354	2.36
z24	2660.445	2660.438	2.32
z25	2774.488	2774.481	2.25
z26	2903.531	2903.524	2.29
z27	3032.573	3032.567	2.03
z28	3161.590	3161.609	-6.12
z28	3161.617	3161.609	2.33
z29	3262.663	3262.657	1.77
z31	3574.864	3574.859	1.50
z43	5032.515	5032.513	0.49
z45	5233.584	5233.588	-0.67
z49	5672.880	5672.878	0.32
z53	6018.020	6018.007	2.16
z54	6133.036	6133.034	0.28
z56	6375.163	6375.160	0.42
z57	6476.183	6476.208	-3.84
z64	7282.751	7282.746	0.66

z66	7552.893	7552.890	0.46
z68	7740.960	7740.952	1.07
z75	8423.200	8423.139	7.16
z84	9549.615	9549.597	1.85
z88	9907.774	9907.746	2.87
z117	13374.397	13374.484	-6.52
z128	14503.175	14503.077	6.78
z155	17877.670	17877.651	1.07
z164	18770.075	18770.128	-2.79
z167	19170.329	19170.303	1.37
z168	19283.390	19283.387	0.15
z169	19411.499	19411.445	2.77
z179	20502.075	20501.976	4.85
z217	24594.994	24594.995	-0.03
z218	24682.009	24682.027	-0.72

B.3 CID of 2NEM-p53_{Lys-C}

Assigned *b* and *y* fragment ions corresponding to the p53 peptide Gln165 - Lys291 alkylated at residues Cys182 and Cys277.

Fragment Ion	Observed Monoisotopic Mass (Da)	Theoretical Monoisotopic Mass (Da)	MME (ppm)
b6	712.301	712.296	6.36
b9	1039.480	1039.476	4.25
b11	1351.685	1351.678	5.25
b12	1454.697	1454.687	6.74
b16	1954.895	1954.900	-2.90
b17	2111.017	2111.001	7.50
b19	2426.085	2426.090	-1.81
b20	2541.113	2541.117	-1.59
b21	2628.137	2628.149	-4.51
b22	2743.180	2743.176	1.68
b23	2800.209	2800.197	4.44
b25	2984.324	2984.318	1.80
b34	4053.905	4053.921	-4.09
b36	4224.964	4224.986	-5.25
b40	4722.283	4722.282	0.27
b43	5113.457	5113.456	0.18
b44	5228.476	5228.483	-1.43
b52	6226.035	6226.004	5.00
b53	6325.082	6325.072	1.53
b54	6424.141	6424.141	0.01
b55	6521.213	6521.193	2.93
b56	6684.259	6684.257	0.31
b57	6813.297	6813.299	-0.34
b58	6910.351	6910.352	-0.22
b60	7136.451	7136.447	0.48
b61	7235.517	7235.516	0.16
b62	7292.559	7292.537	2.99
b64	7494.553	7494.596	-5.72
b68	7912.748	7912.785	-4.61
b69	8049.795	8049.844	-6.07
b91	10567.987	10567.985	0.21
b92	10668.959	10669.033	-6.93
b95	11026.120	11026.186	-6.05
b107	12287.704	12287.791	-7.09
y5	658.381	658.378	4.03
y6	787.422	787.421	1.98
y8	1017.512	1017.511	0.48
y9	1173.619	1173.612	5.78
y10	1329.713	1329.713	-0.32
y11	1444.748	1444.740	5.21
y16	2054.013	2054.009	1.95
y20	2511.261	2511.256	1.82

y22	2787.381	2787.367	4.94
y26	3201.577	3201.564	3.98
y27	3314.661	3314.649	3.80
y28	3427.747	3427.733	4.27
y29	3541.783	3541.776	2.15
y30	3598.787	3598.797	-2.82
y31	3685.841	3685.829	3.34
y32	3772.878	3772.861	4.39
y33	3887.901	3887.888	3.33
y34	4016.939	4016.931	2.10
y35	4130.024	4130.015	2.25
y36	4231.073	4231.062	2.53
y38	4457.186	4457.230	-9.94
y40	4671.378	4671.362	3.31
y49	5683.861	5683.868	-1.16
y50	5786.895	5786.877	2.99
y51	5873.924	5873.909	2.50
y54	6178.008	6177.993	2.38
y55	6309.060	6309.034	4.16
y59	6886.255	6886.262	-1.09
y61	7100.366	7100.394	-3.93
y63	7304.449	7304.451	-0.34
y64	7419.485	7419.478	0.90
y65	7506.512	7506.510	0.22
y66	7563.525	7563.531	-0.88
y67	7662.616	7662.600	2.07
y68	7791.586	7791.642	-7.28
y69	7888.683	7888.695	-1.49
y70	7985.744	7985.748	-0.52
y78	8896.210	8896.203	0.79
y83	9570.502	9570.564	-6.45
y84	9685.576	9685.591	-1.52
y105	12055.792	12055.872	-6.59
y107	12257.853	12257.931	-6.38

B.4 ECD of 2NEM-p53_{Lys-C}

Assigned *c* and *z* fragment ions corresponding to the p53 peptide Gln165 - Lys291 alkylated at residues Cys182 and Cys277.

Fragment Ion	Observed Monoisotopic Mass (Da)	Theoretical Monoisotopic Mass (Da)	MME (ppm)
c5	628.281	628.275	8.85
c6	729.328	729.323	6.97
c7	858.369	858.365	4.88
c9	1056.506	1056.502	3.76
c10	1212.603	1212.603	-0.03
c11	1368.706	1368.704	0.99
c13	1568.768	1568.766	1.15
c14	1705.825	1705.825	0.05
c16	1971.926	1971.927	-0.26
c17	2128.036	2128.028	4.08
c18	2356.091	2356.084	2.97
c19	2443.109	2443.116	-2.72
c20	2558.140	2558.143	-1.28
c21	2645.170	2645.175	-1.86
c24	2930.292	2930.307	-5.24
c28	3323.500	3323.509	-2.55
c29	3460.559	3460.568	-2.57
c31	3686.744	3686.736	2.30
c33	3941.908	3941.905	0.60
c34	4070.940	4070.948	-1.97
c35	4127.952	4127.969	-4.11
c36	4242.012	4242.012	0.02
c37	4355.061	4355.096	-8.10
c40	4739.287	4739.308	-4.57
c42	5015.435	5015.456	-4.08
c43	5130.469	5130.483	-2.75
c44	5245.488	5245.510	-4.11
c45	5401.595	5401.611	-2.95
c46	5515.622	5515.654	-5.73
c48	5763.745	5763.770	-4.37
c49	5919.847	5919.871	-4.07
c56	6701.252	6701.283	-4.66
z5	642.363	642.358	8.58
z6	771.404	771.400	4.95
z7	900.448	900.443	6.03
z8	1001.493	1001.490	2.45
z9	1157.597	1157.592	5.13
z10	1313.697	1313.693	3.45
z11	1428.720	1428.720	0.55
z12	1584.823	1584.821	1.31
z13	1641.838	1641.842	-2.36
z24	2972.404	2972.421	-5.66

z36	4215.017	4215.042	-5.89
z39	4542.240	4542.257	-3.93
z40	4655.303	4655.342	-8.29
z47	5479.766	5479.785	-3.60
z54	6161.994	6161.973	3.47
z55	6293.062	6293.013	7.67
z56	6456.109	6456.077	5.03
z61	7084.339	7084.374	-4.93
z67	7646.592	7646.579	1.68
z68	7775.638	7775.622	2.09
z103	11869.687	11869.746	-4.92
z119	13842.671	13842.619	3.71

B.5 CID of Mono-alkylated p53 Peptide V274-R280

Assigned *b* and *y* fragment ions corresponding to the p53 peptide V274 – R280 (VCACPGR) alkylated at residue Cys277.

Fragment Ion	Observed Monoisotopic Mass (Da)	Theoretical Monoisotopic Mass (Da)	MME (ppm)
b4	501.170	501.171	-2.59
y3	328.185	328.188	-9.84
y4	556.240	556.244	-6.51
y5	627.279	627.281	-3.71
y6	730.287	730.290	-4.82

B.6 CID of 3NEM-p53

Assigned *b* and *y* fragment ions corresponding to p53 core domain alkylated at residues Cys182, Cys277 and Cys229, Cys238 or Cys242.

Fragment Ion	Observed Monoisotopic Mass (Da)	Theoretical Monoisotopic Mass (Da)	MME (ppm)
b21	2290.124	2290.138	-6.20
b22	2427.189	2427.197	-3.26
b23	2514.224	2514.229	-2.01
b26	2743.316	2743.335	-6.93
b27	2871.421	2871.430	-3.29
b29	3057.518	3057.531	-4.19
b30	3158.567	3158.579	-3.54
b33	3525.677	3525.699	-6.23
b34	3612.710	3612.731	-5.82
b36	3780.794	3780.821	-7.03
b37	3893.879	3893.905	-6.61
b38	4007.918	4007.948	-7.45
b43	4645.187	4645.219	-7.00
b44	4758.272	4758.303	-6.55
b45	4829.309	4829.340	-6.56
b46	4957.407	4957.435	-5.78
b48	5161.452	5161.492	-7.83
b51	5485.640	5485.672	-5.90
b52	5598.724	5598.756	-5.75
b53	5784.805	5784.835	-5.21
b114	12838.228	12838.322	-7.31
b128	14538.059	14538.165	-7.31
b129	14635.120	14635.218	-6.64
b131	14861.204	14861.313	-7.32
b169	19107.133	19107.184	-2.70
y11	1157.613	1157.617	-3.46
y12	1254.664	1254.670	-4.52
y13	1351.719	1351.723	-2.69
y14	1464.803	1464.807	-2.86
y15	1593.847	1593.849	-1.56
y16	1730.905	1730.908	-1.84
y18	1965.017	1965.020	-1.46
y25	2790.491	2790.502	-3.99
y26	2919.532	2919.545	-4.32
y31	3590.867	3590.880	-3.68
y41	4772.400	4772.422	-4.65
y85	9805.604	9805.691	-8.93
y87	9949.672	9949.745	-7.29
y90	10274.832	10274.909	-7.51
y91	10371.893	10371.961	-6.57
y105	12071.718	12071.804	-7.14
y162	18722.979	18723.116	-7.31

B.7 CID of 6NEM-p53

Assigned *b* and *y* fragment ions corresponding to p53 core domain alkylated at residues Cys124, 135, 141, 229, 275 and 277.

Fragment Ion	Observed Monoisotopic Mass (Da)	Theoretical Monoisotopic Mass (Da)	MME (ppm)
b19	2029.994	2029.986	4.02
b22	2427.211	2427.197	5.88
b26	2743.354	2743.335	6.63
b27	2871.447	2871.430	5.90
b29	3057.560	3057.531	9.62
b32	3487.714	3487.682	9.10
b33	3650.766	3650.746	5.51
b34	3737.782	3737.778	1.25
b37	4018.977	4018.952	6.29
b38	4133.016	4132.995	5.21
b39	4261.116	4261.090	6.28
b41	4539.222	4539.198	5.21
b43	4895.338	4895.313	5.07
b43	4895.362	4895.313	9.89
b44	5008.419	5008.397	4.30
b45	5079.457	5079.434	4.46
b46	5207.531	5207.529	0.26
b48	5536.657	5536.633	4.21
b50	5732.750	5732.754	-0.74
b51	5860.806	5860.813	-1.17
b52	5973.891	5973.897	-1.06
b53	6159.971	6159.976	-0.88
b54	6259.038	6259.045	-1.03
b55	6374.107	6374.072	5.59
b90	10400.975	10401.049	-7.17
b114	13088.452	13088.416	2.78
b125	14399.075	14399.100	-1.74
b127	14659.253	14659.216	2.52
b128	14788.305	14788.259	3.10
b129	14885.347	14885.312	2.40
b131	15111.403	15111.407	-0.27
y11	1157.617	1157.617	-0.27
y13	1351.734	1351.723	7.97
y14	1464.818	1464.807	7.52
y15	1593.859	1593.849	6.04
y16	1730.919	1730.908	6.25
y18	1965.024	1965.020	1.85
y26	2919.570	2919.545	8.73
y31	3590.897	3590.880	4.87
y41	4897.491	4897.469	4.33
y47	5587.806	5587.778	5.06
y48	5700.860	5700.862	-0.33

y51	5985.036	5985.010	4.29
y52	6072.072	6072.043	4.80
y54	6274.128	6274.101	4.28
y55	6403.171	6403.144	4.28
y56	6516.249	6516.228	3.18
y57	6617.306	6617.276	4.57
y71	8173.126	8173.091	4.37
y73	8347.158	8347.155	0.39
y74	8461.225	8461.198	3.27
y75	8564.237	8564.207	3.53
y85	9930.803	9930.738	6.53
y87	10074.819	10074.792	2.70
y88	10173.882	10173.860	2.15
y89	10302.973	10302.903	6.84
y90	10399.991	10399.956	3.36
y91	10497.041	10497.008	3.06
y105	12196.896	12196.851	3.67
y165	19026.260	19026.223	1.98
y166	19125.348	19125.291	2.98
y167	19311.428	19311.370	2.99
y168	19424.494	19424.454	2.05

Appendix C: Publications, Course and Conference Attendance

C.1 Publications

Vincent I, Scotcher J and Burchmore R (2010) Sixth Exploratory Measurement Science Group symposium. *Expert Rev Proteomics* 7: 19-20

Scotcher J, Clarke DJ, Weidt SK, Mackay CL, Hupp TR, Sadler PJ and Langridge-Smith PRR (2010) Top-Down Mass Spectrometry of p53 Identifies Two Reactive Cysteine Residues Implicated in Redox-Regulation *Submitted to J Am Soc Mass Spectrom*

C.2 Course Attendance

Research, Researchers and the Media: A Hands On Approach to Communicating Your Science. (Oct 2009) *BBC Glasgow & Barony Castle, UK.*

3rd Summer Course on Mass Spectrometry in Biotechnology and Medicine. (July 2009) *Centre for Advanced Academic Studies, Dubrovnik, Croatia.*

Mass Spectrometry: Principles and Practice in the 21st Century. (Apr 2008) *University of Edinburgh, UK.*

Joint DTC Training Course UK-GRAD Programme. (Jan 2008) *Barony Castle, UK.*

C.3 Conference Attendance

2nd Annual RASOR Conference. (September 2007) *Polmont, UK.*

Poster: Investigating p53-DNA Complexes Using ESI-FTICR-MS.

Talk: A CRP Immunoassay Using SERRS Active Microspheres Within a Lab-on-a-Chip.

3rd Annual RASOR Conference. (November 2008) *Drymen, UK.*

Poster: Redox-Regulation of p53: Identifying Redox-Modifications by FT-ICR Mass Spectrometry.

4th Annual RASOR Conference. (December 2009) *Stirling, UK.*

Talk: Using FT-ICR Mass Spectrometry to Investigate the Role of Cysteine Residues in p53.

RASOR Lab-on-a-Chip Symposium. (March 2010) *Glasgow, UK.*

Poster: Investigating the Redox-Regulation of p53 Using FT-ICR Mass Spectrometry.

CBC & RASOR Technology Showcase (July 2010) *Imperial College London, UK.*
Delegate.

4th EMSG Symposium. (October 2007) *Ardgour, UK.*

Talk: p53 (& my PhD).

5th EMSG Symposium. (November 2008) *Ardgour, UK.*

Talk: Characterising the Redox Properties of p53.

6th EMSG Symposium. (September 2009) *Ardgour, UK.*

Talk: Using FT-ICR Mass Spectrometry to Investigate the Role of Cysteine Residues in p53.

7th EMSG Symposium. (September 2010) *Ardgour, UK.*

Talk: Using FT-ICR Mass Spectrometry to Investigate the Role of Cysteine Residues in p53

57th ASMS Conference on Mass Spectrometry and Allied Topics. (May 2009)
Philadelphia, USA.

Poster: Redox-Regulation of p53: Identifying Redox Modifications by Top-Down FT-ICR Mass Spectrometry.

Edinburgh Chemical Biology PhD Meeting. (April 2008) *Firbush, UK.*

Delegate.

Edinburgh Chemical Biology PhD Meeting. (April 2009) *Firbush, UK.*

Poster: Redox-Regulation of p53: Identifying Redox-Modifications by FT-ICR Mass Spectrometry

Edinburgh Chemical Biology PhD Meeting. (March 2010) *Edinburgh, UK.*

Talk: Using FT-ICR Mass Spectrometry to Investigate the Role of Cysteine Residues in p53.

Mass Spectrometry for the Medical & Life Sciences: The Role of High-Field FT-ICR Mass Spectrometry. (September 2010) *Edinburgh, UK.*

Delegate.

Appendix D: Publication Reprints

For reprint orders, please contact reprints@expert-reviews.com

EXPERT
REVIEWS

Sixth Exploratory Measurement Science Group symposium

Expert Rev. Proteomics 7(1), 19–20 (2010)

Isabel Vincent,
Jenna Scotcher and
Richard Burchmore†

†Author for correspondence
Sir Henry Wellcome Functional
Genomics Facility, Institute of
Biomedical and Life Sciences,
Joseph Black Building, Room
B2-25, University of Glasgow,
Glasgow G12 8QQ, UK
Tel.: +44 141 330 8612
Fax: +44 141 330 4600
r.burchmore@bio.gla.ac.uk

Sixth Exploratory Measurement Science Group symposium Ardgour House, Scotland, UK, 14–18 September 2009

The beautiful scenery around Ardgour in the North West of Scotland was the setting for the sixth annual Exploratory Measurement Science Group symposium. The meeting was organized as a study retreat for scientists with an interest in applications of mass spectrometry and associated technologies to discuss ideas in a relaxed, informal setting. Speakers were invited from a wide range of subject areas in the general field of mass spectrometry technology development and application.

KEYWORDS: detection • Exploratory Measurement Science Group • mass spectrometry • measurement • Radical Solutions for Researching the Proteome

The Exploratory Measurement Science Group (EMSG) was developed by the University of Edinburgh's chemistry department under the leadership of Pat Langridge-Smith. The group, based in the Scottish Instrumentation and Resource Centre for Advanced Mass Spectrometry (SIRCAMS), is comprised of a growing network of scientists, researchers and industry partners from around the world, who are interested in the development and application of advanced analytical instrumentation.

Nested at the foot of a hill, surrounded by woodland on the Ardnamurchan Peninsula in West Scotland (UK), Ardgour House has provided a congenial location for successive EMSG symposia. The meeting provides an opportunity for all guests to present their work and ideas through formal oral presentations, providing fuel for discussions and networking over dinner, the snooker table or around the fireplace late at night.

The Ardgour Symposium is also supported by the UK Research Council-sponsored Radical Solutions for Researching the Proteome (RASOR) Consortium, through which the Universities of Glasgow, Strathclyde, Edinburgh and Dundee collaborate to develop novel proteomic workflows and to provide a training conduit for the next generation of scientists.

The meeting advances the aims of the EMSG and RASOR by bringing together users and developers of analytical instrumentation from a wide variety of fields, enabling the cross-disciplinary interaction between scientists who may not otherwise meet. Every year representatives from academia, industry and the Ministry of Defence are invited to present an overview of their research, and are encouraged to illustrate how their expertise could benefit others within a multidisciplinary framework. This year, a wide range of disciplines were discussed including nanotechnology, software engineering and molecular biology, with particular focus on the field of proteomics.

The main ethos of the EMSG symposium is to initiate new collaborative interactions and this aim is recognized in the annual EMSG prize.

Proteomic & beyond

Developments in proteomic technologies were at the forefront of discussions at Ardgour. Presentation topics ranged from the development of novel ion-source technologies to the software solutions for analysis of large-scale MS/MS analyses. Scott Heron, a RASOR-sponsored graduate student working at the University of Glasgow (UK) and the University of Washington (WA, USA), presented his thesis

work on the development of surface acoustic wave technology as a mechanism for the efficient ionization of peptides from very small sample volumes.

Another RASOR student, Jenna Scotcher from the University of Edinburgh (UK), described how the redox state of tumor-suppressing protein p53 has significant effects on its activity. Using Fourier transform ion cyclotron resonance (FTICR) MS, she identified the oxidative modifications to p53 upon hydrogen peroxide treatment. Using top-down FTICR MS she also mapped these modifications to several cysteine residues in the protein.

Melinda McFarland (National Institute of Mental Health, MD, USA) focused on how the function of the neural protein α -synuclein changes upon phosphorylation in familial Parkinson's disease. She described how quantitative and qualitative differences in the interactions of α -synuclein with other proteins could be assessed with MassSieve, a novel software platform for parsimony analysis of large-scale MS/MS experiments. MassSieve allows the comparison of multiple datasets using multiple search engines and has general application where large datasets are generated from complex samples.

David Clarke (University of Edinburgh) described the use of rapid quench FTICR MS to investigate enzyme kinetics. A model system of the chymotrypsin hydrolysis of para-nitrophenyl acetate, which has an intermediate stage where the enzyme is acetylated, was used to validate the methodology with published kinetic data. This technology allows enzyme kinetics to be measured in real time at extremely early time points. Electron-capture dissociation was also exploited to locate the position of the acetylation to a five amino acid portion of the enzyme. Logan McKay (University of Edinburgh) also exploited FTICR MS for top-down proteomic characterization of histone modifications with a role in regulation of gene expression.

Two parasitologists from the University of Glasgow presented work on drug resistance in protozoa. Richard Burchmore described a proteomic approach to analyzing pentamidine resistance in *Leishmania*, which identified a number of changes in proteins associated with the flagellum of the parasite. Isabel Vincent used molecular biology and MS-based metabolomic approaches to identify the mechanism behind eflornithine resistance in *Trypanosoma brucei*, the etiological agent of sleeping sickness in Africa. Dave Goodlett (University of Washington) presented work on the application of MS for lipid structure analysis and the role of lipid A structure in microbial virulence. Richard Goodwin (University of Glasgow) gave an overview of the current state-of-the-art MS imaging, highlighting recent progress and challenges to this approach.

Aside from the biological emphasis, there was a strong representation from the Ministry of Defence. Simon Ellis-Steinborner and David Kilgour from the Defence Science and Technology Laboratory

spoke of their research of detection and analysis of explosives and described how Raman spectroscopy has proved to be of limited use for these applications. Lieutenant Commander Jason White QGM, Commanding Officer of the Royal Navy's Northern Diving Group, gave a fascinating overview of explosive ordnance disposal, both at sea and on land. White illustrated the difficulties in conducting underwater searches for modern naval mines, with particular emphasis on the importance of continued scientific development in the field of explosive detection and disposal. This was followed by a practical demonstration of bomb disposal!

Between and after formal presentations, there was ample opportunity for networking and relaxation. The scientific discussions were taken 'on-deck' for an afternoon when delegates participated in sea fishing around Oban, and the plentiful catch was subsequently served for dinner. Fergus Stokes, a former Baptist Minister and now practicing psychotherapist, gave a stimulating after-dinner talk exploring the interfaces between science, religion, philosophy and psychology. Unsurprisingly, Fergus' speech induced a lively debate!

At the close of the meeting, Ian Sanders (Bruker Daltonics, Coventry, UK) was awarded the annual prize for embracing the spirit of the EMSG. A regular delegate at EMSG symposia, Sanders has consistently made invaluable contributions to both the academic and social fabric of the meeting. Over recent years, Sanders' enthusiasm and curiosity in a breadth of scientific topics has stimulated fruitful partnerships throughout the EMSG community.

Conclusion

Over the years, several international collaborations have resulted from EMSG symposia. These include ongoing research partnerships between the Goodlett and Langridge-Smith laboratories at the Universities of Washington and Edinburgh, and the Defence Science and Technology Laboratory and the Laboratoire de Physique de la Matière Condensée et Nanostructures at the University Claude Bernard Lyon 1 (Lyon, France). These and many other ongoing collaborations typify the cross-fertilization between diverse research areas, which are engendered by the Ardour Symposium.

Financial & competing interests disclosure

Isabel Vincent and Richard Burchmore are employed by the University of Glasgow. Jenna Scotcher is employed by the University of Edinburgh. The authors have no other relevant affiliations or financial involvement with any organization or entity with a financial interest in or financial conflict with the subject matter or materials discussed in the manuscript apart from those disclosed.

No writing assistance was utilized in the production of this manuscript.

Affiliations

- Isabel Vincent
Wellcome Centre for Molecular Parasitology, Glasgow Biomedical Research Centre, Faculty of Biomedical and Life Sciences, University of Glasgow, Glasgow G12 8TA, UK
Tel.: +44 141 330 5650
i.vincent.1@research.gla.ac.uk

- Jenna Scotcher
School of Chemistry, University of Edinburgh, West Mains Road, Edinburgh EH9 3JJ, UK
Tel.: +44 131 651 3034
j.scotcher@sms.ed.ac.uk

- Richard Burchmore
Sir Henry Wellcome Functional Genomics Facility, Institute of Biomedical and Life Sciences, Joseph Black Building, Room B2-25, University of Glasgow, Glasgow G12 8QQ, UK
Tel.: +44 141 330 8612
Fax: +44 141 330 4600
r.burchmore@bio.gla.ac.uk